

**SEDIMENT REMOVAL FROM URBAN RUNOFF USING SEEP  
BERMS AND VEGETATIVE FILTRATION**

A Dissertation  
Presented to  
The Academic Faculty

By

Firas Nadim Hamade

In Partial Fulfillment  
Of the Requirements for the Degree  
Doctor of Philosophy in the  
School of Civil and Environmental Engineering

Georgia Institute of Technology

December, 2013

Copyright © Firas Nadim Hamade 2013

**SEDIMENT REMOVAL FROM URBAN RUNOFF USING SEEP  
BERMS AND VEGETATIVE FILTRATION**

Approved by:

Dr. Terry W. Sturm, Advisor  
School of Civil and Environmental  
Engineering  
*Georgia Institute of Technology*

Dr. Philip J. Roberts  
School of Civil and Environmental  
Engineering  
*Georgia Institute of Technology*

Dr. Donald R. Webster  
School of Civil and Environmental  
Engineering  
*Georgia Institute of Technology*

Dr. James Wray  
School of Earth and Atmospheric  
Sciences  
*Georgia Institute of Technology*

Dr. Thorsten Stoesser  
Cardiff School of Engineering  
*Cardiff University*

Date Approved: August 20, 2013

## ACKNOWLEDGEMENTS

This study was accomplished under the invaluable guidance of Dr. Terry W. Sturm, thesis advisor and chairman of the committee, to whom I express my most profound and heartfelt appreciation for his constructive inspiration, invaluable advice, and limitless patience. He has helped me extensively to enrich my understanding of this study.

I owe much gratitude to the members of my committee: Dr. Thorsten Stoesser, at Cardiff University, Wales, for his invaluable constructive perception and insight into this research; Dr. Donald R. Webster, Dr. Philip J. Roberts, and Dr. James Wray, at the Georgia Institute of Technology, Atlanta, GA, USA.

Heartfelt thankfulness is sincerely expressed to Mr. Andrew I. Udell. With his limitless and invaluable advice, help, and effort, the laboratory apparatus for the experimental trials was transformed from design to reality. Much appreciation is expressed to Mr. Zachariah Worley, who also aided in the laboratory apparatus construction.

Heartfelt gratitude is expressed to my parents and siblings, who have supplied inestimable support and encouragement; my parents: Mr. Nadim Hamade and Mrs. Ahlam Hamade; my brothers: Tarek N. Hamade, PhD., and Bachar N. Hamade, MD; my sister: Diala Hamade. Words cannot express how much I appreciate their support and faith in me.

# TABLE OF CONTENTS

ACKNOWLEDGEMENTS .....	iii
LIST OF FIGURES .....	vii
LIST OF TABLES .....	xii
LIST OF SYMBOLS .....	xiv
SUMMARY .....	xxiii
1. INTRODUCTION .....	1
2. LITERATURE REVIEW .....	6
2.1 Defining the Soil Erosion Problem and Commercial Erosion Control Methods...	6
2.2 The Dirt 2 Committee Report .....	10
2.3 Vegetative Buffer Zones .....	13
2.3.1 Purpose, Benefits, and Design .....	13
2.3.2 Velocity Profiles of Open Channel Flow in Vegetative Zones.....	16
2.3.2.1 Case 1: Emergent Vegetation Velocity Profile.....	17
2.3.2.2 Case 2: Submerged Flexible Vegetation Velocity Profile .....	20
2.3.3 Flow Resistance and Drag in Vegetative Zones in Open Channel Flow .....	22
2.3.3.1 Case 1: Flow Resistance and Drag in Emergent Rigid Vegetation .....	23
2.3.3.2 Case 2: Flow Resistance and Drag in Submerged Flexible Vegetation...	29
2.3.4 Sediment modeling .....	33
2.3.4.1 Suspended Sediment Transport Modeling: Theory .....	33
2.3.4.2 Suspended Sediment Transport Modeling Through Vegetation.....	35
3. SEEP BERMS: EXPERIMENTAL WORK AND RESULTS.....	43
3.1 Project Description.....	43
3.2 Description of Field Sites.....	43
3.3 Project Methodology.....	46
3.4 Project Results .....	50
3.4.1 Alpharetta Site .....	50

3.4.2	The IHM Site .....	53
3.4.3	Outflow Sediment Mass Calculation .....	58
3.5	Summary .....	59
4.	DEFINING THE EXPERIMENTAL PLAN, APPARATUS AND PARAMETERS .....	61
4.1	Experimental Research Objective.....	61
4.2	Experimental Design Plan.....	62
4.2.1	Experimental Flume Design Equations .....	62
4.2.2	Choice of Flume Dimensions and Artificial Vegetation.....	65
4.2.3	Experimental Flume Layout .....	67
4.3	Instrumentation .....	71
4.4	Sediment Feeding Mechanism and Rates .....	72
4.5	Concentration Sampling Mechanism and Rates .....	76
5.	LABORATORY RESULTS AND DISCUSSION.....	80
5.1	Water Surface Profiles .....	80
5.2	Drag Coefficient Calculation .....	83
5.3	ADV Point Velocity Profiles .....	97
5.3.1	Emergent Rigid Vegetation: Density $m = 101.9$ stems/ft <sup>2</sup> .....	99
5.3.2	Emergent Rigid Vegetation: Density $m = 25.5$ stems/ft <sup>2</sup> .....	102
5.3.3	Submerged Flexible Vegetation: Density $m = 101.9$ stems/ft <sup>2</sup> .....	105
5.3.4	Submerged Flexible Vegetation: Density $m = 25.5$ stems/ft <sup>2</sup> .....	108
5.4	Suspended Sediment Concentration Profiles .....	111
5.4.1	Emergent Rigid Vegetation with Density $m = 101.9$ stems/ft <sup>2</sup> .....	114
5.4.2	Emergent Rigid Vegetation with Density $m = 25.5$ stems/ft <sup>2</sup> .....	119
5.4.3	Submerged Vegetation with Density $m = 101.9$ stems/ft <sup>2</sup> .....	123
5.4.4	Submerged Vegetation with Density $m = 25.5$ stems/ft <sup>2</sup> .....	127
5.4.5	Trap Efficiency Analysis .....	131
5.4.6	Trap Efficiency Results.....	134
6.	PERFORMANCE OF SEEP BERM AND VEGETATIVE FILTER IN SERIES ....	139
6.1	Seep Berm Modeling .....	139
6.2	SEDCAD4 Modeling and Determining Vegetation Filter Design Flow Depth .....	142
6.2.1	SEDCAD4 Modeling.....	142
6.2.2	Vegetative Filter Design Depth Technique.....	145

6.2.2.1 Comparing Drag Coefficients from James et al. (2004) and Cheng and Nguyen (2011) .....	145
6.2.2.2 Design Procedure .....	146
6.2.2.3 Numerical Design Example .....	149
7. CONCLUSIONS.....	154
7.1 Summary of the Thesis .....	154
7.2 Conclusions.....	156
7.3 Contributions of this Research.....	158
7.4 Future Research .....	159
APPENDIX A.....	161
APPENDIX B.....	163
APPENDIX C .....	170
REFERENCES .....	181

## LIST OF FIGURES

Figure 1: Flow velocity profiles from Fu Sheng Wu (2008) .....	19
Figure 2: Velocity profile for open channel flow through submerged vegetation (Jarvela, 2005) .....	21
Figure 3 : Schematic showing the control volume and parameters used by Wilson and Horritt (2002) .....	30
Figure 4: Illustration describing the parameters used by Yang and Choi (2010) to obtain the vertical suspended sediment concentration across water depth .....	37
Figure 5: (a) Plan view of the IHM field project location; (b) Plan view of the Alpharetta field project location .....	44
Figure 6: GSD plots for both Alpharetta and IHM sites .....	46
Figure 7: (a) Photo of the Alpharetta silt fence, with the white trapezoidal flume at the end of the silt fence perimeter to collect and direct the silt fence outflow; (b) Photo of the IHM silt fence layout and collection channel, outflow weir, precipitation gage (on wood post), and ISCO sampler in steel cage (Sturm et al., 2007) .....	47
Figure 8: (a) Photo of the Alpharetta seep berm layout and ISCO sampler; (b) Photo of the IHM seep berm layout. The one-in. overflow pipes, three-in. collection pipe, discharge flow meter, and ISCO samplers in steel cages are shown in both photos (Sturm et al., 2007) .....	48
Figure 9: (a) The cross section of the Alpharetta seep berm (not to scale); (b) The cross section of the IHM seep berm (not to scale) (Sturm et al., 2007) .....	49
Figure 10: Cumulative hyetographs for sampled events at Alpharetta site, showing the five different rainfall events in which silt fence samples were collected (Sturm et al., 2007) .....	51
Figure 11: Outflow hydrographs and sedimentgraphs from Alpharetta silt fence for event of 8/12/06 (Sturm et al., 2007) .....	52
Figure 12: Cumulative hyetographs for sampled events at IHM site, showing the five different rainfall events in which silt fence and seep berm samples were collected (Sturm et al., 2007) .....	54
Figure 13: (a) Outflow hydrographs and sedimentgraphs from the IHM silt fence; (b) Outflow hydrographs and sedimentgraphs from the IHM seep berm; both for the event of 8/24/2007 (Sturm et al., 2007) .....	56

Figure 14: Plots of normal depth vs velocity and $k/h$ vs velocity for stem densities ranging from 200 to 1200 stems/m <sup>2</sup> . The $k/h$ vs velocity plots are those curving downwards from left to right. Any $k/h$ values above 1, as bordered by the horizontal line at $k/h=1$ , were discarded as unrealistic values, implying that their corresponding stem densities were not applicable using the Kouwen (1992) design equations for the experimental flume design parameters. ....	66
Figure 15: Front view and plan view of experimental flume.....	69
Figure 16: Plot showing flume length versus still-water depth, to measure the slope of the experimental flume .....	70
Figure 17: Calibration curve for orifice meter in flume flow pipe .....	71
Figure 18: The sediment diffuser with its dimensions.....	73
Figure 19: Grain Size distribution of the sand used in the experimental trials.....	75
Figure 20: (a) ISCO suction inlet mechanism; (b) ISCO suction inlet openings.....	77
Figure 21: Schematic of the ISCO suction inlet location in the vegetation filter .....	78
Figure 22: Water surface profiles for 0.3 cfs; normal depth is 0.43 ft.....	81
Figure 23: The stage-discharge curve for all four vegetation cases.....	83
Figure 24: Drag coefficient results from the four experimental sets of vegetation plotted on the same graph against Stem Re. The experimental vegetation densities are $m = 101.9$ stems/ft <sup>2</sup> and 25.5 stems/ft <sup>2</sup> .....	88
Figure 25: Experimental drag coefficient results plotted against Stem Re, with other researchers' data. The value of $m$ in the legend represents stem density in stems/ft <sup>2</sup> .....	89
Figure 26: The drag coefficient plotted against the submergence ratio $H/d$ , where $H$ is the water depth ( $y_n$ ) and $d$ is the stem diameter (cylindrical rods) or stem width (thin rectangular strips). The experimental vegetation densities are $m = 101.9$ stems/ft <sup>2</sup> and 25.5 stems/ft <sup>2</sup> .....	91
Figure 27: Submergence ratio $H/d$ plotted against the stem Reynolds number. The experimental vegetation densities are $m = 101.9$ stems/ft <sup>2</sup> and 25.5 stems/ft <sup>2</sup> .....	92
Figure 28: Drag coefficient plotted against relative vegetation height $k/H$ . The vegetation is flexible submerged for both cases. The experimental vegetation densities are $m = 101.9$ stems/ft <sup>2</sup> and 25.5 stems/ft <sup>2</sup> .....	93
Figure 29: Relative vegetation height $k/H$ plotted against Stem Re; the vegetation is flexible submerged for both cases. The experimental vegetation densities are $m = 101.9$ stems/ft <sup>2</sup> and 25.5 stems/ft <sup>2</sup> .....	94

Figure 30: Comparison of drag coefficient data between the experimental emergent and submerged vegetation using the Cheng and Nguyen (2011) method, and other researchers' data subjected to the same method. The value of  $m$  in the legend represents stem density in stems/ft<sup>2</sup> ..... 96

Figure 31: Normalized repeatability trial profiles to test ADV accuracy: (a) point velocity; (b) streamwise turbulence intensity; (c) spanwise turbulence intensity; (d) vertical turbulence intensity;  $Q = 0.3$  cfs,  $H =$  normal depth = 5.16 in.,  $U = 0.213$  ft/sec ..... 98

Figure 32: Schematic showing both ADV locations for vegetation density  $m = 101.9$  stems/ft<sup>2</sup> ..... 99

Figure 33: Normalized ADV results for: (a) point velocity; (b) streamwise turbulence intensity; (c) spanwise turbulence intensity; (d) vertical turbulence intensity; for emergent vegetation density  $m = 101.9$  stems/ft<sup>2</sup>,  $Q = 0.4$  cfs,  $H = 6.48$  in.,  $U = 0.226$  ft/sec ..... 100

Figure 34: Schematic showing all four ADV locations for vegetation density  $m = 25.5$  stems/ft<sup>2</sup> ..... 102

Figure 35: Normalized ADV results for: (a) point velocity; (b) streamwise turbulence intensity; (c) spanwise turbulence intensity; (d) vertical turbulence intensity; for emergent vegetation density  $m = 25.5$  stems/ft<sup>2</sup>,  $Q = 0.4$  cfs,  $H = 3.00$  in.,  $U = 0.49$  ft/sec ..... 103

Figure 36: Normalized ADV results for: (a) point velocity; (b) streamwise turbulence intensity; (c) spanwise turbulence intensity; (d) vertical turbulence intensity; for submerged vegetation density  $m = 101.9$  stems/ft<sup>2</sup>,  $Q = 0.4$  cfs,  $H = 3.96$  in.,  $U = 0.37$  ft/sec ..... 106

Figure 37 Normalized ADV results for: (a) point velocity; (b) streamwise turbulence intensity; (c) spanwise turbulence intensity; (d) vertical turbulence intensity; for submerged vegetation density  $m = 25.5$  stems/ft<sup>2</sup>,  $Q = 0.6$  cfs,  $H = 3$  in.,  $U = 0.732$  ft/sec ..... 109

Figure 38: Concentration data points for the repeatability test, plotted against time ..... 114

Figure 39: Streamwise suspended sediment concentration profiles along the vegetation length, for emergent vegetation of density  $m = 101.9$  stems/ft<sup>2</sup>. Exponential trends are shown for two flow rates, to be referred to later in Subsection 5.4.5 ..... 115

Figure 40: Suspended sediment flux per unit width against vegetation length; emergent vegetation of density  $m = 101.9$  stems/ft<sup>2</sup> ..... 119

Figure 41: Streamwise suspended sediment concentration profiles along the vegetation length, emergent vegetation of density  $m = 25.5$  stems/ft<sup>2</sup>. Exponential trends are shown for two flow rates, to be referred to later in Subsection 5.4.5..... 120

Figure 42: Suspended sediment flux per unit width against vegetation length; emergent vegetation of density $m = 25.5$ stems/ft <sup>2</sup> .....	123
Figure 43: Streamwise suspended sediment concentration profiles along the vegetation length, submerged vegetation of density $m = 101.9$ stems/ft <sup>2</sup> . Exponential trends are shown for two flow rates, to be referred to later in Subsection 5.4.5 .....	124
Figure 44: Suspended sediment flux per unit width against vegetation length, submerged vegetation of density $m = 101.9$ stems/ft <sup>2</sup> .....	127
Figure 45: Streamwise suspended sediment concentration profiles along the vegetation length, submerged vegetation of density $m = 25.5$ stems/ft <sup>2</sup> . Exponential trends are shown for two flow rates, to be referred to later in Subsection 5.4.5.....	128
Figure 46: Suspended sediment flux per unit width against vegetation length, submerged vegetation of density $m = 25.5$ stems/ft <sup>2</sup> .....	131
Figure 47: Trap efficiency plotted against sediment settling efficiency, for all four vegetation trials (densities $m = 101.9$ and $25.5$ stems/ft <sup>2</sup> ) and for the theoretical case of no vegetation in the flume.....	137
Figure 48: (a) Hydrograph obtained from SEDCAD4; (b) Sedimentgraph obtained from SEDCAD4.....	144
Figure 49: Drag coefficient using pore velocity $C_{Dv}$ plotted against vegetated Reynolds number $R_v$ (Cheng & Nguyen, 2011) .....	147
Figure 50: Grain size distribution from the theoretical trap efficiency method .....	151
Figure A. 1 : Photo of flume. Flow travels from right to left. ....	161
Figure A. 2: Photo of the cylindrical wooden rods simulating emergent rigid vegetation, $m = 101.9$ stems/ft <sup>2</sup> .....	162
Figure A. 3: Photo of the rectangular plastic strips simulating submerged flexible vegetation, $m = 101.9$ stems/ft <sup>2</sup> .....	162
Figure B. 1: Friction factor $f$ plotted against modified Reynolds number (Andrade et al., 1999).....	165
Figure C. 1: Normalized ADV results for: (a) point velocity; (b) streamwise turbulence intensity; (c) spanwise turbulence intensity; (d) vertical turbulence intensity; for emergent vegetation density $m = 101.9$ stems/ft <sup>2</sup> , $Q = 0.2$ cfs, $H = 4.20$ in., $U = 0.174$ ft/sec .....	170
Figure C. 2: Normalized ADV results for: (a) point velocity; (b) streamwise turbulence intensity; (c) spanwise turbulence intensity; (d) vertical turbulence intensity; for emergent vegetation density $m = 101.9$ stems/ft <sup>2</sup> , $Q = 0.3$ cfs, $H = 5.16$ in., $U = 0.213$ ft/sec .....	171

Figure C. 3: Normalized ADV results for: (a) point velocity; (b) streamwise turbulence intensity; (c) spanwise turbulence intensity; (d) vertical turbulence intensity; for emergent vegetation density  $m = 101.9$  stems/ft<sup>2</sup>,  $Q = 0.5$  cfs,  $H = 7.32$  in.,  $U = 0.250$  ft/sec ..... 172

Figure C. 4: Normalized ADV results for: (a) point velocity; (b) streamwise turbulence intensity; (c) spanwise turbulence intensity; (d) vertical turbulence intensity; for emergent vegetation density  $m = 25.5$  stems/ft<sup>2</sup>,  $Q = 0.3$  cfs,  $H = 2.64$  in.,  $U = 0.416$  ft/sec ..... 173

Figure C. 5: Normalized ADV results for: (a) point velocity; (b) streamwise turbulence intensity; (c) spanwise turbulence intensity; (d) vertical turbulence intensity; for emergent vegetation density  $m = 25.5$  stems/ft<sup>2</sup>,  $Q = 0.5$  cfs,  $H = 3.48$  in.,  $U = 0.526$  ft/sec ..... 174

Figure C. 6: Normalized ADV results for: (a) point velocity; (b) streamwise turbulence intensity; (c) spanwise turbulence intensity; (d) vertical turbulence intensity; for emergent vegetation density  $m = 25.5$  stems/ft<sup>2</sup>,  $Q = 0.6$  cfs,  $H = 3.96$  in.,  $U = 0.554$  ft/sec ..... 175

Figure C. 7: Normalized ADV results for: (a) point velocity; (b) streamwise turbulence intensity; (c) spanwise turbulence intensity; (d) vertical turbulence intensity; for submerged vegetation density  $m = 101.9$  stems/ft<sup>2</sup>,  $Q = 0.2$  cfs,  $H = 3.36$  in.,  $U = 0.218$  ft/sec ..... 176

Figure C. 8: Normalized ADV results for: (a) point velocity; (b) streamwise turbulence intensity; (c) spanwise turbulence intensity; (d) vertical turbulence intensity; for submerged vegetation density  $m = 101.9$  stems/ft<sup>2</sup>,  $Q = 0.3$  cfs,  $H = 3.60$  in.,  $U = 0.310$  ft/sec ..... 177

Figure C. 9: Normalized ADV results for: (a) point velocity; (b) streamwise turbulence intensity; (c) spanwise turbulence intensity; (d) vertical turbulence intensity; for submerged vegetation density  $m = 101.9$  stems/ft<sup>2</sup>,  $Q = 0.5$  cfs,  $H = 4.20$  in.,  $U = 0.436$  ft/sec ..... 178

Figure C. 10: Normalized ADV results for: (a) point velocity; (b) streamwise turbulence intensity; (c) spanwise turbulence intensity; (d) vertical turbulence intensity; for submerged vegetation density  $m = 25.5$  stems/ft<sup>2</sup>,  $Q = 0.5$  cfs,  $H = 2.88$  in.,  $U = 0.635$  ft/sec ..... 179

Figure C. 11: Normalized ADV results for: (a) point velocity; (b) streamwise turbulence intensity; (c) spanwise turbulence intensity; (d) vertical turbulence intensity; for submerged vegetation density  $m = 25.5$  stems/ft<sup>2</sup>,  $Q = 0.7$  cfs,  $H = 3.12$  in.,  $U = 0.821$  ft/sec ..... 180

## LIST OF TABLES

Table 1: A summary of precipitation data that occurred on the Alpharetta site, with their corresponding silt fence peak TSS and turbidity outflow concentrations, analyzed from the sediment runoff samples collected by the ISCO sampler (Sturm et al., 2007).....	51
Table 2: A summary of precipitation data that occurred on the IHM site, with their corresponding silt fence and seep berm peak TSS and turbidity concentrations, analyzed from the sediment runoff samples collected by the ISCO samplers (Sturm et al., 2007). .....	54
Table 3: Suspended sediment outflow mass summary for four precipitation events .....	59
Table 4: Design criteria and guidelines for determining flume dimensions.....	64
Table 5: Final selected flow and vegetation properties for the experimental vegetation filters .....	67
Table 6: The normal depths obtained for the chosen flow rates corresponding to: (a) emergent vegetation of density $m = 101.9$ stems/ft <sup>2</sup> ; (b) emergent vegetation of density $m = 25.5$ stems/ft <sup>2</sup> ; (c) submerged vegetation of density $m = 101.9$ stems/ft <sup>2</sup> ; (d) emergent vegetation of density $m = 25.5$ stems/ft <sup>2</sup> .....	82
Table 7: Tabulated results obtained at different flow rates for: (a) emergent rigid vegetation of density $m = 101.9$ stems/ft <sup>2</sup> ; (b) emergent rigid vegetation of density $m = 25.5$ stems/ft <sup>2</sup> ; (c) submerged flexible vegetation of density $m = 101.9$ stems/ft <sup>2</sup> ; (d) submerged flexible vegetation of density $m = 101.9$ stems/ft <sup>2</sup> .....	87
Table 8: Suspended sediment concentration data obtained from the experimental trials using the ISCO sampler, emergent vegetation of density $m = 101.9$ stems/ft <sup>2</sup> .....	115
Table 9: Tabulated calculated values to obtain the value of trap efficiency for emergent vegetation of density $m = 101.9$ stems/ft <sup>2</sup> .....	117
Table 10: Suspended sediment concentration data obtained from the experimental trials using the ISCO sampler, emergent vegetation of density $m = 25.5$ stems/ft <sup>2</sup> .....	120
Table 11: Tabulated calculated values to obtain the value of trap efficiency for emergent vegetation of density $m = 25.5$ stems/ft <sup>2</sup> .....	122
Table 12: Suspended sediment concentration data obtained from the experimental trials using the ISCO sampler, submerged vegetation of density $m = 101.9$ stems/ft <sup>2</sup> .....	124
Table 13: Tabulated calculated values to obtain the value of trap efficiency for submerged vegetation of density $m = 101.9$ stems/ft <sup>2</sup> .....	126

Table 14: Suspended sediment concentration data obtained from the experimental trials using the ISCO sampler, submerged vegetation of density $m = 25.5$ stems/ft <sup>2</sup> .....	128
Table 15: Tabulated calculated values to obtain the value of trap efficiency for submerged vegetation of density $m = 25.5$ stems/ft <sup>2</sup> .....	130
Table 16: Summary of drag coefficient and trap efficiency results from all four vegetation trials.....	135
Table 17: Table 1 of the Seep Berm Design manual, showing runoff volumes, from Sturm and Warner (2007) .....	140
Table 18: Table 2 from the seep berm design manual, showing berm heights according to slopes, from Sturm and Warner (2007).....	141
Table 19: Seep berm results from SEDCAD4 showing inflow and outflow runoff rates and suspended sediment concentrations .....	143
Table 20: Theoretical trap efficiency calculations ( $Q=3.5$ cfs, $A_s=100$ ft <sup>2</sup> , $Q/A_s=0.035$ ) .....	150
Table 21: Iterations for the numerical design example.....	152

## LIST OF SYMBOLS

$a, b$	Empirical coefficients depending on the degree of bent vegetation in Equations 68 and 69
$b, m$	Property of porous media and a measure of the influence of fluid inertia, respectively, in Equation B – 2 of Appendix B
$A, B$	Constants in the negative power trend equation of Figure 24
$a_x, a_y$	longitudinal and lateral distance between stems, respectively
$a$	Cross-sectional area of flow in Figure 3 and Equations 29 and 30; 5% of the normal depth in Equation 44; vegetation density in Subsection 2.3.4.2; sum of areas of the ports across the sediment diffuser in Section 4.4
$A$	Cross-sectional area of flow, except in Figure 3 and Equations 29 and 30 where it corresponds to $A_p$ ; cross-sectional area of the sediment diffuser in Section 4.4; cross-sectional area of plug-flow reactor model in Subsection 5.4.5
$A_b$	Bed bottom area of a control volume
$A_{inlet}$	Area of the suction head inlet that obtains concentration samples from the experimental flume
$A_p$	Projected area of one or more vegetation stems
$A_{p,tot}$	Projected area of total stems in vegetative filter in Equation 15
$A_s$	Surface area of water in the sedimentation basin or vegetative filter = $bL$
$A_v$	Surface area of voids in Equation B – 6 in Appendix B
$b$	Vegetation filter width, seep berm width, flume width, control volume width
$c'$	Turbulent sediment concentration fluctuation

$C$	Suspended sediment concentration at a point along flow depth; time or flux averaged suspended sediment concentration at a point on the vertical as described when relative in the thesis; Suspended sediment concentration in the runoff from an erosion control in Equation 63; Integration constant in Equation 1
$C_a$	Reference concentration at distance $z = a$ above channel bed in Equation 44
$C_{avg}$	Sediment concentration in the experimental flume after sediment mixing
$C_b$	Concentration at $z = b$ in Subsection 2.3.4.2
$C_d$	Coefficient of drag using $U$
$C_d'$	Vegetal drag coefficient in Equations 33 and 34, equal to $\lambda C_d$ in Equation 33; Vegetal drag coefficient in Equation (36) with a different expression than in Equations 33 and 34
$C_{Dv}$	Coefficient of drag using $U_v$
$C_{feed}$	Sediment concentration fed into flume for each experimental trial
$C_{inflow}$	Initial experimental flume water concentration
$C_{in}$	Suspended sediment concentration entering the experimental flume
$C_{out}$	Suspended sediment concentration exiting the experimental flume
$C_o$	Initial suspended sediment concentration entering a control volume
$C_u$	Vegetation density coefficient in Subsection 2.3.4.2
$d$	Stem diameter (cylindrical) or stem width (rectangular) for vegetative filters; grain diameter where mentioned in Appendix B for porous media
$d_r$	Characteristic plant diameter in Equation 16

$d_s$	Grain diameter
$d_{50}$	Median sediment grain size
$d_{84.13}$	Sediment grain size at 84.13 percent finer
$d^*$	Dimensionless particle diameter
$D$	Flow depth in Equation 33 and 34; sediment diffuser diameter in Section 4.4
$f$	Darcy-Weisbach friction factor; generalized friction factor for porous media in Equation B – 4 in Appendix B
$f'$	Darcy-Weisbach friction factor of the bed due to surface resistance
F or Froude	Froude number
$F_{bedshear}$	Force due to bed shear stress
$F_d$	Vegetation drag Force using $C_d$
$F_D$	Vegetation drag force using $C_{Dv}$ , except in Figure 3 and Equation 27 and Equation 46 where it corresponds to $F_d$
$F_g$	Gravitational force of a control volume
$F_\tau$	Shear force at the vegetation-water interface for submerged vegetation
$g$	Gravity
Ga	Galileo number in Appendix B
Ga*	Modified Galileo number in Appendix B
$h$	Flow depth in Figure 2 and Equation 4; vegetation height in Figure 3 and Equation 35; full flexible stem height in Subsections 4.2.1 and 4.2.2
$h_{deflected}$	Deflected vegetation height in Equations 35 and 36
$h_f$	Head loss

$h_L$	Friction loss parameter preceding Equation B – 17 in Appendix B
$h_{p,m}$	Mean vegetation deflected height in Figure 2 and Equations 2 and 4
$h_{p,low}$	Minimum vegetation deflected height in Figure 2
$h_{p,up}$	Maximum deflected vegetation height in Figure 2
$h_1$	Vegetation height in Subsection 2.3.4.2
$h_2$	Water layer height in Subsection 2.3.4.2
$H$	Water height above vegetation layer only in Equation 31
$H$ or $y_n$	Uniform flow normal depth
$k$	Vertical height of the bent part of the stem measured from bed bottom to the tip of bent stem (deflected stem height); plug-flow reaction parameter in Subsection 5.4.5
$k_s$	Equivalent sand roughness
$K$	Permeability parameter in Appendix B
$l\varepsilon$	Length scale representing the ratio of volume of voids to their flow surface area
$L$ or $l$	Control volume length or Vegetation filter length; Mixing length in Equation 72
$L_s$	Full flexible stem height or length
$m$	Sediment mass in outflow from an erosion control in Equation 63
$m$	Stem density
$M$	Stem density in Subsection 4.2.1
$M_{in}$	Sediment mass entering the vegetative filter
$M_{out}$	Sediment mass exiting the vegetative filter

$M_{settled}$	Mass of sediment that settled out of the flow onto the vegetative filter bed
$MEI$	Stiffness factor of the vegetation
$n$	Manning's $n$ for resistance; number of ports on sediment diffuser in Section 4.4
$N$	Number of stems
$N_{grass}$	Average grass blade number per channel width $b$
$p$	Probability of a particle reaching the bed will remain permanently deposited and not re-suspended into the flow in Equation 62
$P$	Wetted perimeter
$\Delta P$	Pressure drop over a length $L$
$q$	Flow rate per unit width
$q_{feed}$	Slurry feed flow through each port hole on the sediment diffuser pipe
$q_s$	Sediment flux per unit width
$Q$ or $Q_{inflow}$	Flow rate in flume or runoff
$Q_{feed}$	Slurry feed flow from slurry pump to the sediment diffuser
$Q_{ISCO}$	ISCO sampler suction flow rate
$Q_s$	Sediment flux
$r_v$	Vegetation-related hydraulic radius
$R$	Hydraulic radius
$R_0$	Rouse number $R_0 = \frac{w_f}{\beta \kappa u_*}$
Re or Flow Re	Flow Reynolds number
Re'	Modified Reynolds number in porous media flow; equal to $R_v$ in open channel flow through vegetative filters

$R_v$	Vegetation-related Reynolds number
$S$	Bed slope
$S_e$	Energy slope
SEF	Theoretical settling efficiency
Stem Re	Stem Reynolds number
$t$	Time
$t_1$	Start time in Equation 63
$t_2$	End time in Equation 63
$\Delta t$	Interval between two times; duration of an experimental trial
$t_s$	Thickness of the rectangular vegetative LEXAN strip length
$T$	Vegetation height in Equations 32, 33, and 34
$TE$	Trap Efficiency
$TE_{final}$	Final trap efficiency of joint seep berm – vegetative filter erosion control measure in Equation 105
$TE_{seep\ berm}$	Trap efficiency of seep berm in Equation 105
$TE_{veg.filter}$	Trap efficiency of vegetative filter in Equation 105
$u$	Streamwise point velocity in flow
$u_i$	Point velocity components in $x_i$ directions in Equation 59
$u_x$	Streamwise point velocity in flow in Equation 60
$u_2$	Point velocity in water layer above vegetation in Subsection 2.3.4.2

$u^*$	Shear velocity; interfacial shear velocity at the vegetation-water layer interface of submerged vegetation in Subsection 2.3.4.2
$u^*_{crit}$	Critical shear velocity
$u', u_{rms}$	Streamwise turbulence intensity
$-\overline{u'w'}$	Reynolds shear stress
$-\overline{u'w'}_{max}$	Maximum Reynolds shear stress
$-\overline{uw}$	Reynolds shear stress in Subsection 2.3.4.2
$U$	Flow bulk or mean (average) velocity
$U_1$	Mean velocity in the vegetated layer in Subsection 2.3.4.2
$U_2$	Mean velocity in the water layer in Subsection 2.3.4.2
$U_{inlet}$	Velocity of the suction head inlet that obtains concentration samples from the experimental flume
$U_v$	Average pore velocity
$U^*$	Shear velocity estimate in Equation 3 and Equation 4
$v_{feed}$	Velocity of slurry flow from each port hole on the sediment diffuser pipe
$v'$	Spanwise turbulence intensity
$V_{cv}$	Volume of a control volume
$V$	Volume of water in a control volume; volume of vegetative strip control volume in Subsection 5.4.5
$V_p$	Volume of a single grain for porous media in Appendix B
$V_T$	Total volume of the packing in Equation B – 6 in Appendix B
$V_v$	Volume of voids in equation B – 6 in Appendix B
$w_f$	Fall velocity of a sediment particle

$w'$	Vertical turbulence intensity
$\overline{w'c'}$	Mean turbulent flux of sediment per unit area
$x$	Streamwise direction
$\Delta x$	A set measure in the horizontal direction
$x_i$	Denotes all axes in Equation 59
$X$	Size fraction by weight of the sediment sample
$\Delta X$	Difference between two size fractions by weight of the sediment sample
$y$	Spanwise direction; Flow normal depth in Figure 3; vertical direction in Equations 59 through 62 of Subsection 2.3.4.2
$y_o$	Uniform flow depth in Equations 41, 43, and 44
$y_n$ or $H$	Uniform flow normal depth
$z$	Vertical direction
$\Delta z$	A set measure in the vertical direction
$z_b$	5% of flow depth in Subsection 2.3.4.2
$Z_1, Z_2$	Modified versions of the Rouse parameter in Subsection 2.3.4.2
$\alpha$	Reciprocal permeability of the porous material in Equation B – 3 in Appendix B
$\alpha_0, \alpha_1$	Functions of the solid volume fraction $\phi$
$\beta$	Proportionality constant in open channel flow sediment settling; inertial parameter in porous media in Equation B – 3 of Appendix B
$\sigma_g$	Geometric standard deviation of a sediment grain size distribution
$\varepsilon$	Turbulent eddy viscosity; porous media porosity in Appendix B

$\varepsilon_v$	Vertical diffusion coefficient in Equations 71 and 72
$\varepsilon_s$	Turbulent sediment diffusion coefficient
$\varepsilon_i$	Sediment diffusivities in all $x_i$ directions in Equation 59
$\lambda$	Vegetal area coefficient corresponding to the area fraction per channel unit length in Equation 32
$\gamma$	Specific weight of water
$\gamma_s$	Specific weight of the solid
$\mu$	Dynamic viscosity
$\kappa$	von Karman constant
$\phi$	Solid volume fraction
$\rho$	Water density
$\tau$	Shear stress at a point; total boundary shear stress in Subsection 4.2.1
$\tau_b$	Bed shear stress in Subsection 2.3.4.2
$\tau_o$	Average boundary shear stress or bed shear stress; apparent bed shear stress in Equation 76
$\tau_i$	Two-layer interfacial shear stress in Subsection 2.3.4.2
$\nu$	Kinematic viscosity
$\nu_t$	Turbulent eddy viscosity in Subsection 2.3.4.2

## SUMMARY

Previous field demonstration projects in metro-Atlanta have shown that seep berms, which are elongated sedimentation basins at the outlet of a disturbed land area, can provide high suspended sediment trap efficiencies with respect to coarse sediments on construction sites having drainage areas greater than five acres. Previous literature has shown that vegetative filter strips are efficient traps for fine suspended sediment in stormwater runoff. A combination of a seep berm and vegetative filter in series was studied in this thesis as an erosion control measure with quantification of its flow resistance and sediment removal efficiency. First, a field demonstration project was implemented to evaluate seep berms as a viable erosion control measure through a side-by-side comparison with the more commonly-used silt fences on construction sites with drainage areas less than five acres in metro Atlanta. High suspended sediment trap efficiencies were recorded for the seep berm on two separate sites, and the seep berm was shown to be superior to silt fences with respect to sediment control in the site runoff. Then a vegetative filter was studied in the laboratory in a specially-built flume for that purpose. The relationship between vegetative drag coefficient and various parameters reflecting flow conditions and vegetation density in steady, uniform open channel flow was studied in the flume. Both rigid, emergent vegetation and submerged, flexible vegetation were studied at two different plant densities. The application of porous media flow concepts to open channel flow through vegetation resulted in a collapse of data for vegetative drag coefficient for the various vegetation types and densities into a single relationship when plotted against vegetative stem Reynolds number. Point velocity and turbulence intensity profiles at different locations in the vegetative filter were recorded with an acoustic Doppler velocimeter to observe the turbulence structure of the flow and its effects on vegetative drag and settling of sediment. A sediment slurry consisting of a suspension of fine sand was fed into the flume, and an automated sampler was used to measure suspended sediment concentrations along the vegetative filter length for a series of discharges from which sediment flux and trap efficiency could be determined. Experimental data for trap efficiency were plotted against a dimensionless settling

efficiency for each type of vegetation and density. These relationships, along with the one developed for the coefficient of drag, were applied in a numerical design technique that allows designers to determine the flow depth, velocity and trap efficiency of a vegetative filter of known dimensions for a given flow rate, sediment grain size distribution, slope, and vegetation density. In a typical design example, the combined trap efficiency proved that a seep berm followed by a vegetative filter can be a very effective erosion control measure.

# 1. INTRODUCTION

The objective of this thesis is to study methods for reducing the concentration of sediment in urban water runoff from construction sites which is caused by the erosion of soil particles from disturbed land surfaces by the rainfall-runoff process. Erosion control measures (known also as best management practices or BMPs) aimed at addressing the problem are introduced, with seep berms and vegetative buffer zones or filters being the two BMPs of interest in this thesis.

Seep berms are defined as erosion and storm water controls shaped as long and narrow soil berms that form sedimentation chambers placed at the down-gradient boundaries and peripheries of construction sites with the sole purpose of reducing sediment in runoff migrating from disturbed land areas. Vegetative filters are areas of existing native vegetation or planted grass cover that act as physical barriers against the detrimental effects of erosion on cleared farmlands, construction sites, roads, landfills, hill slopes, and many other locations associated with land disturbance.

Previous research and experimentation has shown that seep berms are an efficient BMP, albeit not as popular as other traditional BMPs, such as silt fences, that are currently widely used. One of the most attractive things about seep berms to contractors, consultants, and land developers, is their extremely low cost, since they are built using the fill soil from the construction site itself. Additionally, significant improvements on water quality can be attained over the long term if the berm's use becomes widespread (Sturm et al., 2007). Seep berms are also a great fit into the State NPS plan by offering a certain type of erosion control measure that has extra advantages over conventional erosion control measure like sedimentation ponds and silt fences. A main advantage would be that seep berms can completely contain and store small rainfall events. Moreover, they provide a linear sedimentation control measure, which permits infiltration, sedimentation, and sediment storage behind the berm wall, taking up less land than a sedimentation pond by being constructed downstream along a construction site's perimeter. They can also direct runoff that overtops the berm walls into a vegetative

buffer zone for more extensive treatment of finer sediment particles, through slow flow rates. Seep berm trap efficiencies of 99% have been observed and reported (Sturm et al., 2007).

The successes encountered by Warner et al. (2004), the Dirt 2 Committee (2001), and Sturm et al. (2007) formed the basis of the experimental concept and apparatus described in this thesis. The Dirt 2 Committee of 2001 was formed by the then Lieutenant Governor of Georgia for the purpose of studying erosion control and how its absence on many construction sites was impacting the water quality of the Chattahoochee River. After intensive research and studies, the committee completed a technical report on improving the water quality of the Chattahoochee that was endorsed by the Georgia Environmental Protection Division (EPD) as an improved approach to erosion prevention and sediment control. The Dirt 2 Committee encouraged, through their findings, the treatment of erosion as an imperative issue that must be addressed in the metropolitan Atlanta region, and not as an afterthought, which was the way some developers in the metro Atlanta region viewed it. Unfortunately, the conventional approach to erosion at that time was that it is inevitable due to nature's rainstorm events, and that not a whole lot can be done to prevent it. Due to that approach, the resulting erosion control plans had no expectation of working because they were not based on actual performance (Dirt 2 Committee, 2001). The Dirt 2 Committee encouraged moving away from the conventional approach by working extensively with site planners, developers, and design professionals and showing them how effective erosion control could be achieved on their construction sites of five acres or more, thereby minimizing downstream damage to urban areas and water bodies where they may be held responsible and face litigation. The Dirt 2 Committee promoted thoughtful integration of erosion control into a construction project, meaningful design of a sound and coherent erosion control system by qualified design professionals, and monitoring and maintaining the erosion control measures to assure optimal performance in protecting and safeguarding water quality.

The findings of the Dirt 2 Committee (2001) formed the basis of a joint venture demonstration project between Georgia Tech and the University of Kentucky, supervised by Dr. Terry Sturm of Georgia Tech, and Dr. Richard Warner of the University of

Kentucky. They implemented the findings of the Dirt 2 Committee of 2001 on construction sites of five acres or less using seep berms and silt fences as the erosion control measures of choice. Two sites were chosen for the demonstration project, one in Alpharetta (summer 2006) and one in North Druid Hills (summer 2007) in the Atlanta metro area. The project aimed at showcasing the efficiency of seep berms as an erosion control measure through a direct side-by-side comparison with silt fences, and to promote the use of seep berms as an efficient and less costly alternative to silt fences or sedimentation ponds. The demonstration project successfully achieved its objectives, and will be discussed more thoroughly subsequently in the thesis.

The objective of the thesis research is to further develop the findings of the Dirt 2 Committee (2001) and the joint demonstration project of Sturm et al. (2007). What is proposed and studied in this thesis is the combination of seep berms and vegetative filters installed in series as an effective BMP capable of handling large water runoff rates that may cause water to overtop the seep berm by allowing sedimentation due to temporary storage as well as filtration of the overflow using a vegetative filter. From previous research and literature review, it was shown that vegetative filters are very efficient in reducing sediment in water runoff. Individually, each one of the above-mentioned BMP's has delivered good to excellent results, as is shown in previous experimentation and research, to be discussed in the literature review section of this thesis, but the purpose of this thesis is to investigate how these two BMPs used in series could further improve the water quality of runoff from urban construction sites.

In the thesis, the first stage of erosion control considered is a seep berm that is intended to temporarily store site runoff and allow for sediment removal by settling. During larger storms, however, the seep berm is likely to be overtopped resulting in release of sediment-laden water downstream of the site. In order to improve sediment removal in this eventuality, a vegetative buffer zone is placed directly downstream of the seep berm to provide an additional sediment filtration and settling system for the finer sediment particles that escape the seep berm. Proving the before-mentioned statement is the main objective of the research introduced and described in the thesis.

Since previous work by Sturm et al. (2007), to be discussed later in this thesis, has demonstrated the efficiency of seep berms as BMPs, then the focus of the experimental research undertaken in this thesis is to build on that work by studying the issue of settling and filtration of suspended sediment in flows moving through vegetative strips located directly downstream of the seep berm. Two scenarios will be considered: flows where the vegetation is emergent through the water, and flows where the vegetation is submerged under the water. For the first case, rigid vegetation is used, and for the second case, flexible vegetation is installed. In both cases the performance of the model vegetation is measured in an experimental flume. The experiment is designed to be consistent with runoff rates expected from a properly designed seep berm when it overflows.

The literature review section of the thesis in Chapter 2 is divided into several subsections aimed at defining and discussing the following: First, the process of soil erosion is defined and the problems associated with it are portrayed, introducing commercial and popular best management practices (or BMPs) for erosion control. Second, an introduction to seep berms, and the work of Sturm et al. (2007) with seep berms is discussed. Third, vegetative filters are introduced and a discussion of their use as BMPs follows. Additionally, the discussion covers the settling capacities of vegetation, the velocity profiles in vegetative strips, and the flow resistance of vegetative filters. Fourth and last, various suspended sediment transport modeling methods in vegetative filters are introduced and described.

The research plan in Chapter 4 discusses in detail the engineering concepts behind the design of the experimental apparatus, and how they have been used successfully in previous experiments. The experimental apparatus and its various design features are described also in Chapter 4, including the mechanism used to feed the sediment into the flume, take sediment samples from the flume, and measure velocity profiles in the vegetation strip.

The experimental results are discussed in Chapter 5. The experimental data are used to derive vegetative drag coefficients and to obtain estimates of the trap efficiency of the vegetative filters. The trap efficiencies of the various vegetative filters are shown

to depend on the vegetation density and whether the vegetation is emergent or submerged in the flow. These findings will assist the design engineer in choosing vegetative filters and assessing their performance for use in urban construction sites depending on the storm magnitude, site size, and type of sediment.

Lastly, in Chapter 6, the erosion control design program SEDCAD4 is introduced to show how it can be used to design seep berms through the use of the Sturm and Warner (2007) seep berm design manual. Then a numerical example is given to demonstrate how the seep berm and vegetation filter work in sequence to produce a combined trap efficiency.

## **2. LITERATURE REVIEW**

### **2.1 Defining the Soil Erosion Problem and Commercial Erosion Control**

#### **Methods**

Erosion due to storm water runoff is a long-standing environmental problem caused by land disturbance, especially at urban construction sites. It causes off-site effects, such as clogging of watercourses which results in flooding and water pollution. It also causes landslides (major hillslope erosion) that endanger lives and property (Hudson, 2001). Eroded sediment that is carried downstream can affect the quality of drinking water, increase the costs of water treatment, and reduce reservoir storage capacity through the process of deposition. The reason why reducing sediment in runoff is so important lies in the fact that it is the number one pollutant in U.S. streams, lakes, and estuaries. Most of this sediment is produced by disturbance of soil on construction sites (USEPA, 2002). This type of erosion comprises 70% of the sediment losses in the United States (UM, 2004). Soil losses of over 100,000 tons/sq. mi./yr have been reported throughout the country (Wolman & Schick, 1967). More recent reports put the amount of soil lost in the United States annually at 4 - 4.5 billion tons (Pimentel & Kounang, 1998; UM, 2004). The impacts of this erosion and sediment yield are costly in terms of dollars and aesthetics. Even though many regulations have been formulated to control construction site sediment yield, problems still persist (Kaufman, 2000).

It has been shown that construction sites make up 5% of the total non-point source impacts to surface water in the United States (Morrow et al., 2003). This underlies the importance of dealing with construction site soil erosion. Haan et al. (1994) went further to say that a construction site that has had its soil disturbed and surface cover taken away may increase its sediment yield up to 10,000 times more than a similar undisturbed site. The main reason is that disturbed and eroded sediment boasts a higher percentage of clay as compared to undisturbed sediment. However, local construction sites are not the only sources contributing to construction site soil erosion. As an illustration, in the state of North Carolina (as in many other states), the main source of sediment is highway

construction in addition to housing developments or commercial construction projects (albeit to a lesser extent). Highways stretch in length for many miles, crossing many streams and lakes along the way. These water bodies are very likely to be polluted with heavy amounts of sediment if an ineffective erosion control plan is implemented. Housing projects and commercial construction projects, on the other hand, are concentrated in one area, thus their sediment pollution is localized, although they are still major contributors of sediment to watercourses (Dallaire, 1976).

The process of soil erosion, as theorized by Meyer and Wischmeier (1969), can be divided into two phases. The first phase involves the detachment of the soil particles from the soil mass by raindrop splash impact and/or overland flow. The second phase is the transport of the detached soil particles by either one or both of the two mechanisms at the same time. Morgan (2005) stated that detachment occurs due to raindrop splash impacts and transport results from overland flow due to the limited distance of splash trajectories of raindrops. Overland flow alone may not possess the energy and critical flow shear stress needed to separate soil particles from their surroundings in the field (Rickson, 2006). Hence, when inappropriate land management is involved in construction projects, such as highways and commercial complexes, existing vegetation on the land surface is often stripped from the soil causing it to be more susceptible to erosion by reducing cohesion and erosional strength. The kinetic energy of a rain drop as it hits the soil detaches a larger number of soil particles than it would if a proper vegetation cover was abundant. Surface water runoff also detaches more particles from bare sediment surfaces than from naturally vegetated land (Davies et al., 2006; Kaufman, 2000).

The erosion problem arises when the rate of soil loss exceeds the rate of soil formation. Soil loss can occur immediately after disturbance, whereas soil formation is a process that takes a long time to be accomplished. Soil erosion prevention practices aim to reduce the rate of soil loss by decreasing the runoff velocity and stabilizing the soil using a variety of techniques and products including silt fence which is the most common (Rickson, 2006). Silt fences, usually installed around the perimeter of a construction site on the downslope side, are intended to reduce the sediment concentration in water runoff through forced settling and filtration through the geotextile fabric. Sediment basins are

used at the downstream outlet of a disturbed drainage basin, but they are the sediment trap of last resort and can take up large areas of land in order to be effective (Rickson, 2006).

Other means of combating soil erosion from construction sites include (Rickson, 2006):

- Providing gravel and stabilizing entrances to construction sites to reduce the mud tracking of truck tires.
- Avoiding earthwork during inclement weather.
- Covering of earth stockpiles.
- Grassing or mulching as many exposed areas as possible.
- Applying geotextile mats to exposed areas.

According to Mostaghimi et al. (1994), different kinds of mulches, especially straw, applied as ground covers have been shown to reduce soil erosion by 90%, contributing to a dramatic decrease in the concentration of sediment in storm water runoff. By moderating soil temperature and dissipating rainfall impact, the seed is protected and erosion is reduced, leading to the prevention of the formation of a soil crust and reduction of evaporation losses (Turgeon, 2002).

In comparing different types of ground covers, Turgeon (2002) found that hydraulically applied mulches and excelsior erosion control blankets (ECB) form a thick and uniform cover as opposed to plain straw or even straw ECBs. They promote a good environment for seed germination and grass growth, in addition to the main goal of reducing soil erosion (McLaughlin & Brown, 2006).

Using a rainfall simulator to induce sediment runoff in a controlled environment, McLaughlin and Brown (2006) showed that the presence of ground covers significantly reduced runoff volume, sediment loss, and turbidity in all of their simulated rainfall events. Straw and MBFM (mechanically bonded fiber matrix) provided the most ground

coverage and the biggest reduction of sediment in water runoff, with straw having the advantage in providing a more consistent and uniform ground coverage. McLaughlin and Brown (2006) also observed that the highest turbidities were obtained from the most clayey soil, such as sandy clay loam. Another result showed that ground covers minimized runoff turbidity by a factor of 4 as compared to bare soil.

Most conventional methods of soil erosion, especially geotextile silt fences, fail to trap the fines in the eroded sediment due to inadequate detention time (Barfield et al., 2005). According to a study by Haan et al. (1994), the percentage of clays and fines in eroded sediment is much higher than the percentage found in non-eroded sediment. The fact that conventional BMPs such as silt fences have a low detention time can be translated into the presence of suspended fine particles high in the water column that are discharged easily with the water runoff through the BMP. Moreover, studies have shown that conventional BMP's, specifically silt fences and sediment basins, cannot trap particles smaller than 20 microns (Barfield et al., 2005). Thus, extra measures need to be applied in order to enhance conventional BMP performance.

In BMP performance, the particle settling velocity is one of the most important factors in the determination of efficiency. This settling velocity is dependent on particle size, shape, and density, and the water properties of temperature and viscosity. A California study on three different highway sites showed that 97% of the particle size distribution of sediment in highway runoff was less than 30 micrometers in diameter (Li et al., 2005). Moreover, by using the Stokes' law and assuming spherical shapes for all sediment particles with a uniform density of  $2.6 \text{ g/cm}^3$ , Li et al. (2005) calculated the particle settling velocity. However, the settling column of freshwater showed much lower removal rates than predicted due to non-uniform distributions of densities and deviation from a spherical shape. These two observations show the importance of installing BMPs capable of removing the fine sediment, and that common BMPs, such as silt fences, perform poorly when using only sedimentation for removing small particles (Li et al., 2006). This conclusion was further reinforced by Sturm et al. (2007), in which several runoff tests were conducted in the lab and on a field site using silt fence which produced low trap efficiency rates.

In conclusion, the BMP's mentioned in this sub-section are very common, but they do not provide a high rate of reduction in sediment concentration in water runoff unless they are installed as a system of integrated control measures (Sturm et al., 2007). Unfortunately, they are not always implemented properly. Most importantly, they are costly to the contractor, who may try to minimize their usage to cut costs and save overhead. Consequently, construction sites contribute large sediment loads to small areas in short time periods (Kaufman, 2000). Furthermore, the most common best management practice used today, the geotextile silt fence, has proved to be inefficient when it comes to trapping fines and clays, specifically particles smaller than 20 microns. As mentioned previously, that is due to the fact that silt fences are inadequate in terms of detention time. If the particles were flocculated to produce a larger size with higher settling velocity, or if the suspended sediment detention time could be increased using a combination of two BMPs or more, then BMP trap efficiency could be increased dramatically (Haan et al., 1994).

## **2.2 The Dirt 2 Committee Report**

A viable, efficient, and cost-effective way of dramatically reducing sediment concentration in storm water runoff is the implementation of seep berms, which are defined as erosion and storm water controls shaped as long and narrow soil berms or sedimentation chambers placed at the down-gradient boundaries and peripheries of construction sites. They are a passive dewatering system, and are relatively simple to construct and use. They discharge water slowly after suspended sediment settling has been maximized and the water quality is acceptable. The seep berm idea and concept was implemented in the state of Georgia on a construction site that required very low effluent sediment concentration (Warner et al., 2004). The concept was shown to be successful; thus, furthering the use of this BMP can reap many benefits in cost and efficiency.

The “Dirt 2” committee (formally known as the Erosion and Sedimentation Control Technical Study Committee) in the metro Atlanta area was formed to continue the work of the original Dirt Committee of 1993. It set out to determine whether it would be technically possible to achieve Georgia state recommended water quality standards in a cost effective manner. Dirt 2 was a thorough and meticulous effort to create and implement a system of erosion and sedimentation controls for large construction sites, and evaluate the water quality performance of these measures in a quantitative manner. The committee was established in order to change the old paradigm of “mud just happens”, where erosion prevention and sediment control plans usually came as an afterthought (Dirt 2 Committee, 2001). The committee’s bottom line was “good site management makes good business sense”. Regulations regarding erosion control were difficult to enforce due to a lack of funding of a sufficient number inspectors. What the Dirt 2 Committee showed is that the major consequence of inadequate erosion control is the transfer of the erosion costs to the off-site downstream private owners or cities through loss in property values, increased water treatment costs, and reduced water quality (Dirt 2 Committee, 2001).

The Dirt 2 Committee sought a complete reorientation of erosion control planning and implementation. The new paradigm that the Dirt 2 Committee encouraged can be summarized as follows (Dirt 2 Committee, 2001):

- Integrating the design of erosion prevention and sediment control systems into the total project effort, and eliminate their treatment as a secondary afterthought.
- Insuring that the designed control systems perform up to standard and specified levels.
- Maintenance and monitoring of the systems and adjusting them when needed.
- Minimizing exposed soils on site by clearing it in phases.
- Allowing water to infiltrate the site as much as possible, to reduce runoff.

- Maximizing the use of vegetative buffer zones to halt sediment as much as possible before it leaves the site.
- Making sure that the implementation of the above-listed objectives result in the protection of water quality by minimizing sediment concentrations, and minimizing the transfer of erosion costs to downstream property owners.

Implementing the new paradigm results in a winning situation for all parties involved. The water bodies downstream of a construction site and the ones surrounding it will have little to no mud in them, and their water quality would be protected. No costs due to sediment erosion damages would be transferred to off-site downstream property and business owners and towns. Plus, the credibility of all parties entrusted with maintaining the state's water quality standards would remain intact.

The Dirt 2 Committee, in an effort to deviate from the old paradigm of erosion control, sponsored extensive technical research and policy analysis by nationally renowned experts, and concluded that it was possible to keep Georgia's waters clean while reducing public and private costs associated with development. The main demonstration project used to test and validate that conclusion was the Big Creek Elementary School in Alpharetta, Georgia. It proved that erosion can be controlled much more effectively through a team effort involving owners, developers, builders, regulators and public-interest advocates, putting to rest the old paradigm of "mud just happens" (Dirt 2 Committee, 2001).

On the Big Creek site, Dirt 2 proved that erosion control was not an engineering problem or a significant on-site expense. The new erosion control paradigm was implemented in the Big Creek site through the development of a construction schedule and site plan that incorporated a sediment control system into the project. The sediment control system included seep berms, floating siphons, and sand filters. Construction was sequenced in phases that would minimize the effects of the construction process on sediment erosion through minimizing the amounts of disturbed and erodible soil. Moreover, the construction site's existing vegetation was also used to aid in the erosion control process through holding soil together in certain key areas, and used as an extra

sediment trapping measure. Those techniques were simple to implement and highly effective in eliminating costs to downstream property owners. They were successful in preventing water and measurable sediments in reaching downstream streams during most of the rainfall events that occurred while the construction process was under way. The Dirt 2 Committee proved that seep berms, as a cheap erosion control alternative, are extremely effective when used on areas of five acres and more (Dirt 2 Committee, 2001).

Based on the success of the Big Creek site demonstration project, EPA funded an additional demonstration project for disturbed land sites smaller than five acres because of the expanding scope of water quality control regulations (Sturm et al., 2007). That project will be described in more detail in Chapter 3.

## **2.3 Vegetative Buffer Zones**

### **2.3.1 Purpose, Benefits, and Design**

Vegetative buffer zones are areas of existing natural vegetation such as trees, grass, and shrubs, or they consist of grass sowed downstream of disturbed land areas to slow the velocity of runoff, promote infiltration, and filter excess sediment. They act as physical barriers against the detrimental effects of erosion (from cleared farmlands to construction sites). In addition, vegetative buffer zones help reduce other eroding factors, such as weed seeds, erosive winds, and nutrients (Ocktmann, 2000; Rickson, 2006).

Riparian and aquatic vegetation is recently and quickly becoming integral to river restoration schemes which are an integral component in plans for the preservation of river ecology (Stoesser et al., 2003b). Vegetation plays a major role in reducing the mean flow velocity in open channels, induces turbulence production, and has strong interactions with local hydraulics and sediment dynamics (Kadlec & Knight, 1996; Stoesser et al., 2003a). This causes vegetation to exert a major and powerful influence on the physical and ecological functions of rivers and wetlands, translating into a bigger use for vegetation in open channels as a means to reduce sediment in rivers and streams, and consequently to be used as erosion control measures in urban construction areas (Stoesser

et al., 2003a). The removal of sediment by vegetative buffers, referred to as "filters" in the realm of erosion control, is not performed efficiently through common separation mechanism such as sieving or impaction, but most commonly through slowing down the flow as water passes through the vegetative zone (Kadlec & Knight, 1996).

As previous research and studies have shown, having a vegetative cover on a land surface is extremely effective at combating soil erosion. The plant canopy reduces the raindrop kinetic energy and fall velocity by changing the raindrop size distribution; plant stems cause distortions to overland flow, and reduce the flow velocity and kinetic energy needed to detach and transport soil by imparting form roughness. Plant roots reduce overland flow by promoting water infiltration into the ground, and by counteracting the shearing forces of overland flow (Rickson, 2006). The vegetation slows down the water flow, hence consequently removing sediment from the water by settling (Elliott, 2000).

Even though vegetation can be extremely effective in controlling erosion when it is low-growing with uniform and dense swards, it requires a period of time for establishment that ranges from one to two seasons. Erosion risk is high in the establishment period, and measures such as geotextile blankets can be installed to protect the slope during this time. After the period of establishment, the geotextiles can be used in combination with the vegetation for more effective erosion control purposes (Rickson, 2006).

Due to their efficacy, vegetation covers recently are becoming more popular as landfill caps. The two primary objectives of landfill caps are to minimize water percolation into landfill waste and to prevent surface soil erosion, and vegetative caps meet these two main requirements in a manner that promotes efficacy, viability, and cost-optimization (Licht et al., 2001).

Vegetative covers, however, do have limitations and are not appropriate for some sites that experience excessive rainfall or snowfall. In addition, an area with too little rainfall may not support tree viability; however it might support grass or shrubs. Other environmental stresses, such as drought, excessive winds, ice storms, and high soil

concentrations of salts, toxic metals, metalloids, or organics, can also negatively impact plant health and cover performance (Licht et al., 2001).

Effective vegetative buffer zones share some common properties: regeneration, weed invasion resistance, and resistance of natural disturbances. The vegetation stores a large quantity of seed in the soil it nourishes on, and in the case of a natural disturbance, such as a fire, the seeds sprout and regenerate, spreading foliage on the soil surface and thus helping to suppress weeds and minimize erosion that can occur after the fire. Some plants re-sprout stems, which also promote regeneration. Moreover, the existence of microscopic plants, such as fungi, can result in crust formation on the soil surface which helps to suppress weed growth and provide nutrients for the vegetative zone to regenerate itself. Toxins, released by decaying vegetation into the soil, provide barriers against detrimental weed formation and allow native plants to re-sprout (Ocktmann, 2000).

It has been shown that edge effects affect mostly vegetative zones that are characterized as being thin or small. When attempting to protect or restore vegetative areas, the size and shape of the zone has to be taken into consideration. It has been noted, from previous attempts in the West Australian wheatlands, that large round or square zones possess a better chance at survival than long and narrow zones, thus promoting erosion control with more effect and for longer time durations (Morgan, 2005).

Elliott (2000) conducted flume experiments in which he showed the settling capabilities of vegetation in general, and compared the settling efficiencies of three vegetative types in particular. He ran sediment-laden water with known concentration through the flume, and collected the outflow in a collection tank downstream of the flume. The three types of vegetation modeled were vertical cylindrical rods (made of 6.4 mm PVC representing reed stems or stems of cylindrical vegetation), rigid inclined strips (made of steel strips 0.9 mm thick and 9 mm wide, representing bladed grass bent over by the water flow), and imitation boxwood vines (made of artificial polyethylene plant stems with 40 mm<sup>2</sup> leaves attached to the stem, representing long trailing vegetation such as watercress). At the end of the experiment, settling of sediment had occurred around all three imitation vegetation types, with the vines having significantly the best sediment

removal efficiency, a fact attributed to the larger leaf trapping area. However, at higher velocities, the fact that some areas of the flume were bare around the three simulated vegetation types suggested the re-entrainment of the sediment into the flow again, decreasing sediment removal efficiency. Sediment was still removed though, regardless of the high water velocity (Elliott, 2000).

### **2.3.2 Velocity Profiles of Open Channel Flow in Vegetative Zones**

Studies on flow resistance in vegetated channels have been ongoing since 1926 (Fu Sheng Wu, 2008). The importance of drag coefficient research and evaluation is occurs in several topographic scenarios and locations: open channels, hill slopes, irrigated lands, and wetlands.

The drag that the vegetation exerts upon the flow is influenced by several parameters (a dimensionless analysis is presented in Chapter 5). Those parameters are namely the plant's form and dimensions, the plant population per unit area, the spatially heterogeneous distribution of the vegetation, bed slope, Reynolds number (both flow and stem), and the degree of submergence (Lee et al., 2004).

Studies by Hsieh (1964) showed decreased flow velocity with increasing vegetation density by checking the waves behind wooden cylinders simulating non-submerged vegetation in flowing water. According to Jarvela (2004), vegetation in flow systems or open water bodies are divided into two types: stiff vegetation, which is typically woody plants, and flexible vegetation, which is usually used in the role of protective liner in agricultural waterways. For water flow over vegetation in a river channel, for example, two types of flow are distinguished: flow that submerges vegetation and flow in which the vegetation is unsubmerged (emergent vegetation). According to Stone and Shen (2002), the flow phenomenon increases in complexity in the case where flow depth exceeds the plant height.

### 2.3.2.1 Case 1: Emergent Vegetation Velocity Profile

The presence of vegetation can dramatically affect and alter the bulk, time-averaged, and instantaneous flow characteristics of turbulent open channel flow, in addition to having a major effect on sediment transport. For the same discharge and channel slope, the presence of vegetation induces flow blockage and increased channel resistance, as compared to unvegetated flow through the same channel. This leads to an increase in the flow depth and a decrease in the flow velocity to satisfy momentum conservation and continuity (Neary et al., 2012). Nezu and Nakagawa (1993) defined the increased channel resistance due to vegetation as largescale roughness, quantified as channel bed roughness heights in the flow that completely obstruct the near-wall region of the velocity profile with heights of 10 to 15% of the channel flow depth. Kubrak et al. (2008) and Liu et al. (2008) showed that the presence of vegetation in open channel flow also alters local velocities and turbulence intensities, and their vertical and horizontal distributions. Thus, Neary et al. (2012) advise caution while using popular and commonly used classical resistance relationships that lump flow resistance into a single parameter, like the Manning's equation and the Manning's  $n$  flow resistance coefficient, to qualitatively evaluate the effect of vegetation on bulk flow parameters.

Kouwen and FathiMaghadam (1997) found that for emergent flexible vegetation, momentum is not only absorbed by the projected frontal area of the vegetation, but also by foliage hidden behind the frontal areas. They concluded that the momentum absorbing area is based on total foliage area, hidden and projected, per unit volume, in the direction of the flow. Reynolds stresses and turbulence fluctuations are usually small in emergent vegetation conditions. However for submerged conditions, a horizontal shear layer forms at the top of the plant canopy. Thus, the Reynolds stresses reach a peak at this shear layer and decay upward into the surface flow region above the canopy. This is due to the influence of the shear layer, acting over a certain depth in the surface flow region above the canopy (Stoesser et al., 2003b).

Tanino and Nepf (2009) showed that vegetation density and the stem Reynolds number (Stem  $Re$ ) affect the bulk drag coefficient in vegetated open channel flow by

interfering with the stem wake. Their research also showed the difference between using the depth of the flow  $H$  and the stem diameter  $d$  as two different length scales when calculating the Reynolds number in vegetated open channel flow. In their paper, the flow Reynolds number  $Re$  was shown to be correlated with the level of turbulence of the flow, while Stem  $Re$ , the Reynolds number using the stem diameter as the length scale, was correlated with the drag force resisting the flow. This validates the use of Stem  $Re$  as the main dimensionless parameter in relationships involving drag coefficients in vegetated open channel flow.

Liu et al. (2008) studied open channel flow through emergent vegetation in a flume to observe velocity profile variation over the flow depth. They measured the profiles of time-averaged longitudinal velocity  $u$ , longitudinal turbulence intensity  $u'$ , and vertical turbulence intensity  $w'$ . In their experiments, the stem diameter  $d$  was 0.635 cm with a stem density  $m = 17.66$  stems/sq.ft, channel slope of  $S = 0.003$ , a flow rate of  $Q = 0.155$  cfs, and a flow depth of  $H = 0.21$  ft. They took profile measurements at four downstream locations in line with the stem ( $2d$ ,  $6d$ ,  $10d$ ,  $14d$ ) and two locations in the free stream region halfway between the stems in the unvegetated flow region. They observed a near-bed velocity spike directly downstream of the stem at distance  $2d$  away. The spike was less pronounced further downstream at locations behind the stem. They found that in the vicinity of the flume bed, local fluid behind a dowel was displaced upward away from the bed due to the higher momentum fluid approaching from the free stream region. The velocity differential behind a dowel, as compared to the velocity differential between two dowels, was very large. In addition, they obtained near-uniform velocity profiles above the spike at each vertical measurement location within the stems. They also observed the streamwise variability of the velocity profiles with the smallest velocities occurring in the location directly behind the stem, and increasing for profile locations further downstream of the stem. The highest velocity magnitudes were obtained in the free stream region between stems. The same observation was made for the longitudinal and vertical spatial variability of the turbulence intensity magnitudes but in the opposite direction, where the highest turbulence intensity magnitudes occurred immediately downstream of the stem and decreased in magnitude further downstream,

with the lowest magnitudes occurring in the free stream region. Near-uniform turbulence intensity profiles were observed at all locations.

Fu Sheng Wu (2008) found that the flow discharge capacity of a channel decreases with increasing vegetation density. Nehal et al. (2005) showed that flow roughness and resistance increased with increasing vegetation density. Much experimental work has been done on studying the velocity profile of water in the emergent vegetation. Fu Sheng Wu (2008) studied subcritical water flow through a 12.5 m long by 0.4 m wide flume having a slope of 0.001. Emergent rigid vegetation covered the flume mid-section over a flume length of 4 m. Figure 1 shows the measured velocity profiles. The vegetation densities used were 0, 125, 175, and 225 IP/m<sup>2</sup> (individual plant number/m<sup>2</sup>):

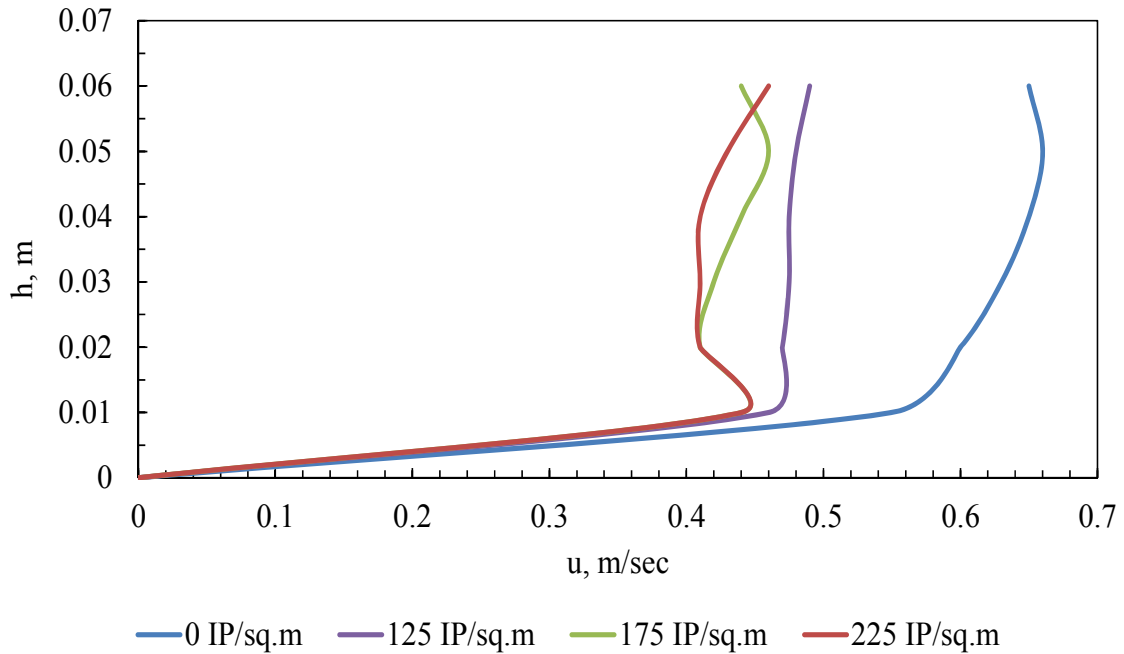


Figure 1: Flow velocity profiles from Fu Sheng Wu (2008)

Fu Sheng Wu (2008) showed clearly that the velocity profile deviates from the logarithmic law due to increased flow resistance caused by the vegetation. The vegetation also reduces the mean velocity. He confirmed experimentally that the drag coefficient increases proportionally to the flow Reynolds number and water depth.

### 2.3.2.2 Case 2: Submerged Flexible Vegetation Velocity Profile

From numerous experimental studies, it is now widely accepted that when flexible roughness (or vegetation) is submerged, then a log velocity profile will exist in the water depth above the vegetation beginning from the top of the vegetation and extending to the water surface (Jarvela, 2005). The Prandtl log law as given by Nikuradse is:

$$\frac{u}{u_*} = \frac{1}{\kappa} \ln \frac{z}{k_s} + C \quad (1)$$

where  $u$  is the point velocity,  $u_*$  is the shear velocity,  $\kappa$  is the von Karman constant,  $k_s$  is the equivalent sand roughness,  $z$  is the vertical coordinate, and  $C$  is the integration constant (Jarvela, 2005). However, Stephan (2002) suggested a different form of the log law for velocity profiles above submerged flexible vegetation as given by:

$$\frac{u}{u_*} = \frac{1}{\kappa} \ln \frac{z - h_{p,m}}{h_{p,m}} + 8.5 \quad (2)$$

As shown in Figure 2,  $h_{p,m}$  is the mean deflected height of the vegetation, while  $h_{p,up}$  and  $h_{p,low}$  (the latter not shown in the figure) are the maximum and minimum deflected heights of vegetation.

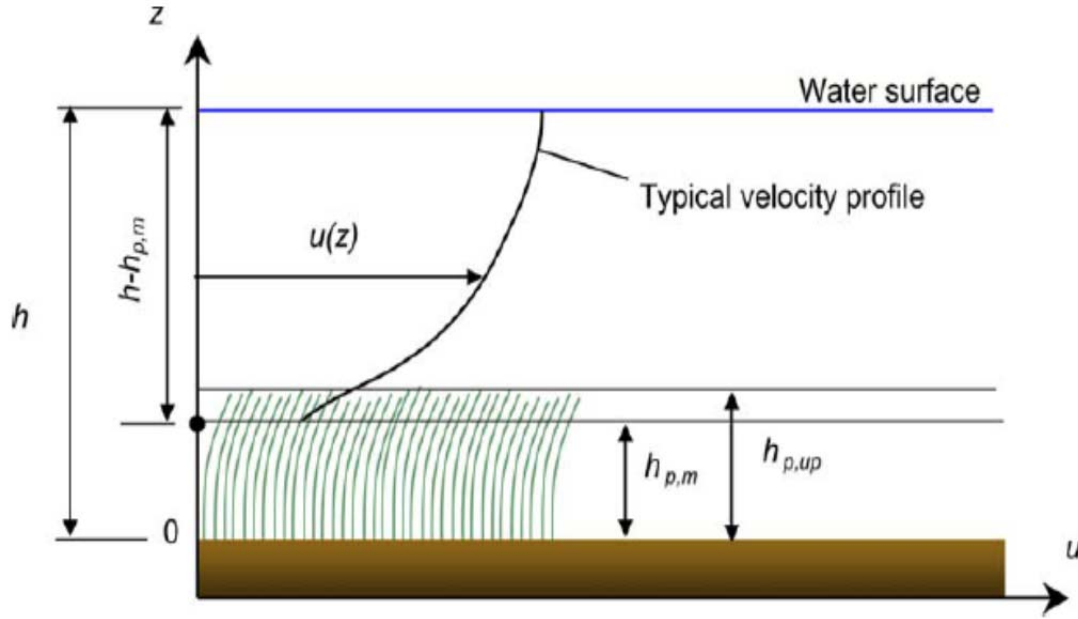


Figure 2: Velocity profile for open channel flow through submerged vegetation (Jarvela, 2005)

By increasing the discharge through a 50 m long by 1.1 m wide flume, with flexible submerged vegetation located only in the middle section of the flume, Jarvela (2005) found that flow velocity increased quickly and assumed a linear profile in the region between the minimum and maximum plant deflected height in each test run. Turbulence intensity ( $u_{rms}$ ) and Reynolds stress  $-\overline{u'w'}$  had maximum values at the maximum deflected plant height location. This varies slightly with results from Tsujimoto et al. (1992), who found that the turbulence intensity and Reynolds stress were at their maximum at  $h_{p,up}$ . Using the Stephan (2002) equation, Jarvela (2005) obtained good results comparing the predicted velocity profiles with the experimentally measured ones. However, Stephan (2002) used a shear velocity estimate that depended on measured Reynolds stresses, whereas Jarvela (2005) argued that better results can be obtained by introducing plant geometry and using the equation of uniform flow to calculate the shear velocity. Stephan (2002) used:

$$U_* = \sqrt{-\overline{(u'w')}}_{\max} \quad (3)$$

while Jarvela (2005) used:

$$U_* = \sqrt{g(h - h_{p,m})S_e} \quad (4)$$

where  $S_e$  is the energy slope.

Using both techniques, Jarvela (2005) concluded that the Stephan (2002) equation characterizes the velocity profile above the submerged flexible grass, but the shear velocity must be calculated by Equation 4 to obtain agreement between measured and predicted velocity profiles. This in turn allows a simplified calculation of shear velocity without complicated measurements of turbulence (Jarvela, 2005).

Experiments run by Stoesser et al. (2003b) on submerged vegetation, with different water depths, in a 10 m long by 0.5 m wide flume showed that the velocity profiles do not follow the logarithmic law profile where the flow was extensively retarded within the plant layer due to the drag forces exerted by the plant canopy. The results were consistent with previous experimental work and research. The turbulence intensity,  $u_{rms}$ , peaked at the top of the rods, which showed similarities with Jarvela (2004), no matter what the water depth in the flume was. Once the water depth relative to the rod height exceeded 1.9 (water depth/rod height = 1.9), then the shape of the turbulence intensity profile in the surface flow region was preserved regardless of the flow depth (Stoesser et al., 2003a). Plots of the Reynolds stress showed that the shear layer penetrated through the rod canopy, reaching its maximum at the top of the rods. High levels of Reynolds stress values were also found in the surface region above the rods, suggesting significant vertical momentum exchange between the plant canopy and surface flow region (Stoesser et al., 2003b).

### **2.3.3 Flow Resistance and Drag in Vegetative Zones in Open Channel Flow**

Recent research on open channel flow resistance has focused on mean flow and turbulence characteristics of open channel flow through vegetation as informed by the

case of atmospheric flow over plant canopies. One of the important factors driving research into the atmospheric flow case has been the need to understand related transport processes in natural environments such as transport of pollutants, heat, and carbon dioxide. For open channel flow through vegetation in streams, estimation of resistance laws is the main topic of interest and research. Most research deals with two cases of vegetation: rigid and flexible (Lopez & Garcia, 1997).

Previous research on the effects of vegetation in open channel flow has shown that vegetation increases flow resistance. The vegetative lining exerts a significant drag force on the open channel flow (Wilson & Horritt, 2002). Vegetation also plays a major role in changing backwater profiles, and as mentioned previously in this chapter, affects sediment deposition and transport (Yen, 2002). More specifically, the type of vegetation plus the density and various vegetative combinations directly affect the flow resistance (Jarvela, 2002a). The conventional approach for estimating open channel flow roughness in vegetative channels has been to lump up all forms of flow resistance, which also includes the flow resistance caused by the vegetative lining, into the Manning's  $n$  coefficient (Jarvela, 2004).

Recent studies have attempted to develop specific formulas designed to calculate the coefficient of flow resistance of vegetative linings in open channels as a separate parameter. A summary of flow resistance relationships for emergent rigid vegetation and flexible submerged vegetation is given next.

#### 2.3.3.1 Case 1: Flow Resistance and Drag in Emergent Rigid Vegetation

The drag force  $F_d$  is defined as:

$$F_d = \frac{1}{2} \rho C_d A_p U^2 \quad (5)$$

where  $C_d$  is the drag coefficient,  $\rho$  is the density,  $A_p$  is the projected area of one or more stems of vegetation (assumed cylindrical), and  $U$  is the bulk velocity of the flow in an open channel. Jarvela (2004) applied the momentum principle on a control volume in an open channel to estimate the flow resistance caused by natural vegetation by equating the drag force to the gravitational force  $F_g$  given by:

$$F_g = \rho g(A_b H)S \quad (6)$$

where  $S$  is the channel slope,  $A_b$  is the bottom area, and  $H$  is the flow depth). By setting  $F_d = F_g$ , and using the known relationship between shear velocity  $u_*$  and Darcy-Weisbach  $f$  for friction, i.e.

$$\frac{U}{u_*} = \left(\frac{8}{f}\right)^{1/2} \quad (7)$$

$$u_* = (gHS)^{1/2} \quad (8)$$

then the friction factor for an emergent vegetative lining in an open channel can be obtained as (Jarvela, 2004):

$$f = 4C_d \frac{A_p}{A_b} \quad (9)$$

Lindner (1982) improvised on the above friction factor equation, and through successful experimental trials, modified it slightly by introducing the plant diameter  $d$ , water depth  $H$ , and the longitudinal and lateral distances ( $a_x$  and  $a_y$ , respectively) between the plant stems, to produce the following equation (Lindner, 1982):

$$f = \frac{4dH}{a_x a_y} C_d \quad (10)$$

The Lindner (1982) equation has been used with good success in a number of experimental studies, most recently the research of Stoesser et al. (2003a) dealing with numerical modeling of a heterogeneously vegetated floodplain. For the drag coefficient

$C_d$  used in the Lindner (1982) equation, Jarvela (2002b) showed it to vary between 1.43 and 1.55 from laboratory experiments, with the German Association for Water and Wastewater (DVWK, 1991) recommending it to be equal to 1.5 for uniform rigid vegetation.

A more recent study by Tanino and Nepf (2008) on mean drag of flow through emergent, rigid cylinders formulated an alternative definition of the mean vegetal drag coefficient  $C_d$ . They related  $C_d$  to two parameters. The first is the stem Reynolds number:

$$\text{Stem Re} = \frac{Ud}{\nu} \quad (11)$$

where  $U$  is the mean channel velocity,  $d$  is the stem diameter, and  $\nu$  is the kinematic viscosity. The second is solid volume fraction:

$$\phi = (m\pi d^2)/4 \quad (12)$$

where  $m$  is the stem density, or stems per unit horizontal area. From laboratory measurements, Tanino and Nepf (2008) suggested the following empirical equation for  $C_d$ :

$$C_d = 2 \left( \frac{\alpha_0}{\text{Stem Re}} + \alpha_1 \right) \quad (13)$$

where  $\alpha_0$  and  $\alpha_1$  are functions of  $\phi$ . Through linear regression, they formulated the following formula for  $\alpha_1$ :

$$\alpha_1 = (0.46 \pm 0.11) + (3.8 \pm 0.5)\phi \quad (14)$$

For  $\alpha_0$ , Tanino and Nepf (2008) plotted it against  $\phi$ , and showed that  $\alpha_0$  increased with increasing  $\phi$  until  $\phi=0.15$ . After that,  $\alpha_0$  remained reasonably constant. Numerically,  $\alpha_0$  increased from 25 to 84 when  $\phi$  changed from 0.091 to 0.15, and remained nearly constant in the range of 84 to 85 for  $\phi$  between 0.15 and 0.35.

Plotting  $C_d$  versus Stem Re for various  $\phi$  values, Tanino and Nepf (2008) observed, on the basis of their experiments, that  $C_d$  monotonically decreases as Stem Re increases. They concluded that for a given value of  $\phi$ , the value of  $C_d$  can be predicted by finding  $\alpha_1$  using Equation 14 and then using interpolation of obtained  $\alpha_0$  values to get the  $\alpha_0$  for the given  $\phi$ . The  $\alpha_0$  values in question can be obtained from Table 2 of Tanino and Nepf (2008).

Jarvela (2004) provided a slightly different approach to the Lindner (1982) equation for the friction factor. He used the DVWK (1991) recommendation for the  $C_d$  value, but determined the projected area  $A_p$  as a function of plant stem height  $L_s$  and total projected area  $A_{p,tot}$ , where  $A_{p,tot}$  is projected area of each stem multiplied by the total number of stems in the vegetative lining of study. The equation is (Jarvela, 2004):

$$A_p(H) = \frac{H}{L_s} A_{p,tot} \quad (15)$$

for  $0 \leq H \leq L_s$ , where  $H$  is the water depth. From Equation 15, Jarvela (2004) described a characteristic plant diameter  $d_r$  as a function of water depth  $H$ , as follows:

$$d_r(h) = \frac{A_p(H)}{H} \quad (16)$$

Finally, Jarvela (2004) inserted his modifications into the Lindner (1982) friction factor formula and obtained:

$$f = \frac{4d_r h}{a_x a_y} C_d \quad (17)$$

Using the above formulations to predict values for  $f$  (friction factor),  $U$  (average velocity), and  $Q$  (flow rate), the predicted values were compared to actual measured values obtained by experimental runs conducted by Jarvela (2004), with excellent correlations between predicted and measured values. The Jarvela (2004) equation is deemed applicable to estimate flow resistance for any canopy density and height, as long as  $H/L_s$  is less than or equal to 1.

Cheng and Nguyen (2011) derived a method that allowed the drag coefficients of emergent vegetation obtained from different experiments to collapse onto the same curve. They implemented principles from porous media flow. This assumption has been used in the past with good results for the drag coefficient (Hoffmann, 2004). They used the pore velocity instead of the bulk velocity:

$$U_v = U/(1 - \phi) \quad (18)$$

where  $U_v$  is the average pore velocity through the vegetation, and  $U$  is the bulk flow velocity. Moreover, the average volume fraction was defined by:

$$\phi = \left(\frac{N}{bL}\right) \left(\frac{\pi d^2}{4}\right) \quad (19)$$

where  $N$  is the number of stems,  $b$  is the vegetation filter width, and  $L$  is the vegetation filter length. They devised a new length parameter, the vegetation-related hydraulic radius  $r_v$ . It is defined as the ratio of the volume occupied by the water to the wetted surface area of all cylinders, hence it is a form of the common hydraulic radius  $R=A/P$ . It should be noted that  $A$  is the cross-sectional area of the flow, and  $P$  is the wetted perimeter. The volume of the control volume would be  $V_{cv}=bLH$  (where  $H$  is the flow depth), and the volume of water only in the control volume would be  $V_w = bLH(1 - \phi)$ . Cheng and Nguyen (2011) highlighted the importance of form drag induced by vegetation over skin friction, thus for the vegetation-induced form drag, they only used the planar frontal area of the stems, which is equal to  $NHd$ , and not the whole wetted surface area. The parameter  $d$  represents the stem diameter. Thus, Equation 20 is obtained after substituting for  $N$  from Equation 19:

$$r_v = \frac{(1-\phi)bHL}{NHd} = \frac{\pi(1-\phi)}{4(\phi)} d \quad (20)$$

Consequently, they defined a vegetation-related Reynolds number, similar to the modified Reynolds number in porous media flow. They used pore velocity and the vegetated hydraulic radius as a length scale.

$$R_v = \left( \frac{U_v r_v}{\nu} \right) \quad (21)$$

Once expanded, the Reynolds number in Equation 21 has the following expression:

$$R_v = Re' = \frac{Re}{\phi} = \frac{\left( \frac{Ud}{\nu} \right)}{\phi} \quad (22)$$

where  $Re$  is the flow Reynolds number,  $\nu$  is the kinematic viscosity, and  $U$  is the flow bulk velocity.  $Re'$  is the modified Reynolds number used in porous media flow, as described by Holdich (2002) and Niven (2002), where the commonly used flow Reynolds number is divided by the solid fraction. The application of porous media concepts to explain the relationship between drag coefficient and modified Reynolds number will be thoroughly investigated in Appendix B. In the case of flow through vegetation filters, the stems are the solids, and the “solids” fraction is designated by  $\phi$ . This modified Reynolds number is called  $Re'$ .

Cheng and Nguyen (2011) used the pore velocity  $U_v$  to define the drag force as

$$F_D = C_{Dv} \rho H d \frac{U_v^2}{2} \quad (23)$$

where they multiplied each side of Equation 23 by  $\phi$ , since only the drag force from the stems only in the control volume was needed. Consequently, they obtained the drag force/unit bed area by dividing both sides of Equation 23 with the cross-sectional area of one stem,  $\pi d^2 / 4$ .

Hence, the drag per unit-bed area is:

$$\frac{4\phi}{\pi d^2} F_D = \frac{4\phi}{\pi d^2} C_{Dv} \rho H d \frac{U_v^2}{2} = C_{Dv} \frac{2\phi \rho H U_v^2}{\pi d} \quad (24)$$

which is equivalent to the streamwise component of the water weight only in the control volume for the condition of uniform flow, and considering the shear forces from the sidewalls and bed to be negligible:

$$C_{Dv} \frac{2\phi\rho H U_v^2}{\pi d} = (1 - \phi)\rho gHS \quad (25)$$

Equation 25 is an expression of (*form drag for all stems/Bed unit surface area*) = (*Streamwise weight component/Bed unit surface area*). Equation 25 can be re-written in terms of  $r_v$  as defined by Equation 20 to obtain:

$$C_{Dv} = 2 \frac{gS r_v}{U_v^2} \quad (26)$$

### 2.3.3.2 Case 2: Flow Resistance and Drag in Submerged Flexible Vegetation

Unlike rigid vegetation, flexibility in submerged vegetation plays an important role in determining flow resistance. Most researchers recommend using a logarithmic law for the vertical profile of mean velocities above the submerged plant canopy. This recommendation implicitly assumes the existence of an equilibrium layer where turbulence production is balanced by dissipation (Lopez & Garcia, 1997).

Kouwen and Li (1980) studied the relation between the deflected height of the vegetation to the drag and drag coefficient with good results. A recent study by Wilson and Horritt (2002) equated the average boundary shear stress  $\tau_o$  to the average drag force  $F_D$  of the plants per unit plan area, neglecting the gravitational force:

$$\tau_o = F_D/bL \quad (27)$$

where  $b$  is width of the flume and  $L$  is the control volume length. The drag force is described by Equation 5, in which  $C_d$  is the vegetation drag coefficient, and  $U$  is the bulk velocity in the open channel, and  $A$  is the projected area or momentum-absorbing area of the vegetation, and  $\rho$  is the water density. The factors that mainly affect the vegetative drag coefficient are the vegetation's shape, dimensions, surface roughness and Reynolds number (Wilson & Horritt, 2002). The characteristic length term in the Reynolds number in this case is defined by using the blade thickness or diameter  $d$ , and is described previously by Equation 11.

Kouwen and Li (1980) cited a porosity parameter,  $A/a$ , where  $a$  is the cross-sectional flow area. Figure 3 shows the dimensions used.  $N_{grass}$  is the average grass blade number per channel width  $b$ :

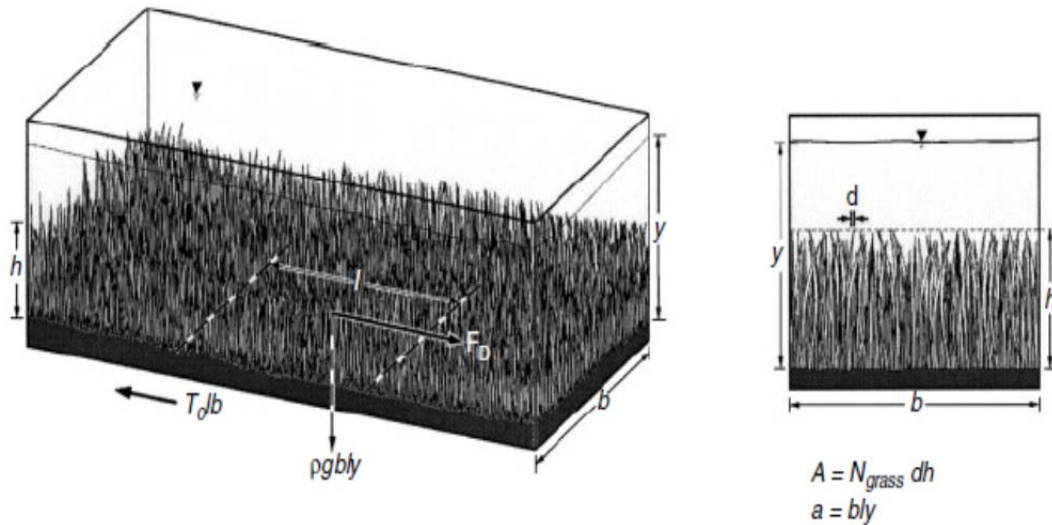


Figure 3 : Schematic showing the control volume and parameters used by Wilson and Horritt (2002)

Wilson and Horritt (2002) then converted shear and drag forces into resistance coefficients in terms of with the Darcy-Weisbach  $f$ :

$$f = 8 \frac{\tau_0}{\rho U^2} \quad (28)$$

Inserting the drag and porosity parameter, Equation 28 becomes:

$$f = 4C_d \frac{A}{a} \quad (29)$$

Translating  $f$  into Manning's  $n$ , the following is obtained (Wilson & Horritt, 2002):

$$n = \left( \frac{1}{2g} R^{1/3} C_d \frac{A}{a} \right)^{1/2} \quad (30)$$

Wilson and Horritt (2002) ran laboratory flume experiments to relate relative submergence ( $y/h$ , see Figure 3) to Darcy-Weisbach's  $f$ , and Manning's  $n$ . They showed that the hydraulic resistance of grass ( $f$  or  $n$ ) is at its maximum when the flow depth is level comparable to the submerged grass height. As the flow depth increases to more than the height of grass, the hydraulic resistance decreases until it levels out and becomes constant when the flow depth reaches twice the height of grass (Wilson & Horritt, 2002). This observation is consistent with previous research results (Kouwen et al., 1969); it is attributed to the exposure of grass when the flow depth is small. The porosity parameter  $A/a$  decreases as the flow depth increases,  $a$  increases and Manning's  $n$  and Darcy-Weisbach's  $f$  decrease.

A more practical approach to calculating the drag coefficient of submerged flexible vegetation has been suggested by Wilson (2007), who applied the approach of Wu et al. (1999) on rigid submerged vegetation and modified it for flexible submerged vegetation. Wu et al. (1999) considered four forces on a control volume in equilibrium and solved for the drag coefficient  $C_d$ . Above the vegetated layer, they considered the shear force at the vegetation water interface to balance the gravitational force of the water body above the vegetation. The resulting shear force is given by:

$$F_\tau = \rho g (bHL)S \quad (31)$$

where  $b$  = channel width,  $H$  = water height above vegetation layer,  $L$  = length of vegetative layer control volume, and  $S$  = channel bed slope. Through the vegetation, they considered the drag force caused by the vegetation resisting both the gravitational force of water through the vegetation and the vegetation-water interface shear force. The drag force is defined as (Wu et al., 1999):

$$F_d = C_d (\lambda T b L) \frac{\rho U^2}{2} \quad (32)$$

where  $T$  is the vegetation height as defined by Wu et al. (1999),  $U$  is the mean channel velocity, and  $\lambda$  is a vegetal area coefficient corresponding to the area fraction per channel unit length. Hence,  $\lambda T b L$  symbolizes the total frontal vegetation area in channel reach  $L$ . Wu et al. (1999) assumed the vegetation to be stiff; hence  $T$  was constant. The drag coefficient, after performing equilibrium, becomes (Wu et al., 1999):

$$C_d' = \left( \frac{D}{T} \right) \left( \frac{2gS}{U^2} \right) \quad (33)$$

where  $C_d' = \lambda C_d$ , and  $D$  is the depth of flow. Wu et al. (1999) also derived a relationship between vegetal drag coefficient and Manning's  $n$ , for rigid submerged vegetation.

$$n = \left( \frac{D^{1/6} T^{1/2}}{\sqrt{2g}} \right) \sqrt{C_d'} \quad (34)$$

Wilson (2007) used experimental data of her own, plus data from Carollo et al. (2002) and Jarvela (2005), to plot  $\frac{h_{deflected}}{h}$  vs  $U$ , where  $h_{deflected}$  is the deflected vegetation height,  $h$  is the original vegetation height, and  $U$  is the mean flow velocity. The Wilson (2007) empirical equation is:

$$\frac{h_{deflected}}{h} = (1.44U + 1) \quad (35)$$

Wilson (2007) used  $h_{deflected}$  instead of the vegetation thickness as the characteristic length to calculate the vegetation Reynolds number, citing flexibility as the reason to use deflected height, whereas the vegetation thickness would be useful in the Wu et al. (1999) study of rigid submerged vegetation. Similar reasons were cited for including  $h_{deflected}$  instead of the original vegetation height (as Wu et al. (1999) did by using  $T$ , the original height of vegetation) while calculating the vegetal drag coefficient  $C_d'$ , which was described by Wilson (2007) as:

$$C_d' = \left( \frac{y_n}{h_{deflected}} \right) \left( \frac{2gS}{U^2} \right) \quad (36)$$

where  $y_n$  is the water depth. An increasing Reynolds number means a decreasing vegetal drag coefficient, and for a given Reynolds number higher vegetal drag coefficient values are obtained with higher vegetation heights. More submergence or higher water depth means a decrease in the vegetal drag coefficient (Wilson, 2007).

## 2.3.4 Sediment modeling

### 2.3.4.1 Suspended Sediment Transport Modeling: Theory

In steady open channel flow, vertical turbulent velocity fluctuations move suspended sediment particles upward, keeping them in suspension (Sturm, 2001). The mean turbulent flux of sediment per unit area is designated by  $\overline{w'c'}$ , where  $w'$  is the vertical velocity fluctuation due to turbulence, and  $c'$  is the turbulent sediment concentration fluctuation. Assuming a system in equilibrium, the positive upward flux  $\overline{w'c'}$  is balanced by gravitational settling of the sediment from the flow. The downward flux is designated by  $w_f C$  per unit area, where  $w_f$  is the fall velocity of the sediment particles and  $C$  designates, at a given point on the vertical, the time-averaged concentration of sediment.

Assuming a Fickian diffusive process for the turbulent flux, and designating  $z$  as the height in the vertical direction, the equation governing the vertical distribution of suspended sediment in equilibrium sediment transport is given by (Sturm, 2001):

$$\varepsilon_s \frac{dC}{dz} + w_f C = 0 \quad (37)$$

where  $\varepsilon_s$  designates the turbulent sediment diffusion coefficient.

The value of  $\varepsilon_s$  is not a constant, and can be related to the parameter  $\mathcal{E}$ , which is the turbulent eddy viscosity, by the equation (Sturm, 2001):

$$\varepsilon_s = \beta \mathcal{E} \quad (38)$$

where  $\beta$  is a proportionality constant. An expression for  $\beta$  can be found in Cellino and Graf (2002):

$$\beta = \frac{3}{10} + \frac{3w_f}{4u_*} \quad (39)$$

where  $u_*$  is the shear velocity. The turbulent eddy viscosity  $\varepsilon$  is related to the shear stress at a point and the longitudinal velocity by:

$$\tau = \rho\varepsilon \frac{du}{dz} \quad (40)$$

and  $\rho$  designates the water density. Since the flow is steady and uniform, the vertical shear distribution is linear, given by:

$$\tau = \tau_o \frac{(y_o - z)}{y_o} \quad (41)$$

where  $\tau_o$  is the bed shear stress and  $y_o$  is the depth of uniform flow. Using the Pandtl-von Karman velocity law, then:

$$\frac{du}{dz} = \frac{u_*}{\kappa z} \quad (42)$$

where  $u_*$  is the shear velocity and  $\kappa$  is the von Karman constant usually taken to be 0.4 for clear fluids (Sturm, 2001). Combining these equations, the expression for the turbulent sediment diffusion coefficient from Graf (1971) is :

$$\varepsilon_s = \beta\kappa u_* \frac{z}{y_o} (y_o - z) \quad (43)$$

Finally, to obtain the concentration  $C$  at a point on the vertical, the equation for  $\varepsilon_s$  can be substituted into Equation 37 and integrated to give the Rouse (1937) equation for vertical suspended sediment concentration with respect to distance from the bed,  $z$  :

$$\frac{C}{C_a} = \left[ \frac{(y_o - z)}{z} \frac{a}{(y_o - a)} \right]^{R_0} \quad (44)$$

in which  $C_a$  is the reference concentration at the distance  $z = a$  above the channel bed. The parameter  $a$  is taken as 5% of the normal depth.  $R_0$  is defined as the Rouse number with the expression  $R_0 = \frac{w_f}{\beta \kappa u_*}$ .

A smaller value of  $R_0$  corresponds to finer sediments in the flow and a more uniform concentration distribution, while a higher Rouse number value means coarser sediments in the flow with the bulk of the suspended sediment located in the lower portion of the flow. According to Sturm (2001), the Rouse equation has been tried and compared favorably against existing data sets of measured suspended sediment concentrations from rivers and flumes in equilibrium sediment transport. However, net settling is expected in flow through vegetative filters at the channel bed, so the Rouse equation does not directly apply to this case unless the sediment concentration is unchanging in the flow direction.

#### 2.3.4.2 Suspended Sediment Transport Modeling Through Vegetation

The Rouse equation does not take into account the presence of vegetation, whether emergent or submerged, in the flow. Vegetation plays a significant role in filtering suspended sediment particles and causing them to settle out of the flow. The role of vegetation in enhancing settling is explored in the next sections.

One approach for modeling suspended sediment transport concentration in uniform flows with submerged vegetation is to adopt a two-layer model approach. The first layer is taken from the channel bed to the top of the vegetation, and the second layer is defined from the top of the vegetation to the free water surface. Figure 4 depicts the parameters used in the analysis. Assuming the flow velocity in the vegetation layer to be uniform (Yang & Choi, 2010), and also assuming the flow velocity in the upper layer

above the vegetation to follow a logarithmic profile dependent on vegetation density, then by applying a force balance to the vegetation layer, the result was:

$$\rho g h_1 S + \tau_i = F_D + \tau_b \quad (45)$$

where  $h_1$  is the vegetation height (and corresponds to deflected vegetation height if the vegetation is flexible),  $S$  is the channel slope,  $\tau_i$  is the two-layer interfacial shear stress,  $\tau_b$  is the bed shear stress, and  $F_D$  is the drag force from the vegetation as given by (Yang & Choi, 2010):

$$F_D = 0.5aC_dU_1^2h_1 \quad (46)$$

where  $a$  is the vegetation density,  $U_1$  is the mean velocity in the vegetated layer,  $C_d$  is the vegetation drag coefficient, and  $h_1$  is the vegetation height. For the upper flow layer, the force balance equation was taken to be:

$$\rho g(H-h_1)S = \tau_i \quad (47)$$

The interfacial shear stress plays two different roles between the vegetation and upper flow layer. In the vegetation layer, it accelerates the flow, while in the upper flow layer, it balances gravity and reduces mean velocity (Yang & Choi, 2010). Figure 4 below illustrates that concept.

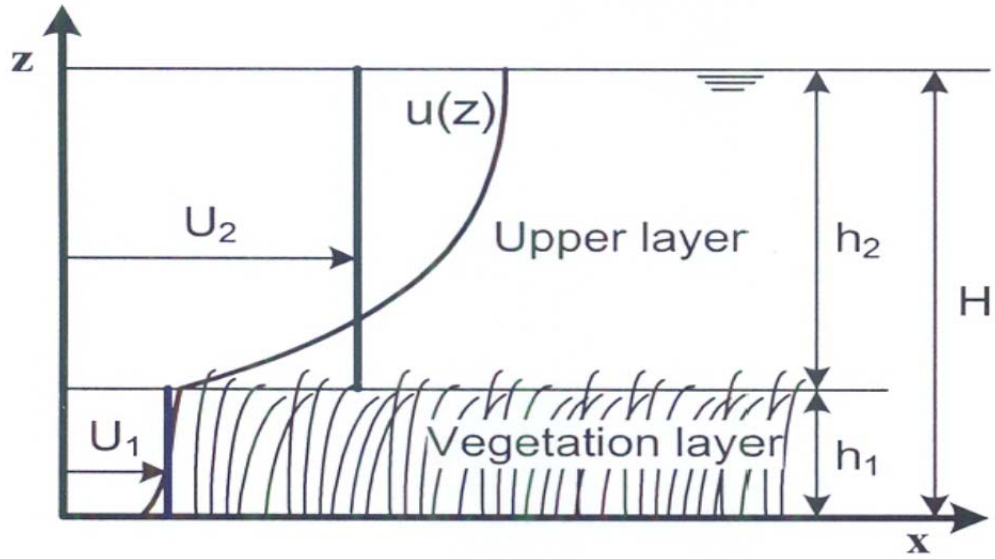


Figure 4: Illustration describing the parameters used by Yang and Choi (2010) to obtain the vertical suspended sediment concentration across water depth

According to several experimental studies, flow in the vegetative layers can be assumed to be uniform at a specific flow rate. This has been verified by Kubrak et al. (2008) and Yang and Choi (2010); hence, a uniform expression can be obtained for the mean velocity in the vegetation by using Equations 45 to 47 for vegetation layer force balance and ignoring the bottom shear stress. The resulting equation for  $U_1$  is expressed by:

$$U_1 = \sqrt{\frac{2gHS}{aC_d h_1}} \quad (48)$$

For the upper flow layer, the log-law velocity profile is assumed by Yang and Choi (2010):

$$\frac{u_2(z)}{u_*} = \frac{1}{\kappa} \ln\left(\frac{z}{h_1}\right) + \frac{U_1}{u_*} \quad (49)$$

where  $u_*$  is the interfacial shear velocity atop of the vegetation layer at  $z = h_1$ , and equal to  $(gh_2S)^{1/2}$ .

Equation 49 is modified to include  $C_u$ , which is a vegetation density coefficient. Hence the equation becomes:

$$\frac{u_2(z)}{U_1} = \frac{u_*}{U_1} \frac{C_u}{\kappa} \ln\left(\frac{z}{h_1}\right) + 1 \quad (50)$$

where  $C_u = 1$  if  $a < 5 \text{ m}^{-1}$  and  $C_u = 2$  if  $a > 5 \text{ m}^{-1}$  (Yang & Choi, 2010). The mean velocity expression for the upper flow layer becomes:

$$U_2 = \frac{1}{h_2} \int_{h_1}^h u_2(z) dz = \frac{C_u u_*}{\kappa} \left[ \frac{H}{h_2} \ln\left(\frac{H}{h_1}\right) - 1 \right] + U_1 \quad (51)$$

where  $h_2 = H - h_1$ , the upper flow layer height. The vertical direction is denoted by  $z$ .

Equations 48 and 51 were tested against several existing measured data sets, such as Stoesser et al. (2003b), and delivered good comparison results, reinforcing the validity of assuming a uniform flow velocity profile in the vegetated layer (Yang & Choi, 2010).

Consequently, in order to obtain a suspended sediment concentration model, the expression for the turbulent eddy viscosity,  $v_t$ , needs to be obtained for both layers. The expression for eddy viscosity is:

$$v_t = \frac{-\overline{uw}}{\frac{\partial u}{\partial z}} \quad (52)$$

where  $-\overline{uw}$  is the Reynolds shear stress. Yang and Choi (2010) reported that the Reynolds shear stress in the upper layer can be successfully approximated by a linear function, where the Reynolds shear stress varies between zero at the water surface to a maximum at  $h_1$ . This assumption also results in the eddy viscosity varying between zero at the free surface to a maximum at  $h_1$  in the upper layer, albeit in a parabolic manner. In the vegetation layer, the assumption of a uniform velocity profile does not allow the use

of Equation 52. Thus, Yang and Choi (2010) assumed a linear relationship for eddy viscosity in the vegetation layer, where  $\nu_t$  varies from a maximum at  $h_1$  to zero at the channel bed. The Yang and Choi (2010) assumption for Reynolds stress variation in both the upper and vegetation layers was also observed in Stoesser et al. (2003b), where experimental trials on submerged vegetation yielded Reynolds stress values with a maximum at the top of the deflected vegetation, and zero at the free surface and channel bed. Thus, the eddy viscosity expressions derived for the upper flow layer and lower vegetation layer, respectively, are:

$$\nu_t = z \frac{u_* \kappa}{C_u} \left( \frac{H-z}{h_2} \right) \quad (53)$$

$$\nu_t = z \frac{u_* \kappa}{C_u} \quad (54)$$

Yang and Choi (2010) validated Equations 53 and 54 by comparing existing experimental data sets and numerical simulations using the Reynolds stress turbulence model from Choi and Kang (2004). The results were compatible, validating the use of both equations. The eddy viscosity expressions for both layers were obtained by incorporating the log-law turbulent velocity distribution (Nezu & Nakagawa, 1993; Nezu & Rodi, 1986).

To obtain the vertical distribution of suspended sediment equation, Yang and Choi (2010) assumed Fickian diffusivity and the flux balance equation as given previously by Equation 37 was used. Assuming eddy diffusivity to be equal to eddy viscosity, i.e.  $\nu_t = \varepsilon_s$ , and using the eddy viscosity Equations 53 and 54, the following expressions for distribution of suspended sediment concentration for both upper and vegetation layers, respectively, are as follows:

$$\frac{C}{C_b} = \left( \frac{z_b}{h_1} \right)^{Z_1} \left( \frac{H-z}{z} \frac{h_1}{h_2} \right)^{Z_2} \quad (55)$$

$$\frac{C}{C_b} = \left( \frac{z_b}{z} \right)^{Z_1} \quad (56)$$

Similarities between the two-layer model and the Rouse model are very obvious. In the two-layer model,  $C_b$  is the concentration at  $z = z_b$ , and  $z_b = 0.05 * \text{flow depth}$ . The parameters  $Z_1$  and  $Z_2$  are a modified version of the Rouse parameter  $R_0$ , to account for the presence of the vegetation layer. Their definitions are (Yang & Choi, 2010):

$$Z_1 = \frac{w_f}{\kappa u_*} \quad (57)$$

$$Z_2 = \frac{w_f h_2}{H \kappa u_*} \quad (58)$$

The proposed two-layer model was tested against several existing experimental cases with suspended sediment concentration data sets, taken in open channels with submerged vegetation. The comparison yielded acceptable results, validating the two-layer model as a good approximation of the vertical suspended sediment concentration distribution in open channel flows with submerged vegetation (Yang & Choi, 2010).

However, the absence of streamwise gradients in the concentration distribution imply that Yang and Choi (2010) assumed equilibrium suspended sediment transport through the vegetative filter with no settling. James and Sharpe (2006) modeled suspended sediment transport through emergent vegetation by arguing that the effects of vegetation be incorporated by introducing them into an expression for sediment eddy diffusivity.

The advection-diffusion equation can be stated as:

$$\frac{\partial C}{\partial t} = -u_i \frac{\partial C}{\partial x_i} + \frac{\partial}{\partial x_i} \left( \varepsilon_i \frac{\partial C}{\partial x_i} \right) \quad (59)$$

where  $t$  is time,  $u_i$  corresponds to velocity components in the  $x_i$  directions, and  $\varepsilon_i$  corresponds to the sediment diffusivities in the corresponding directions. In their model, the vertical direction was referred to as  $y$ . The fall velocity  $w_f$  was equal to  $-u_y$ , and

longitudinal sediment diffusion was assumed to be negligible compared to convection ( $\varepsilon_x = 0$ ), simplifying the steady-state advection-diffusion equation to:

$$0 = -u_x \frac{\partial C}{\partial x} + w_f \frac{\partial C}{\partial y} + \frac{\partial}{\partial y} \left( \varepsilon_s \frac{\partial C}{\partial y} \right) \quad (60)$$

The boundary condition at the free water surface states that there is no transport flux across the surface or bed, so the boundary condition is for the surface is given by:

$$\varepsilon_s \frac{\partial C}{\partial y} + w_f C = 0 \quad (61)$$

whereas at the bed, the boundary condition is given by:

$$\varepsilon_s \frac{\partial C}{\partial y} + (1 - p)w_f C = 0 \quad (62)$$

where  $p$  denotes the probability where a particle reaching the bed will remain permanently deposited and not re-suspended into the flow (James & Sharpe, 2006). James and Sharpe (2006) covered their experimental flume bed with fully absorbing filament, rendering the value of  $p = 1$ . They ran several experimental trials with varying densities of emergent vegetation and quantified the sediment deposited at designated intervals along the flume bed after each trial, then plotted the deposit distributions along the flume length.

Direct estimates for vertical diffusivity were not available since James and Sharpe (2006) did not measure for vertical sediment diffusivity within the stems in their experiments. Instead, they used Equation 43 to express vertical sediment diffusivity  $\varepsilon_s$ , and Equation 39 to express the  $\beta$  parameter in Equation 43. Since Equations 39 and 43 are used for suspended sediment transport in unobstructed flow. James and Sharpe (2006) attempted to compensate for that fact by adjusting the diffusivity to achieve satisfactory agreement between their measured deposit distributions and the simulated ones obtained from Equations 60 to 62. Preliminary simulations using uniform and parabolic diffusivity distributions showed that the results were insensitive to diffusivity distribution; hence

James and Sharpe (2006) adopted a uniform diffusivity distribution for all their subsequent simulations. The vertical diffusivity values obtained from the data fitting were an order of magnitude less than the values of vertical diffusivity from Equation 43.

Based on the satisfactory performance of the diffusion-convection model, James and Sharpe (2006) suggested its use for describing deposition patterns if reliable vertical diffusivity values were available. Also, they recommended further research be done on sediment settling in near-bed conditions to obtain a better value for the deposition probability  $p$  and enhance the diffusion-convection model performance.

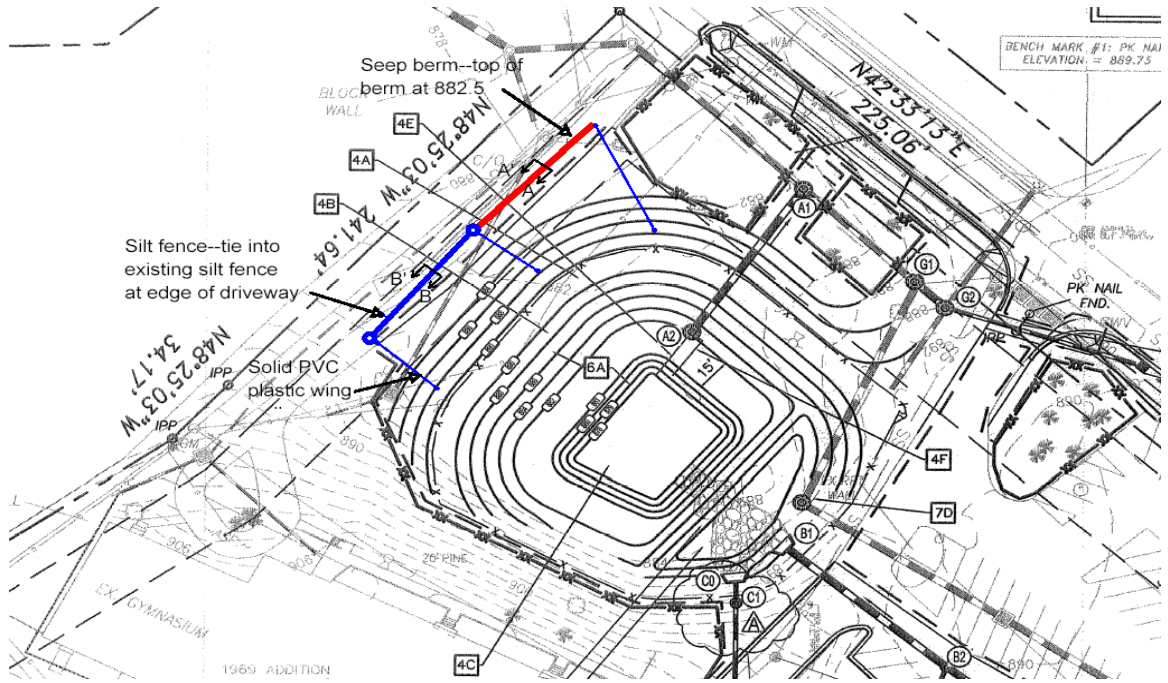
### **3. SEEP BERMS: EXPERIMENTAL WORK AND RESULTS**

#### **3.1 Project Description**

The first step in the thesis research was to test the efficiency of seep berms as a viable erosion control alternative to traditional measures. A field project that was a joint collaboration with the University of Kentucky was introduced with the objective of comparing the treatment efficiency and cost effectiveness of seep berms side by side with silt fences. The joint project was comprised of two site demonstrations in the metro Atlanta area, with the first implemented in the summer of 2006, and the second in the summer of 2007. Both site demonstrations were applied to disturbed areas of five acres or less, which usually is the typical area for the small residential and commercial construction sites that characterize the Georgia Piedmont river basins and metro Atlanta areas (Sturm et al., 2007). The results of the two site demonstration projects showed that the sediment contribution to receiving waters of small construction sites can be significantly reduced through the correct implementation of seep berms around the downslope side of a construction site, and that they perform better than silt fences.

#### **3.2 Description of Field Sites**

The first field site was an environmental park site in Alpharetta in the Big Creek drainage basin (Summer 2006), and the second was the Immaculate Heart of Mary (IHM) church site in Atlanta in the Peachtree Creek drainage basin (Summer 2007). Figure 5 presents both overall site layouts to illustrate where the demonstration projects were within the construction project site:



Those two specific sites were chosen due to the fact that both Big Creek and Peachtree Creek are major tributaries to the Chattahoochee River, and major contributors to the sediment load in the Chattahoochee (Sturm et al., 2007). Big Creek is the drainage basin for the new and developing urban areas north of the city of Atlanta, while Peachtree Creek is the drainage basin for old suburban Atlanta neighborhoods in Dekalb County. These old neighborhoods are specifically undergoing a resurgence, with in-fill housing and new commercial development replacing older residential properties (Sturm et al., 2007). Both field demonstrations placed seep berms side-by-side with silt fences on those two small construction sites.

At the Alpharetta site, the seep berm and silt fence each had drainage areas that were approximately 0.75 acres. The IHM erosion control demonstration site was located at the outer slope of the permanent sedimentation pond of the IHM construction site. The drainage areas of the seep berm and silt fence were only about 0.06 acres each. However, the small drainage area size for each of the two IHM erosion control measures was adequately compensated by its steep runoff area, which produced high yields of sediment. Through monitoring and comparing the performances of seep berms and silt fences in reducing suspended sediment concentrations in storm water runoff, the objective of the study was to demonstrate that seep berms are an effective substitute to silt fences on construction sites. Moreover, the data accumulated from the demonstration projects can be used to develop design guidelines that would encourage the use of seep berms as a viable erosion control measure (Sturm et al., 2007).

The Alpharetta and IHM construction sites were located in areas characterized by woods, providing dense vegetation. However, the sites themselves were stripped of all vegetation prior to the commencement of the construction projects. The stripping of the surface cover disturbs the native soil and increases sediment erodibility and yield. Thus, the seep berm-silt fence demonstrations were installed on a bare ground cover. The grain distribution size plots for the soil on both sites are given in Figure 6. The  $d_{50}$  of the Alpharetta soil is 0.28 mm, with a geometric standard deviation of  $\sigma_g = 1.14$ , while the  $d_{50}$  of the IHM soil is 0.19 mm, with a geometric standard deviation of  $\sigma_g = 1.21$ .

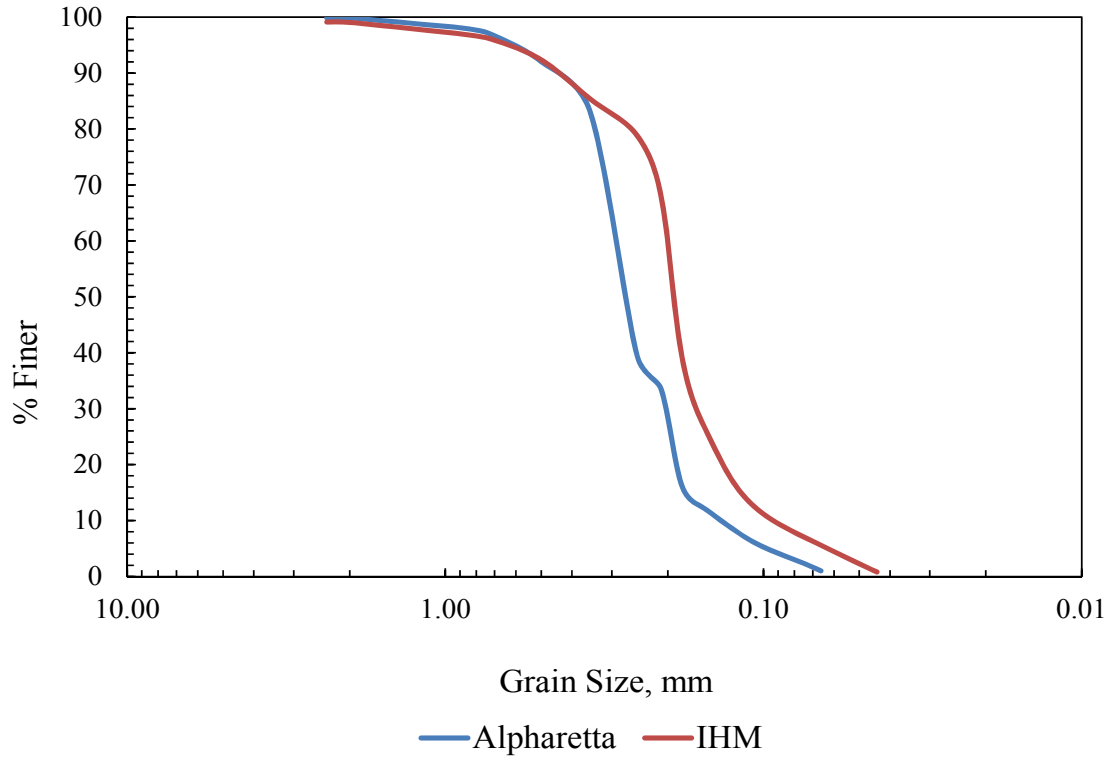


Figure 6: GSD plots for both Alpharetta and IHM sites

### **3.3 Project Methodology**

The treatment efficiency and viability of seep berms as an erosion control when compared to silt fences were studied by performing a direct comparison between the two in terms of turbidity and concentration of total suspended solids (TSS) in the outflow using a split watershed approach. As mentioned earlier in Section 3.1, the two erosion control measures were placed side by side in parallel on the downslope side of the construction site, and their performance was evaluated in terms of successful sediment trapping through a sequence of rainfall events. Outflow data from overland flow on water quality was collected for comparison between the two BMPs.

Outflow from the silt fence for both demonstration sites was collected in a ditch lined with plastic sheets. A trapezoidal flume was used to measure the runoff rate at the

Alpharetta site and a sharp-crested weir was used on the IHM site. Photos of these details are presented in Figure 7.



(a)

(b)

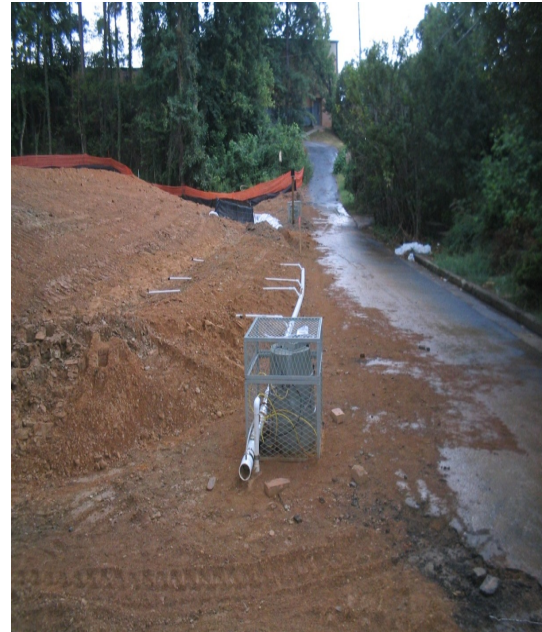
Figure 7: (a) Photo of the Alpharetta silt fence, with the white trapezoidal flume at the end of the silt fence perimeter to collect and direct the silt fence outflow; (b) Photo of the IHM silt fence layout and collection channel, outflow weir, precipitation gage (on wood post), and ISCO sampler in steel cage (Sturm et al., 2007)

The cross section of the Alpharetta seep berm has a height of 2.5 feet, a 2:1 slope, and nine one-in. PVC pipes embedded at 0.5 feet from the top of the berm. The nine one-in. pipes all are attached to one three-in. PVC collecting pipe, which poured into the ISCO sampler. The cross section of the IHM seep berm has a height of 1.5 feet, a 2:1 slope, and four one-in. PVC pipes embedded at 0.75 feet from the top of the berm. The four one-in. pipes all are attached to one three-in. PVC collecting pipe, which poured into the ISCO sampler. The IHM seep berm is smaller than the Alpharetta one due to space limitations, but effective nonetheless (Sturm et al., 2007). The seep berm layout for both

demonstration sites is presented in the photos of Figure 8. Figure 9 presents schematics showing the cross-section of the seep berms on both demonstration sites.



(a)



(b)

Figure 8: (a) Photo of the Alpharetta seep berm layout and ISCO sampler; (b) Photo of the IHM seep berm layout. The one-in. overflow pipes, three-in. collection pipe, discharge flow meter, and ISCO samplers in steel cages are shown in both photos (Sturm et al., 2007)

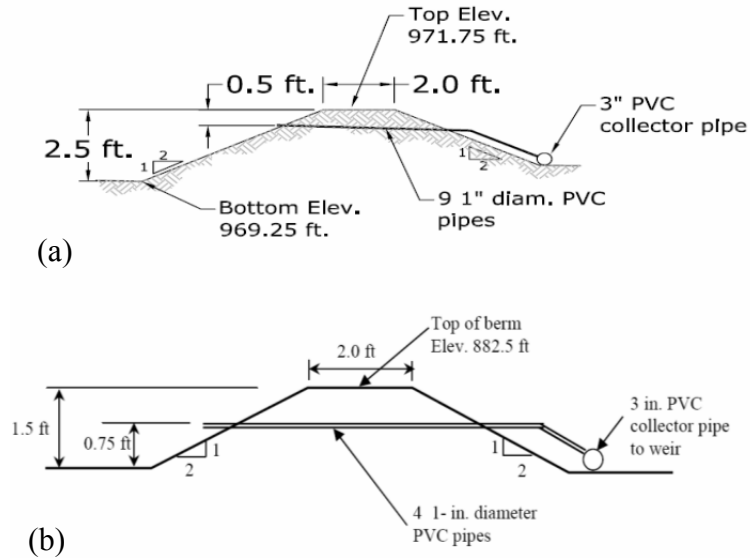


Figure 9: (a) The cross section of the Alpharetta seep berm (not to scale); (b) The cross section of the IHM seep berm (not to scale) (Sturm et al., 2007)

The upstream depths at the flume and the weir were measured and converted into volumetric flow rates through the use of Mini-Troll pressure transducers that measured depths at 0.06 ft increments. The transducers measured depths at one-minute intervals and used calibration relationships to transform the measured depths into volumetric flow rates. Outflow from the silt fences in both sites was collected through the use of one-in. diameter PVC pipes that were placed through the seep berm at a height of 2 feet above the channel bottom of the seep berm in the Alpharetta site, and 0.75 feet for the IHM site. The one-in. pipes channeled the outflow into a three-in. diameter PVC collection pipe with a free discharge. The collection pipe had a small weir embedded at its invert near the outfall. Pressure transducers were also used to measure depth increments at that location and to convert the depth increments into volumetric flow rates (Sturm et al., 2007). Figure 8 can be referred to again for photographs of the overflow pipes and collection pipe.

Programmable samplers (ISCO 3700) with liquid-level actuators were used to collect outflow water samples in order to test the outflow suspended sediment concentration from both erosion control measures at each of the field sites. The ISCO samplers pumped outflow water samples at five minute intervals for the first 45 minutes of a storm, then at ten minute intervals. Suspended sediment concentration from the pumped samples was determined in the lab and reported in turbidity units (NTU) and total suspended solids (TSS, mg/l).

Rainfall events at both demonstration site locations were measured using a tipping bucket rain gage connected to a rainfall event data logger. The rain gage was mounted on a post in the vicinity of both erosion control measures at both demonstration sites.

### **3.4 Project Results**

#### **3.4.1 Alpharetta Site**

For the Alpharetta site, all of the five precipitation events logged, with the exception of the 8/12/2006 event, were brief thunderstorms with durations of approximately 30 minutes, and with total depths of precipitation that reached 1.10 inches. Figure 10 shows the cumulative hyetographs of the sampled rainfall events at the Alpharetta site:

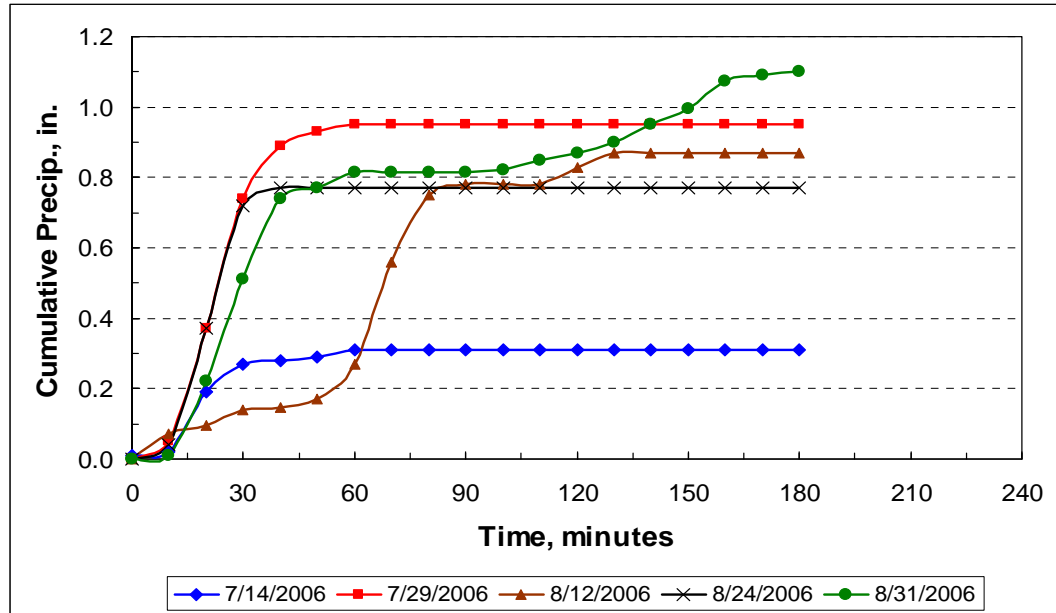


Figure 10: Cumulative hyetographs for sampled events at Alpharetta site, showing the five different rainfall events in which silt fence samples were collected (Sturm et al., 2007)

The first logged storm on July 14 had the smallest maximum rainfall intensity while the second logged storm on July 29 had the highest maximum rainfall intensity. The logged storm on August 12 had the lowest initial rainfall intensity but the longest rainfall event duration. The silt fence monitoring data for the Alpharetta site is given in Table 1 below. The seep berm fully contained all runoff so that no sediment runoff samples were recorded (Sturm et al., 2007).

Table 1: A summary of precipitation data that occurred on the Alpharetta site, with their corresponding silt fence peak TSS and turbidity outflow concentrations, analyzed from the sediment runoff samples collected by the ISCO sampler (Sturm et al., 2007)

Event	Precip., in.	Max Intensity, in./hr	Peak TSS, mg/L	Peak Turbidity, NTU	Peak Outflow Discharge, cfs
7/14/2006	0.31	1.02	196	22	0.55
7/29/2006	0.95	2.22	370	10	0.562
8/12/2006	0.87	1.74	5194	1312	3.604
8/24/2006	0.77	2.10	4136	468	0.424
8/31/2006	1.10	1.74	647	155	1.565

Peak TSS effluent sediment concentrations were found to be 5194 mg/l and 4136 mg/l, measured for the rainfall events of 8/12/2006 and 8/24/2006. These large values of TSS illustrate the poor performance of silt fences with respect to sediment removal. Figure 11 shows the outflow discharge, turbidity, and TSS values from the Alpharetta silt fence for the rain event of 8/12/2006, which was the event that produced the most samples due to its longer duration:

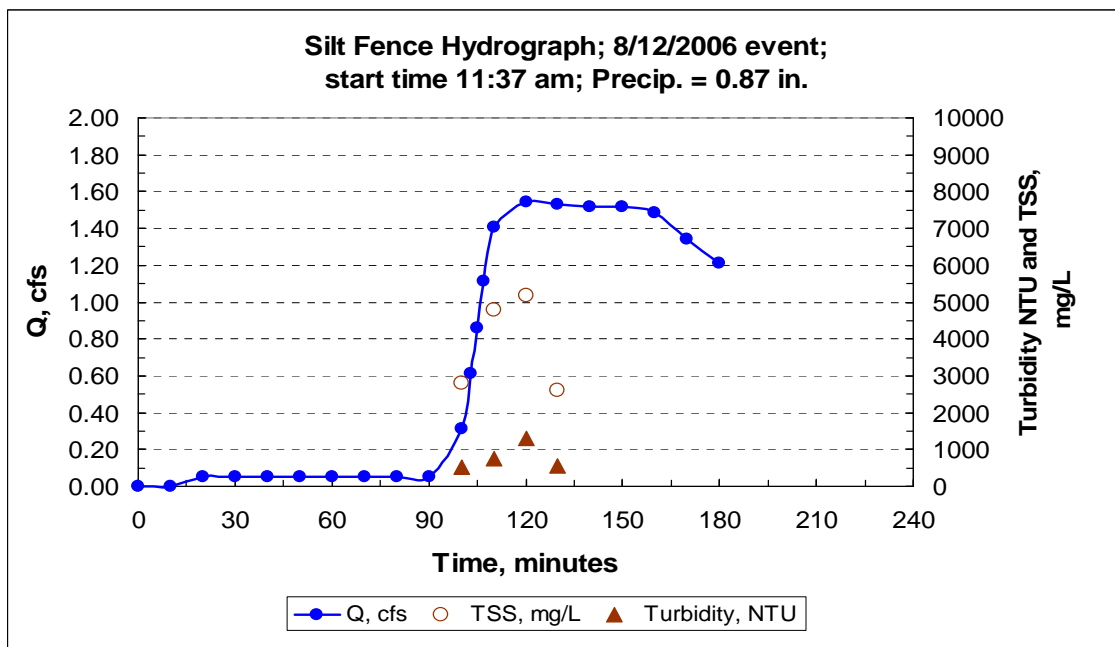


Figure 11: Outflow hydrographs and sedimentgraphs from Alpharetta silt fence for event of 8/12/06 (Sturm et al., 2007)

Since the 8/12/2006 rainfall event occurred over a longer time duration in comparison with the other events, and was characterized by low initial rainfall intensity followed by a burst of high rainfall intensity, it resulted in the highest number of ISCO samples. Figure 11 shows water flowing directly through the silt fence without being detained; hence the rise and fall of the hydrograph and sediment graphs coincide in time.

The rise of the sediment concentrations correspond to the rise in the hydrograph, where the TSS maximum value of 5,194 mg/L corresponds to the hydrograph rise resulting from the brief intense period of rainfall occurring about 70 minutes into the storm (Sturm et al., 2007). This behavior indicates that higher rainfall intensity provides higher sediment erodibility and higher sediment loads in the runoff. This is also reflected in the fact that the TSS and NTU values drop off after the brief intense period of rainfall, which created a water column behind the silt fence that allowed for some sediment settling. Thus, the outflow leaving the silt fence was less turbid even though the silt fence outflow rate remained relatively constant. In addition, an initial period of high intensity rainfall carries away most of the easily erodible sediment in the drainage area, which is translated into an initial higher turbidity in the surface runoff, with the subsequent surface runoff after that period being less turbid.

The Alpharetta seep berm did not exhibit any kind of overflow for any of the logged rain events, and no outflow samples were obtained from the seep berm to be tested for their TSS and NTU values. However, this does not signify the failure of the seep berm as an erosion control measure. On the contrary, it proves that the seep berm managed to contain all of the sediment-laden runoff from the logged rainfall events, and infiltrate it into the ground, a major advantage of seep berms over silt fences.

### **3.4.2 The IHM Site**

The IHM site is almost 25 miles south of the Alpharetta site, and is closer to the city of Atlanta. The maximum logged rainfall event had a maximum precipitation of 1.04 in., and rainfall events varied in duration from 30 to 90 minutes. Figure 12 shows the cumulative hyetographs of the sampled rainfall events at the IHM site:

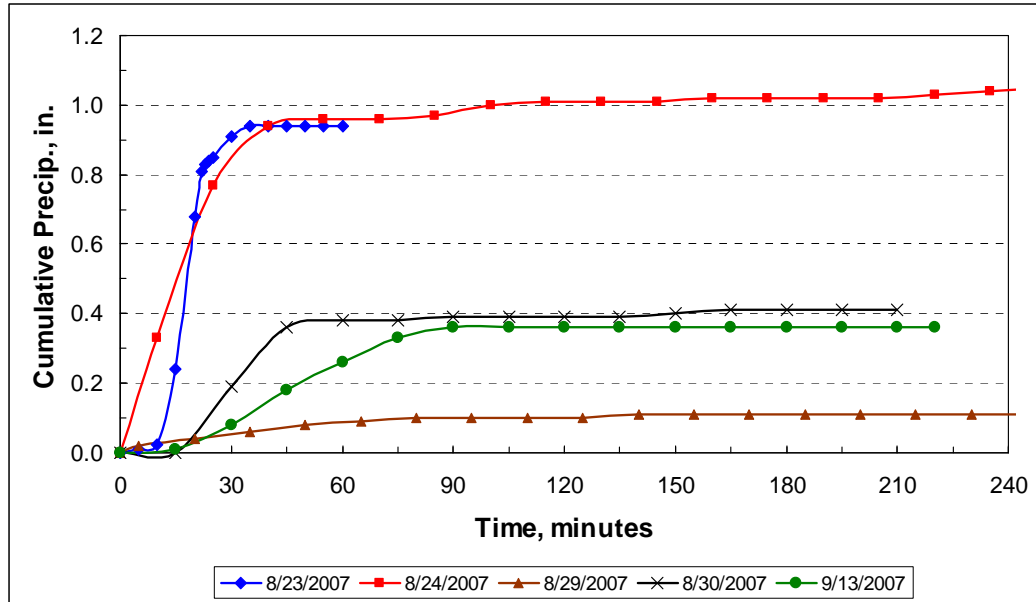


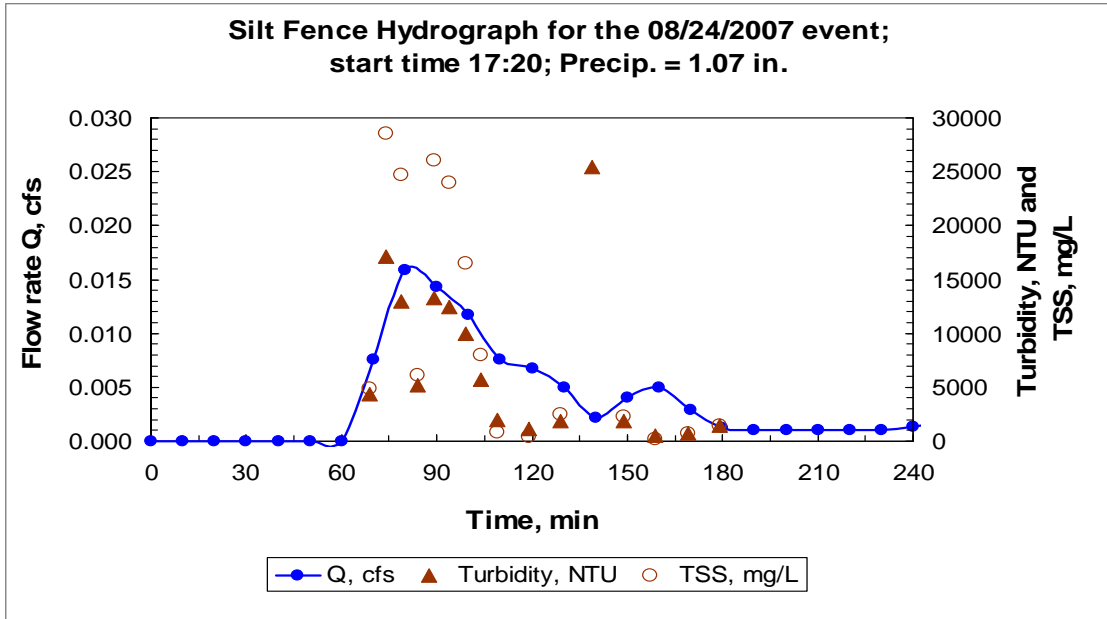
Figure 12: Cumulative hyetographs for sampled events at IHM site, showing the five different rainfall events in which silt fence and seep berm samples were collected (Sturm et al., 2007)

Silt fence and seep berm monitoring data is given in Table 2. The largest two rainfall events occurred on 8/23/2007 and 8/24/2007, with maximum precipitation intensities of 5.28 in./hr and 1.98 in./hr, respectively. It is clear that the seep berm was more efficient in containing sediment runoff, as projected by its zero or smaller TSS and turbidity values, when compared to the silt fence (Sturm et al., 2007).

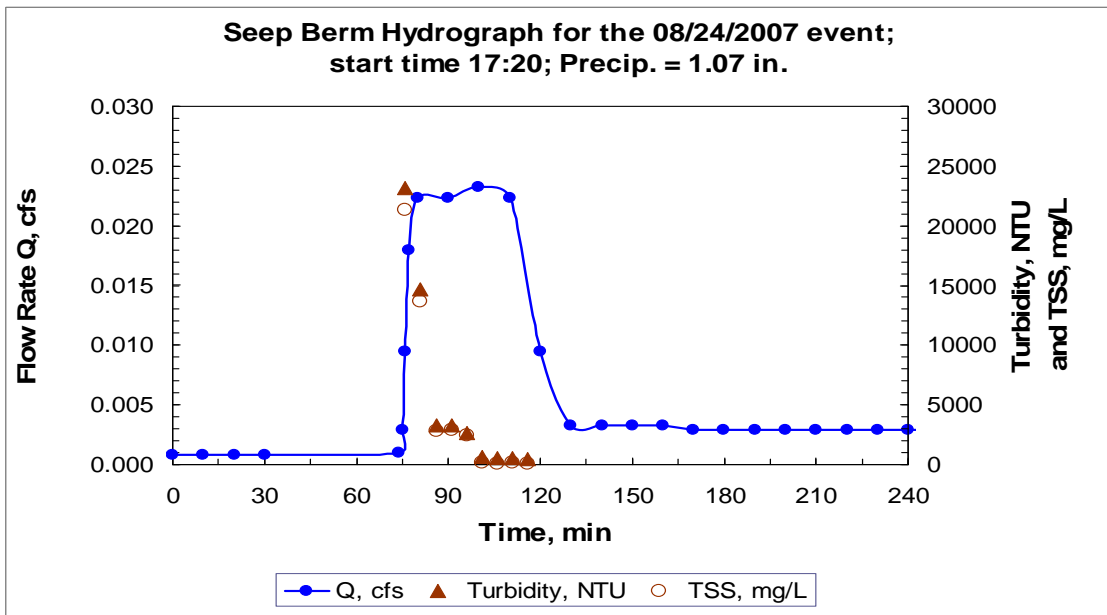
Table 2: A summary of precipitation data that occurred on the IHM site, with their corresponding silt fence and seep berm peak TSS and turbidity concentrations, analyzed from the sediment runoff samples collected by the ISCO samplers (Sturm et al., 2007)

Event	Precip. in.	Max Intensity in./hr	S.F. Peak Turbidity NTU	S.B. Peak Turbidity NTU	S.F. Peak TSS mg/L	S.B. Peak TSS mg/L	S.F. Peak Outflow Discharge cfs	S.B. Peak Outflow Discharge cfs
8/23/2007	0.94	5.28	12440	none	28750	none	0.0208	none
8/24/2007	1.07	1.98	25480	23200	41300	21300	0.0159	0.0233
8/29/2007	0.11	0.24	2180	none	2875	none	0.00054	none
8/30/2007	0.41	0.76	1848	none	1138	none	0.00071	none
9/13/2007	0.36	0.40	6200	3636	10400	3840	0.0194	0.0581

The outflow from the silt fence and seep berm for the events of 8/23/2007 and 8/24/2007 show the highest peak turbidity and TSS values of any of the rainfall events logged, and are larger than the peak turbidity and TSS values of the other rainfall events by an order of magnitude. It should be noted that, even though the 8/23/2007 event had a significantly higher rainfall intensity than the 8/24/2007 event, the peak turbidity and TSS values for the latter are higher. This can be most likely attributed to the fact that the rainfall event of 8/23/2007 was preceded by a long dry period, causing much larger infiltration losses than normal. The silt fence exhibited an outflow peak TSS value of 28750 mg/l for the 8/23/2007 event, and an outflow peak TSS value of 41300 mg/l for the 8/24/2007 event. These values are extremely high and demonstrate the inefficiency of the silt fence when used alone as an erosion control. The seep berm did not overflow for the 8/23/2007 event, showing that the storm runoff was totally contained and infiltrated at the base of the upstream side of the seep berm, a main advantage of seep berms over silt fences. The seep berm also exhibited a much lower peak TSS value than the silt fence for the 8/24/2007 event, which was 21300 mg/l. The storm water runoff from the 8/24/2007 event flowed freely through the silt fence, while it built-up on the upstream side of the seep berm wall before reaching the overflow pipe discharge level. The storage of water on the upstream side of the berm wall allowed for suspended sediment settling from the runoff, which was reflected by the lower TSS values from the seep berm outflow. The results of the 8/24/2007 rainfall event again show the efficiency of seep berms as an erosion control measure when compared to silt fences. Figure 13 shows the outflow discharge, turbidity, and TSS values from the IHM silt fence and seep berm for the event of 8/24/2007.



(a)



(b)

Figure 13: (a) Outflow hydrographs and sedimentgraphs from the IHM silt fence; (b) Outflow hydrographs and sedimentgraphs from the IHM seep berm; both for the event of 8/24/2007 (Sturm et al., 2007)

It can be seen that the rise of the seep berm hydrograph lags behind the silt fence hydrograph. This is due to the buildup of the water behind the berm, whereas the water flows directly through the silt fence without being detained. Even though the seep berm peak TSS value for the 8/24/2007 event is still considered high, significant differences are observed when comparing the hydrographs and sedimentgraphs for both erosion controls from that particular rainfall event. It is notable that the silt fence hydrograph has a longer time duration, and is characterized by a triangular shape, while the seep berm hydrograph is delayed and lags behind the silt fence hydrograph, and is characterized by a square wave shape. This particular square shape can be attributed to the storage building of water runoff behind the seep berm, prior to the berm overflow pipes beginning to discharge.

The silt fence sedimentgraphs of TSS and turbidity rise and fall slowly in synchronization with the silt fence hydrograph on the 8/24/2007 event. This points to a direct correlation between rainfall intensity and sediment load in the runoff, reflected by a free flow of water through the silt fence with no detention. On the other hand, the seep berm sedimentgraphs of TSS and turbidity fall more abruptly when compared to the seep berm hydrograph, reflecting a rapid decrease of downstream sediment concentration in the seep berm runoff. Initially, the suspended sediment in the water storage behind the berm is thoroughly mixed across the water column, and is reflected through higher sediment concentrations in the downstream seep berm outflow. However, the rapid decrease of downstream sediment concentration is an indicator of the seep berm filtration of suspended sediment out of the water storage upstream of the berm wall, and is attributed to the one-in. discharge pipes skimming the surface of the water behind the seep berm, which is less turbid due to sediment settling. This explains why the water effluent discharged from the berm is much less turbid and has less storm-event sediment load than the effluent discharged from the silt fence (Sturm et al., 2007).

### 3.4.3 Outflow Sediment Mass Calculation

Further analysis was conducted to quantify the total mass of sediment flowing out of both the seep berm and the silt fence at the IHM site, for the precipitation events of 08/12/2006, 08/23/2007, 08/24/2007, and 09/13/2007. The 08/24/2007 event was chosen to illustrate the methodology behind the suspended sediment mass outflow calculation. Figure 13 shows the hydrographs for both silt fence and seep berm to occur over a time period of 240 minutes for the 08/24/2007 event. The sediment graph for the seep berm occurred over a time period of 40 minutes, while the sediment graph of the silt fence occurred over a time period of 110 minutes. The seep berm delivered suspended sediment concentration samples over a shorter time frame, indicating that the suspended sediment mass in the seep berm outflow runoff was much less than that of the silt fence, and that the seep berm contained the suspended sediment for longer time durations than the silt fence.

The integral equation of the sediment mass in the outflow from an erosion control is given as:

$$m = \int_{t_1}^{t_2} QCdt \quad (63)$$

where  $t_1$  and  $t_2$  are the recorded start and end times of the first and last grabbed suspended sediment concentration sample,  $Q$  is the runoff volumetric flow rate, and  $C$  is the concentration of suspended sediment in the runoff. The first step to numerically quantifying the mass of sediment leaving an erosion control was to calculate the mass flow rate of the outflow. The mass flow rate (lbs/min) at a particular moment in time ( $t$ , min) is defined as the product of the volumetric outflow rate of the erosion control ( $Q$ , ft<sup>3</sup>/min) and the suspended sediment TSS concentration ( $C$ , lbs/ft<sup>3</sup>) of that outflow. Next, the concentration and volumetric flow data for each erosion control was multiplied together at each time a concentration sample was grabbed. Since the time interval ( $\Delta t$ ) between every two samples was non-uniform, the  $QC$  product was subsequently integrated using the trapezoidal rule for each  $\Delta t$  and over the entire duration of the rainfall event to obtain the mass of sediment in the outflow. The calculated sediment mass values

for each time interval were then summed up to give the total sediment mass in the erosion control outflow over the precipitation duration.

Using the methodology just described, the mass of suspended sediment in the outflow runoff for the 08/24/2007 event was calculated to be 13.09 lbs for the seep berm and 39.77 lbs for the silt fence, a value three times that of the seep berm. The uncertainty for the sediment outflow mass for the seep berm and silt fence was 1.9% and 2.1%, respectively. This quantitatively illustrates the superiority of seep berms over silt fences as an erosion control measure under the same precipitation event conditions.

Table 3 summarizes the results from the four precipitation events:

Table 3: Suspended sediment outflow mass summary for four precipitation events

Event	S.F. Suspended Sediment Outflow Mass, lbs	S.B. Suspended Sediment Outflow Mass, lbs	S.F. Outflow Volume, ft <sup>3</sup>	S.B. Outflow Volume, ft <sup>3</sup>	S.F. Outflow Volume, in.	S.B. Outflow Volume, in.
8/23/2007	6.0	0.0	4.7	0.0	0.002	0.000
8/24/2007	39.8	13.1	50.8	55.1	0.020	0.021
9/13/2007	4.7	3.1	39.3	18.5	0.015	0.007
8/12/2006	635.0	0.0	7000	0.0	0.100	0.000

### 3.5 Summary

The analysis of the data collected showed the superiority of seep berms compared to silt fences in terms of significantly reducing downstream runoff due to storage at the beginning of the runoff event and subsequent infiltration. The TSS and turbidity values of runoff downstream of the seep berm, if there were any, provided lower values than those collected downstream of silt fences. The seep berm effluent suspended sediment load can be controlled to some degree by the designer, through the amount of storage provided behind the berm, and through regular maintenance of the berm at predesigned time

intervals. Silt fences were shown to transmit significant values of downstream runoff TSS and turbidity, and can do so over long time frames that are dependent on the size, duration, and intensity of the storm. Consequently, their sediment control efficiency was poor.

In summary, seep berms were shown to achieve a significant reduction of sediment concentrations in effluent storm water runoff samples, and consequently in terms of total effluent suspended sediment event load, as compared to silt fences. The joint project successfully presented seep berms as a viable and more efficient alternative to silt fences. The sedimentation, storage, and infiltration capacities of the seep berm provide it with an excellent advantage over silt fences, which provide minimal sedimentation and allow significant flow-through capacity without allowing for sedimentation. Thus, seep berms can be recommended as an erosion control choice for construction sites, especially small sites.

It should be emphasized that the joint demonstration project does not attempt to prove that seep berms are the sole solution for erosion control, but rather an alternative to the more commonly used silt fences in terms of efficiency. The field data collected showed that seep berms performed well in settling medium to large particles of sediment out of the storm water runoff; however, finer sediment particles remained suspended in the water stored upstream of the seep berm, and constituted a major component of the suspended sediment in the berm overflow. This observation demonstrates the need for another erosion control measure to be used in series with the seep berm that has the capacity to remove the fine sediment from the berm overflow. Chapter 2 presented a literature review of vegetation filters as a viable erosion control measure for removing finer sediment particles. Therefore, the lab experimental section of the thesis in Chapter 4 is intended to study the sediment filtering capacity of vegetative filters when subjected to storm water runoff transporting fine suspended sediments.

## **4. DEFINING THE EXPERIMENTAL PLAN, APPARATUS AND PARAMETERS**

### **4.1 Experimental Research Objective**

The experimental research described in this and the following chapter addresses settling of suspended sediment in storm water runoff flowing through emergent and submerged vegetative filters in order to estimate the additional water quality benefits of directing seep berm outflow through a vegetative filter. The effect of emergent and submerged vegetation on the vegetation drag coefficient, flow velocity profiles, and the settling efficiency of suspended sediment are all studied.

A recirculating wooden flume with a width of 3.28 ft, length of 32 ft, and a fixed bed slope of 0.00629 ft/ft was designed for the experimental study in which rigid cylindrical wooden rods and flexible Lexan strips were installed at different plant densities to simulate vegetation. Depth measurements were taken along the flume centerline to plot the water surface profiles through emergent and submerged vegetation from which the normal depth was determined for several flow rates varying between 0.2 cfs and 0.7 cfs. The friction factor and the vegetation drag coefficient were then calculated and generalized so that they can be used in determining the design depth of flow in a particular vegetative filter design. Detailed velocity and turbulence profiles were measured in the wake of the artificial vegetation elements to suggest the appropriate type of sediment filtering model needed to predict trap efficiency. In addition, a series of flume experiments was conducted in which a fine-sediment slurry was fed at the flume entrance at a constant rate. The concentration profiles were measured and the trap efficiency was calculated from these experimental data for comparison with a theoretical trap efficiency model. In this chapter, the design of the experimental flume and the flexible artificial vegetation is summarized. In addition, the experimental instrumentation and the experimental procedure are described. In Chapter 5, the experimental results are given and analyzed.

## 4.2 Experimental Design Plan

### 4.2.1 Experimental Flume Design Equations

The design adopted for the flume construction, in addition to the determination of the optimal flume bed slope, was based on the concept of biomechanics of vegetation and relative roughness, introduced by Kouwen (1992). Kouwen suggested that the amount of flexure in a flexible grass lining under varying flow conditions can be predicted. Biomechanical properties of the grass and the channel flow conditions are the two major factors affecting the flexure of a grass lining. Based on a prediction of the degree of bending over of the vegetation for varying flow rates, the relative roughness is determined from which the resistance parameter (Darcy-Weisbach friction factor  $f$ , Chezy's  $C$ , or Manning's  $n$ ) is quantified.

The nucleus of the Kouwen (1992) design equation is the  $k/h$  ratio, also known as relative deflection of the vegetative lining. The parameters  $h$  and  $k$  refer to the flexible stem length and the height of the bent part of the flexible stem measured vertically from the bottom of the bed to the tip of the bent stem, respectively. Kouwen and Li (1980) and Kouwen et al. (1980) introduced an equation to predict  $k$ , which is dependent on the amount of drag exerted by the flow:

$$k = 0.14h \left[ \frac{\left( \frac{MEI}{\tau} \right)^{0.25}}{h} \right]^{1.59} \quad (64)$$

where  $MEI$  = the stiffness factor of the vegetation and  $\tau$  = the total boundary shear stress. Since deflection is perpendicular to the applied load, the value of  $MEI$  is dependent on  $h$ . The longer the grass, the more biomass that is available, and the stronger the resistance to deflection by the flow is.

The Kouwen (1992) method involves calculating the  $MEI$  (introduced in Equation 64) of the vegetative strip, which is defined as the biomechanics coefficient. The  $MEI$  is the product of stem density, stem modulus of elasticity, and second moment of area of a

stem, corresponding to  $M$ ,  $E$ , and  $I$ , respectively. Subsequently, the use of hydraulic and flow design equations (presented below) completes the calculations resulting in the flow velocity and depth in the vegetative channel. The relative roughness method, based on the calculation of the friction factor of the vegetative channel is essential in determining the flow resistance of a certain vegetative strip, and the capacity design of a vegetative channel. Alternatively, the relative roughness and  $MEI$  method provides a calculation method to obtain the flow velocity and depth over a vegetative strip at a specified discharge, which are parameters needed to determine the sediment removal capability of the vegetative strip.

The  $MEI$  method is summarized as follows (Kouwen, 1992):

- Height =  $h$  of plastic stem is chosen, with a range of flume normal depths,  $y_n$  or  $H$
- Width  $b$  and slope  $S$  of flume are chosen
- Flexible plastic stem dimensions are selected (width, length, thickness)
- $M = \text{stem density/m}^2$  (or  $\text{ft}^2$ ) is chosen, and stem second moment of area is calculated
- The  $MEI$  coefficient is subsequently calculated, to be used in critical shear velocity calculation
- Shear velocity, critical shear velocity, and total boundary shear are calculated from:

$$u_{*crit} = \min( 0.028 + 6.33 MEI^{-2}, 0.23 MEI^{0.106} ) \quad (65)$$

$$\tau = \gamma y_n S \quad (66)$$

$$u_* = \sqrt{g y_n S} \quad (67)$$

- Deflected height of stem =  $k$  is calculated from Equation 64
- Darcy- Weisbach friction factor =  $f$  is calculated from a Keulegan type equation (Sturm, 2001):

$$\frac{1}{\sqrt{f}} = a + b \log_{10} \left( \frac{y_n}{k} \right) \quad (68)$$

where “ $a$ ” and “ $b$ ” are empirical coefficients dependent on the degree the vegetation is bent, and:

$$a, b = fn \left( \frac{u_*}{u_{*crit}} \right) \quad (69)$$

- After calculating the Darcy-Weisbach friction factor, the mean flow velocity is calculated from the uniform flow equation below, followed by the flow rate  $Q$  from continuity.

$$U = \sqrt{\frac{8g}{f}} \sqrt{y_n S} \quad (70)$$

Table 4 presents the design criteria and guidelines that were essential in determining the flume dimensions prior to construction.

Table 4: Design criteria and guidelines for determining flume dimensions

<b>Parameter</b>	<b>Measurable Ranges</b>
$Q$ , cfs	0.2 – 2.0
$U$ , ft/sec	0.1 – 1.6
$y_n$ , ft	0.2 – 1.2
Flow Re	3000 - 60000
Froude	0.05 – 0.5
$H/d$ ( $y_n/d$ )	8 - 30
$k/h$ (submerged case)	0.3 – 0.99

#### 4.2.2 Choice of Flume Dimensions and Artificial Vegetation

Design of the flume slope and range of flow depths for a given range of experimental discharges was based on Kouwen's method summarized in the previous section. In the case of flexible vegetation, the height, width, and thickness of the vegetation had to be carefully selected in conjunction with the flume dimensions and slope and the desired flow properties. Strips of thin flexible plastic were cut manually from large plastic sheets to simulate flexible vegetation. The flexible plastic material LEXAN, which has a modulus of elasticity of  $2.39 \times 10^9$  Pa, as stated by the manufacturer, was the material chosen for the flexible vegetation experimental trials.

The LEXAN strip dimensions were chosen by taking into consideration the height of the flume's sidewall and the normal depth range desired in the experimental trials for the available pump recirculating discharge range. The strip dimensions were: 7.62 cm long (3 in.), with a width of 1.0 cm (0.39 in.) and a thickness of 0.25 mm (0.0098 in.). The selected width and thickness of the LEXAN strips were the result of making numerous trial and error calculations from the Kouwen (1992) equations and filtering out the results that met the flow criteria established in Table 4, including a realistic range of values of MEI and a value of  $k/h \leq 1.0$ . The results of a few trial calculations are shown in Figure 14 with  $M$  ranging from 200 to 1200 stems/m<sup>2</sup>. From these results, which are shown as plots of normal depth and  $k/h$  ratio versus bulk velocity in Figure 14, the selected values of  $M$  were 275 stems/m<sup>2</sup> (25.5 stems/ft<sup>2</sup>) and 1100 stems/m<sup>2</sup> (101.9.0 stems/ft<sup>2</sup>). It can be observed in Figure 14 that normal depth increases with increasing velocity while the  $k/h$  ratio decreases as the stems are bent over further with increasing velocity. Once the stem density increases above 350 stems/m<sup>2</sup>, the plots move closer to one another for both normal depth and  $k/h$ . This implies that an increase in stem density while keeping the normal depth constant does not cause a significant change in velocity and  $k/h$  ratio.

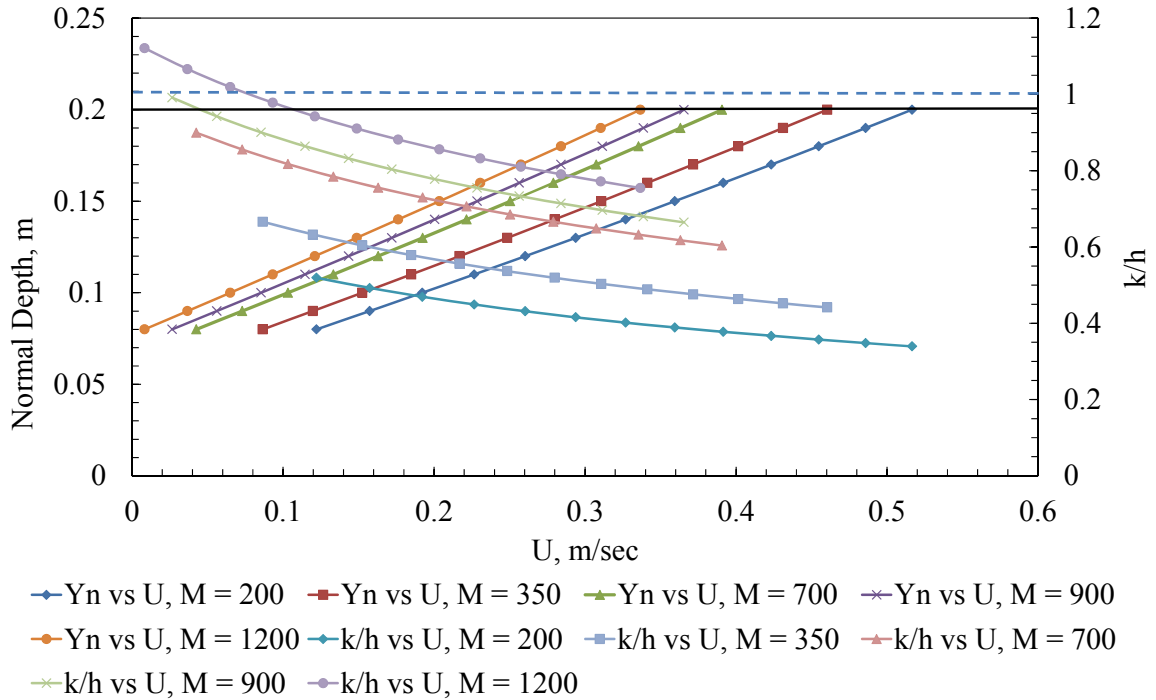


Figure 14: Plots of normal depth vs velocity and  $k/h$  vs velocity for stem densities ranging from 200 to 1200 stems/m<sup>2</sup>. The  $k/h$  vs velocity plots are those curving downwards from left to right. Any  $k/h$  values above 1, as bordered by the horizontal line at  $k/h=1$ , were discarded as unrealistic values, implying that their corresponding stem densities were not applicable using the Kouwen (1992) design equations for the experimental flume design parameters.

The final values of various flow and vegetation properties for the two chosen vegetation densities are given in Table 5. These values are not the experimental results; however they are guidelines that indicated the expected values and ranges of the measured parameters obtained from the experimental trials. The flow and velocity values are well within the range of maximum allowable values dictated by the allowable value of bed shear stress that provides channel stability. The flexible plastic strips simulated natural Bermuda grass with a good stand (retardance class D), with a permissible bed shear stress of 29 Pa (Chen & Cotton, 1988; Sturm, 2001). The maximum permissible normal depth and flow rate resulting from that bed shear stress were much higher than the

experimental depth and flow rate ranges to be used, hence the vegetative flume strip used simulated a stable natural vegetative channel. Moreover, Kouwen and Li (1980) provided tables stating the MEI for different types of natural vegetation. The Bermuda grass simulated by the experimental Lexan strips had given MEI ranges of 0.06 to 0.135. The MEI values calculated from the experimental Lexan strips fall within that range.

Table 5: Final selected flow and vegetation properties for the experimental vegetation filters

<b>Parameter</b>	<b>Measurable Ranges</b>
$Q$ , cfs	0.2 – 0.7
$U$ , ft/sec	0.1 – 1.0
$y_n$ , ft	0.2 – 0.7
Flow Re	3000 - 20000
Froude	0.05 – 0.2
$H/d$ ( $y_n/d$ )	8 - 20
$k/h$ (submerged case)	0.5 – 0.99

Rigid cylindrical rods were used to simulate emergent vegetation. The rods had a diameter of one cm (same as the flexible strip width) and a length equal to the height of the flume sidewalls to ensure emergent vegetation regardless of the normal depth. The same two vegetation densities as for the flexible vegetation were utilized.

#### **4.2.3 Experimental Flume Layout**

The flume was constructed of wood with a width of 3.28 ft (1 m), a side wall height of 15.75 in. (0.4 m), and a length of 26 ft (7.9 m), with an additional 6 ft (1.82 m) to accommodate the head box length and flow straighteners as shown in Figure 15. The head box width was equal to the flume width. The purpose of the flow straighteners was

to ensure a uniform flow distribution across the flume width and to absorb and dissipate excess turbulence just upstream of the flume entrance. The flow straighteners were comprised of a perforated steel sheet and a horsehair filter layer. Additionally, water was introduced into the head box through the use of a diffuser across the flume width and then passed over a sharp-crested weir inside the head box to provide the initial flow stilling and uniformity conditioning.

A sharp-crested weir, with adjustable heights from two in. to seven in. (for maximum experimental flexibility), was installed at the downstream end of the flume to provide tailwater depth control and thus to set the flume normal depth and aid in maintaining uniform flow. Water exiting the flume was released onto a 10-ft long steep trough of 5% slope where the sediment-laden flow was channeled into a large steel sedimentation tank with the following dimensions: 10.4 ft long by 3.5 ft wide by 3 ft deep. The sedimentation tank featured a built-in weir at the downstream end extending 2.5 ft vertically from the bottom of the tank to form an intake area for the re-circulating pump and to prevent short-circuiting of any suspended sediment through the sedimentation tank.

The vegetation strip, spanning the flume width, was installed beginning at a streamwise station of five ft downstream of the flume entrance, and extending 16 ft in length. The artificial vegetation stems were inserted into pre-drilled holes in one-inch thick PVC plastic sheets affixed to the flume bed. Gravel, with a  $d_{50}$  of 0.617 in., was spread on the bed upstream and downstream of the vegetation strip in order to develop fully-rough turbulent flow. The vegetation densities in the experimental trials (for both rigid and flexible vegetation) were 25.5 stems/ft<sup>2</sup> and 101.9 stems/ft<sup>2</sup>, or 1338 stems and 5350 stems in the whole strip, respectively, and were chosen as explained in the previous section.

The experimental apparatus was an independent closed-loop re-circulation system. Water was drawn out of the full sedimentation tank by a pump which discharged into a six in. diameter pipe laid on the concrete lab floor along the length of the flume. Midway along this pipe, an orifice meter was installed with a gate valve downstream of it

for flow control. At the head box, the pipe rose vertically and discharged into a six in. PVC diffuser on the floor of the head box. The head box, main channel, and return chute were all covered with a waterproof rubber membrane to prevent leaks and deterioration of the flume due to moisture. The structural design of the flume is presented in Figure 15, in front and plan view. A photo of the flume is provided in Figure A. 1 of Appendix A.

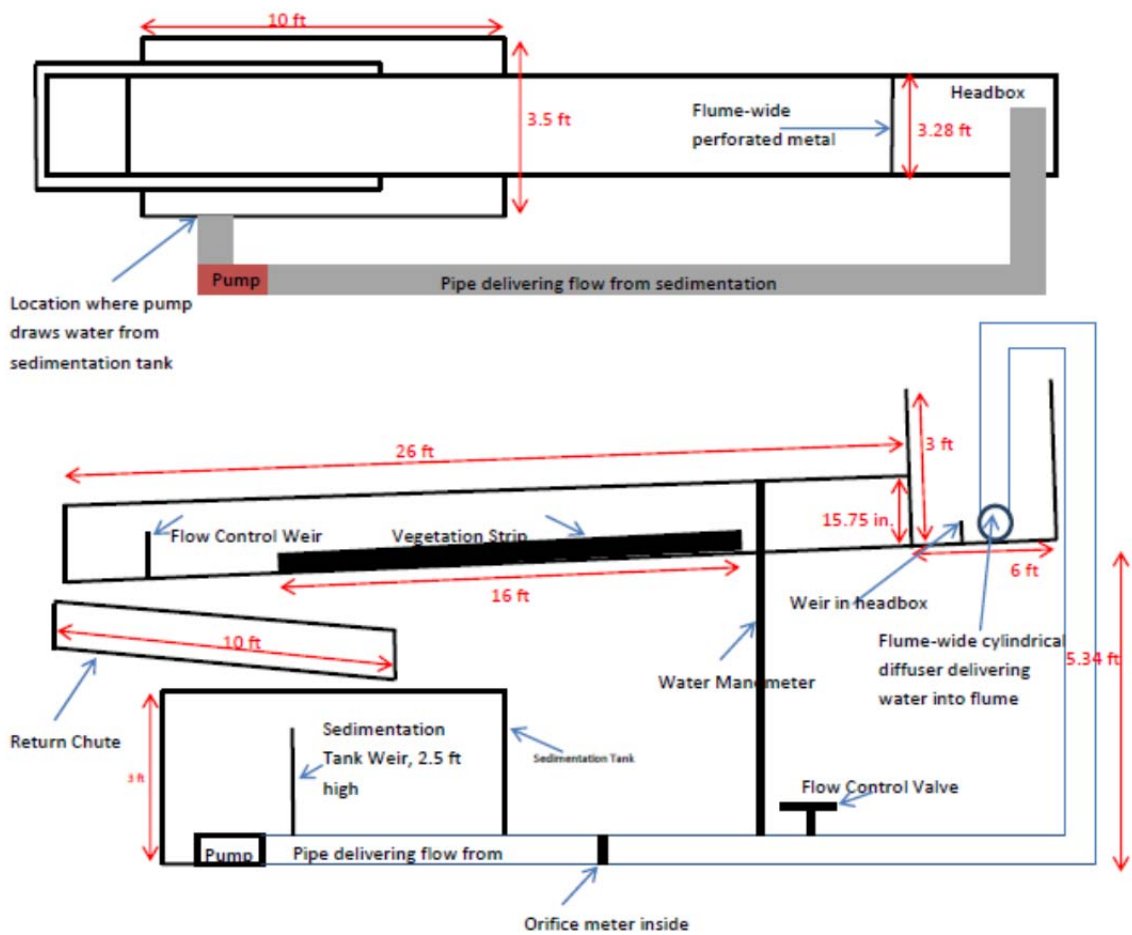


Figure 15: Front view and plan view of experimental flume

Upon completion of the flume construction, the bed slope was re-measured to determine its actual constructed value and standard error. Figure 16 shows a plot of the depth measurements. The flume was filled with water, and then the water supply was shut off to allow the water to come to rest overnight. Subsequently, water depth was measured using a point gage at horizontal intervals of 20 in. along the flume length to obtain the flume slope. The measured slope of the flume was 0.00629, while the standard error obtained from the regression analysis was 0.00012 (1.9%). The value of  $S = 0.00629$  was used in all experimental calculations and subsequent analyses.

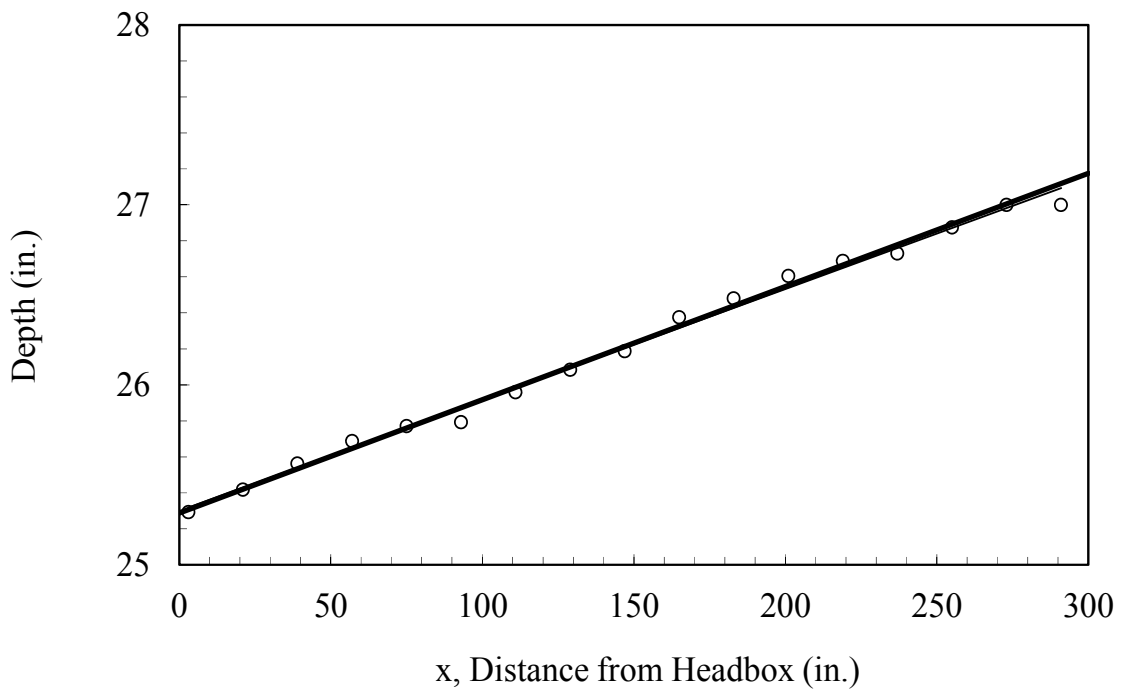


Figure 16: Plot showing flume length versus still-water depth, to measure the slope of the experimental flume

### 4.3 Instrumentation

Flow rates in the experimental flume were measured with an orifice meter calibrated by weighing. The calibration curve is shown in Figure 17 with a calibration equation of  $Q = 0.0868(\text{Manometer Deflection})^{0.4952}$ , and a standard error in flow rate of  $\pm 0.0047$  cfs. The orifice diameter was 3.25 in. Upstream and downstream pressure taps for the orifice meter were connected to either a water or mercury manometer through a switching valve. The water manometer accurately measured flow rates up to 0.7 cfs, while the mercury manometer measured higher flow rates that were not needed for these experiments. The water manometer was allowed to come to equilibrium and was stable for flow rates greater than 0.1 cfs. The minimum flow rate for these experiments was 0.2 cfs.

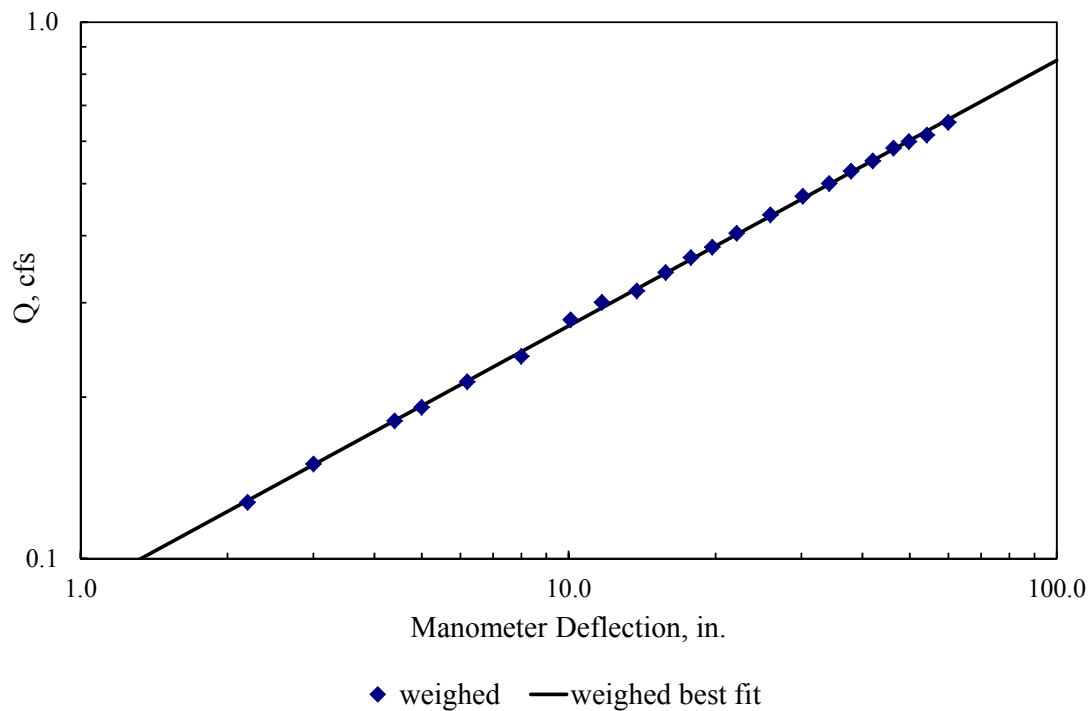


Figure 17: Calibration curve for orifice meter in flume flow pipe

Velocity and turbulence profiles were measured inside the vegetative strip which required removing some of the artificial roughness elements. A 3D downward-looking Son-Tek ADV (acoustic Doppler velocimeter) was employed for these measurements. The measuring volume was cylindrical with a diameter of 6 mm and a height of 9 mm located 5 cm below the receiver of the probe. Velocity and turbulence measurements were sampled for a duration of two minutes at 25 Hz at each measuring point. The sample was filtered for spikes and monitored for quality control by requiring a signal to noise ratio greater than 25 and a minimum correlation of 70.

#### **4.4 Sediment Feeding Mechanism and Rates**

Sediment was fed into the flume by a small feeding pump. The required sediment was mixed with water in a cylindrical bucket. The sediment diffuser was connected by a 0.25 in. rubber tube to the sediment feed pump, which in turn was connected to the mixing bucket. The sediment feeding pump drew water from the mixing tank and fed it to the flume through the sediment diffuser, which was located horizontally across the flume bed at the entrance of the channel directly downstream of the head box. Figure 18 shows the sediment diffuser.

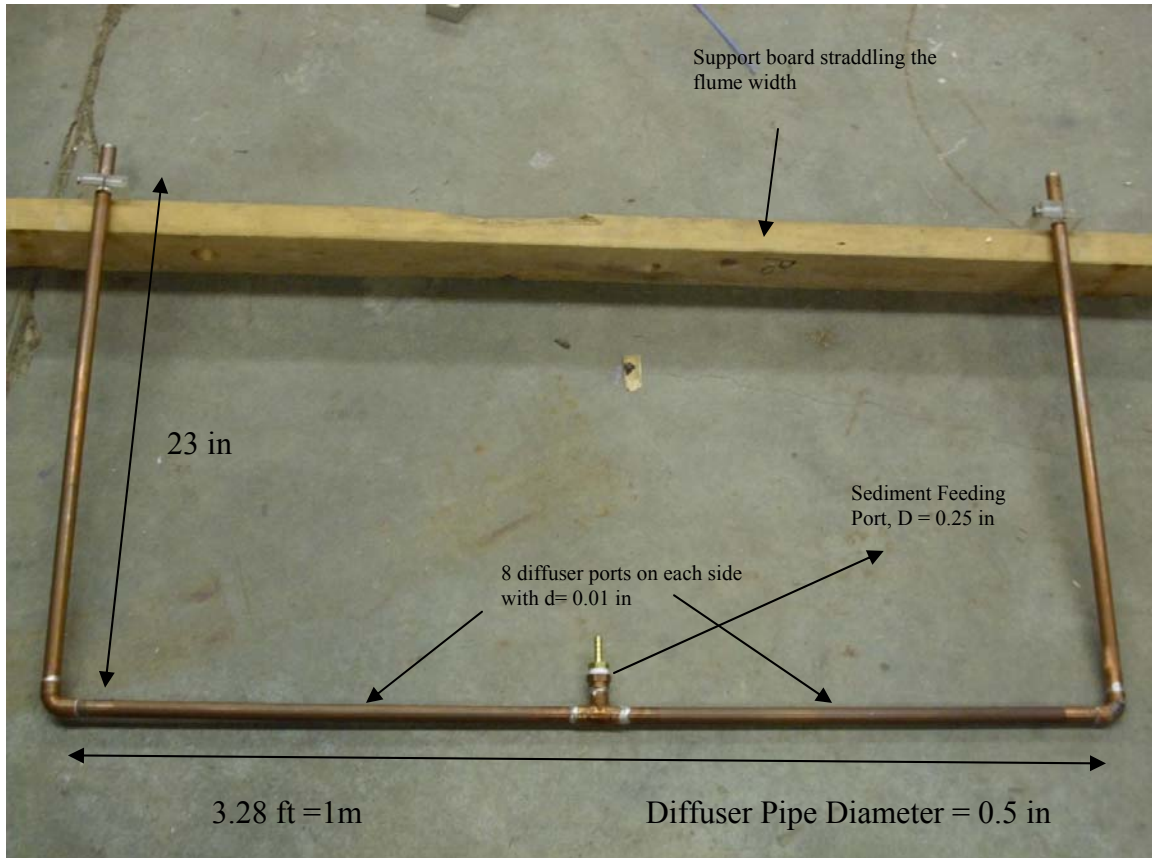


Figure 18: The sediment diffuser with its dimensions

The sediment diffuser spanned the width of the flume and was located a distance of five ft upstream of the beginning of the vegetative strip to allow for full mixing. To calculate that mixing length, the shear velocity  $u_*$  was calculated for the maximum normal depth ( $y_n$ ) measured in the experimental trials, which was 0.12 m. The vertical diffusion coefficient was calculated from the Fischer et al. (1979) equation:

$$\varepsilon_v = 0.067y_n u_* \quad (71)$$

and consequently the mixing length of the horizontal diffuser on the flume bed was calculated from (Fischer et al., 1979):

$$L = 0.4Uy_n^2 / \varepsilon_v \quad (72)$$

in which  $U$  is the mean flow velocity. The mixing length was calculated to be 1.47 m (4.8 ft), implying sufficient vertical mixing of suspended sediment in the water flow upstream of the submerged vegetation strip.

The length of the sediment diffuser was 3.28 ft (flume width), with a diameter  $D = 0.5$  in. = 0.0417 ft. Thus, the cross-sectional area of the sediment diffuser was  $A = 0.00136$  ft<sup>2</sup>. The number of ports on the diffuser was assumed to be  $n = 15$ , and the ratio of the sum of the port areas to the cross-sectional area of the diffuser pipe was assumed to be  $a/A = 0.7$ . Hence, the diameter  $d$  of each port was calculated by:  $d = D(0.7/n)^{0.5} = 0.009$  ft, giving a diffuser port diameter  $d = 0.108$  in.

The slurry feed pump had a maximum voltage of 9.5 volts, corresponding to a flow rate of 0.062 l/sec (0.0022 cfs) based on the feeding pump calibration. Since  $Q_{feed} = 0.0022$  cfs, the flow through each port hole was  $q_{feed} = 0.000146$  cfs. Consequently, the velocity from each port hole was calculated as  $v_{feed} = q_{feed}/(\pi d^2/4) = 2.3$  ft/sec. Thus, a total of 16 ports were drilled into the diffuser of Figure 18, with a diameter of 0.01 in. each. Since the sediment diffuser was flume-wide, lateral mixing was established through the release of the sediment from all the ports across the flume width.

The sediment feeding flow rate was fixed for all the experimental trials. However, the amount of sediment in the mixing bucket varied prior to each experiment, depending on the flume flow rate used. The mass continuity equation was used to calculate the sediment concentration fed for each experiment,  $C_{feed}$  :

$$Q_{feed} C_{feed} + Q_{inf\ low} C_{inf\ low} = (Q_{feed} + Q_{inf\ low}) C_{avg} \quad (73)$$

where  $Q_{feed}$  and  $Q_{nflow}$  were respectively the flow rates of the sediment flow and flume flow,  $C_{feed}$  and  $C_{inflow}$  were respectively the sediment concentration and the initial flume water concentration, and  $C_{avg}$  was the sediment concentration in the flume after sediment mixing, which was set at  $C_{avg} = 250$  mg/l for each flow rate of the experimental trials. Thus, the amount of sediment mixed in the mixing bucket, and consequently the feed

concentration, was based on the fixed  $C_{avg}$  value and the fixed feed flow rate of  $Q_{feed} = 0.0022$  cfs, while assuming  $C_{inflow} = 0$  during the experimental run.

The sand used in the experiments was fine, with a  $d_{50} = 0.11$  mm. The grain size distribution of the sand is shown in Figure 19. The grain size distribution clearly exhibits a wider spread at the finer side of the distribution, with a geometric standard deviation of  $\sigma_g = d_{84.13}/d_{50} = 1.88$ .

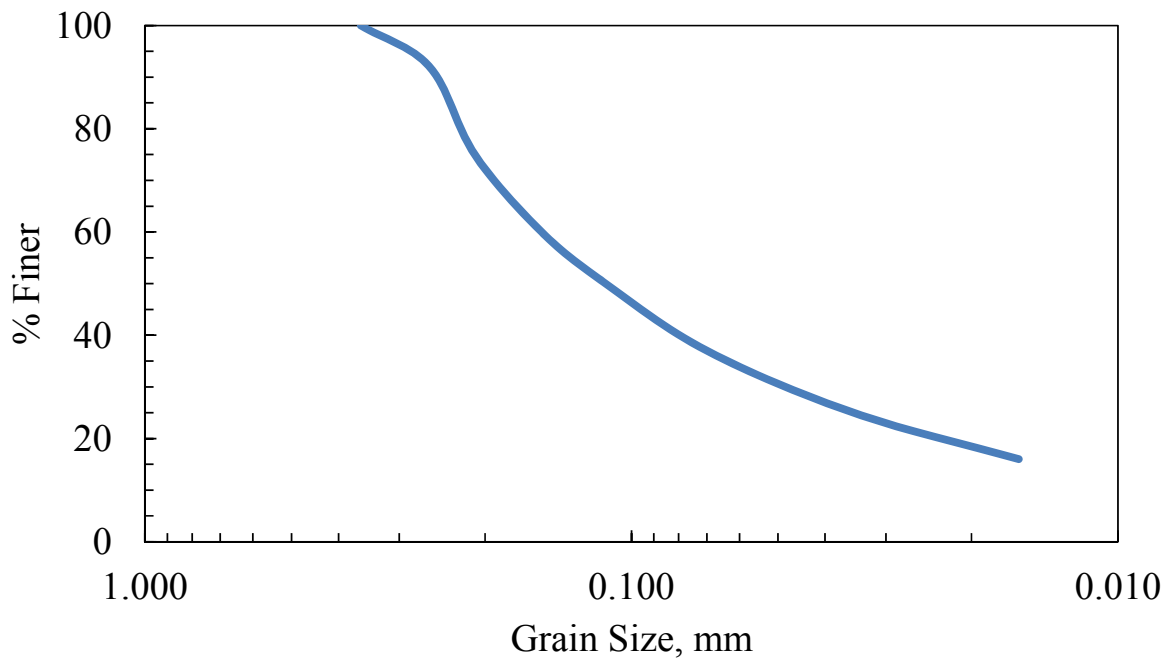


Figure 19: Grain Size distribution of the sand used in the experimental trials

#### 4.5 Concentration Sampling Mechanism and Rates

An automatic sampler (ISCO sampler) was used to collect samples at four different locations along the length of the vegetative strip. Four locations were chosen instead of one to capture the longitudinal sediment concentration profile through the vegetation as well as the streamwise sediment flux profiles for calculating the trapping efficiency of the vegetation. The sampler was programmed to take samples at one minute intervals. The samples were pumped into one-liter bottles.

A copper tube connected to the suction hose of the ISCO sampler was used as the grab sample suction mechanism. The suction inlet was designed so that the fluid entering the inlet had a velocity close to the flow velocity in the flume, as measured by the ADV. From the velocity data collected by the ADV for flow rates between 0.2 to 0.5 cfs through emergent vegetation of volumetric fraction density  $\phi = 0.086$  (i.e. 101.9 stems/ft<sup>2</sup>), and minding that the velocity for each flow rate varied depending on the measuring location (directly behind a stem or in the free stream between two stems), the value of  $U_{inlet} = 0.225$  ft/sec was chosen. The suction inlet was designed using  $U_{inlet}$  and an ISCO suction flow rate of  $Q_{ISCO} = 0.0017$  cfs. The suction inlet area was calculated to

$$\text{be } A_{inlet} = \frac{Q_{ISCO}}{U_{inlet}} = 0.0073 \text{ ft}^2 = 6.78 \text{ cm}^2.$$

The value of the inlet suction velocity was selected after observing the point velocity values for all experimental runs, obtained from the ADV at both behind the stem and in the free stream. It was observed that at the location behind the stem, the point velocity values revolved around 0.15 ft/sec, while they revolved around 0.3 ft/sec in the free stream location. Hence, the inlet suction velocity selected was the average between the two before-mentioned velocity values. Moreover, the near-bed velocity values obtained from the ADV at both locations was observed to be fairly stable and unchanging through all the experimental trials. As a further justification for the inlet suction velocity choice, equations related to initiation of sediment motion from Sturm (2001) were used to calculate the critical velocity needed to move a sediment particle off the bed. The critical

velocity calculated was 0.92 ft/sec, which is a larger value than any of the bulk or point velocities observed in the flume.

The suction inlet area was divided into two openings in a horizontal copper cylindrical casing. The openings were located at the front face of the horizontal cylinder, while the back face was connected to a 0.5-in. diameter vertical copper tube that directed the suction flow to the bottles in the ISCO sampler. The horizontal sampling cylinder had a length of 8.5 cm (3.35 in.), covering the center-to-center length of three vegetation stems in the same row in the cross-stream direction, where the distance between two stems was 4.25 cm (1.67 in.) from center to center. The horizontal cylinder length was chosen so as to obtain a representative sample from the flow between three stems as influenced by the wakes of the staggered stems in the upstream row. The two openings in the horizontal suction cylinder (which has a one-in. diameter) were each 2.35 cm (0.925 in.) in length and 1.5 cm (0.59 in.) in width. The openings were separated by 1.27 cm (0.5 in.). Figure 20 and Figure 21 show the ISCO sampling head and its position relative to the stems.

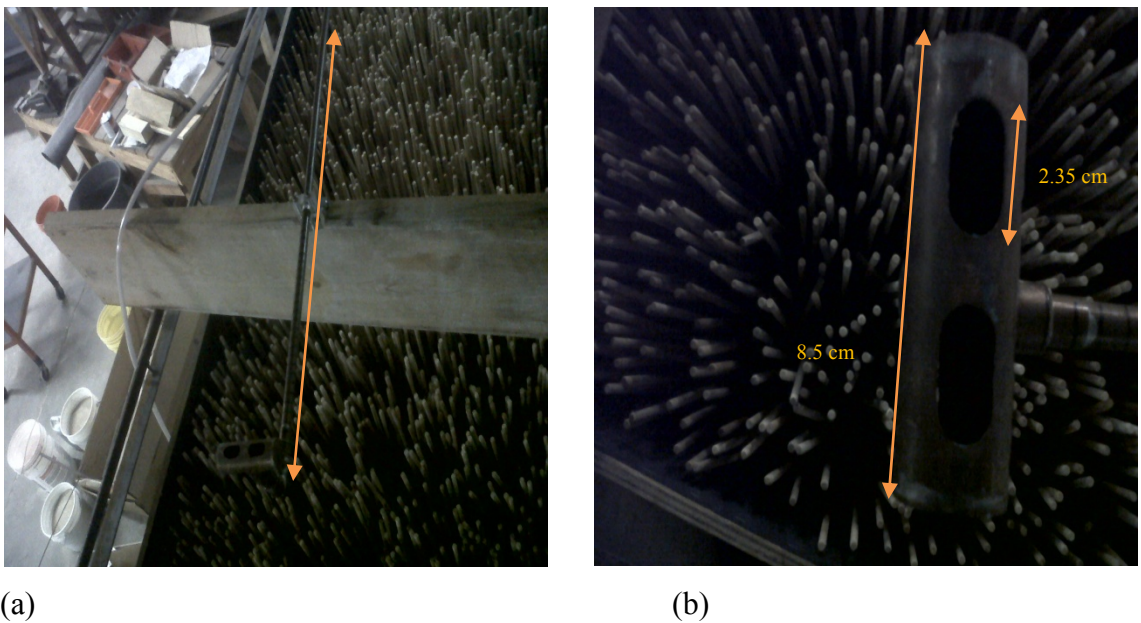


Figure 20: (a) ISCO suction inlet mechanism; (b) ISCO suction inlet openings

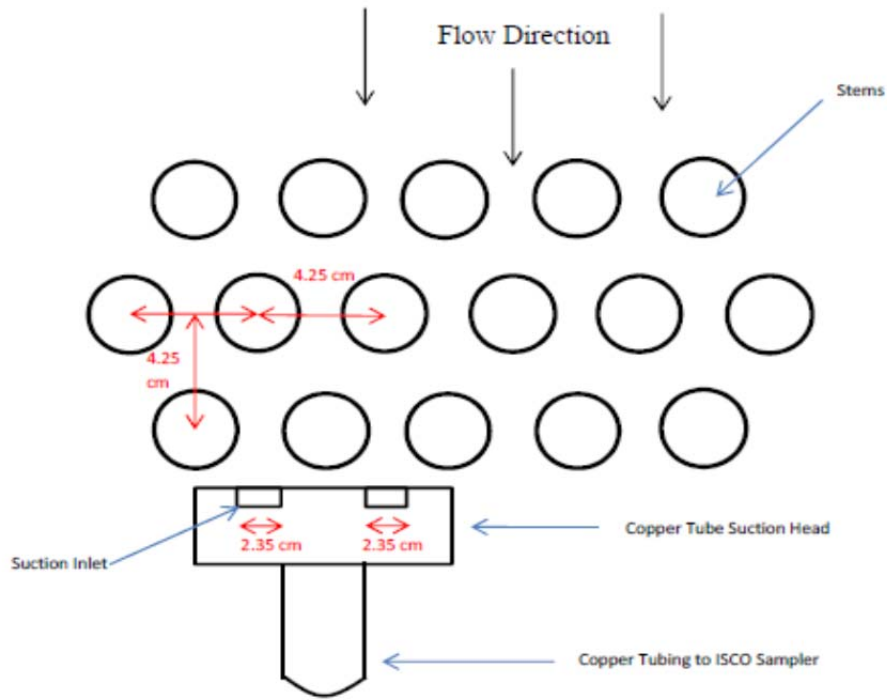


Figure 21: Schematic of the ISCO suction inlet location in the vegetation filter

The vertical copper tube was marked along its length to act as a measuring scale. For support, the copper tube was fixed to a wooden board spanning the flume width and mounted on top of the flume sidewalls. The board was moved manually along the flume length and positioned successively above the sampling locations during an experimental run. To properly collect samples across the flow depth at each sampling location, the suction inlet of the copper tube was moved vertically and rested at the sample depth needed. The four locations designated for sample stations in the streamwise direction were:

- At the beginning of the vegetation ( $x = 0.00$  ft)
- At 1/3 of the vegetation length ( $x = 5.33$  ft)
- At 2/3 of the vegetation length ( $x = 10.67$  ft)
- At the end of the vegetation ( $x = 16.00$  ft)

Once an experimental run was started, the sediment sample collection was delayed several minutes to allow an equilibrium concentration profile to develop in the flume. The initial sampling location was at  $x = 0.00$  ft on the vegetation filter. Once those samples were collected, the suction inlet was then moved and successively placed at stations of  $x = 5.33$  ft,  $10.67$  ft, and  $16.00$  ft until samples from all locations were obtained for the experimental run.

At each of the four vegetative filter sampling stations, three samples were taken over the flow depth, with a one minute time interval between initiation of pumping for each sample (pumping duration for each sample was approximately 20 seconds). The three samples were taken in the following order: on the flume bed, at mid-depth, and at the water surface. Once the third sample was collected, the suction inlet was moved to the next downstream station. The time between the third sample at one station and the first sample at the next downstream station was exactly one minute. The process was repeated until all samples were taken. The duration of sampling for each experimental run was 12 minutes.

The suspended sediment concentration (SSC) test was performed to obtain the concentration of sediment from each collected sample. The samples were filtered, dried, and weighed according to ASTM Standards D 1140 and D 4753. The data from the SSC test were then plotted as sediment concentration profiles at each station to show variation in concentration with depth. Subsequently, the suspended sediment flux at each of the four sampling stations was computed using a point-by-point integration of the product of the concentrations obtained across the flow depth and the flow point velocities obtained from the ADV. The trapezoidal rule was used to evaluate the integral, expressed as:

$$q_s = \int_a^{y_n} uCdz \quad (74)$$

where  $q_s$  is the sediment flux per unit width,  $u$  is the point velocity at a particular depth  $z$ , and  $C$  is the concentration at  $z$ .

## 5. LABORATORY RESULTS AND DISCUSSION

In this chapter, the experimental data are analyzed and discussed, and a relationship is suggested for trap efficiency of a vegetative filter for four cases: rigid emergent vegetation at density  $m = 101.9$  stems/ft<sup>2</sup> (volumetric fraction  $\phi = 0.086$ ), rigid emergent vegetation at density  $m = 25.5$  stems/ft<sup>2</sup> ( $\phi = 0.022$ ), flexible submerged vegetation at density  $m = 101.9$  stems/ft<sup>2</sup> ( $\phi = 0.0027$ ), and flexible submerged vegetation at density  $m = 25.5$  stems/ft<sup>2</sup> ( $\phi = 0.0007$ ). Photos of the emergent cylindrical rigid stems and the submerged rectangular flexible strips are provided in Figure A. 2 and Figure A. 3 of Appendix A, respectively.

### 5.1 Water Surface Profiles

Depths of uniform flow for varying flume discharges were obtained by measuring water surface profiles for multiple tailgate positions at the same value of discharge. Because the flume slope is mild, the convergence of M1 and M2 profiles near the upstream end of the flume provided a measured value of normal depth. A point gage mounted on steel rails installed above the flume side walls was used to measure water depths at one-ft intervals along the length of the flume.

Through a series of tailgate settings and water surface profile measurements, it was possible to determine the asymptote of the M1 and M2 profiles which was taken as the normal depth for a given discharge. Tailgate positions were chosen so as to find as closely as possible the asymptote and then that tailgate position which produced uniform flow (at the measured normal depth) for a given discharge was recorded for future experiments. This procedure was carried out for all the flow rates associated with each of the four vegetation cases used in the experiments. The resulting uncertainty in normal depth measured in this manner is estimated to be  $\pm 2.5\%$ .

In the case of emergent rigid vegetation of density  $m = 101.9$  stems/ft<sup>2</sup>, the flow rates chosen for the experimental plan were: 0.20, 0.25, 0.30, 0.35, 0.40, and 0.50 cfs. The water surface profiles for the flow rate of 0.30 cfs are shown in Figure 22. The water surface profile plots begin at the upstream entrance to the vegetation filter ( $x = 0.00$  ft), and finish at the downstream end of the filter ( $x = 16.00$  ft) with the flume station increasing in the downstream direction.

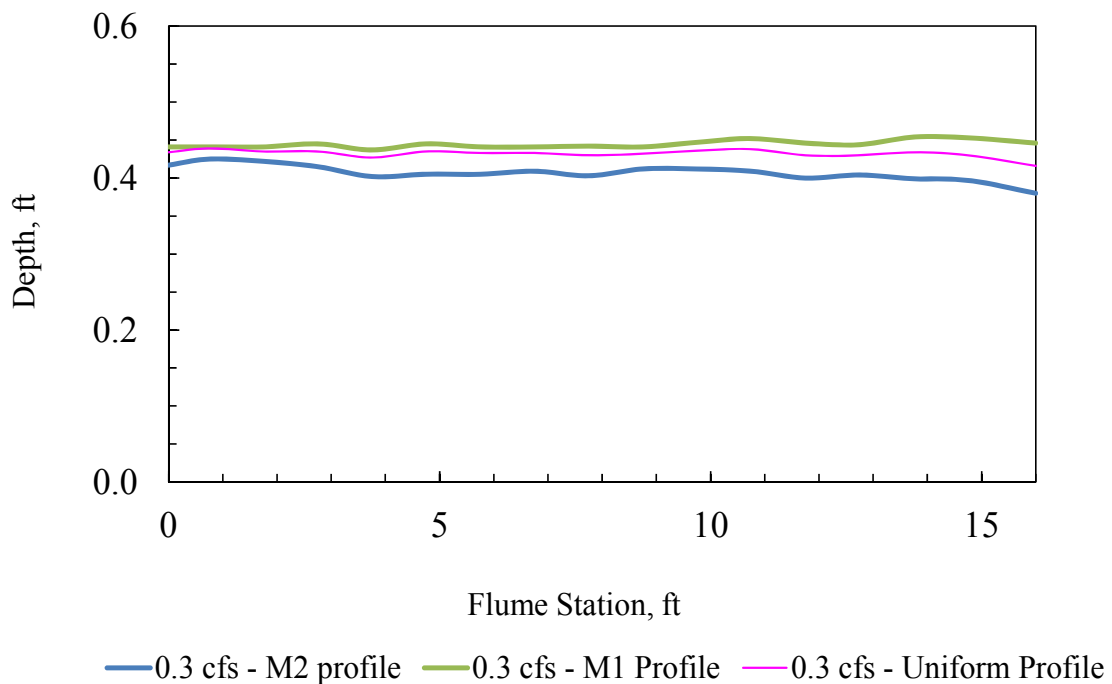


Figure 22: Water surface profiles for 0.3 cfs; normal depth is 0.43 ft.

The plots for other flow rates and for other vegetation types and densities are not shown to avoid repetition. Nevertheless, the uniform depths measured for each flow rate in each vegetation case are presented below in tabular form (Table 6), along with their stage-discharge curves (Figure 23). Flows less than 0.3 cfs were not presented for the emergent vegetation of  $m = 25.5$  stems/ft<sup>2</sup> because the normal depth observed was too

shallow, not allowing for proper ADV readings. Flows less than 0.5 cfs were not presented for the submerged vegetation of  $m = 25.5$  stems/ft<sup>2</sup> because they failed to achieve uniform flow profiles.

Table 6: The normal depths obtained for the chosen flow rates corresponding to: (a) emergent vegetation of density  $m = 101.9$  stems/ft<sup>2</sup>; (b) emergent vegetation of density  $m = 25.5$  stems/ft<sup>2</sup>; (c) submerged vegetation of density  $m = 101.9$  stems/ft<sup>2</sup>; (d) emergent vegetation of density  $m = 25.5$  stems/ft<sup>2</sup>.

(a)

Flow $Q$ , cfs	Normal Depth $y_n$ , ft
0.202	0.353
0.251	0.380
0.301	0.429
0.353	0.472
0.399	0.540
0.503	0.613

(c)

Flow $Q$ , cfs	Normal Depth $y_n$ , ft
0.200	0.281
0.249	0.290
0.299	0.297
0.354	0.308
0.402	0.332
0.500	0.350

(b)

Flow $Q$ , cfs	Normal Depth $y_n$ , ft
0.303	0.220
0.353	0.243
0.402	0.252
0.500	0.288
0.601	0.330

(d)

Flow $Q$ , cfs	Normal Depth $y_n$ , ft
0.503	0.241
0.602	0.252
0.705	0.261

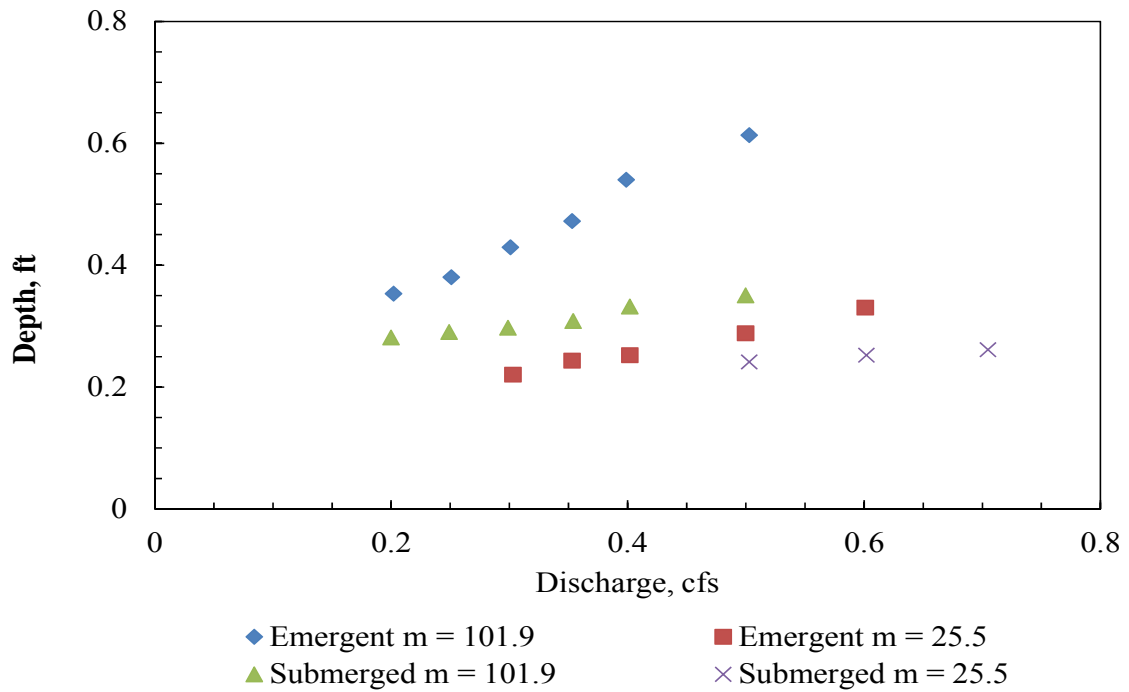


Figure 23: The stage-discharge curve for all four vegetation cases.

## 5.2 Drag Coefficient Calculation

Several methods exist for calculating the drag coefficient of a vegetative filter. This section describes three common drag calculation methods, then shows the tabulated drag coefficient data for all experiments using the James et al. (2004) method, which takes into account all forces acting on a control volume in the flume.

### Method 1 (Kouwen & FathiMaghadam, 1997):

This method equates the drag force of the vegetative filter to an apparent bed shear stress in the flume even though the drag force is primarily from drag on the stems. By definition, the Darcy-Weisbach friction factor  $f$  is:

$$f = \frac{8gRS}{U^2} \quad (75)$$

in which  $R$  = hydraulic radius and  $S$  = bed slope =  $h_f/L$  with  $h_f$  = head loss and  $L$  = flow length. In terms of the Darcy-Weisbach friction factor,  $f$ , the apparent bed shear stress is given by:

$$\tau_o = \frac{f\rho U^2}{8} \quad (76)$$

The apparent drag force is  $F_d = \tau_o bL$ , where the vegetation Area = width \* length of filter =  $b*L = 3.28 * 16 = 52.48 \text{ ft}^2$ . Now expressing the drag force on the stems in terms of the drag coefficient  $C_d$  and equating it to the apparent bed drag force, the following is obtained:

$$\frac{1}{2} \rho C_d A_p U^2 = \frac{f\rho U^2 bL}{8} \quad (77)$$

where  $A_p$  is the projected area of 5350 or 1338 stems of  $d = 1 \text{ cm}$  (0.0328 ft). In this method,  $f$  is evaluated from Equation 75 and then  $C_d$  can be determined.

Method 2 (Jarvela, 2004):

This method assumes the bed shear stress to be negligible, and uses a momentum approach to solve for the drag coefficient, excluding the total stem volume from the vegetative filter total control volume. The gravitational force of the fluid in the vegetative filter control volume (excluding the volume occupied by the stems) is equated to the drag force of the vegetative filter, assuming the apparent bed shear as negligible.

Equating  $F_d = F_g$ , where  $F_g$  is the gravitational force down the slope, and  $F_d$  is obtained from the definition of the coefficient of drag, Equation 5, the result is:

$$F_g = \gamma S \left[ \left( (bLy_n) - (N\pi y_n \frac{d^2}{4}) \right) \right] = \frac{1}{2} C_d \rho N (y_n d) U^2 \quad (78)$$

where  $N = 5350$  or  $1338$  = total number of stems in the vegetative filter strip, and the frontal area for rigid stems is  $y_n d$ , the normal depth times the stem diameter.

Method 3 (James et al., 2004):

This method was proposed by James et al. (2004). It is an all-encompassing method, in which the gravitational force of the vegetative filter control volume is equated to the sum of both the drag force of the vegetative filter and the bed shear stress. This method is used in the calculations performed on the experimental data to obtain the drag coefficients for the vegetative filter under different flow rates.

The expression for gravitational force after removing the volume occupied by the stems from the vegetative filter control volume is:

$$F_g = \gamma y_n \left( bL - \frac{N\pi d^2}{4} \right) S \quad (79)$$

and the expression of the drag force is taken from Equation 5, where  $A_p = N y_n d$ . Hence, the sum of forces is  $F_g = F_d + F_{bedshear}$ , and the shear stress can be defined as:

$$\tau_o = \left( 1 - \frac{m\pi d^2}{4} \right) \gamma y_n S - \frac{1}{2} C_d \rho m y_n d U^2 \quad (80)$$

where  $m = \frac{N}{bL}$  is the stem density per unit surface area.

James et al. (2004) assume that the bed shear stress equation in free surface flow also can be used in the case of stems, thus Equation 76 is used for  $\tau_o$ . This expression for shear stress is substituted into Equation 80 and rearranged to calculate  $C_d$ , giving the following expression for drag coefficient:

$$C_d = \frac{-\frac{f}{8}\rho U^2 + (1 - \frac{m\pi d^2}{4})\gamma y_n S}{\frac{1}{2}\rho m y_n d U^2} \quad (81)$$

in which  $f$  is understood to be the friction factor of the bed, which in the experiments reported in this thesis was a smooth sheet of PVC plastic. When calculating the drag coefficient for the rectangular strips,  $mdt_s$  is substituted for  $(m\pi d^2)/4$  in the numerator of Equation 81, where  $t_s$  is the thickness of a rectangular strip. Moreover, the deflected stem height  $k$  is used instead of  $y_n$  in Equation 5, as it provides a more accurate representation of the frontal area of the deflected stems.

Table 7 presents the values of drag coefficients from the experimental trials for each vegetation case as calculated from Equation 81. Each table shows the flow rates, bulk velocities, normal depths, drag coefficients, and stem Reynolds numbers. The Darcy-Weisbach  $f$  for the flume bed is obtained from the Moody diagram for smooth turbulent flow. It is representative of bed friction, not vegetative stem resistance. The bulk velocity is defined by  $U$ , whereas  $U_v$  designates the pore velocity after being divided by the porosity of the vegetation. If the flow volume over the vegetative filter strip is taken as the control volume, then the porosity is defined as the ratio of: the total control volume minus the volume occupied by the stems, divided by the total control volume:

$$Porosity = \left( \frac{bLy_n - Ny_n\pi\frac{d^2}{4}}{bLy_n} \right) = (1 - \phi) \quad (82)$$

The volume occupied by the submerged rectangular strips is  $NL_s dt_s$  in Equation 82, where  $L_s$  is the full length of a rectangular strip. However, the solid volume fraction  $\phi$  in this study can be approximated by  $[N/(bL)](dt_s) = md t_s$  because  $L_s/y_n \sim 1$  and  $\phi \ll 1$ .

Table 7: Tabulated results obtained at different flow rates for: (a) emergent rigid vegetation of density  $m=101.9$  stems/ft<sup>2</sup>; (b) emergent rigid vegetation of density  $m=25.5$  stems/ft<sup>2</sup>; (c) submerged flexible vegetation of density  $m=101.9$  stems/ft<sup>2</sup>; (d) submerged flexible vegetation of density  $m=101.9$  stems/ft<sup>2</sup>

(a)

$Q$ , cfs	$y_n$ (or $H$ ), ft	$U$ , ft/sec	$f$ , from Moody	$m$ , stems/ft <sup>2</sup>	porosity	$U_v$ , ft/sec	$C_d$	Stem Re	Flow Re
0.202	0.353	0.174	0.0390	101.94	0.914	0.191	3.63	480	5000
0.301	0.429	0.214	0.0330	101.94	0.914	0.234	2.41	590	7600
0.399	0.540	0.225	0.0303	101.94	0.914	0.246	2.18	620	10000
0.503	0.613	0.250	0.0270	101.94	0.914	0.274	1.76	680	12700

(b)

$Q$ , cfs	$y_n$ (or $H$ ), ft	$U$ , ft/sec	$f$ , from Moody	$m$ , stems/ft <sup>2</sup>	porosity	$U_v$ , ft/sec	$C_d$	Stem Re	Flow Re
0.303	0.220	0.420	0.0330	25.50	0.978	0.429	2.64	1150	7600
0.402	0.252	0.486	0.0303	25.50	0.978	0.497	1.97	1300	10000
0.500	0.288	0.529	0.0270	25.50	0.978	0.541	1.66	1450	12700
0.601	0.330	0.555	0.0250	25.50	0.978	0.567	1.51	1500	15300

(c)

$Q$ , cfs	$y_n$ (or $H$ ), ft	$U$ , ft/sec	$f$ , from Moody	$m$ , stems/ft <sup>2</sup>	$k$ , ft	$k/H$	porosity	$U_v$ , ft/sec	$C_d$	Stem Re	Flow Re
0.200	0.281	0.217	0.0390	101.94	0.250	0.89	0.998	0.218	2.87	600	5000
0.299	0.297	0.307	0.0330	101.94	0.245	0.83	0.998	0.308	1.54	850	7600
0.402	0.332	0.369	0.0303	101.94	0.238	0.72	0.998	0.370	1.23	1000	10000
0.500	0.350	0.436	0.0270	101.94	0.225	0.64	0.998	0.436	0.98	1200	12700

(d)

$Q$ , cfs	$y_n$ (or $H$ ), ft	$U$ , ft/sec	$f$ , from Moody	$m$ , stems/ft <sup>2</sup>	$k$ , ft	$k/H$	porosity	$U_v$ , ft/sec	$C_d$	Stem Re	Flow Re
0.503	0.241	0.636	0.0270	25.50	0.209	0.87	0.999	0.637	1.34	1700	12700
0.602	0.252	0.728	0.0250	25.50	0.205	0.81	0.999	0.729	1.08	2000	15300
0.705	0.261	0.824	0.0235	25.50	0.199	0.76	0.999	0.824	0.90	2250	18000

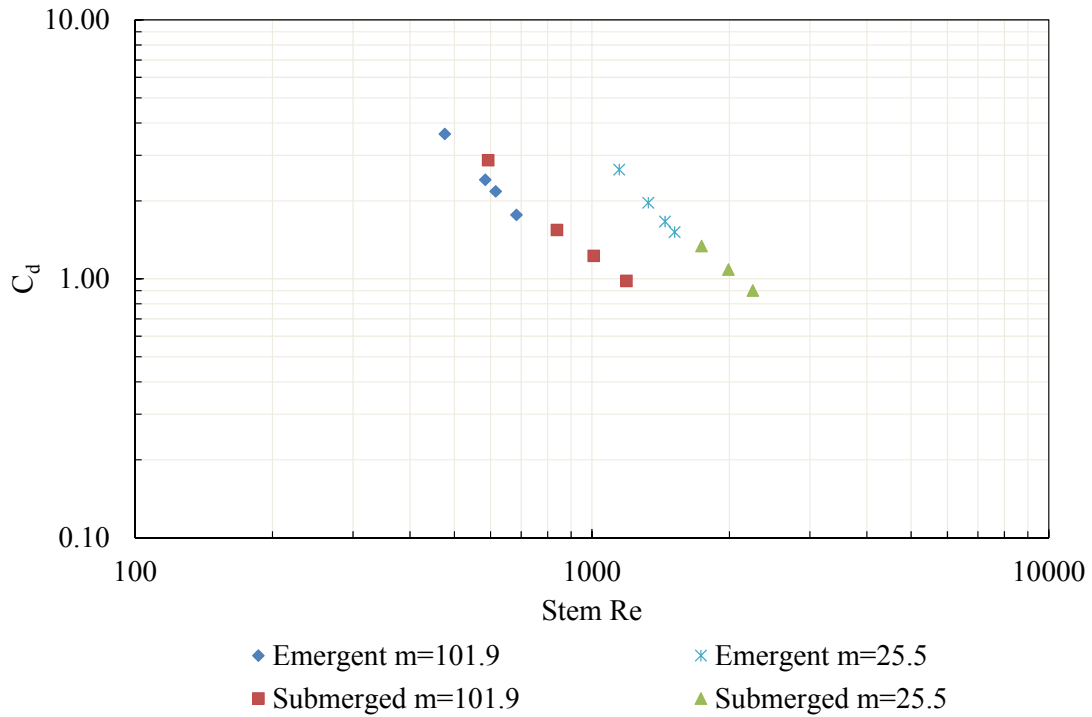


Figure 24: Drag coefficient results from the four experimental sets of vegetation plotted on the same graph against Stem Re. The experimental vegetation densities are  $m = 101.9$  stems/ft<sup>2</sup> and 25.5 stems/ft<sup>2</sup>

The results for coefficient of drag as a function of stem Reynolds number are shown in Figure 24. A decreasing negative power trend for the drag coefficient is observed for all vegetation cases as the Stem Re increases, which is consistent with previous research and literature (Tanino & Nepf, 2008). The trend power equation is  $C_d = A(\text{StemRe})^B$ , where  $A$  and  $B$  are constants. The value of  $B$  is approximately -2 for both cases of emergent rigid vegetation density, and is approximately -1.5 for both cases of submerged flexible vegetation. The change in the value of  $B$  signifies the change of the vegetation states from emergent to submerged. Thus, Stem Re is concluded to have a significant effect on drag coefficient. It is also observed that the drag coefficient trends of Figure 24 exhibit sharp decreases as Stem Re increases.

Figure 25 presents the drag coefficient data from the lab experiments plotted along with rigid emergent data from James et al. (2004) and Tanino and Nepf (2008). The range of drag coefficients is similar, and all drag coefficients exhibit a decreasing trend as the stem Reynolds number increases. The curves for multiple stems are steeper than that for a single circular cylinder of infinite length, also plotted in Figure 25, from Munson et al. (1999).

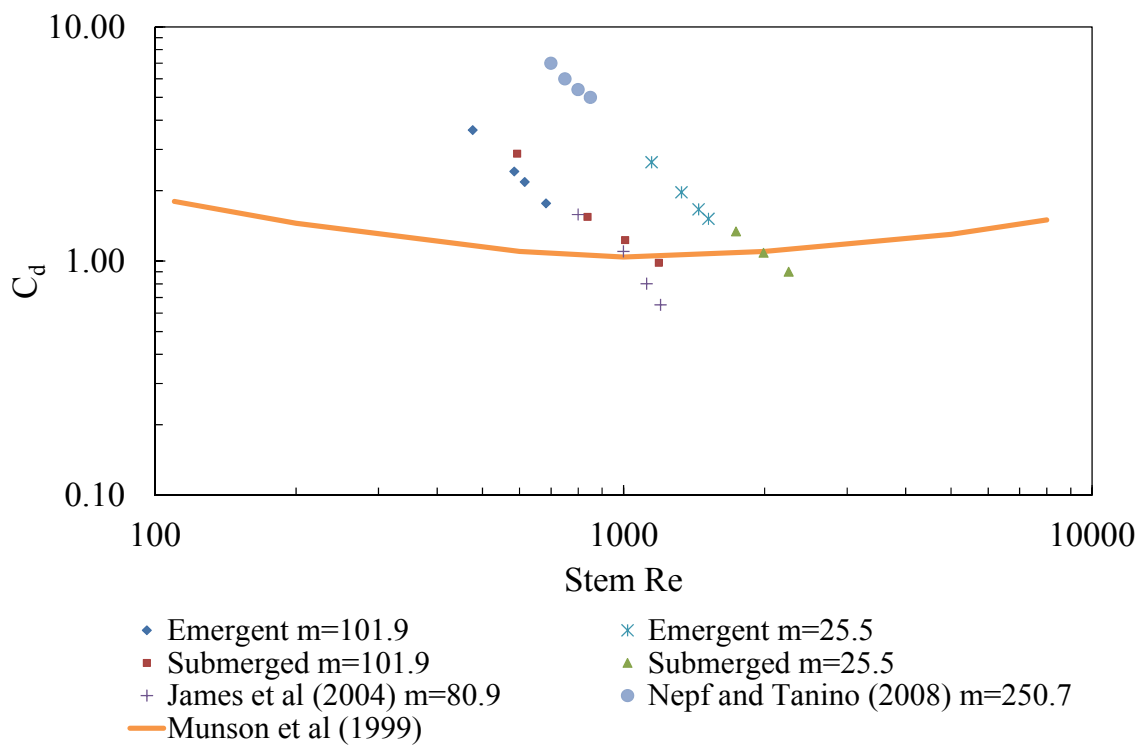


Figure 25: Experimental drag coefficient results plotted against Stem Re, with other researchers' data. The value of  $m$  in the legend represents stem density in stems/ft<sup>2</sup>

### Dimensional Analysis

Dimensional analysis is performed on the drag coefficient to evaluate the roles of the parameters affecting it. Dependence of the drag coefficient on these parameters is discussed.

The drag coefficient can be written as:

$$C_d = f(\rho, g, \mu, y_n, d, k, U, f', \phi)$$

where  $f'$  = Darcy-Weisbach friction factor of the bed due to surface resistance, obtained from Moody diagram;  $\rho$  = water density;  $g$  = gravity;  $U$  = water bulk velocity;  $d$  = stem diameter;  $y_n$  = normal depth;  $k$  = deflected submerged flexible stem height (if applicable);  $\mu$  = dynamic viscosity;  $\phi$  = solid volume fraction =  $m(\pi d^2)/4$  for the cylindrical stems, and  $mdt_s$  for the rectangular strips, where  $t_s$  is the strip thickness, and  $m = N/bL$ , where  $N$  = number of stems. Implicit in the dimensional analysis is a staggered stem pattern with equidistant spacing in the span-wise and stream-wise directions in this study of  $4.25d$  and  $8.50d$ .

Using dimensional analysis, the drag coefficient is rewritten as:

$$C_d = f\left(\frac{y_n}{d}, \frac{k}{y_n}, \text{StemRe}, F, f', \phi\right) \quad (83)$$

where Stem Re is the stem Reynolds number, and F is the flow Froude number but using  $y_n$  as the length scale.

In the following graphical comparisons, the coefficient of drag and the stem Reynolds number are defined in terms of the stem diameter  $d$  and the bulk velocity  $U$  for the length and velocity scales, respectively. Figure 26 shows the drag coefficient plotted against  $H/d$  ( $H = y_n$ ).

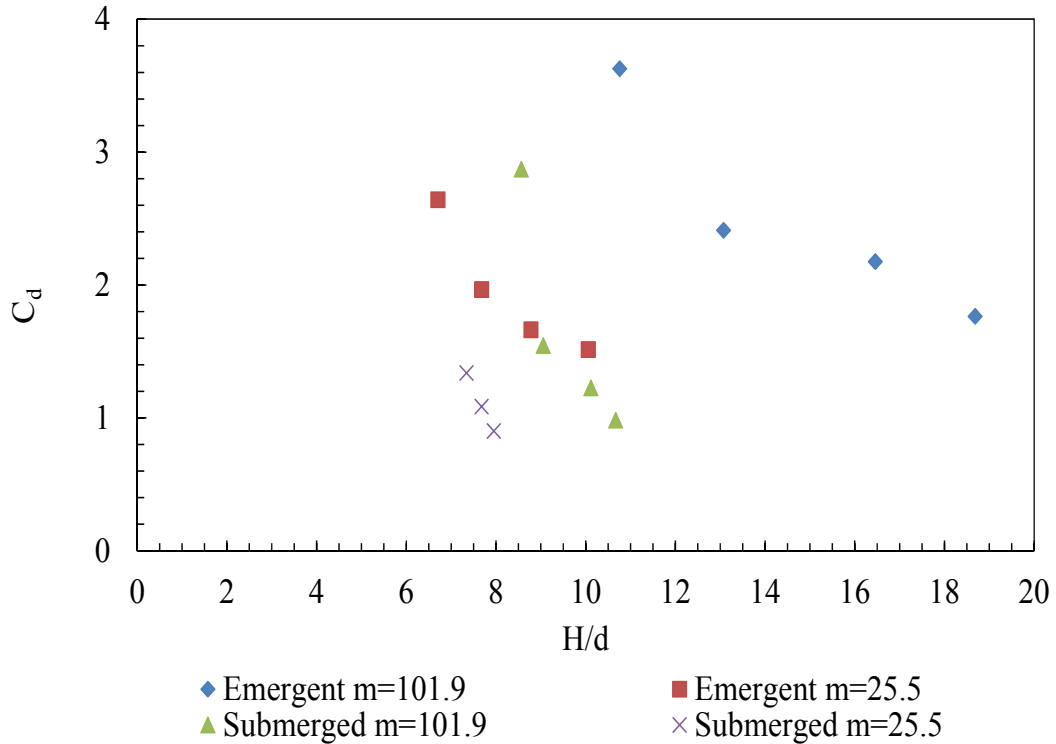


Figure 26: The drag coefficient plotted against the submergence ratio  $H/d$ , where  $H$  is the water depth ( $y_n$ ) and  $d$  is the stem diameter (cylindrical rods) or stem width (thin rectangular strips). The experimental vegetation densities are  $m = 101.9$  stems/ft<sup>2</sup> and 25.5 stems/ft<sup>2</sup>

Figure 26 shows a decreasing trend for the drag coefficient as  $H/d$  increases. For emergent rigid vegetation, the decreasing trend of drag coefficient is more gradual across the range of  $H/d$  values, as opposed to the submerged flexible vegetation case, where the decreasing trend of drag coefficient is much sharper. For all vegetation cases, it is observed that as  $H/d$  increases with an increase of flow rate, so does the bulk velocity and therefore the Stem Re.

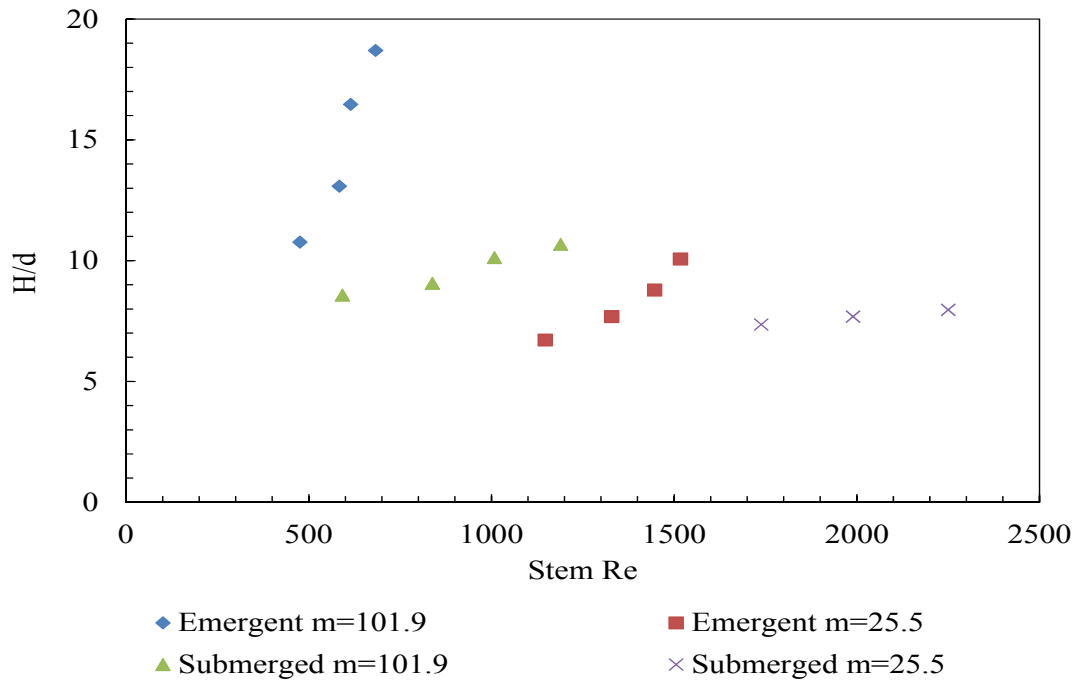


Figure 27: Submergence ratio  $H/d$  plotted against the stem Reynolds number. The experimental vegetation densities are  $m = 101.9$  stems/ft<sup>2</sup> and  $25.5$  stems/ft<sup>2</sup>

Figure 27 shows  $H/d$  displaying a sharp increasing trend across the range of Stem Re values for the emergent rigid vegetation cases, especially the case with density of 101.9. For the submerged flexible cases,  $H/d$  displays a milder increasing trend. This appears to indicate that Stem Re and  $H/d$  are nearly independent in the submerged case, while they are correlated in the emergent vegetation case. In fact, Figure 26 and Figure 27 seem to reflect the correlation between depth and bulk velocity as  $Q$  increases. In the submerged flexible vegetation case, the relative vegetation height  $k/H$  is a parameter that must be observed to determine its effect on the drag coefficient, where  $k$  is the deflected vegetation height measured from the bottom of the flume to the bent tip of the vegetation stem, and  $H$  is the normal depth of water. Figure 28 and Figure 29 present that effect graphically.

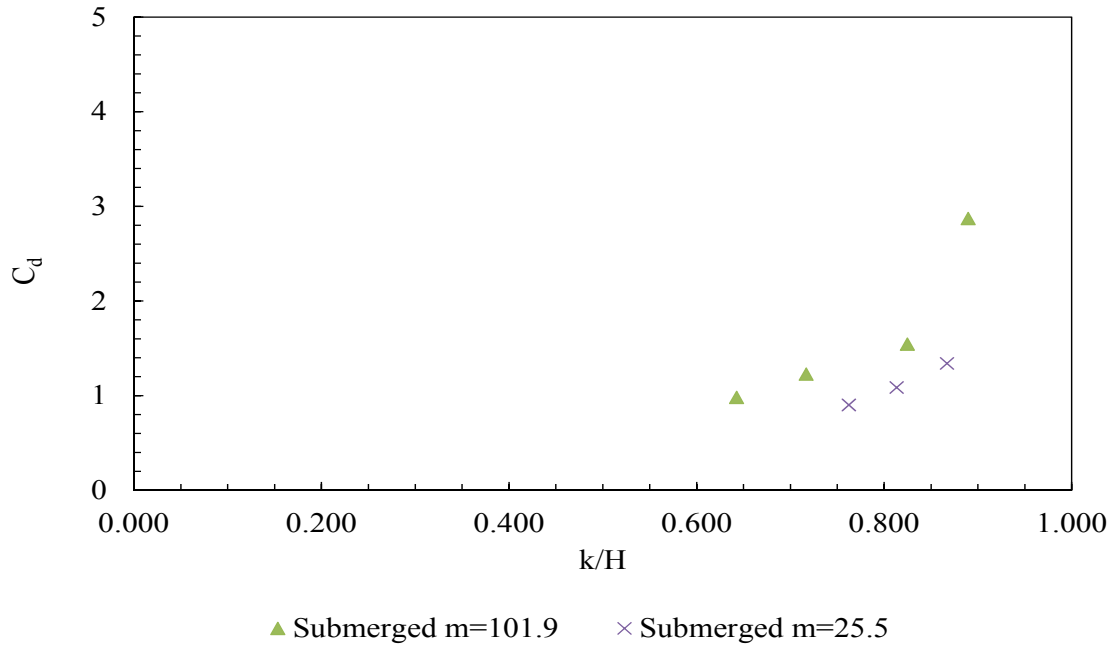


Figure 28: Drag coefficient plotted against relative vegetation height  $k/H$ . The vegetation is flexible submerged for both cases. The experimental vegetation densities are  $m = 101.9$  stems/ $\text{ft}^2$  and  $25.5$  stems/ $\text{ft}^2$

From Figure 28, it is clear that the relative vegetation height  $k/H$  has a significant effect on the drag coefficient; the drag coefficient decreases as the relative vegetation height decreases corresponding to greater submergence of the vegetation. The relative vegetation height decreases with an increase of flow rate and normal depth, corresponding to an increase in bulk velocity which is consistent with the trend shown in Figure 29 with stem Reynolds number.

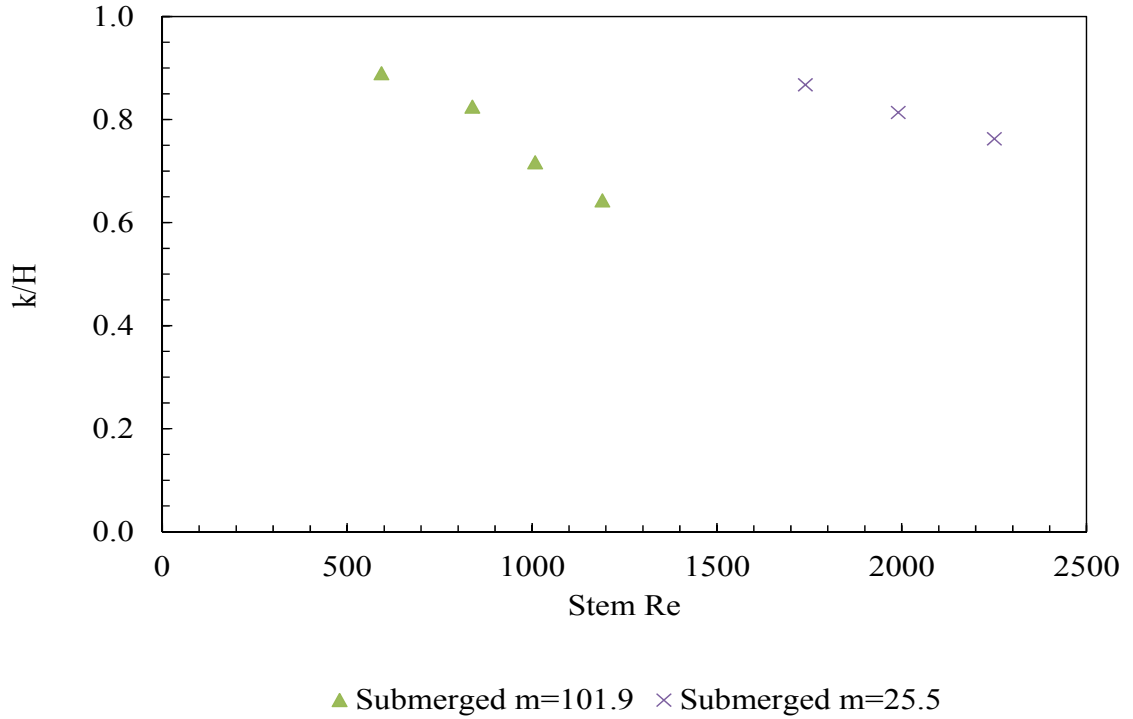


Figure 29: Relative vegetation height  $k/H$  plotted against Stem Re; the vegetation is flexible submerged for both cases. The experimental vegetation densities are  $m = 101.9$  stems/ft<sup>2</sup> and 25.5 stems/ft<sup>2</sup>

Using the Cheng and Nguyen (2011) technique discussed earlier in Chapter 2, in which the coefficient of drag and the stem Reynolds number are based on a stem hydraulic radius,  $r_v$ , and the pore velocity,  $U_v$ , Figure 30 shows a plot of drag coefficients obtained from the experiments versus the stem Reynolds numbers for both emergent and submerged cases. However, it differs from Figure 24 since the drag coefficients (termed  $C_{Dv}$ ) and stem Reynolds numbers (termed  $R_v$ ) for the experimental emergent vegetation were calculated using Equation 26 and Equation 21, respectively. Moreover, modifications were applied to those two equations when calculating  $C_{Dv}$  and  $R_v$  for the experimental submerged vegetation. Since the submerged vegetation was made of thin rectangular strips and not cylindrical stems, it was not possible to calculate the  $\phi$  value from Equation 19. Instead,  $\phi = md_t_s$  was used, where  $t_s$  is the thickness of the submerged

vegetation strips. Using the new definition of  $\phi$  for rectangular strips, the drag coefficient  $C_{Dv}$  was calculated from:

$$C_{Dv} = \frac{\left[ \frac{(2gS(1-\phi)^3)}{mdU^2} \right]}{\frac{k}{H}} \quad (84)$$

and  $R_v$  was calculated from:

$$R_v = \frac{\frac{Ud}{\nu}}{md^2} \quad (85)$$

where  $U$  is the bulk velocity,  $\nu$  is the kinematic viscosity,  $m$  is the stem density in stems/ft<sup>2</sup>,  $d$  is the stem diameter,  $S$  is the flume slope,  $g$  is gravity,  $\phi$  is the solid volume fraction,  $k$  is the deflected height of the vegetation, and  $H$  is the normal depth of flow. The coefficient of drag in Equation 84 was derived from Equation 81 after neglecting the effect of bed shear stress, and was divided by the parameter  $k/H$  to reflect the effect of submergence on the drag coefficient with respect to the frontal area of the deflected stem. The stem Reynolds number in Equation 85 was derived by using a new length scale  $l_\varepsilon$  in place of the stem diameter  $d$ , where  $l_\varepsilon$  is a length scale representation that is common in porous media flow applications, and represents the ratio of volume of voids to their flow surface area (Niven, 2002). More detail is given in Appendix B about the relationship and similarities between porous media flow and open channel flow through vegetative filters. The length scale  $l_\varepsilon$  for submerged flexible vegetation was derived as:

$$l_\varepsilon = \frac{1-\phi}{md} \quad (86)$$

Substituting  $l_\varepsilon$  into Equation 21 and using the definition of  $\phi = mdt_s$  for thin rectangular strips, Equation 85 is obtained. Using these definitions for the coefficient of drag and stem Reynolds number, it is observed that the data points for the emergent and submerged vegetation collapse onto a single relationship regardless of the vegetation density.

Figure 30 also shows a comparison of the experimental drag coefficient data and other researchers' data after the application of Equation 26 and Equation 21. The

experimental drag coefficients fall in the same range of magnitude as the data provided from the researchers, for similar ranges of stem Reynolds numbers. In addition, Figure 30 presents a plot of the empirical equation describing the relationship between  $C_{Dv}$  and  $R_v$  as provided by Cheng and Nguyen (2011):

$$C_{Dv} = \frac{50}{R_v^{0.43}} + 0.7 \left[ 1 - \exp\left(-\frac{R_v}{15000}\right) \right] \quad (87)$$

The experimental data and the data of other researchers show a good fit with the relationship of Equation 87, where all data points collapse onto the curve.

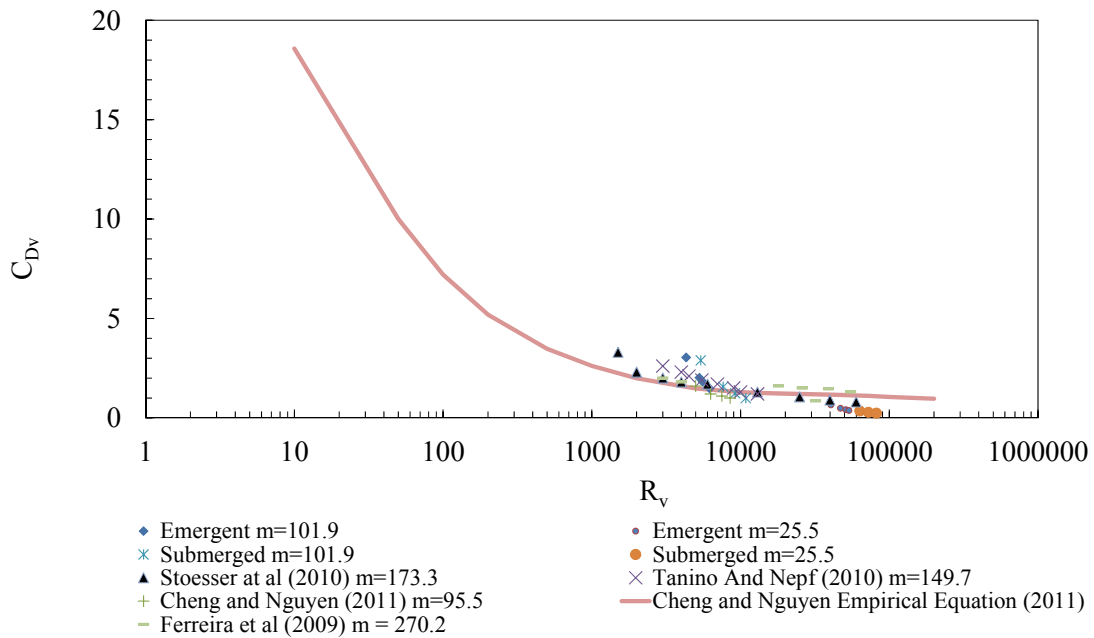


Figure 30: Comparison of drag coefficient data between the experimental emergent and submerged vegetation using the Cheng and Nguyen (2011) method, and other researchers' data subjected to the same method. The value of  $m$  in the legend represents stem density in stems/ft<sup>2</sup>

From Figure 30, it was observed that the experimental vegetated drag coefficient data ( $CD_v$ ) deviated from the empirical curve of Equation 87 depending on the value of vegetated Reynolds number ( $R_v$ ). Deviations in the drag coefficient were  $\pm 40\%$  for  $R_v$  values less than 6000 and  $\pm 5\%$  for  $R_v$  values between 6000 and 30000. Data obtained from Ferreira et al. (2009) showed a good correlation with the empirical relationship. Equation 87 was derived for a wider range of data than for the present experiments, and the left half of the curve depends on additional unpublished data by Tanino and Nepf (2010). While a new empirical curve could have been developed for the Reynolds number range of these experiments, it was decided to use Equation 87 because of its development from a larger data set.

### **5.3 ADV Point Velocity Profiles**

This section introduces the point velocity profiles and turbulence intensities measured over the water depth using an acoustic Doppler velocimeter (ADV) as described in Chapter 4. The ADV sampling rate was 25 Mhz and the sampling duration was two minutes. The ADV was inserted in the flow at specific locations across the flume width relative to the location of the vegetation stems at a longitudinal station of 10.33 ft from the flume mouth. This location is at 1/3 of the vegetative filter length, when measured from the beginning of the vegetation strip. For open channel flow over a smooth bed, Dombroski and Crimaldi (2007) reported errors of  $\pm 5\%$  in the velocity measurements in the proximity of the bed. The measured data from the ADV showed the effect of the vegetation on the flow velocity profiles inside the vegetation. Some stems had to be removed downstream of the ADV profile locations in order to provide room for the instrument. All ADV plots were normalized by bulk velocity so as to observe the relative magnitude of point velocities and turbulence intensities as affected by the stems of the vegetation.

Prior to the commencement of the point velocity measurements, a repeatability test was performed with the ADV, where the ADV sensor was placed in the vegetation-free flow immediately upstream of the vegetation filter. The objective was to verify

repeatability of the ADV data by measuring the velocity profiles and turbulence intensity profiles at different times at the same location. The test was performed twice at a flow rate of 0.3 cfs. Figure 31 presents the normalized (by bulk velocity) point velocity and streamwise turbulence intensity profiles.

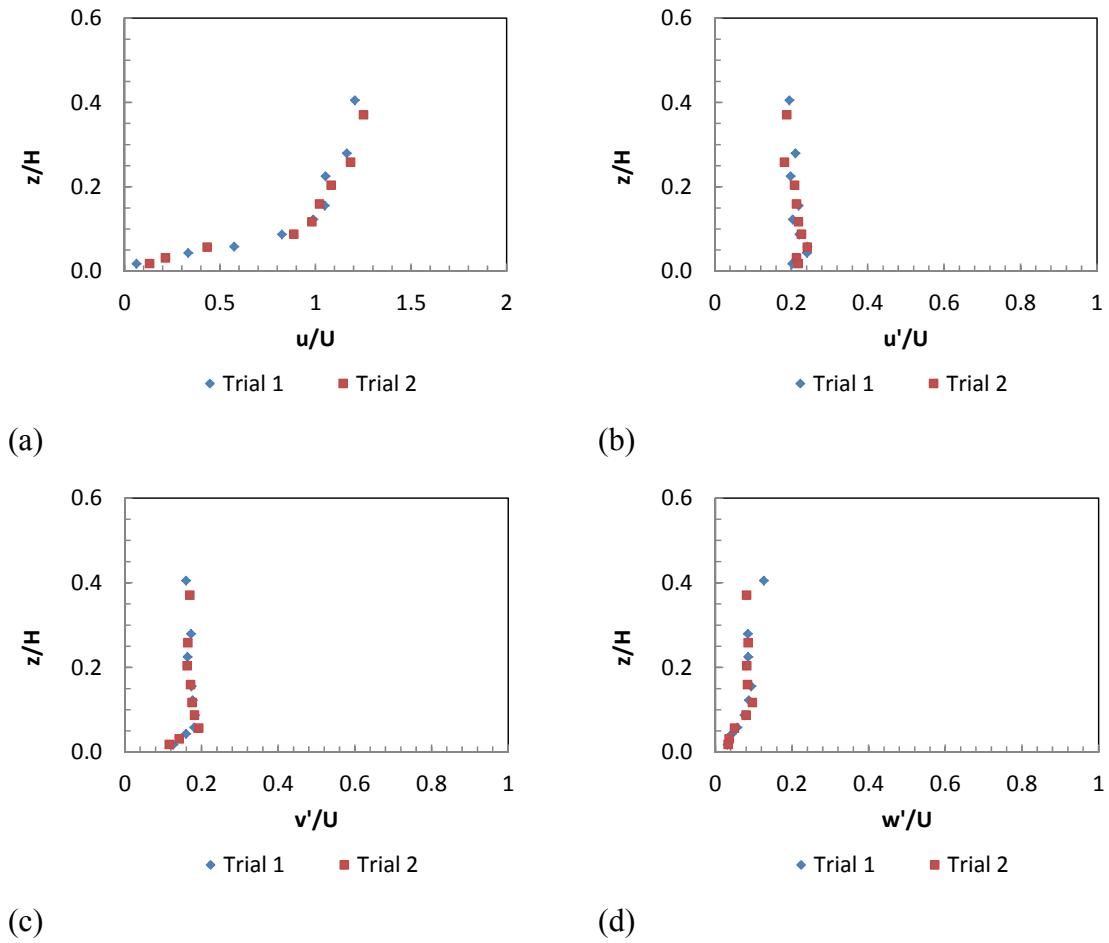


Figure 31: Normalized repeatability trial profiles to test ADV accuracy: (a) point velocity; (b) streamwise turbulence intensity; (c) spanwise turbulence intensity; (d) vertical turbulence intensity;  $Q = 0.3$  cfs,  $H =$  normal depth = 5.16 in.,  $U = 0.213$  ft/sec

From Figure 31, the ADV data demonstrate good repeatability. The turbulence intensities in all three directions are relatively uniform over the flow depth, and are significantly smaller in magnitude than those obtained from within the vegetative filter, irrespective of vegetation type and density.

### 5.3.1 Emergent Rigid Vegetation: Density $m = 101.9$ stems/ft<sup>2</sup>

To capture the full effects of vegetation on the velocity profiles, two sets of ADV measurements were performed for each flow rate. For a given flow rate, measurements were taken with the ADV sensor placed directly behind a stem, and in the free stream behind and between two stems. These two positions will be termed Location 1 and Location 2, respectively, as shown in Figure 32. The ADV was located at a distance of  $4.25d$  behind the stem for Location 1, and at  $4.25d$  behind and between two stems in the free stream for Location 2. This distance is the same as the spacing of the rows of vegetation in the flow direction.

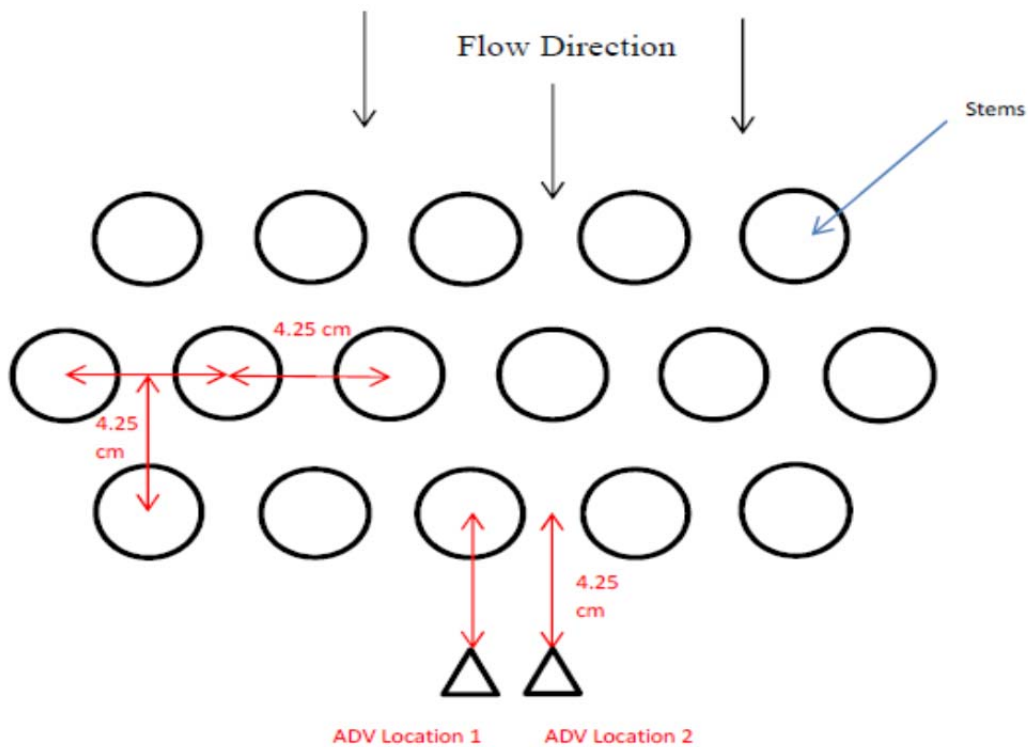


Figure 32: Schematic showing both ADV locations for vegetation density  $m = 101.9$  stems/ft<sup>2</sup>

The plots presented in Figure 33 compare the normalized point velocity and turbulence intensity profiles for a flow rate of 0.4 cfs at both ADV locations for the rigid emergent vegetation. Bulk velocity was used to normalize all the plots. The plots for the other flow rates are shown in Appendix C.

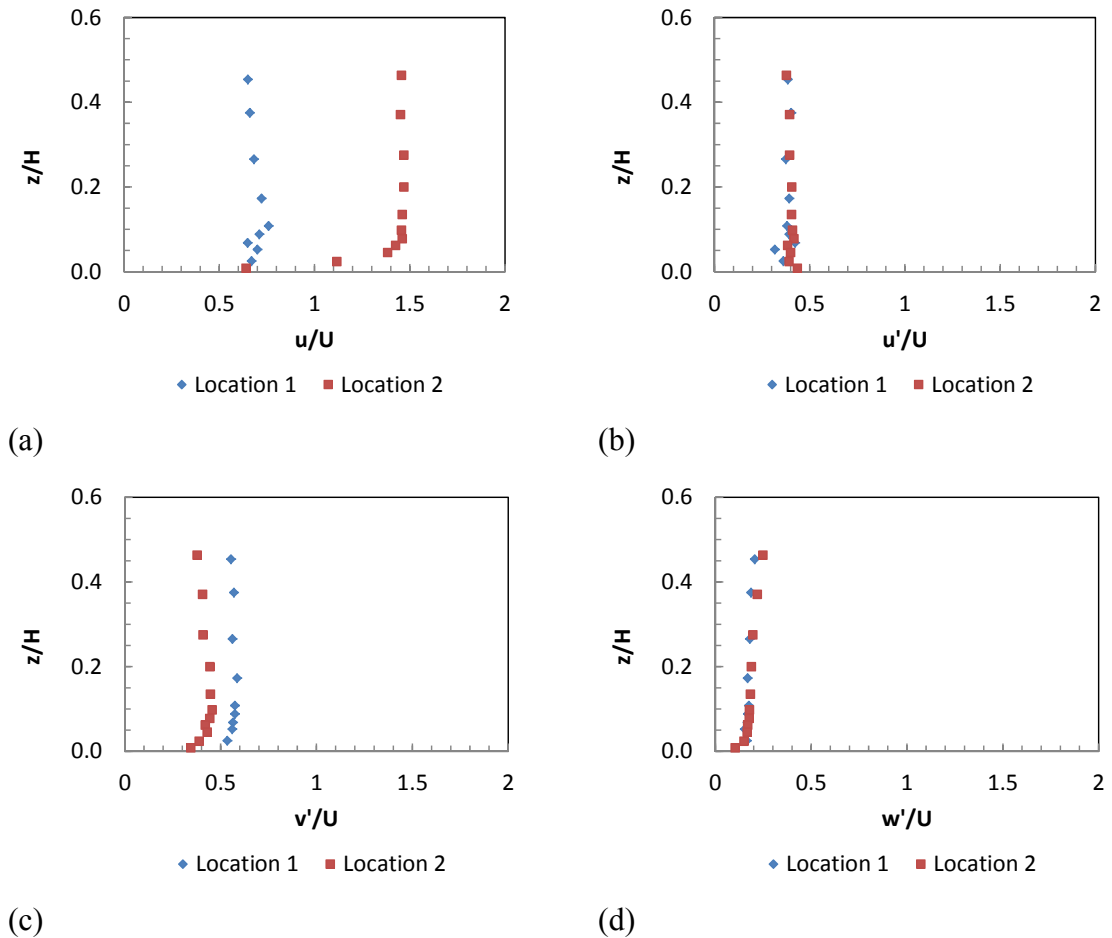


Figure 33: Normalized ADV results for: (a) point velocity; (b) streamwise turbulence intensity; (c) spanwise turbulence intensity; (d) vertical turbulence intensity; for emergent vegetation density  $m = 101.9$  stems/ft<sup>2</sup>,  $Q = 0.4$  cfs,  $H = 6.48$  in.,  $U = 0.226$  ft/sec

From Figure 33, it is evident that the velocity profiles in the streamwise flow direction (x-direction) for each flow rate at both ADV locations can be assumed to be

uniform except very close to the bed, a generalization that has been made by other researchers (Jarvela, 2005; Yang & Choi, 2010) when discussing velocity profiles in emergent vegetation. Another observation is that the point velocity values measured behind the stem (Location 1) are significantly smaller than those measured in the free stream location (Location 2). The difference in magnitude can be attributed to the wake and turbulent effects that occur just downstream of the stem. The normalized point velocity profile at Location 1 varies from 60% to 70% of the bulk velocity depending on the flow rate, while the velocity in the free stream region (Location 2) is almost 150% of the bulk velocity for all flow rates. This difference in velocities can be attributed to the high density of the vegetation, that allows for jet-like flow passing between two stems just upstream of Location 2, while a wake is identified immediately downstream of a stem (Liu et al., 2008; Stoesser et al., 2010).

All velocity profiles at Location 1 showed a velocity bulge near the flume bed, irrespective of flow rate magnitude. According to Liu et al. (2008), the velocity bulge is probably caused by a horseshoe or junction vortex that formed at the bed directly downstream of the vegetative stem. However, Stoesser et al. (2010) showed that the bulge is a result of the prevailing secondary flow entraining high momentum fluid into the wake near the bed. The velocity profiles in the free stream location (Location 2) did not exhibit this kind of velocity bulge in support of the hypothesis of Stoesser et al. (2010).

For all flow rates, the turbulence intensity plots as in Figure 33 show that the spanwise turbulence intensity,  $v'$ , has a larger magnitude in the wake at Location 1 than in the free stream at Location 2 due to the effects of the turbulent eddies shedding from a stem. The measured values of  $u'$  are almost identical between Locations 1 and 2 and are relatively uniform over the depth as are the profiles of vertical turbulence intensity. The overall picture created by Figure 33 is a wake-dominated flow in the horizontal plane with almost no variation in the vertical coordinate.

### 5.3.2 Emergent Rigid Vegetation: Density $m = 25.5$ stems/ft<sup>2</sup>

In this case, four sets of measurements were performed for each flow rate. For a given flow rate, measurements were taken with the ADV sensor placed directly behind a stem (two locations), and in the free stream behind and between two stems (two locations). These four positions will be termed Locations 1 through 4, as shown in Figure 34. For Locations 1 and 2, the ADV was located at a distance of  $4.25d$  behind the stem and at  $4.25d$  behind and between two stems in the free stream, respectively, midway between two rows. For Locations 3 and 4, the ADV was located at  $8.5d$  behind the stem and at  $8.5d$  behind and between two stems in the free stream, respectively, at the location of the next row of stems.

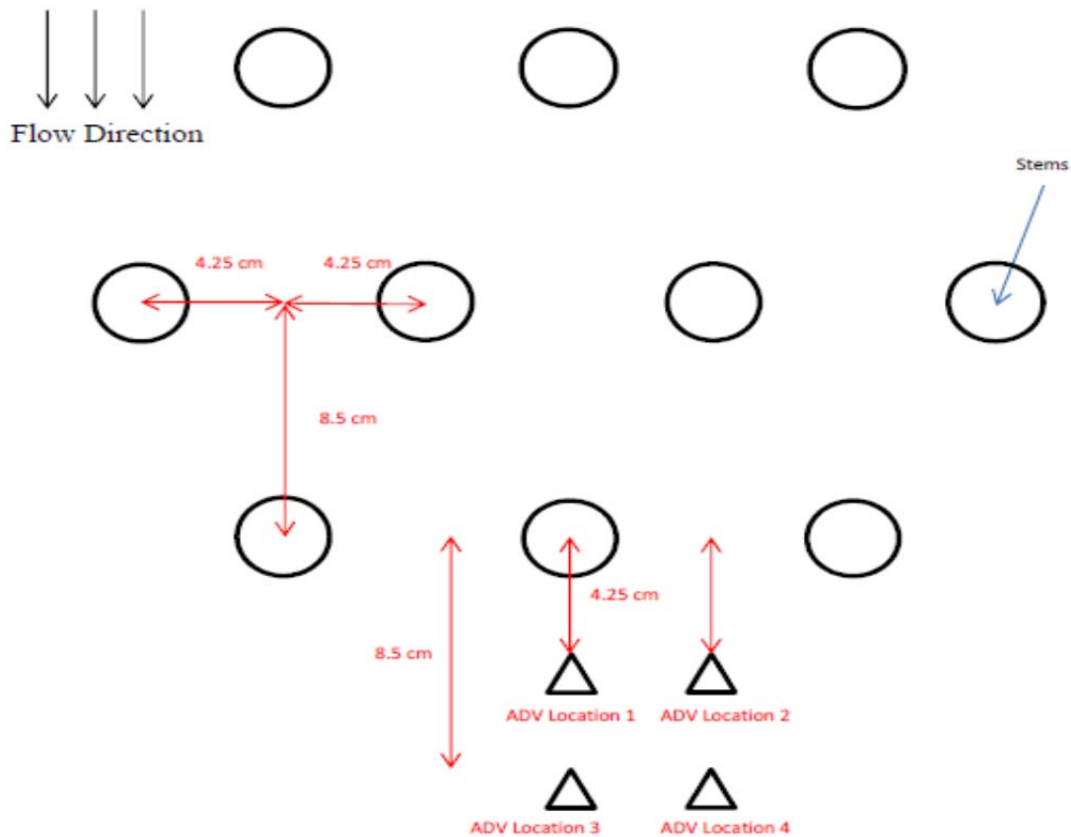


Figure 34: Schematic showing all four ADV locations for vegetation density  $m = 25.5$  stems/ft<sup>2</sup>

The plots presented in Figure 35 compare the normalized point velocity and turbulence intensity profiles for a flow rate of 0.4 cfs at all four ADV locations for the rigid emergent vegetation. Bulk velocity was used to normalize all the plots. The plots for the other flow rates are shown in Appendix C.

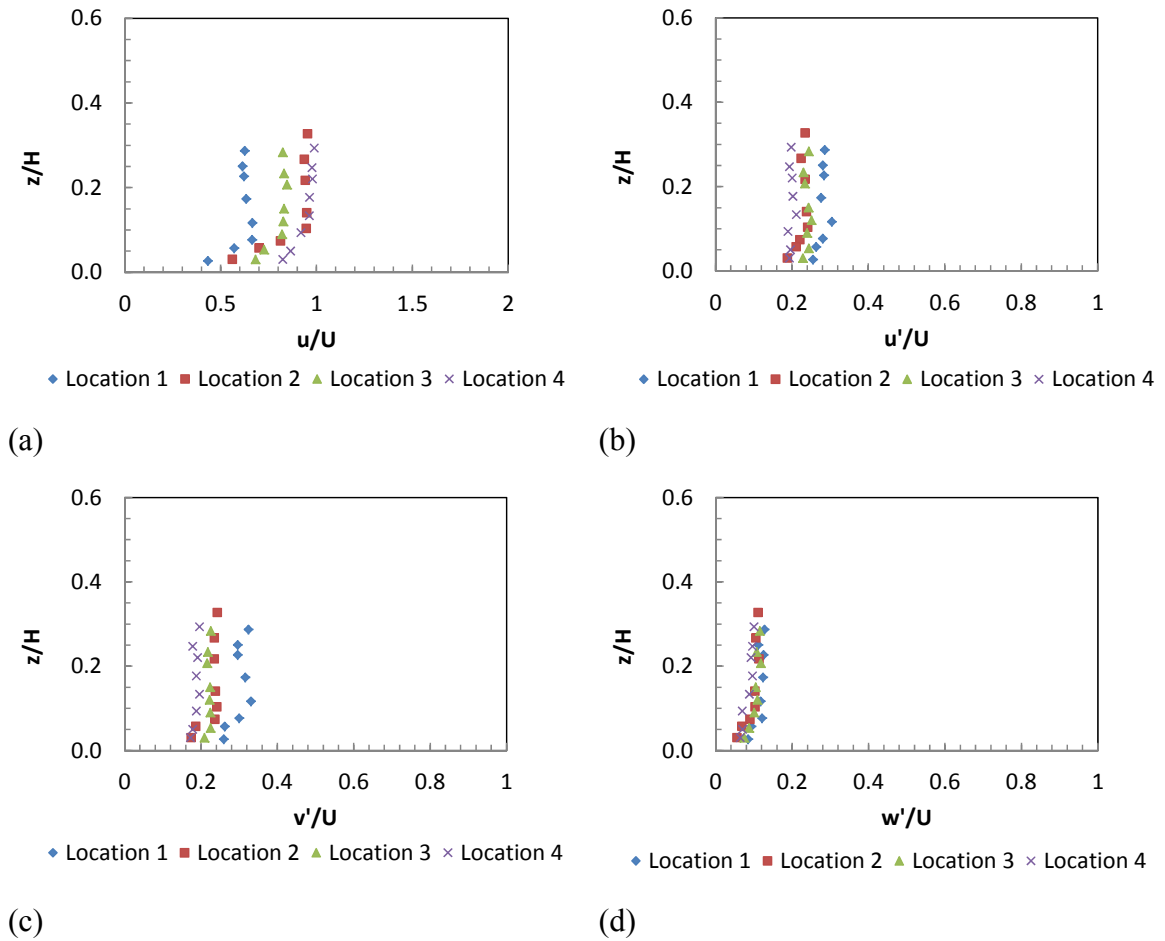


Figure 35: Normalized ADV results for: (a) point velocity; (b) streamwise turbulence intensity; (c) spanwise turbulence intensity; (d) vertical turbulence intensity; for emergent vegetation density  $m = 25.5$  stems/ft<sup>2</sup>,  $Q = 0.4$  cfs,  $H = 3.00$  in.,  $U = 0.49$  ft/sec

From Figure 35, it can be observed that the velocity profiles are nearly uniform in the vertical direction, but the velocity deficit between “wake” and “free stream” locations

is less for this lower stem density ( $m = 25.5$  stems/ft<sup>2</sup>) as compared with Figure 33 ( $m = 101.9$  stems/ft<sup>2</sup>). At locations 3 and 4, behind the stem and between stems, respectively, the streamwise velocity increases from Location 1 to 3 while it remains about the same from Location 2 to Location 4 as the wake deficit begins to mix with the jet flow in the streamwise direction.

The normalized point velocity profiles at Location 1 showed magnitudes between 70% to 80% of the bulk velocity, while the profiles at Location 3 showed magnitudes of 80% to 90% of the bulk velocity, depending on the flow rate magnitude. On the other hand, for the point velocity profiles in the free stream, the velocity profiles at Location 2 were 100% to 110% of the bulk velocity magnitude, while they were 100% of the bulk velocity magnitude at Location 4. The point velocity profiles at Location 1 exhibited a velocity spike near the flume bed for all flow rates, as was observed previously with emergent vegetation of density  $m = 101.9$  stems/ft<sup>2</sup>. It should be noted, however, that the velocity spike observed in the emergent vegetation case of density  $m = 25.5$  stems/ft<sup>2</sup> at Location 1 was more pronounced than its counterpart in emergent vegetation of density  $m = 101.9$  stems/ft<sup>2</sup>, indicating that lower vegetation density had a significant role in increasing the magnitude of the velocity spike.

For all flow rates, the turbulence intensity plots showed that the streamwise and spanwise turbulence intensities,  $u'$  and  $v'$  respectively, had larger magnitudes at Location 1 than the other three locations. The effects of turbulent eddy shedding were more predominant at Location 1 than the other three locations, allowing for larger turbulence intensity magnitudes. In addition, at any of the four ADV locations, it was observed that the 0.3 cfs flow rate had the largest streamwise and spanwise relative turbulence intensity magnitudes, and the 0.6 cfs flow rate had the lowest. This was mostly evident for Location 1, and least evident for Location 4, where eddy shedding effects on the turbulence intensity values were very minimal. Moreover, the streamwise and spanwise normalized turbulence intensity profiles at all four ADV locations were uniform in the vertical direction.

The turbulence intensity in the  $z$ -direction,  $w'$ , exhibited turbulence profiles that were identical in magnitude for Locations 2, 3, and 4, irrespective of the flow rate. The  $w'$  profile magnitudes at Location 1 were slightly larger than those at the other three locations, but that was to be expected since turbulence was at its highest at Location 1. Nonetheless, it could be concluded that location in the vegetative strip had no significant effect on the vertical turbulence intensity profiles. The profiles exhibited a high degree of uniformity from the bed to the free surface. The values of  $w'$  at any flow rate and at any ADV measuring location were significantly smaller than those of  $u'$  and  $v'$ . When comparing the magnitudes of turbulence intensity in all three directions, the magnitudes were all less for the lower stem density in Figure 35.

### **5.3.3 Submerged Flexible Vegetation: Density $m = 101.9$ stems/ft<sup>2</sup>**

Two sets of measurements were performed for each flow rate. For a given flow rate, measurements were taken with the ADV sensor placed directly behind a stem, and in the free stream behind and between two stems. These two positions were termed Location 1 and Location 2, respectively. The ADV was located at  $4.25d$  behind the stem for Location 1, and at  $4.25d$  behind and between two stems in the free stream for Location 2. This arrangement is identical to the one shown in Figure 32 for emergent vegetation with  $m = 101.9$  stems/ft<sup>2</sup>.

The plots presented in Figure 36 compare the normalized point velocity and turbulence intensity profiles for a flow rate of 0.4 cfs at both ADV locations for the flexible submerged vegetation. Bulk velocity was used to normalize all the plots. The plots for the other flow rates are shown in Appendix C.

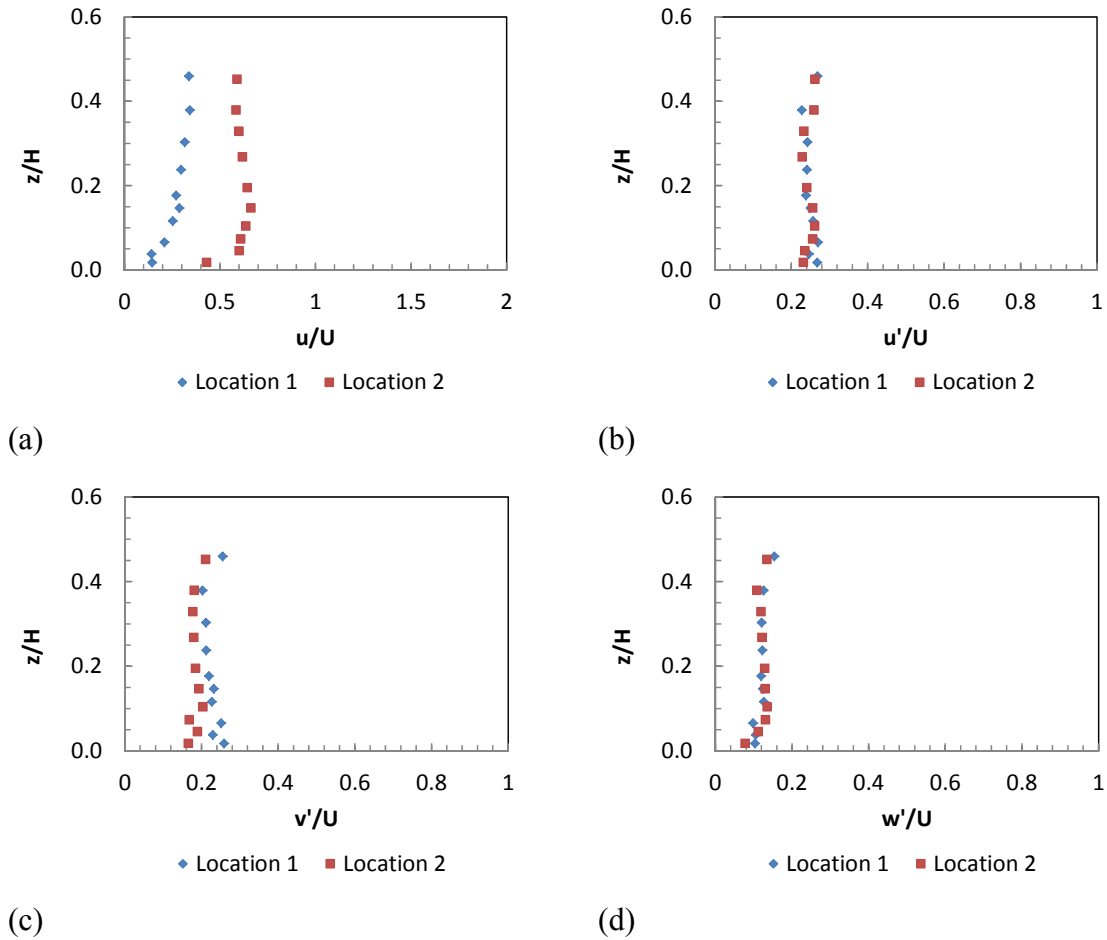


Figure 36: Normalized ADV results for: (a) point velocity; (b) streamwise turbulence intensity; (c) spanwise turbulence intensity; (d) vertical turbulence intensity; for submerged vegetation density  $m = 101.9$  stems/ft<sup>2</sup>,  $Q = 0.4$  cfs,  $H = 3.96$  in.,  $U = 0.37$  ft/sec

It was evident from Figure 36 that the velocity profiles in the streamwise flume direction (x-direction) for each flow rate at both locations can be assumed to be uniform within the stem layer. As  $z/H$  increased, the point velocity measurements assumed almost identical magnitudes, validating the assumption of uniform velocity profiles in submerged vegetation flow within the stem layer mentioned in previous literature (Cheng & Nguyen, 2011). It should be noted, however, that the magnitudes of the point velocity profiles for the 0.2 cfs flow rate at both locations were significantly larger than the other three flow rates. This could be attributed to the fact that the vegetation was barely

submerged when uniform flow was achieved for the 0.2 cfs flow rate, which may have caused the vegetation to exhibit emergent vegetation properties.

For any flow rate, it was observed that the point velocity magnitudes at Location 1 were significantly smaller than those at Location 2. This was attributed to the wake and turbulent effects at Location 1.

The normalized point velocity profiles at Location 1 exhibited magnitudes varying between 30% to 40% of the bulk velocity for the range of 0.3 cfs to 0.5 cfs. This percentage decreased as the flow rate increased. The 0.2 cfs profile achieved 80% of the bulk velocity magnitude, attributed to the fact that the vegetation exhibited emergent vegetation properties at that flow rate. At Location 2, those magnitudes ranged from 60% to 80% of the bulk velocity for the range of 0.3 cfs to 0.5 cfs as a result of a significant portion of the flow being transported in the region above the submerged stems. The 0.2 cfs flow rate case achieved 120% of the bulk velocity magnitudes at Location 2, similar to emergent vegetation properties with the same density. Compared to emergent vegetation of the same density, and excluding the 0.2 cfs flow rate case, these observations show how the turbulence and wake effects have significantly larger effects in terms of inducing a lag effect on the velocity profiles, where the normalized point velocity profiles did not achieve magnitudes greater or equal to 100%.

For all flow rates, it was observed that the streamwise and spanwise turbulence intensities,  $u'$  and  $v'$  respectively, had larger magnitudes in the location downstream of the vegetative stem (Location 1) than in the free stream location (Location 2). That was caused by the effects of the eddy turbulence shedding from a stem, as explained in the previous subsections. The magnitudes of  $u'$  and  $v'$  measured were larger in Location 1 than in Location 2, indicating that the shedding of turbulent eddies was larger behind a stem than in the free stream region, and caused an increase in turbulence intensity. The  $u'$  and  $v'$  profiles were also observed to decrease in magnitude as the flow rate increased. The larger flow depth associated with larger flow rates caused a reduction in the turbulent effects of the vegetative stems as measured by the streamwise and spanwise turbulence

intensities. At both locations, the streamwise and spanwise normalized turbulence intensity profiles were observed to be uniform in the vertical direction.

For all flow rates, the turbulence intensity in the  $z$ -direction,  $w'$ , exhibited profiles that were uniform in the stem layer, at both locations. For a given flow rate, the magnitude of the  $w'$  profiles was almost identical between Location 1 and Location 2. Hence, location in the vegetative strip had no significant effect on the vertical turbulence intensity profiles. The  $w'$  profiles were observed to be uniform from the bed to the free surface. Moreover, they were smaller in magnitude than the  $u'$  and  $v'$  magnitudes at both locations, irrespective of flow rate magnitude. This implied that the effects of turbulence in the  $z$ -direction were much smaller on flow velocity profiles, drag, and suspended sediment settling, when compared to the streamwise and spanwise turbulence effects.

#### **5.3.4 Submerged Flexible Vegetation: Density $m = 25.5$ stems/ft<sup>2</sup>**

In this case, four sets of measurements were performed for each flow rate. For a given flow rate, measurements were taken with the ADV sensor placed directly behind a stem (two locations), and in the free stream behind and between two stems (two locations). Those four positions will be termed Locations 1 through 4 as defined previously in Figure 34.

The plots presented in Figure 37 compare the normalized point velocity and turbulence intensity profiles for a flow rate of 0.6 cfs at all four ADV locations for the flexible submerged vegetation. Bulk velocity was used to normalize all the plots. The plots for the other flow rates are shown in Appendix C.

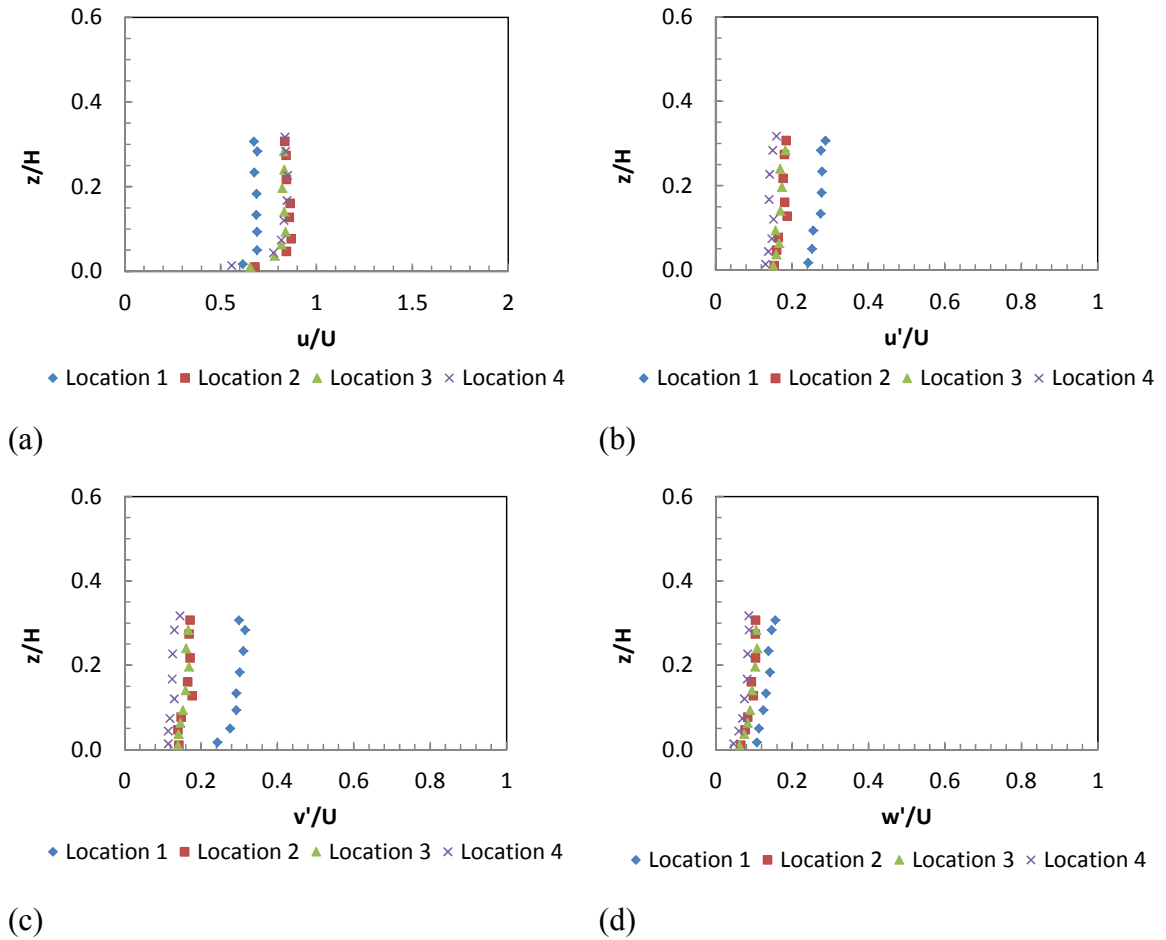


Figure 37 Normalized ADV results for: (a) point velocity; (b) streamwise turbulence intensity; (c) spanwise turbulence intensity; (d) vertical turbulence intensity; for submerged vegetation density  $m = 25.5$  stems/ft<sup>2</sup>,  $Q = 0.6$  cfs,  $H = 3$  in.,  $U = 0.732$  ft/sec

It was evident from Figure 37 that the velocity profiles in the streamwise flume direction (x-direction) for each flow rate at all locations could be assumed to be uniform within the stem layer. As  $z/H$  increased, the point velocity measurements assumed almost identical magnitudes, validating the assumption of uniformity for velocity profiles within the stem layer (Cheng & Nguyen, 2011).

The point velocity profiles at Location 1 exhibited magnitudes varying between 50% to 80% of the bulk velocity, with the 80% being at the lowest flow rate of 0.5 cfs.

At Location 2, those magnitudes ranged between 80% to 100%. At Locations 3 and 4, those magnitudes ranged between 70% to 90%, with the highest percentages observed at the lowest flow rate of 0.5 cfs. These observations indicated that the turbulence and wake effects had relatively smaller lag effects on the velocity profiles as the ADV location moved downstream. The point velocity magnitudes at Locations 1 and 2, when compared to the same locations for submerged vegetation of density  $m = 101.9$  stems/ft<sup>2</sup>, were larger, indicating that the turbulence and wake lag effects decrease as vegetation density decreases. However, the relative point velocity magnitudes were smaller when compared to emergent vegetation of the same density due to a portion of the flow being carried above the submerged vegetation.

For all flow rates, it was observed that the streamwise and spanwise turbulence intensities,  $u'$  and  $v'$  respectively, had the highest magnitudes at Location 1. Locations 2, 3, and 4 exhibited streamwise and spanwise turbulence intensity profiles that were similar in magnitude to each other but less than for the submerged vegetation of higher density. In contrast to the higher density submerged vegetation for which streamwise and spanwise turbulence intensities were nearly the same at Locations 1 and 2, the values at Location 2 as well as at Locations 3 and 4 were all less than at Location 1 and similar to each other. It appears that the lateral nonuniformity in turbulence due to the wake does not extend all the way to Locations 3 and 4 for the less dense submerged vegetation. Variability of the turbulence intensities was removed by mixing at Locations 3 and 4. This recovery of the velocity deficit at Locations 3 and 4 was also observed for the low density rigid vegetation although it was perhaps not quite as pronounced.

For all flow rates, the turbulence intensity in the  $z$ -direction,  $w'$ , exhibited uniform profiles within the stem layer at all four locations as in all other cases except that Location 1 had a slightly larger magnitude than the other three locations. Locations 2, 3, and 4 exhibited very similar values to each other and had values similar to all other cases.

In summary, the presence of vegetation increases drag and flow depth, leading to a decrease in flow bulk velocity, which allows for suspended sediment settling out of the flow. The upstream lateral velocity profile approaching a single stem is fairly uniform.

However, it loses its uniformity immediately downstream of a stem and gradually regains as it moves further downstream of a stem. Velocity values have negative measurements immediately behind a cylinder, and a highly turbulent wake is formed directly downstream of a cylinder due to the low pressure region caused by boundary layer separation. Hence, velocity drops immediately downstream of a stem and follows a non-smooth oscillatory line until it reaches the edge of the wake, where it becomes equal to the free stream velocity (Kundu & Cohen, 2004). The wake is not fully formed yet at a location immediately downstream of a stem, exhibiting high turbulence intensity values in that region. The velocity defect in the wake causes suspended sediment to settle in the wake region. Moving further downstream away from the stem, the wake becomes fully formed and the turbulence intensity magnitude and variability decreases as the wake undergoes complete mixing. What is seen from the ADV turbulence intensity measurements at a location of  $4.25d$  downstream from the stem is wake interference in the vegetation of density  $m = 101.9$  stems/ft<sup>2</sup>. The wake of each stem is not fully formed and interferes with the wakes of the stems adjacent to it. This in turn provides a wake dominated flow in the horizontal plane which is relatively uniform over the depth, and it has a large effect on increasing the vegetative filter trapping efficiency and allowing more suspended sediment to settle out of the flow. For the vegetation of density  $m = 25.5$  stems/ft<sup>2</sup>, the ADV measurements show less turbulence at a distance of  $8.5d$  downstream from the stems, implying that the lateral non-uniformity of turbulence does not extend to those locations, where the wake was subjected to complete mixing with no wake interference from the adjacent stems. The result is lower turbulence intensity magnitudes when compared to the turbulence intensity measurements at  $4.25d$  downstream of a stem for the same vegetation density, that have a lesser effect on suspended sediment settling.

#### **5.4 Suspended Sediment Concentration Profiles**

This section presents the suspended sediment concentration data from the experimental trials. In addition, it presents plots exhibiting the longitudinal changes in suspended sediment concentration through the vegetation filter, plus the trap efficiencies

for each vegetation type at different densities. However, it was essential to initially verify that the flume setup satisfied mass continuity. The mass continuity equation was checked to verify that the sediment mass settled in the vegetation filter was the difference between the mass entering and the mass leaving the filter. The mass flow rate into the flume is equal to the mass flow rate out of the flume, expressed by:

$$QC_{in}\Delta t = QC_{out}\Delta t + M_{settled} \quad (88)$$

where  $Q$  is the flow rate into the flume,  $C_{in}$  and  $C_{out}$  are respectively the suspended sediment concentrations entering and exiting the flume, and  $M_{settled}$  is the mass of sediment that settled out of the flow onto the vegetative filter bed. The time duration of the experiment is denoted by  $\Delta t$ . Hence, Equation 88 was rewritten as:

$$M_{settled} = M_{in} - M_{out} \quad (89)$$

where the mass of settled sediment in the vegetative filter was equal to the difference between the mass entering and exiting the filter during the experiment. The vegetation chosen for the mass continuity verification experiment was the emergent vegetation of density  $m = 101.9$  stems/ft<sup>2</sup>.

The flume was run at a flow of 0.3 cfs, while sediment was injected through the feeding apparatus. The ISCO sampler was used to obtain samples of the suspended sediment concentration flowing in and out of the vegetation filter. The initial suspended sediment concentration entering the vegetation filter was 65 mg/l, while the concentration leaving was 20 mg/l. After obtaining the relevant suspended sediment concentrations, the sediment fluxes in and out of the filter were calculated using the following equation, similar to Equation 74:

$$Q_s = b \int_a^{y_n} u.C.dz \quad (90)$$

where  $Q_s$  is the sediment flux,  $b$  is the flume width,  $u$  is the point velocity at a certain depth  $z$ , and  $C$  is the concentration at that depth as well. The sediment fluxes were then

multiplied by the time duration of the experiment to obtain the sediment mass going in and out of the filter, and consequently the mass of settled sediment onto the filter bed.

The verification experiment was repeated twice, with the flume bed left to dry after both experiments were concluded. Once the flume bed was dry, sediment was scraped off the vegetative filter bed and collected, oven-dried, and weighed. In the first experiment, the sediment mass entering the vegetation was calculated to be 352 g and the mass exiting was 120.5 g, leaving a settled mass of 231.5 g. The mass scraped off and obtained from the filter bed was 227 g, which was a 2% error (4.5 grams) compared to the difference between input and output fluxes. In the second experiment, the sediment mass entering the vegetation was calculated to be 343.9 g and the mass exiting was 118.3 g, leaving a settled mass of 225.6 g. The mass scraped off and obtained from the filter bed was 222.5 g, which is a 1.4% error (3.1 grams) compared to the difference between input and output fluxes. Hence, the experimental results satisfied mass continuity.

To verify repeatability and to validate that the flume flow is in steady-state flow, it was shown that the concentration of suspended sediment at a specific streamwise flume station did not change with time. Seven sediment samples were obtained using the ISCO at the  $x = 5.33$  ft station in the vegetative filter, at mid-depth. The flow rate used for this repeatability test was 0.4 cfs. The data are presented in Figure 38. It is evident from Figure 38 that the experimental setup provided satisfactory storage and sedimentation in the receiving tank to avoid recirculation of any of the sediment being fed into the flume. Thus it can be concluded that the suspended sediment concentration at a particular station in the vegetative filter does not vary with time during the experimental trials.

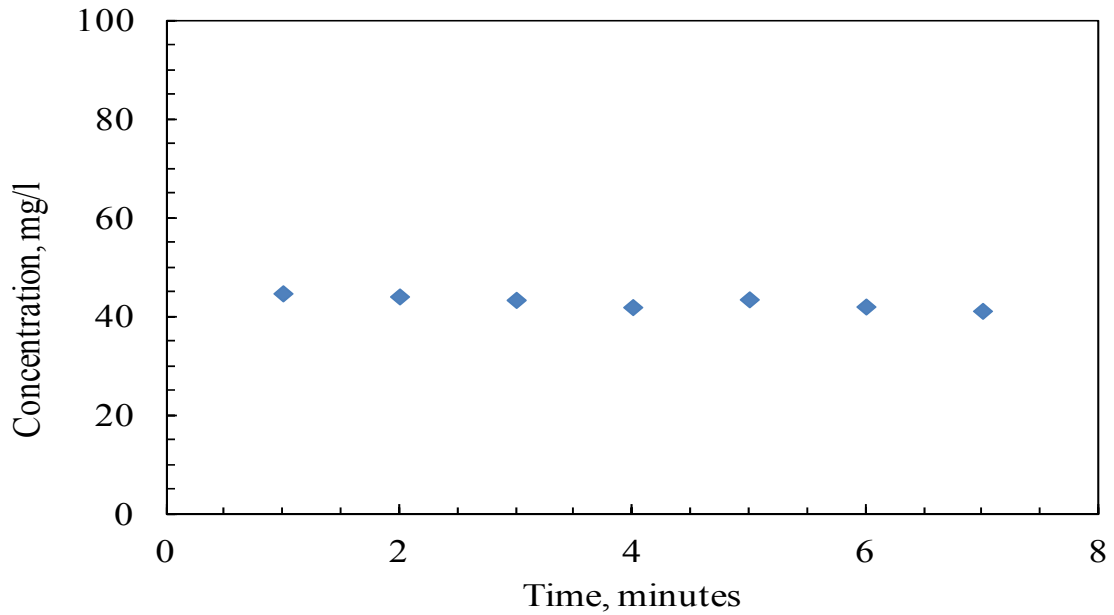


Figure 38: Concentration data points for the repeatability test, plotted against time

#### 5.4.1 Emergent Rigid Vegetation with Density $m = 101.9 \text{ stems/ft}^2$

Figure 39 presents the streamwise concentration profiles through the vegetative filter from the four flow rates used. The figure is based on the concentration data accumulated from the four sample locations along the vegetative filter, with three samples for each location. Then, the flux-averaged concentration for each location was used to plot the streamwise suspended sediment profiles. The data is tabulated in Table 8. The flow rates used for the experiments were 0.2, 0.3, 0.4, and 0.5 cfs.

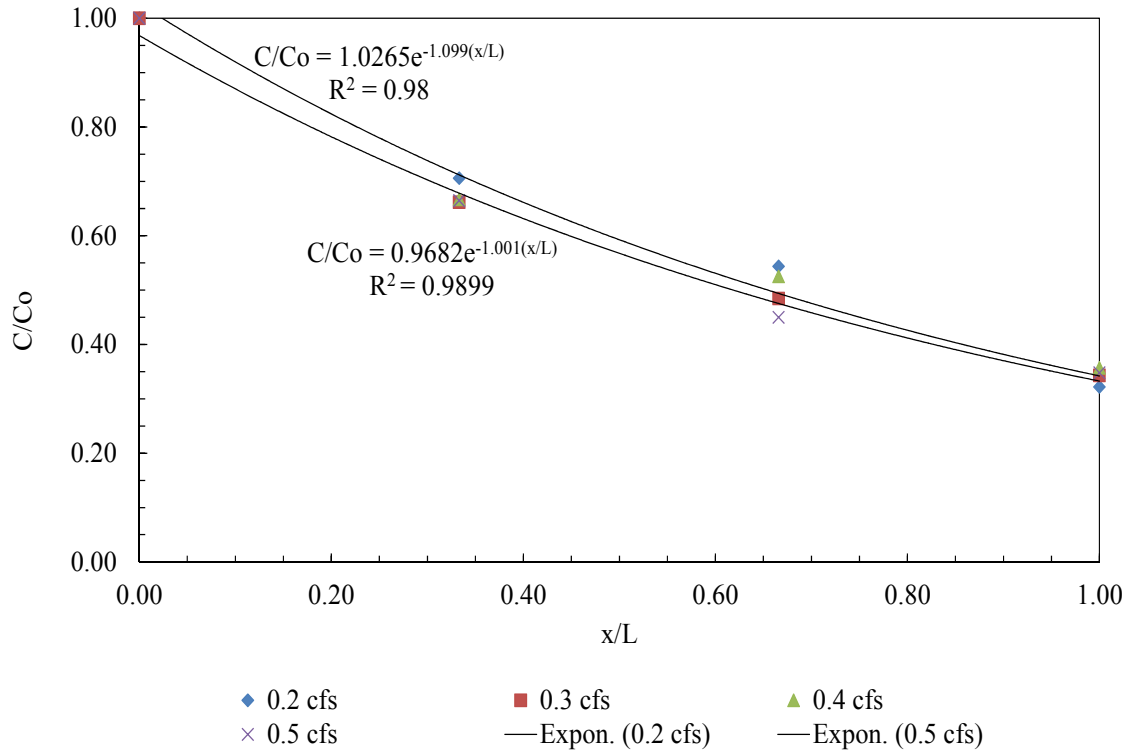


Figure 39: Streamwise suspended sediment concentration profiles along the vegetation length, for emergent vegetation of density  $m = 101.9$  stems/ft<sup>2</sup>. Exponential trends are shown for two flow rates, to be referred to later in Subsection 5.4.5

Table 8: Suspended sediment concentration data obtained from the experimental trials using the ISCO sampler, emergent vegetation of density  $m = 101.9$  stems/ft<sup>2</sup>

Bottle no.	Concentration, mg/l, for $Q = 0.2$ cfs	Concentration, mg/l, for $Q = 0.3$ cfs	Concentration, mg/l, for $Q = 0.4$ cfs	Concentration, mg/l, for $Q = 0.5$ cfs	Distance Along Vegetation $x$ , ft
1	40.56	60.12	80.10	115.47	0.00
2	37.42	57.23	62.99	98.35	0.00
3	33.19	42.78	51.97	70.39	0.00
4	29.45	45.78	50.00	76.34	5.33
5	25.34	33.42	43.66	64.89	5.33
6	23.67	26.77	36.36	47.62	5.33
7	25.12	31.23	38.87	43.77	10.67
8	19.67	25.13	34.93	43.50	10.67
9	15.63	21.20	28.57	40.53	10.67
10	15.12	22.12	27.32	40.88	16.00
11	10.34	18.34	23.11	32.11	16.00
12	10.32	14.45	19.15	25.78	16.00

From Figure 39, it can be seen that the streamwise suspended sediment concentration profile follows the plug-flow reactor model and shows an exponential decrease of suspended sediment concentration as the flow moves through the emergent vegetative filter. This conformed with previous literature indications regarding concentration profile trends in emergent vegetation (Elliott, 2000).

The data tables in Table 9 present the results of the suspended sediment flux and trap efficiency calculations for the denser, emergent vegetation. From the calculations in Table 9, the streamwise suspended sediment flux per unit width is plotted against the vegetation length in Figure 40.

Table 9: Tabulated calculated values to obtain the value of trap efficiency for emergent vegetation of density  $m = 101.9$  stems/ft<sup>2</sup>

(a)

Location 1, $x=0$ ft	Location 2, $x=5.33$ ft	Location 3, $x=10.67$ ft	Location 4, $x=16$ ft	
Initial Flux In, mg/s/ft	Flux after 1st third of veg length, mg/s/ft	Flux 2nd third of veg length, mg/s/ft	Flux Out, mg/s/ft	$Q$ , cfs
71.3	50.4	39.6	23.4	0.2
145.5	98.7	71.2	50.5	0.3
245.8	161.3	126.6	86.7	0.4
395.9	266.7	180.9	142.7	0.5

(b)

net flux lost between 1--2, mg/s/ft	net flux lost between 2--3, mg/s/ft	net flux lost between 3--4, mg/s/ft	net flux lost between 1--4, mg/s/ft
20.9	10.8	16.2	47.9
46.8	27.5	20.7	95.0
84.6	34.7	39.9	159.1
129.2	85.8	38.1	253.2

(c)

net mass flow rate between 1--2, mg/s	net mass flow rate between 2--3, mg/s	net mass flow rate between 3--4, mg/s	net mass flow rate between 1--4, mg/s
68.5	35.5	53.3	157.3
153.5	90.2	67.9	311.6
277.4	113.7	130.8	521.8
423.9	281.5	125.0	830.4

(d)

mass deposited between 1--2, mg	mass deposited between 2--3, mg	mass between deposited 3--4, mg	mass deposited between 1--4, mg
49000	25500	38000	113000
110000	65000	49000	224000
200000	82000	94000	375000
305000	200000	90000	580000

(e)

$Q$ , cfs	Initial Flux In, mg/s/ft	Mass coming in, mg	% deposited between 1&2	% deposited between 1&3	% deposited between 1&4 = $TE$
0.2	71.3	170000	29.27	44.45	67.25
0.3	145.5	343000	32.17	51.07	65.31
0.4	245.8	581000	34.40	48.49	64.72
0.5	395.9	935000	32.64	54.32	63.95

Part (a) Table 9 in shows the sediment flux per unit width in each of the four specified locations along the vegetative filter in the streamwise direction, designated 1, 2, 3, and 4. Part (b) shows the net flux lost in each vegetative filter segment. Part (c) gives the calculation of the net mass flow rate in each filter segment, by multiplying the values of the second table by the width of the flume. Part (d) provides the calculated values of mass deposited in each filter segment, by multiplying the values of the third table by 12 minutes, which is the duration of the experiment. Finally, part (e) of the table shows the mass percentage of sediment deposited in each filter segment, or the trap efficiency of each filter segment. The last column in the table is the overall trap efficiency of the vegetative filter at different flow rates.

It is clear that the trap efficiency of the vegetative filter decreased as the flow rate increased, an observation consistent with previous research. Higher flow rates keep sediment suspended in water longer than lower flow rates, thus reducing the chance of settling and decreasing the vegetative filter trap efficiency in the process. Figure 40 presents the suspended sediment flux per unit width as a function of flow distance.

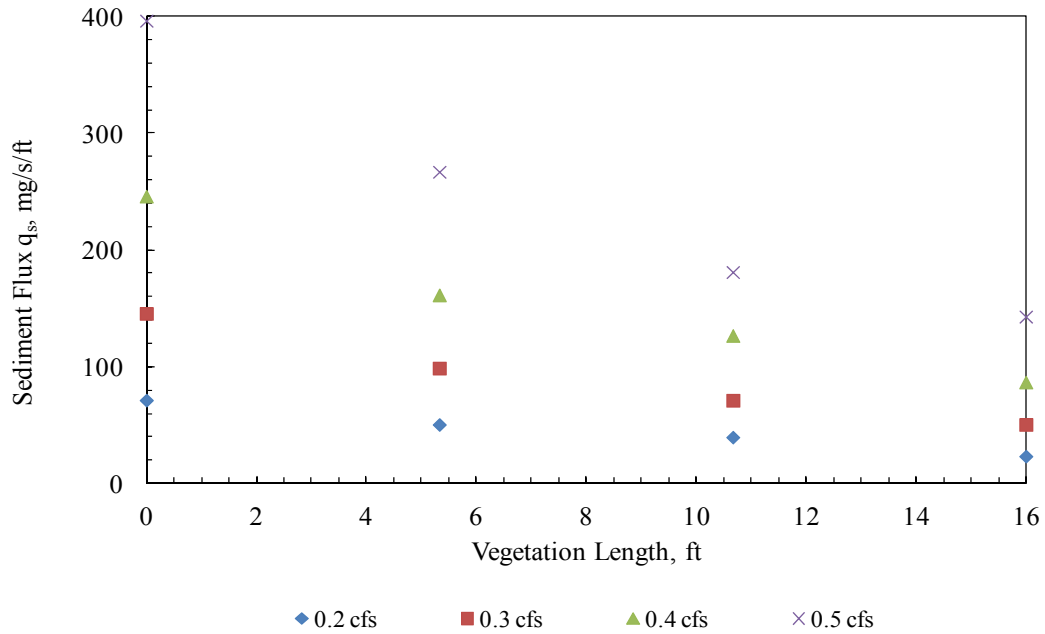


Figure 40: Suspended sediment flux per unit width against vegetation length; emergent vegetation of density  $m = 101.9 \text{ stems/ft}^2$

#### 5.4.2 Emergent Rigid Vegetation with Density $m = 25.5 \text{ stems/ft}^2$

The same plots pertaining to the main parameters of Subsection 5.4.1 are presented. The trends and reasoning are identical to Subsection 5.4.1.

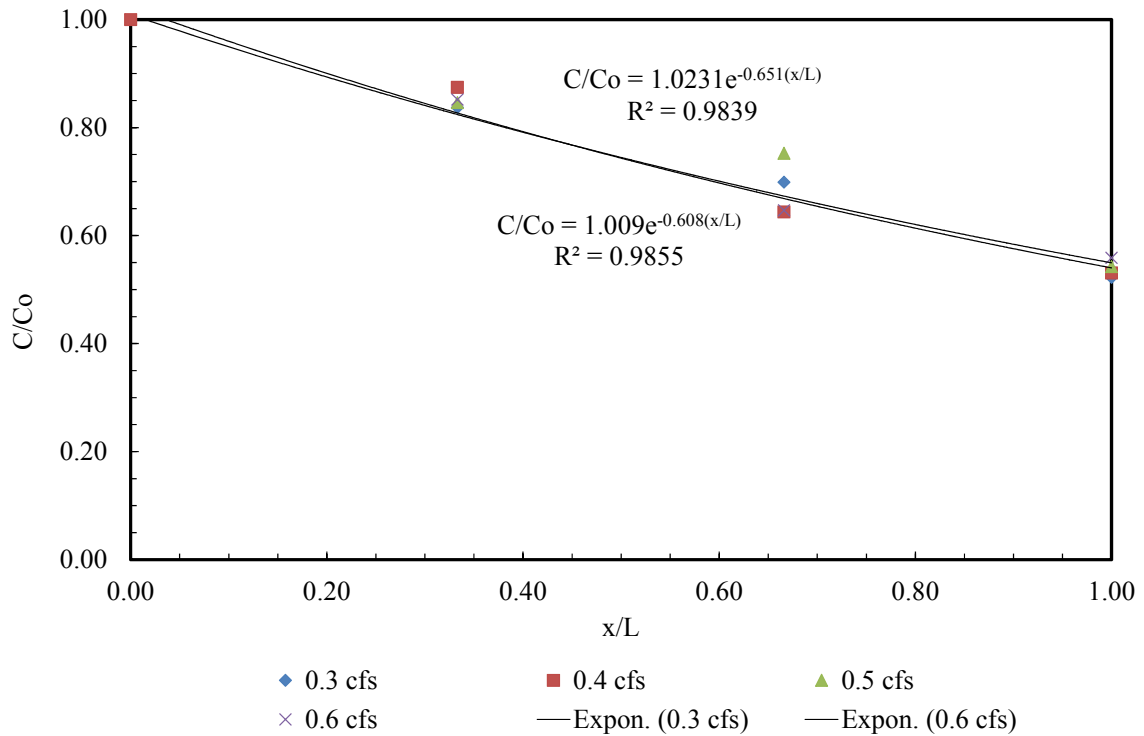


Figure 41: Streamwise suspended sediment concentration profiles along the vegetation length, emergent vegetation of density  $m = 25.5$  stems/ft<sup>2</sup>. Exponential trends are shown for two flow rates, to be referred to later in Subsection 5.4.5

Table 10: Suspended sediment concentration data obtained from the experimental trials using the ISCO sampler, emergent vegetation of density  $m = 25.5$  stems/ft<sup>2</sup>

Bottle no.	Concentration, mg/l, for $Q = 0.3$ cfs	Concentration, mg/l, for $Q = 0.4$ cfs	Concentration, mg/l, for $Q = 0.5$ cfs	Concentration, mg/l, for $Q = 0.6$ cfs	Distance Along Vegetation $x$ , ft
1	36.04	45.10	61.11	85.73	0.00
2	34.07	41.20	56.34	75.92	0.00
3	31.36	38.10	53.32	73.71	0.00
4	31.93	41.80	50.76	75.06	5.33
5	27.72	37.54	48.23	65.50	5.33
6	25.28	29.45	45.50	59.71	5.33
7	27.61	29.44	47.12	54.42	10.67
8	22.80	25.10	42.55	50.69	10.67
9	20.47	25.56	38.78	46.86	10.67
10	19.15	26.69	35.87	48.04	16.00
11	17.32	20.11	30.32	42.61	16.00
12	16.53	19.20	26.44	40.68	16.00

The data tables in Table 11 present the results of the suspended sediment flux and trap efficiency calculations for the less dense, emergent vegetation. From the calculations in Table 11, the streamwise suspended sediment flux per unit width is plotted against the vegetation length in Figure 42.

Table 11: Tabulated calculated values to obtain the value of trap efficiency for emergent vegetation of density  $m = 25.5$  stems/ft<sup>2</sup>

(a)

Location 1, $x=0$ ft	Location 2, $x=5.33$ ft	Location 3, $x=10.67$ ft	Location 4, $x=16$ ft	
Initial Flux In, mg/s/ft	Flux after 1st third of veg length, mg/s/ft	Flux 2nd third of veg length, mg/s/ft	Flux Out, mg/s/ft	$Q$ , cfs
72.8	60.7	50.3	37.8	0.3
110.7	94.9	75.0	59.1	0.4
207.7	175.6	141.8	113.9	0.5
357.6	305.3	240.6	199.7	0.6

(b)

net flux lost between 1--2, mg/s/ft	net flux lost between 2--3, mg/s/ft	net flux lost between 3--4, mg/s/ft	net flux lost between 1--4, mg/s/ft
12.1	10.4	12.5	34.9
15.9	19.9	15.9	51.5
32.1	33.7	28.3	94.1
52.2	64.7	40.9	157.9

(c)

net mass flow rate between 1--2, mg/s	net mass flow rate between 2--3, mg/s	net mass flow rate between 3--4, mg/s	net mass flow rate between 1--4, mg/s
39.8	34.1	40.8	114.6
51.8	65.1	52.2	169.1
105.4	110.6	92.7	308.7
171.3	212.2	134.5	517.9

(d)

mass deposited between 1--2, mg	mass deposited between 2--3, mg	mass between deposited 3--4, mg	mass deposited between 1--4, mg
28600	24500	29000	82500
37200	47000	37500	122000
75900	79600	66700	222000
123000	153000	96800	373000

(e)

$Q$ , cfs	Initial Flux In, mg/s/ft	Mass coming in, mg	% deposited between 1&2	% deposited between 1&3	% deposited between 1&4 = $TE$
0.3	72.8	172000	16.66	30.92	48.02
0.4	110.7	261000	14.26	32.21	46.57
0.5	207.7	490000	15.48	31.71	45.31
0.6	357.6	844000	14.60	32.70	44.16

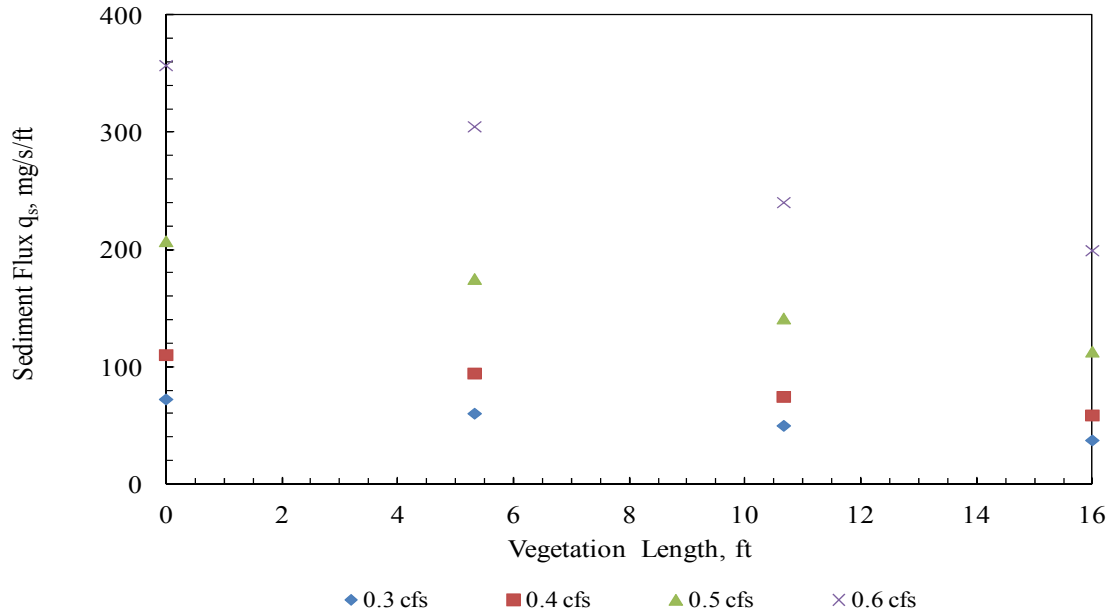


Figure 42: Suspended sediment flux per unit width against vegetation length; emergent vegetation of density  $m = 25.5$  stems/ft<sup>2</sup>

### 5.4.3 Submerged Vegetation with Density $m = 101.9$ stems/ft<sup>2</sup>

The same plots pertaining to the main parameters of Subsection 5.4.1 are presented. The trends and reasoning are identical to Subsection 5.4.1.

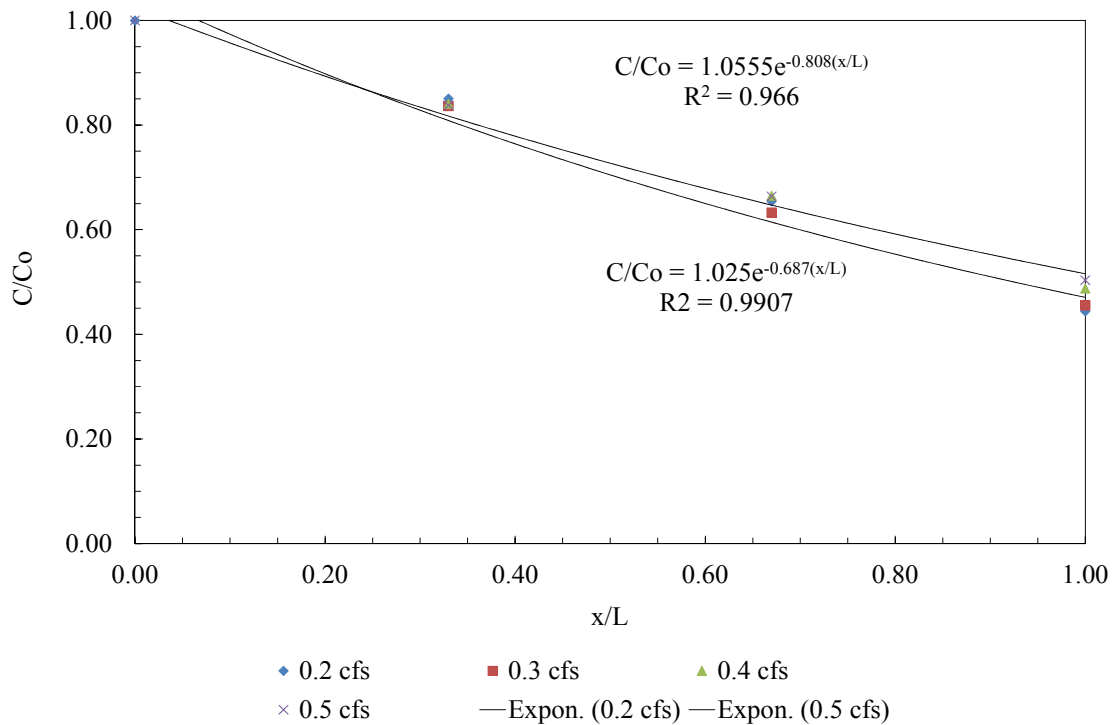


Figure 43: Streamwise suspended sediment concentration profiles along the vegetation length, submerged vegetation of density  $m = 101.9$  stems/ft<sup>2</sup>. Exponential trends are shown for two flow rates, to be referred to later in Subsection 5.4.5

Table 12: Suspended sediment concentration data obtained from the experimental trials using the ISCO sampler, submerged vegetation of density  $m = 101.9$  stems/ft<sup>2</sup>

Bottle no.	Concentration, mg/l, for $Q = 0.2$ cfs	Concentration, mg/l, for $Q = 0.3$ cfs	Concentration, mg/l, for $Q = 0.4$ cfs	Concentration, mg/l, for $Q = 0.5$ cfs	Distance Along Vegetation $x$ , ft
1	13.26	19.12	24.34	27.78	0.00
2	10.25	17.05	23.45	25.36	0.00
3	9.48	15.74	22.12	22.30	0.00
4	9.87	15.61	22.56	23.47	5.33
5	9.43	14.22	19.32	20.36	5.33
6	8.76	13.57	16.87	19.36	5.33
7	7.82	12.50	17.67	18.45	10.67
8	7.61	10.76	15.30	16.58	10.67
9	6.15	9.58	13.50	15.03	10.67
10	5.17	8.49	12.30	14.23	16.00
11	4.93	7.71	10.99	13.26	16.00
12	4.55	7.42	10.78	10.47	16.00

The data tables in Table 13 present the results of the suspended sediment flux and trap efficiency calculations for the denser, submerged vegetation. From the calculations in Table 13, the streamwise suspended sediment flux per unit width is plotted against the vegetation length in Figure 44.

Table 13: Tabulated calculated values to obtain the value of trap efficiency for submerged vegetation of density  $m = 101.9$  stems/ft<sup>2</sup>

(a)

Location 1, $x=0$ ft	Location 2, $x=5.33$ ft	Location 3, $x=10.67$ ft	Location 4, $x=16$ ft	
Initial Flux In, mg/s/ft	Flux after 1st third of veg length, mg/s/ft	Flux 2nd third of veg length, mg/s/ft	Flux Out, mg/s/ft	$Q$ , cfs
17.9	15.1	11.7	7.9	0.2
25.3	21.1	16.1	11.5	0.3
36.5	31.4	24.7	17.9	0.4
48.1	40.4	31.9	24.3	0.5

(b)

net flux lost between 1--2, mg/s/ft	net flux lost between 2--3, mg/s/ft	net flux lost between 3--4, mg/s/ft	net flux lost between 1--4, mg/s/ft
2.8	3.4	3.8	10.0
4.3	4.9	4.7	13.9
5.2	6.6	6.8	18.6
7.8	8.4	7.6	23.8

(c)

net mass flow rate between 1--2, mg/s	net mass flow rate between 2--3, mg/s	net mass flow rate between 3--4, mg/s	net mass flow rate between 1--4, mg/s
9.3	11.1	12.5	32.9
13.9	16.3	15.3	45.5
17.0	21.7	22.4	61.1
25.4	27.7	25.0	78.1

(d)

mass deposited between 1--2, mg	mass deposited between 2--3, mg	mass between deposited 3--4, mg	mass deposited between 1--4, mg
6700	8000	9000	23700
10000	11700	11000	32700
12300	15600	16100	44000
18300	20000	18000	56000

(e)

$Q$ , cfs	Initial Flux In, mg/s/ft	Mass coming in, mg	% deposited between 1&2	% deposited between 1&3	% deposited between 1&4 = $TE$
0.2	17.9	42300	15.84	34.69	56.03
0.3	25.3	60000	16.76	36.36	54.72
0.4	36.5	86000	14.22	32.29	50.94
0.5	48.1	114000	16.11	33.64	49.49

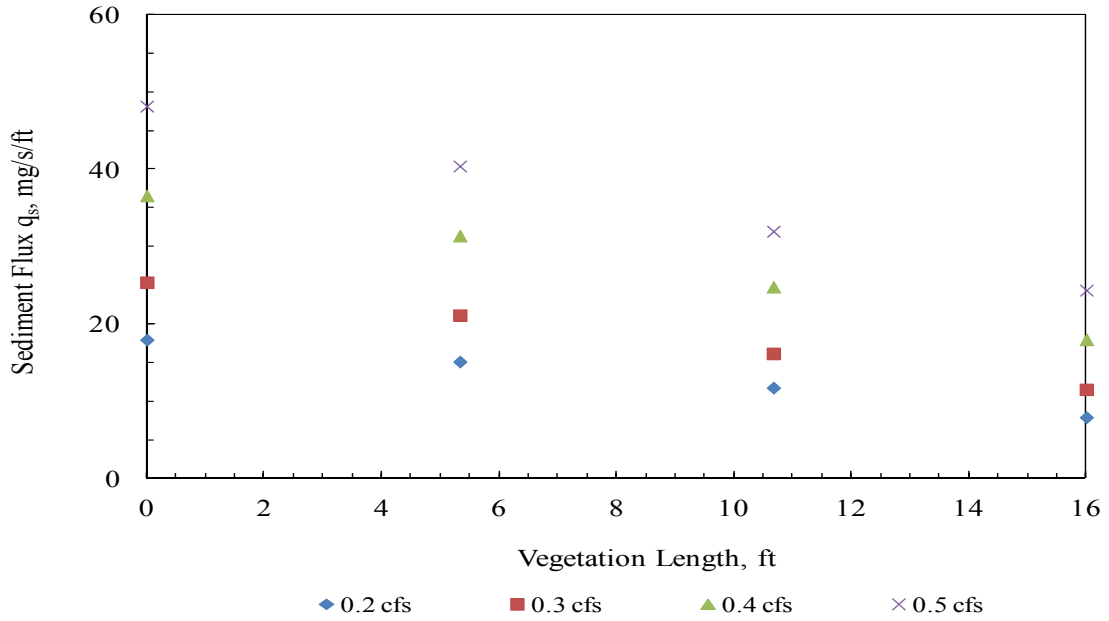


Figure 44: Suspended sediment flux per unit width against vegetation length, submerged vegetation of density  $m = 101.9$  stems/ft<sup>2</sup>.

#### 5.4.4 Submerged Vegetation with Density $m = 25.5$ stems/ft<sup>2</sup>

The same plots pertaining to the main parameters of Subsection 5.4.1 are presented. The trends and reasoning are identical to Subsection 5.4.1.

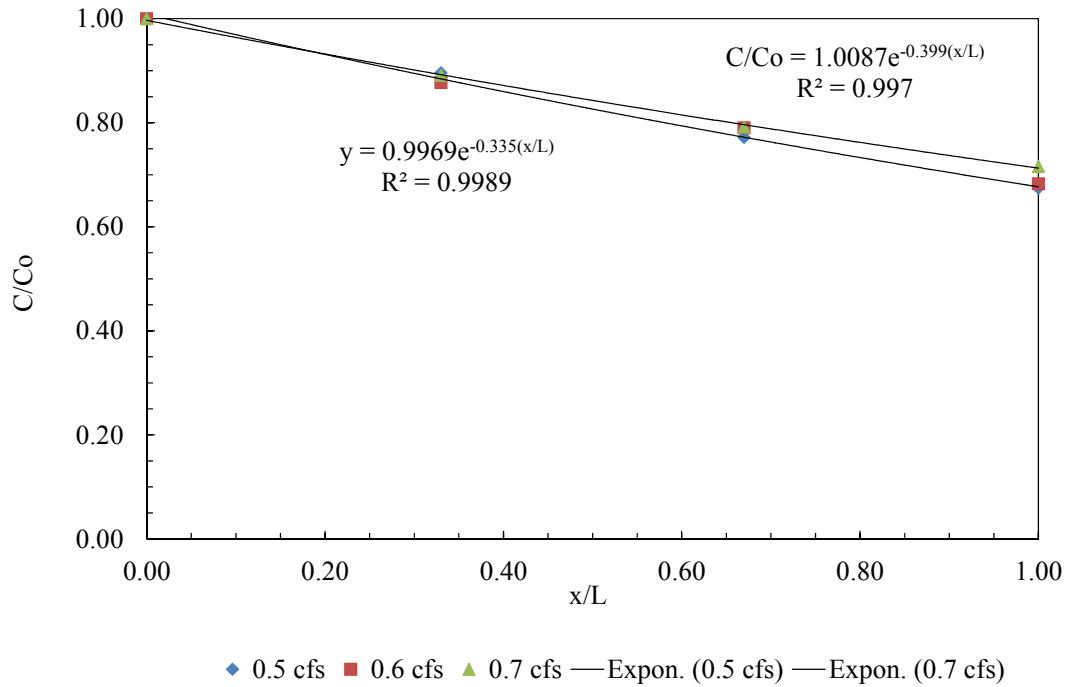


Figure 45: Streamwise suspended sediment concentration profiles along the vegetation length, submerged vegetation of density  $m = 25.5$  stems/ft<sup>2</sup>. Exponential trends are shown for two flow rates, to be referred to later in Subsection 5.4.5

Table 14: Suspended sediment concentration data obtained from the experimental trials using the ISCO sampler, submerged vegetation of density  $m = 25.5$  stems/ft<sup>2</sup>

Bottle no.	Concentration, mg/l, for $Q = 0.5$ cfs	Concentration, mg/l, for $Q = 0.6$ cfs	Concentration, mg/l, for $Q = 0.7$ cfs	Distance Along Vegetation $x$ , ft
1	35.15	44.21	53.77	0.00
2	32.76	43.98	50.65	0.00
3	31.17	42.51	46.30	0.00
4	32.26	40.39	45.87	5.33
5	29.08	38.24	44.90	5.33
6	27.46	36.02	43.48	5.33
7	27.15	36.16	41.21	10.67
8	26.04	34.61	39.67	10.67
9	23.28	32.52	38.44	10.67
10	23.81	31.44	38.56	16.00
11	23.37	30.41	36.76	16.00
12	19.62	27.36	32.59	16.00

The data tables in Table 15 present the results of the suspended sediment flux and trap efficiency calculations for the less dense, submerged vegetation. From the calculations in Table 15, the streamwise suspended sediment flux per unit width is plotted against the vegetation length in Figure 46.

Table 15: Tabulated calculated values to obtain the value of trap efficiency for submerged vegetation of density  $m = 25.5$  stems/ft<sup>2</sup>

(a)

Location 1, $x=0$ ft	Location 2, $x=5.33$ ft	Location 3, $x=10.67$ ft	Location 4, $x=16$ ft	
Initial Flux In, mg/s/ft	Flux after 1st third of veg length, mg/s/ft	Flux 2nd third of veg length, mg/s/ft	Flux Out, mg/s/ft	$Q$ , cfs
129.4	116.3	100.2	87.8	0.5
169.6	149.5	132.4	116.6	0.6
194.2	173.3	154.4	139.2	0.7

(b)

net flux lost between 1--2, mg/s/ft	net flux lost between 2--3, mg/s/ft	net flux lost between 3--4, mg/s/ft	net flux lost between 1--4, mg/s/ft
13.2	16.1	12.4	41.6
20.1	17.1	15.8	53.0
21.0	18.9	15.1	55.0

(c)

net mass flow rate between 1--2, mg/s	net mass flow rate between 2--3, mg/s	net mass flow rate between 3--4, mg/s	net mass flow rate between 1--4, mg/s
43.1	52.7	40.6	136.4
65.9	56.1	51.9	173.8
68.7	62.0	49.6	180.3

(d)

mass deposited between 1--2, mg	mass deposited between 2--3, mg	mass between deposited 3--4, mg	mass deposited between 1--4, mg
31000	38000	29200	98000
47000	40000	37400	125000
49500	44600	35700	130000

(e)

$Q$ , cfs	Initial Flux In, mg/s/ft	Mass coming in, mg	% deposited between 1&2	% deposited between 1&3	% deposited between 1&4 = $TE$
0.5	129.4	305000	10.16	22.57	32.13
0.6	169.6	400000	11.83	21.91	31.25
0.7	194.2	459000	10.79	20.52	28.30

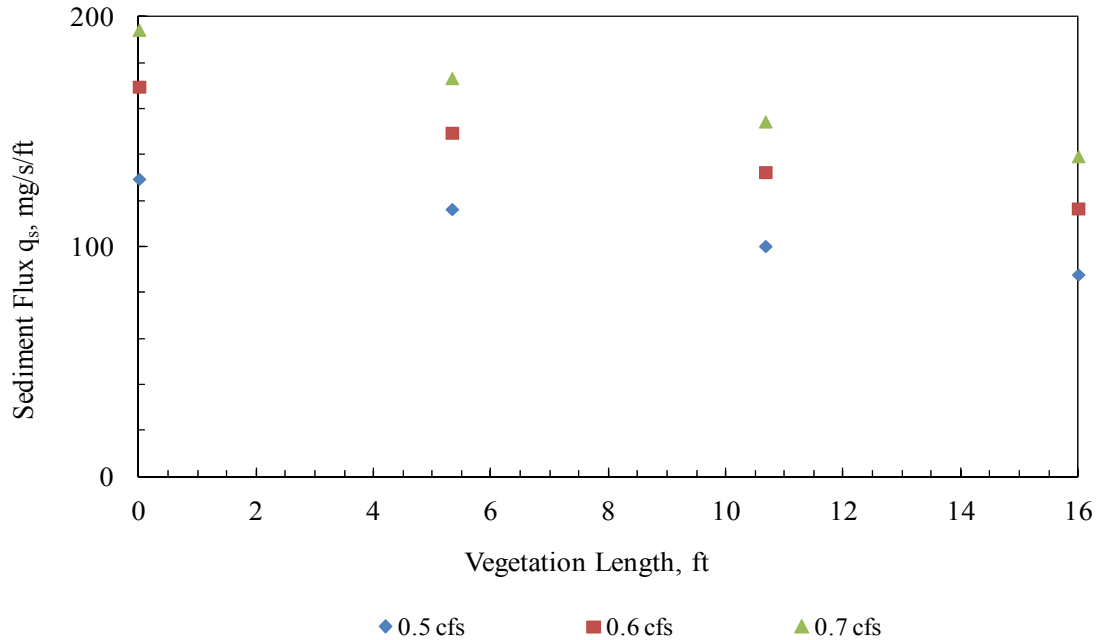


Figure 46: Suspended sediment flux per unit width against vegetation length, submerged vegetation of density  $m = 25.5$  stems/ft<sup>2</sup>

#### 5.4.5 Trap Efficiency Analysis

Previous research has shown that the vegetative strip can be modeled as a plug-flow reactor (Elliott, 2000). The governing equation can be expressed as:

$$\frac{C(x)}{C(0)} = \exp(-kA/Q)x \quad (91)$$

where  $x$  is the longitudinal direction  $A$  is the cross-sectional area of the reactor,  $Q$  is the flow rate through the reactor, and  $k$  is the plug-flow reaction parameter. For a vegetative strip of length  $L$ , the equation becomes:

$$\frac{C(L)}{C(0)} = \exp(-kV/Q) \quad (92)$$

where  $V$  is the volume of the vegetative strip control volume, defined as the product of  $bLH$ , in which  $H$  is the normal depth and  $b$  is the width of the vegetative filter.

The theoretical basis of Equation 92 results from the plug-flow assumption in a sedimentation tank, where the velocity of the fluid is assumed to be constant across any cross-section. Assuming a horizontal slice across the tank, with a width of  $\Delta x$ , and assuming that the flow is steady and uniform in the tank; these assumptions are also satisfied in the vegetative filter as described previously. Analyzing the concentration variation of suspended sediment moving horizontally in a control volume taken over the full depth of the tank with unit width, length =  $\Delta x$  and height  $\Delta z = H =$  depth of water, the inflow and outflow of sediment can be described as:

Inflow:  $HUC$

Outflow:  $w_f C \Delta x$  and  $HUC + \frac{\partial UC}{\partial x} H \Delta x$ , and  $H$  is a constant.

Therefore from mass continuity:

$$HU\left(\frac{\partial C}{\partial x}\right)\Delta x + w_f C \Delta x = 0 \quad (93)$$

where  $U$  is the flow bulk velocity, and  $w_f$  is the fall velocity of the sediment grains. The concentration at any value of  $x$  is assumed constant with  $z$  in Equation 93. It varies slightly with  $z$  in these experiments, so the concentration has been taken to be the flux-averaged value over the vertical coordinate as explained previously. The boundary conditions for the differential equation are as follows:

At  $x = 0$ , then  $C(x) = C(0) = C_o$ , where  $C_o$  is the initial suspended sediment concentration entering the tank. The governing differential equation becomes:

$$\frac{U\partial C}{\partial x} = -\frac{w_f C}{H} \quad (94)$$

and the solution is given by:

$$\frac{C(x)}{C_o} = e^{-\frac{xw_f}{UH}} \quad (95)$$

For the full length  $L$  of the tank in the flow direction, the solution becomes

$$\frac{c(L)}{c_o} = e^{\frac{-w_f}{q/L}} \quad (96)$$

where  $q = Q/b = UH$  and  $b$  is the width of the tank.

Theoretical trap efficiency for a sedimentation tank is then given by:

$$TE = \frac{c(0)-c(L)}{c(0)} = 1 - e^{\frac{-Lw_f}{UH}} = 1 - e^{\frac{-w_f}{q/L}} \quad (97)$$

in which  $L$  is the length of the tank in the flow direction.

If it is assumed that a vegetation filter also experiences plug flow, Equation 95 is the basis for the exponential plots for concentration vs. flow distance given previously in Figure 39, Figure 41, Figure 43, and Figure 45 for the vegetation filter. An additional parameter reflecting the porosity or volume density of the vegetation would be expected to modify the theoretical equations for a sedimentation tank to fit the vegetative filter case.

The negative exponential decreasing trend in Equation 95 is reflected in Figure 39, Figure 41, Figure 43, and Figure 45, which presented the best fit trends for the highest flow rate and the lowest flow rate for each vegetation case. For both emergent and submerged cases, the numerical value of the power in the exponential decreased as the flow rate increased, indicating an increase in flow turbulence, hence an increase in the value of turbulent diffusivity coefficient  $\varepsilon_s$ .

Treating the vegetative filter as a sedimentation basin for sediment with non-uniform grain sizes, the theoretical settling efficiency of the different grain sizes, or SEF, is defined as:

$$SEF = \frac{w_f}{Q/A_s} = \frac{w_f}{q/L} \quad (98)$$

where  $w_f$  is the sediment fall velocity of a grain size,  $Q$  is the flow rate,  $b$  is the width of the vegetation perpendicular to the flow direction,  $L$  is the length of the filter in the flow direction,  $q = Q/b$  is the flow rate per unit width, and  $A_s$  is the surface area of water in the sedimentation basin equal to  $bL$ , which is the bed area of the vegetation filter. The ratio  $Q/A_s$  is defined as the surface loading rate, and in cases of ideal settling, is equal to  $w_f$ , indicating that a sedimentation basin's depth has no role in determining the SEF. Sturm and Kirby (1991) described the theoretical trap efficiency as the integration of SEF across the whole grain size distribution of the sediment used:

$$TE = 1 - \int_0^1 e^{\frac{-w_f}{Q/A_s} \cdot dX} \quad (99)$$

where  $X$  is the size fraction by weight of the sediment sample. To calculate the fall velocity of a certain grain size, Equation 100 is used (Sturm, 2001):

$$\frac{w_f d_s}{\nu} = 8 \left( \sqrt{1 + 0.0139 d_*^3} - 1 \right) \quad (100)$$

where  $d_s$  is the grain diameter, and  $d_*$  is the dimensionless particle diameter defined as:

$$d_* = \left[ \frac{(\gamma_s / \gamma - 1) g d_s^3}{\nu^2} \right]^{1/3} \quad (101)$$

where  $\gamma_s$  is the specific weight of the solid.

#### 5.4.6 Trap Efficiency Results

The drag coefficient and trap efficiency experimental results from all types of vegetation tested in this research, along with the respective bulk and shear velocities, are summarized in Table 16:

Table 16: Summary of drag coefficient and trap efficiency results from all four vegetation trials

(a) Emergent Vegetation with density  $m = 101.9$  stems/ft<sup>2</sup>

$Q$ , cfs	$y_n$ , ft	$U$ , ft/sec	$u^*$	$C_d$	Stem Re	$TE$ %
0.202	0.353	0.174	0.238	3.63	480	67.25
0.301	0.429	0.214	0.260	2.41	590	65.31
0.399	0.540	0.225	0.282	2.18	620	64.72
0.503	0.613	0.250	0.292	1.76	680	63.95

(b) Emergent Vegetation with density  $m = 25.5$  stems/ft<sup>2</sup>

$Q$ , cfs	$y_n$ , ft	$U$ , ft/sec	$u^*$	$C_d$	Stem Re	$TE$ , %
0.303	0.220	0.420	0.194	2.64	1150	48.02
0.402	0.252	0.486	0.204	1.97	1300	46.57
0.500	0.288	0.529	0.218	1.66	1450	45.31
0.601	0.330	0.555	0.230	1.51	1500	44.16

(c) Submerged Vegetation with density  $m = 101.9$  stems/ft<sup>2</sup>

$Q$ , cfs	$y_n$ , ft	$U$ , ft/sec	$u^*$	$C_d$	Stem Re	$TE$ , %
0.200	0.281	0.217	0.215	2.87	600	56.03
0.299	0.297	0.307	0.221	1.54	850	54.72
0.402	0.332	0.369	0.230	1.23	1000	50.94
0.500	0.350	0.436	0.236	0.98	1200	49.49

(d) Submerged Vegetation with density  $m = 25.5$  stems/ft<sup>2</sup>

$Q$ , cfs	$y_n$ , ft	$U$ , ft/sec	$u^*$	$C_d$	Stem Re	$TE$ , %
0.503	0.241	0.636	0.200	1.34	1700	31.23
0.602	0.252	0.728	0.204	1.08	2000	31.25
0.705	0.261	0.824	0.208	0.90	2250	28.30

The trap efficiency values for the emergent rigid vegetation of density  $m = 25.5$  stems/ft<sup>2</sup> and the submerged flexible vegetation of density  $m = 101.9$  stems/ft<sup>2</sup> are close in magnitude, with the submerged vegetation of density  $m = 101.9$  stems/ft<sup>2</sup> possessing slightly larger trap efficiency values. The highest trap efficiency values are displayed by the emergent rigid vegetation of density  $m = 101.9$  stems/ft<sup>2</sup>, and the lowest are displayed by the submerged flexible vegetation of density  $m = 25.5$  stems/ft<sup>2</sup>.

The suspended sediment concentration measuring locations along the flume length at  $x = 0.00$ , 5.33, 10.67, and 16.00 ft divided the vegetative filter length into three

equal segments. These measured concentrations were used to calculate the suspended sediment flux  $Q_s$  in each segment of the filter using Equation 90, in addition to the net flux lost in each filter segment. The initial sediment mass entering the vegetative filter and the mass deposited in each filter segment are subsequently calculated over the time duration of the whole experimental trial. The experimental trap efficiency calculated for each vegetation case at each flow rate and plotted in Figure 47 is the ratio of the deposited mass along the full vegetative filter length and the initial sediment mass entering the filter.

Equation 97 represents the theoretical trapping efficiency describing settling with no presence of vegetation; it is not applicable to the experimental trials. Nonetheless, it is plotted with the experimental trap efficiencies against the dimensionless SEF variable in Figure 47 to graphically show the effect that different types and densities of vegetation have on sediment settling out of open channel flow when compared to settling out of unobstructed flow.

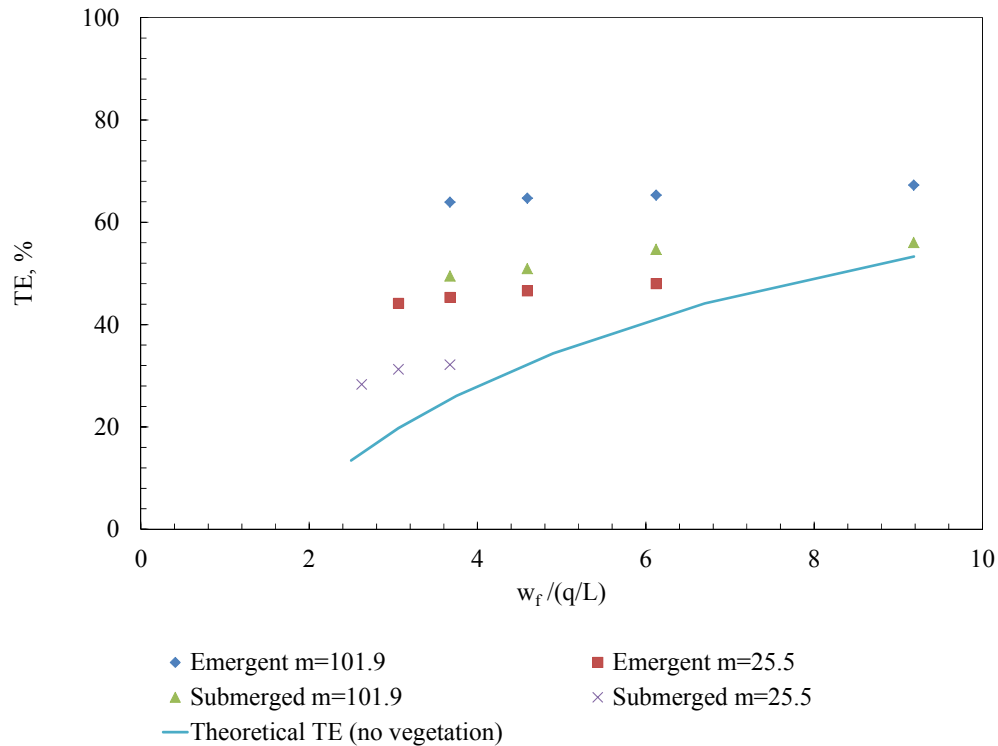


Figure 47: Trap efficiency plotted against sediment settling efficiency, for all four vegetation trials (densities  $m = 101.9$  and  $25.5$  stems/ft<sup>2</sup>) and for the theoretical case of no vegetation in the flume.

From Figure 47, it can be observed that as  $SEF = w_f/(q/L)$  increases, the trap efficiency of the vegetation increases. The highest trap efficiencies were observed for the lowest flow rates, in accordance with previous analysis in this section and the literature review in Chapter 2. Higher flow implies higher flow turbulence as depicted by a higher flow Reynolds number. The higher flow and turbulence keep the sediment suspended in the flow for longer time periods and allow for re-entrainment. The lowest trap efficiencies were recorded for the theoretical trap efficiency model at the same SEF values when compared to the four vegetation cases, where no vegetation was available to help settle and trap the suspended sediment out of the flow. It is also observed in Figure 47 that as the SEF value increases, the trap efficiencies of the four vegetation cases and the theoretical trap efficiency all begin to converge closer to one another, indicating that for the same grain size sediment distribution and vegetative filter length, the rate of

increase of trap efficiency decreases as the flow rate increases. Although the grain size distribution was not varied in these experiments, the presentation in Figure 47 allows the results to be used for other grain size distributions as long as the plug flow assumption applies. Finally, it can be observed that the trap efficiency curves level off for  $SEF > 6$ , so that the maximum filter length required can be estimated from this value.

## 6. PERFORMANCE OF SEEP BERM AND VEGETATIVE FILTER IN SERIES

### 6.1 Seep Berm Modeling

Chapter 3 presented a field demonstration project that showed seep berms to be a viable alternative for erosion control on construction sites. However, finer suspended sediment particles in surface water runoff have a longer settling time behind the berm wall compared to coarser particles. Thus, in the event of a storm, the runoff overtopping the seep berm normally carries a significant load of finer suspended sediment particles. It is for that reason that the use of vegetation filters located downstream of the berm is essential to trap the finer particles escaping the berm. The lab experiments on vegetation filters detailed in Chapters 4 and 5 addressed the capability of vegetation filters to trap and settle those fine particles. This chapter presents a numerical case study in which seep berms and vegetation filters working in series comprise a joint erosion control measure. The study will focus on the hydraulic performance and design of the seep berm, followed by applying the seep berm outflow results as the runoff inflow entering the vegetation filter for the subsequent calculation of the total trap efficiency of the whole system.

The SEDCAD4 software was used to theoretically model the hydrological performance of the seep berm and to obtain the berm inflow from stormwater runoff and berm outflow, in addition to the suspended sediment concentrations entering and leaving the seep berm (Warner et al., 1998). Subsequently, experimental results on emergent rigid vegetation with a density of  $m = 101.9$  stems/ft<sup>2</sup> were used to simulate a vegetation filter located directly downstream of the seep berm, where the runoff inflow rate through the vegetation filter equaled the outflow rate exiting the berm. The inflow suspended sediment concentration through the vegetation filter was taken to be the exact sediment concentration in the berm outflow runoff, mostly consisting of finer sediment particles. The suspended sediment concentration exiting the vegetation filter was taken as the final output of the sequential seep berm – vegetation filter erosion control measure.

First, seep berm design calculations were performed. The methodology described by Sturm and Warner (2007) in their seep berm design manual was used for the calculations described in the next paragraph.

Given a 2 yr-24 hr storm of 4.08 in. (the design storm dictated the berm height), on a 2.5 acre land disturbance area, with a width of 100 ft and a 2.5% slope, the required storage of the berm was calculated as follows:

For the 4.08 in. storm: Run-off volume =  $2.5 * 0.258 \text{ ac-ft/ac} = 0.645 \text{ ac-ft}$

where the number 0.258 represents the runoff volume in ac-ft/acre for the hydrologic soil group class C for the storm event, taken from Table 1 of the seep berm design manual presented in Table 17.

Table 17: Table 1 of the Seep Berm Design manual, showing runoff volumes, from Sturm and Warner (2007)

Hydrologic Soil Group	A	B	C	D
Infiltration Rate (in/hr)	>0.30	0.15 – 0.30	0.05 – 0.15	<0.05
Curve Number	77	86	91	94
	Runoff Volume (ac-ft)/acre disturbed			
1.20 in. design storm	0.008	0.025	0.042	0.056
4.08 in. design storm	0.156	0.218	0.258	0.284

The Georgia Green book (GASWCC, 2000) recommends 67 cubic yards/disturbed acre ( $1,809 \text{ ft}^3 / \text{disturbed acre}$ ) to be provided for sediment storage. Therefore, for a site with an area of 2.5 acres, required sediment storage was calculated as  $2.5 \text{ acre} * 1809 \text{ ft}^3 = 4522.5 \text{ ft}^3 = 0.103 \text{ ac-ft}$ . Since the values of Table 2 of the seep berm design manual (presented in Table 18 below) are given for storage volume/100 ft of berm length, then the required berm height needed to only contain the calculated sediment storage for a berm with a length of 100 ft and a slope of 2.5% was, by interpolation, approximately 1.46 ft.

Table 18: Table 2 from the seep berm design manual, showing berm heights according to slopes, from Sturm and Warner (2007)

Berm Height (ft.)	Land Slope (%)						
	0.5	1	1.5	2	2.5	3	4
0.50	0.0578	0.0291	0.0196	0.0148	0.0119	0.0100	0.0076
1.00	0.2313	0.1165	0.0782	0.0591	0.0476	0.0400	0.0304
1.50	0.5204	0.2621	0.1760	0.1330	0.1072	0.0900	0.0684
2.00	0.9252	0.4660	0.3130	0.2365	0.1905	0.1599	0.1217
2.50	1.4456	0.7282	0.4890	0.3695	0.2977	0.2499	0.1901
3.00	2.0816	1.0486	0.7042	0.5320	0.4287	0.3598	0.2738
3.50	2.8333	1.4272	0.9585	0.7241	0.5835	0.4898	0.3726
4.00	3.7006	1.8641	1.2519	0.9458	0.7622	0.6397	0.4867

Berm Height (ft.)	Land Slope (%)						
	5	6	7	8	9	10	5
0.50	0.0062	0.0052	0.0045	0.0040	0.0036	0.0033	0.0062
1.00	0.0247	0.0209	0.0181	0.0161	0.0145	0.0132	0.0247
1.50	0.0555	0.0469	0.0408	0.0362	0.0326	0.0297	0.0555
2.00	0.0987	0.0834	0.0725	0.0643	0.0579	0.0528	0.0987
2.50	0.1542	0.1303	0.1132	0.1004	0.0905	0.0825	0.1542
3.00	0.2221	0.1877	0.1631	0.1446	0.1303	0.1188	0.2221
3.50	0.3023	0.2554	0.2220	0.1969	0.1773	0.1617	0.3023
4.00	0.3949	0.3336	0.2899	0.2571	0.2316	0.2112	0.3949

The PVC pipe invert elevation required to completely contain the 2 yr-24 hr design storm was determined by adding the required storage to the sediment storage to obtain  $0.645 + 0.103 = 0.748$  ac-ft of total sediment storage. For a berm width of 100 ft, the pipe invert height was calculated, by interpolation, from Table 18 to be almost 3.96 ft to satisfy the given design watershed conditions. Thus, the minimum required design seep berm height was set at 4.00 ft.

## **6.2 SEDCAD4 Modeling and Determining Vegetation Filter Design Flow Depth**

### **6.2.1 SEDCAD4 Modeling**

The subsequent step after acquiring the structural design parameters of the seep berm was to analyze its hydrological performance and erosion control efficiency using SEDCAD4. The software was designed to aid in designing and evaluating hydraulic systems, erosion control measures, and BMPs such as seep berms. SEDCAD4 is a microcomputer-based model developed for quality modeling and runoff quantity as affected primarily by land erosion. The runoff is generated using triangular unit hydrographs and the SCS runoff curve number, after allowing the input of standard SCS storm distributions. Sediment concentration is taken to be proportional to hydrograph ordinates to the 0.5 power, while continuously-stirred-tank or plug-flow reactors in series are used to model a sediment basin divided into ten layers of uniform depth. At each time step, the mass balance equation is solved using discrete particle settling and uniform apportionment of inflow and outflow among the ten layers (Sturm & Kirby, 1991). SEDCAD4 studies the hydrological performance of any erosion control measure through analyzing effluent outflow, effluent suspended sediment concentrations, and trap efficiency. The following paragraphs demonstrate the use of SEDCAD4 to obtain seep berm inflow and outflow runoff rates and suspended sediment concentrations, after inputting the seep berm dimensions calculated in Section 6.1.

Using SEDCAD4, a seep berm design was created with a berm height of 4.00 ft. The design storm chosen was a 2 yr – 24 hr storm with a rainfall depth of 4.08 inches. The sedimentology input into SEDCAD4 was the same sedimentology used in the IHM field demonstration project described in Chapter 3.

The next step was to define the watershed that would contribute the runoff flowing downstream into the seep berm. The watershed area used for the design was 2.5 acres. Three effluent straight pipes with a diameter of two in. and an emergency spillway with a width of 30 ft were chosen for the seep berm wall. The pipes and emergency spillway were located at 0.5 ft and 0.25 ft below the top of the berm wall, respectively.

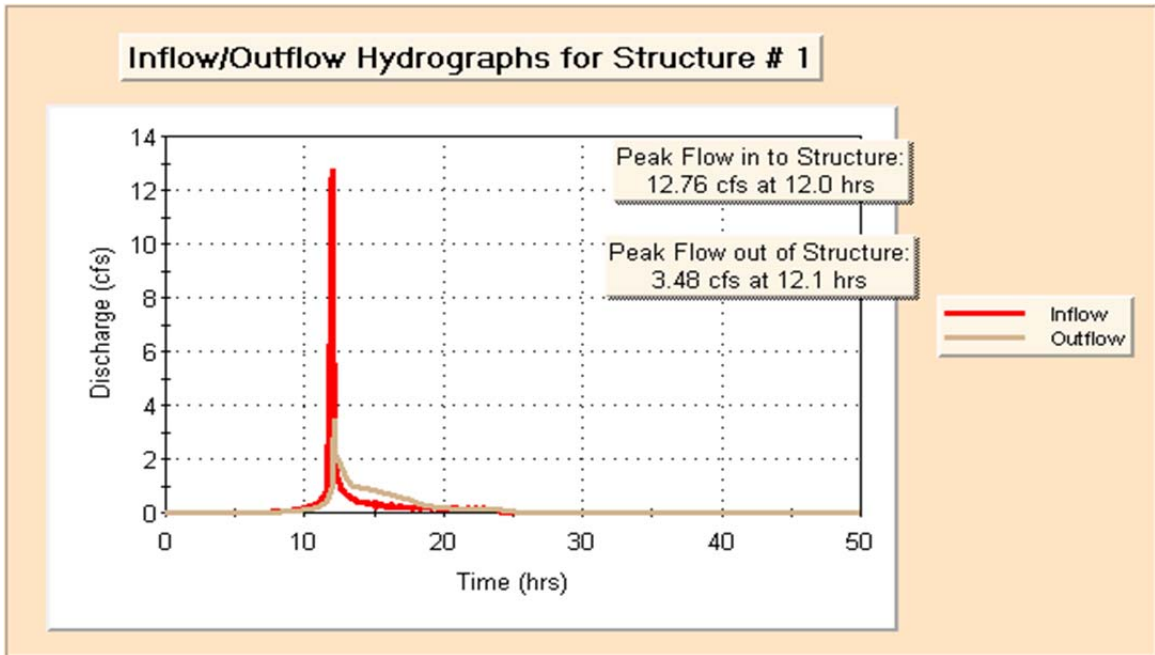
The time of concentration for the watershed was 0.12 hours, the land cover coefficient was 0.89, and the runoff curve number was 91. The seep berm had a bottom width of one ft, and side slopes of 1.5:1. SEDCAD4 provided the results shown in Table 19 after creating the inflow hydrograph and routing it through the seep berm.

Table 19: Seep berm results from SEDCAD4 showing inflow and outflow runoff rates and suspended sediment concentrations

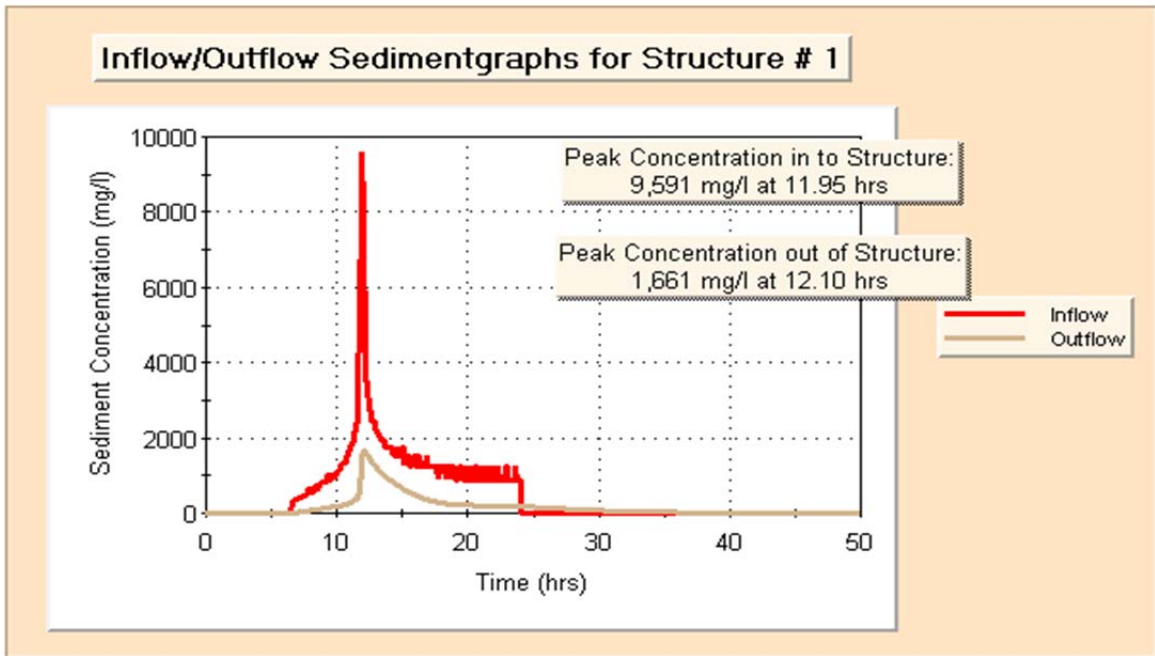
<b>Design Results</b>	<b>In</b>	<b>Out</b>
Peak Discharge, cfs	12.76	3.48
Peak Sediment Concentration, mg/l	9600	1660
Trap Efficiency = 81.9%		

Table 19 showed that SEDCAD4 calculated the peak inflow discharge into the berm at 12.76 cfs, and the peak outflow at 3.48 cfs. The maximum stage of the berm was 3.82 ft. The calculated peak berm outflow would later represent the simulated inflow rate entering the vegetative strip downstream of the berm.

A significant drop was observed in suspended sediment concentration levels between the seep berm inflow and outflow, from 9600 mg/l to 1660 mg/l. The outflow suspended sediment value is expressed by  $C_{avg}$ , the average suspended sediment concentration in the vegetative filter as described by Equation 73 in Chapter 4. SEDCAD4 provided the trap efficiency of the berm at 81.9%. The following two graphs (in Figure 48) provided by the SEDCAD4 output present the seep berm inflow and outflow hydrographs and sedimentgraphs, respectively:



(a)



(b)

Figure 48: (a) Hydrograph obtained from SEDCAD4; (b) Sedimentgraph obtained from SEDCAD4

## 6.2.2 Vegetative Filter Design Depth Technique

The technique allowing a designer to calculate a vegetative filter water design depth combines the information presented in the appendix with the drag coefficient expression derived through the use of the James et al. (2004) method in Chapter 5, after proving its similarity to the Cheng and Nguyen (2011) expression for vegetated drag coefficient  $C_{Dv}$ . This similarity allows the future use of the Cheng and Nguyen (2011) graph of drag coefficient versus modified Reynolds number for site erosion control design purposes, presented in Figure 49.

### 6.2.2.1 Comparing Drag Coefficients from James et al. (2004) and Cheng and Nguyen (2011)

Equation 81 is used to calculate the drag coefficient. From the results of the experimental trials, and from previous research, it is observed that  $F_d \gg F_{bedshear}$ . Hence, the force due to bed shear can be ignored, and Equation 81 can be written as (using algebraic manipulation and using  $H$  instead of  $y_n$  to represent normal depth):

$$C_d = \frac{2(1-\phi)gS}{mdU^2} \quad (102)$$

The Cheng and Nguyen (2011) definition of vegetation-related hydraulic radius ( $r_v$  from Equation 20) is modified to give:

$$r_v = \frac{(1-\phi)}{md} \quad (103)$$

thus the James et al. (2004) expression for drag coefficient (of Equation 81) can be written as:

$$C_d = \frac{2gSr_v}{U^2} \quad (104)$$

and the vegetated Reynolds number is given by Equation 21, expressed again as:

$$R_v = \left( \frac{U_v r_v}{\nu} \right)$$

where  $U_v$  represents pore velocity.

The expression for drag coefficient in Equation 104 has also been used in James et al. (2008) and Tanino and Nepf (2008). Cheng and Nguyen (2011) use the same expression for drag coefficient in Equation 26, but with use pore velocity  $U_v$  instead of bulk velocity  $U$ , and termed their drag coefficient  $C_{Dv}$ , expressed again as:

$$C_{Dv} = 2 \frac{g S r_v}{U_v^2}$$

Cheng and Nguyen (2011) collapsed their experimental data and other researcher's data into a single relationship when plotting drag coefficient against the Reynolds number, by using the bulk pore velocity in their expressions of drag and stem Reynolds number, and using the vegetated hydraulic radius as the length scale in the stem Reynolds number, changing it into the vegetated Reynolds number  $R_v$  expressed in Equation 21, a concept used in porous media flow, as shown in Appendix B.

#### 6.2.2.2 Design Procedure

For design purposes, the analysis in the previous subsection validates the use of the Cheng and Nguyen (2011) plot presented as Figure 49 (shown below), and is recommended for determining the depth of water  $H$  in the vegetative filter, since it encompasses extensive researchers' experimental data into one collapsed single curve using porous media flow as a basis for derivation of the length scale  $r_v$ .

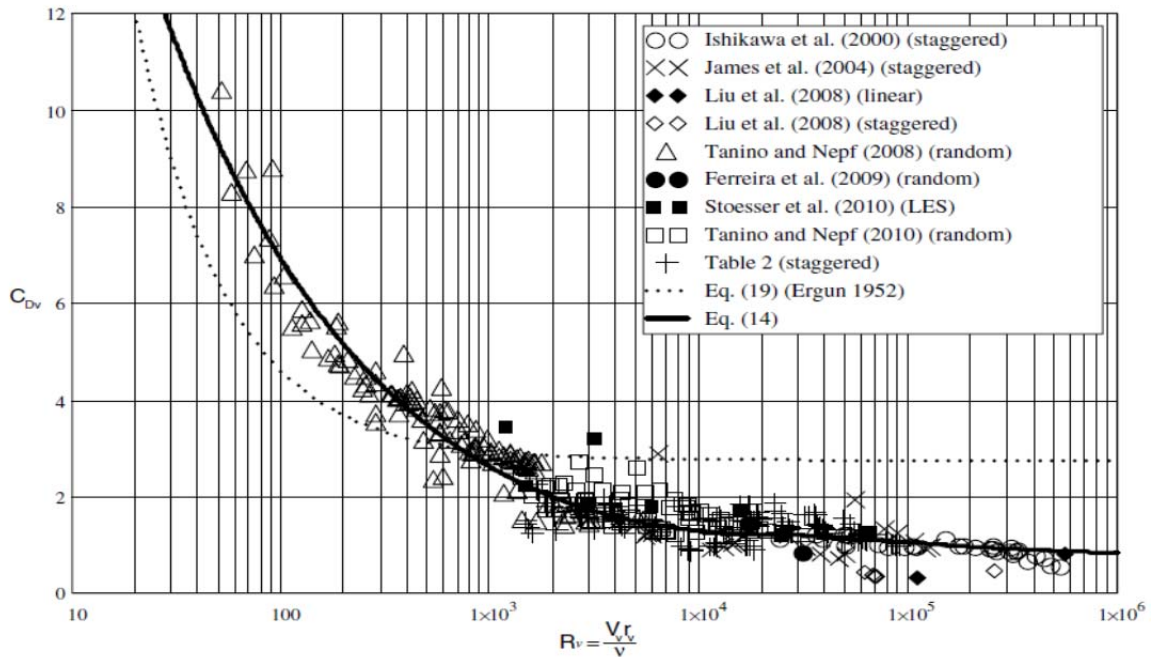


Figure 49: Drag coefficient using pore velocity  $C_{Dv}$  plotted against vegetated Reynolds number  $R_v$  (Cheng & Nguyen, 2011)

The design method is an iterative process and is described as follows:

- Step 1: The parameters  $S$ ,  $\phi$ ,  $d$ ,  $Q$ ,  $b$ , and  $L$  are known. The depth  $H$  and bulk velocity  $U$  are unknown. Initially,  $k/H$  is assumed to be 1, irrespective of whether the design vegetation was chosen to be emergent or submerged. For the first iteration, a vegetated Reynolds number ( $R_v$ ) is chosen randomly with the vegetated hydraulic radius ( $r_v$ ) used as a length scale for a selected vegetation of density  $m$ , stem diameter  $d$ , and solid density  $\phi$ .
- Step 2: The corresponding drag coefficient ( $C_{Dv}$ ) is determined from Figure 49, and the pore velocity is solved for by Equations 20 (or 103) and 26 (or 104 with  $U$  replaced by  $U_v$ ). Then, a new value of  $R_v$  is calculated from Equation 21, mentioned again above in this chapter. Figure 49 is revisited with the new value of  $R_v$ , and another iteration is performed. The iterative procedure is repeated until the error in the pore velocity values  $U_v$  is acceptable to the designer. Once the value of  $U_v$  is determined, then the bulk velocity  $U$  is calculated from Equation 18, where  $U = U_v (1 - \phi)$ .

Subsequently, the depth of water  $H$  is calculated from continuity:  $Q = UA = UHb$ . The shear stress of the vegetative filter is subsequently calculated and compared with the permissible shear stresses for vegetative linings in Sturm (2001) and Chen and Cotton (1988), depending on the vegetative retardance class selected for the design.

- Step 3: If the design vegetation was chosen to be flexible and submerged, then an additional step is required, where  $k$  is calculated from Equation 64. The final drag coefficient design value from Step 2 is then divided by  $k/H$ , where  $H$  is also obtained from Step 2. The pore velocity is subsequently calculated. If the error between the new  $U_v$  value and the final  $U_v$  value from Step 2 is unacceptable, then a new  $R_v$  value is calculated from the new  $U_v$  value, and Figure 49 is revisited for a new drag coefficient. Subsequently,  $U_v$ ,  $U$ ,  $H$ ,  $k$ , and  $k/H$  are calculated. The most recent drag coefficient value is then divided by the most recent  $k/H$  value, and a new pore velocity is subsequently calculated and compared with the value preceding it. The process is repeated until the error in the pore velocity values is acceptable to the designer. Once the value of  $U_v$  is decided, then the bulk velocity  $U$  is calculated from Equation 18. Subsequently, the depth of water  $H$  is calculated from continuity:  $Q = UA = UHb$ . The shear stress of the vegetative filter is subsequently calculated and compared with the permissible shear stresses for vegetative linings in Sturm (2001) and Chen and Cotton (1988), depending on the vegetative retardance class selected for the design.
- Step 4: Based on: (1)  $d_{50}$  of the sediment leaving the seep berm which determines  $w_f$ , (2)  $q = UH$ , (3) the length  $L$  of the vegetative filter in the flow direction, and (4) the type and density of vegetation, the trap efficiency of the vegetative filter is determined from Figure 47. Finally, the combined trap efficiency of both the seep berm and the vegetative filter is determined.

Through SEDCAD4, a designer can design a seep berm for a construction site based on the land, cover, sediment, and storm parameters. SEDCAD4 provides the trap efficiency of the seep berm, the peak outflow from the seep berm, and the concentration

of suspended sediment in the outflow. A designer can then decide on a certain vegetation type and density for the vegetative strip to be installed immediately downstream of the seep berm. Using the iterative procedure just described, it is fairly simple for a designer to determine the flow depth, and length and density of stems, needed in the vegetative filter, and then to determine its trap efficiency as well as the combined trap efficiency.

### 6.2.2.3 Numerical Design Example

The IHM field demonstration project soil was the design sediment chosen for the subsequent design example. In Subsection 6.2.1, the IHM sediment was used in SEDCAD4 to design a seep berm and obtain its trap efficiency. The seep berm sediment outflow of 3.48 cfs from Table 19 was used as the vegetative filter inflow for the design example. Most of the suspended sediment in that inflow was comprised of finer sediment, as the coarser sediment had already settled behind the berm wall. However, the suspended sediment flowing through the outlet pipes and emergency spillway of the seep berm and entering the vegetative filter possess a different grain size distribution than the original distribution entering the seep berm. Thus, it was necessary to find the new grain size distribution entering the vegetative filter. It should be noted that the seep berm overflow can be collected in a perforated diffuser pipe for uniform distribution across the vegetative filter.

Equation 99 was used to calculate theoretical trap efficiency for the seep berm. The IHM sediment sample was divided into size fractions, then the dimensionless particle diameter and fall velocity were calculated for each size fraction  $X$  from Equation 101 and Equation 100, respectively. The settling efficiency for each size fraction was calculated from Equation 98, and the peak overflow rate per unit length of seep berm was obtained from SEDCAD4. Since the size fractions were non-uniform, the exponential part of Equation 99 was integrated using the trapezoidal rule for each  $\Delta X$ . Subsequently, the trap efficiency of each size fraction was calculated from Equation 99, and all size fraction trap efficiencies were summed up to give the theoretical trap efficiency of the seep berm, which was 83.1%. Table 20 provides calculations to find theoretical trap efficiency after

calculating fall velocities for different grain sizes from the IHM grain size distribution in Chapter 3. The last column is summed up and the theoretical trap efficiency was calculated from Equation 99. The portion of each size fraction overflowing the seep berm was determined from the percent of each size fraction trapped by the berm.

Table 20: Theoretical trap efficiency calculations ( $Q=3.5$  cfs,  $A_s=100$  ft<sup>2</sup>,  $Q/A_s=0.035$ )

$d, mm$	Size Fraction	(Fraction 1 – Fraction 2) = Fraction Interval	$w_f / (Q/A_s)$	$e^{-w_f / (Q/A_s)}$	[(Exp1 + Exp2)*(Fraction Interval)]/2
0.840	0.97	0.12	9.45	7.85E-05	0.0005
0.350	0.85	0.06	4.85	0.008	0.0014
0.250	0.79	0.11	3.37	0.034	0.0055
0.210	0.68	0.29	2.70	0.067	0.0265
0.180	0.39	0.14	2.17	0.114	0.0215
0.150	0.25	0.13	1.61	0.199	0.0398
0.105	0.12	0.09	0.95	0.416	0.0556
0.055	0.03	0.02	0.25	0.776	0.0176
0.045	0.01		0.17	0.845	

The theoretical value of trap efficiency of 83.1% agrees closely with the seep berm trap efficiency of 81.9% obtained from SEDCAD4. The trap efficiency of each size fraction was then used to calculate the remaining mass of sediment from the original sediment sample in each size fraction, and an output grain size distribution was plotted, shown in Figure 50, with a  $d_{50} = 0.15$  mm, and a geometric standard deviation  $\sigma_g =$

$$d_{84.13} / d_{50} = 1.33.$$

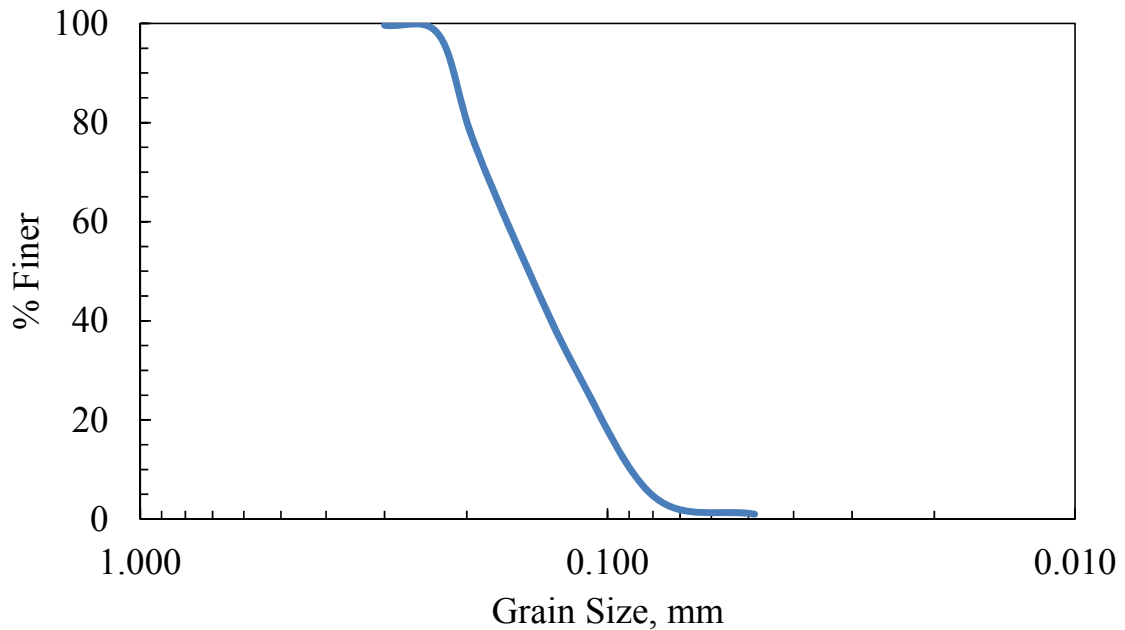


Figure 50: Grain size distribution from the theoretical trap efficiency method

Prior to determining the vegetative filter design water depth  $H$ , the following parameters are known or selected by the designer:

$S$  = slope

$N$  = number of stems

$m$  = vegetation density

$\phi$  = solid volume fraction

$b$  and  $L$  = width and length of the vegetation filter, respectively

$d$  = stem diameter

$Q$  = runoff flow rate

Since the theoretical trap efficiency of the seep berm agreed closely with that of SEDCAD4, then the latter was used in the subsequent steps of the design example. From

the SEDCAD4 output in Subsection 6.2.1, the suspended sediment concentration in the runoff entering the seep berm is 9600 mg/l, and the suspended sediment concentration exiting the seep berm and entering the vegetative filter is 1660 mg/l with  $d_{50} = 0.15$  mm. Bermuda grass of retardance class C is selected, and the stems are assumed to be cylindrical. The vegetative filter has the following known parameters:

- Emergent rigid vegetation
- stem diameter  $d = 1$  cm = 0.0328 ft
- solid volume fraction  $\phi = 0.086$ , and stem density  $m = 101.94$  stems/ft<sup>2</sup>
- Slope  $S = 1\% = 0.01$
- Flow rate  $Q = 3.48$  cfs
- Vegetative filter width  $b = 100$  ft
- Vegetative filter length  $L = 6$  ft

The iterations for the design procedure parameters are shown in Table 21:

Table 21: Iterations for the numerical design example

Iteration No.	$R_v$	$C_{Dv}$	$U_v$ , ft/sec
1	2000	2.00	0.297
2	6800	1.70	0.322
3	7300	1.60	0.332
4	7600	1.55	0.337
5	7700	N/A	N/A

The new  $R_v$  value for Iteration 5 is 7700. However, the error between the values of  $R_v$  in Iterations 3 and 4 was 1.53%, considered an acceptable value. Using  $U_v = 0.337$  ft/s, the bulk velocity  $U$  is obtained through Equation 18, giving  $U = 0.308$  ft/sec. Thus,  $Q = UA = UbH$ , so  $H = 1.36$  in., the design depth of the water flow in the vegetative filter.

The design depth of water flow is used to obtain the shear stress of the vegetative filter, calculated at 3.50 Pa. The calculated shear stress is less than the permissible shear

stress of 48 pa for the chosen vegetation retardance class, given in Sturm (2001) and Chen and Cotton (1988).

Using the  $d_{50}$  calculated for the suspended sediment exiting the seep berm, the fall velocity is calculated, and  $SEF = 8.9$  from Equation 98. For that value of SEF, a trap efficiency  $TE = 0.670 = 67.0\%$  was obtained from Figure 47. With both trap efficiencies of the seep berm and vegetative filter now available, the combined trap efficiency of the joint erosion control mechanism was calculated to be 94% from Equation 105:

$$TE_{final} \% = 100 * [TE_{seep\ berm} + TE_{veg.filter} (1 - TE_{seep\ berm})] \quad (105)$$

where the suspended sediment concentration in the runoff exiting the vegetative filter is 575 mg/l, from the original concentration of 9600 mg/l entering the seep berm.

## 7. CONCLUSIONS

### 7.1 Summary of the Thesis

This thesis research was focused on studying and introducing methods that reduce suspended sediment concentration in urban stormwater runoff from construction sites in a quantifiable manner. Two BMPs were introduced as alternative erosion control measures: seep berms and vegetative filters. The objective of this thesis was to build on the findings of the Dirt 2 Committee (2001), Warner et al. (2004), and the joint demonstration project of Sturm et al. (2007) by developing performance-based measures of seep berms and vegetative filters employed in series.

Seep berms act as sedimentation basins and have high suspended sediment trapping efficiencies; however outflow from the berm contains finer sediment particles that need very lengthy detention times to settle out of the flow. Thus, vegetative filters located directly downstream of the berm can accept the overflowing berm flow and provide additional settling and filtration of the finer sediment particles, through slow flow rates. Hence, a combined seep berm – vegetative filter erosion control measure, working in series, was proposed as an effective BMP with the potential and capability of handling large water runoff rates that may cause water to overtop the seep berm. The objective of the experimental trials described in this thesis was to develop the data needed for estimating the flow resistance of the vegetative filter and its settling efficiency as part of a proposed joint best-management practice (BMP).

The installation, methodology, and results of the side-by-side field comparison of a seep berm and silt fence in terms of suspended sediment trapping efficiency were detailed in the thesis. The side-by-side demonstration project showed seep berms to be a viable erosion control measure compared to silt fences in terms of sediment settling efficiency and cost-effectiveness. This step in the thesis was important because silt fences are more commonly used in the Atlanta metro area but were shown to be inferior to seep berms in sediment removal efficiency.

The addition of vegetative filters to seep berms required an experimental study of their flow resistance as well as their sediment trapping efficiency. This thesis introduces and details the experimental research objective, apparatus, and methodology for open channel flow through vegetative filters. The objective was to study the trapping efficiency of both emergent cylindrical rigid and submerged rectangular flexible vegetation, with two vegetation densities for each case. The experimental process was divided into several phases for each flow rate used in each vegetation filter case: (1) obtaining uniform water surface profiles and measuring the normal depth; (2) calculating the drag coefficient of the vegetative filter; (3) measuring velocity and turbulence profiles within the vegetation using an acoustic Doppler velocimeter (ADV); (4) using ISCO samplers to collect flow samples at four different locations across the vegetative filter length; and (5) measuring the trap efficiency.

The first step in the experimental trials was to establish uniform flow for all the flow rates used. Uniform flow depths were measured as the asymptotic approach depth of M1 and M2 profiles for the same  $Q$ . Once uniform flow depths were determined, a specific tailgate setting could be used to reproduce the uniform flow depth along the full length of the vegetative filter. Subsequently, the drag coefficient for each flow rate case was calculated, and plotted against the dimensionless parameters affecting the drag force exerted by flow through vegetation.

An ADV was used to measure velocity profiles and turbulence intensities within the vegetation. The ADV was inserted in the flow at a streamwise station of 1/3 of the vegetative filter length, at different locations across the filter width. The point velocity and turbulence intensity profiles at each location were measured for the flow rate ranges specified.

The suspended sediment flux for each experimental trial was calculated from the concentration samples obtained by an ISCO sampler, and subsequently the trap efficiency for each trial was calculated and was observed to decrease as the flow rate increased. Experimental trap efficiencies were expressed as a function of the dimensionless variable  $SEF = w_s/(q/L)$ , and type and density of vegetation.

The thesis presented a numerical example explaining the hydraulic performance and trap efficiency of the joint erosion control comprised of a seep berm and a vegetative filter working in series. The objective was to develop a technique that would allow designers to determine the design normal flow depth through a vegetative filter when used as an erosion control measure, and its trapping efficiency as well as that of the joint BMP. The SEDCAD4 software was used to model the seep berm; it uses the SCS runoff model and reservoir routing along with an erosion and sedimentation model to predict the peak outflow and its sediment concentration from the seep berm. The SEDCAD4 outflow rate and suspended sediment concentration results were then applied to the vegetative filter as the inflow runoff rate and inflow suspended sediment concentrations. An iterative methodology was introduced to determine the depth of flow in the vegetated filter based on the experimental data presented as dimensionless graphs of vegetative drag coefficient as a function of vegetated Reynolds number, and trap efficiency as a function of settling efficiency.

## **7.2 Conclusions**

Seep berms were found to be superior to silt fences with respect to trap efficiency and structural stability as an erosion control measure. The fact that they are also a much cheaper alternative than silt fences, and can be constructed using excavated soil fill from the construction site itself, makes them a more cost effective alternative than silt fences or other erosion control measures.

The vegetative drag coefficient in the flume follows a decreasing power trend when plotted against Stem  $Re$  for both emergent rigid stems as well as submerged flexible stems. This follows trends observed in previous research for rigid cylinders. Using the Cheng and Nguyen (2011) drag coefficient expression that incorporates pore velocity instead of bulk velocity, the experimental drag coefficient data collapses onto a single empirical relationship when plotted against vegetated Reynolds number, which is the stem Reynolds number divided by the solid volume fraction of the vegetation. The analogy with porous media flow can be extended to flat stems as well as cylindrical

stems, and it was shown how these flexible, submerged vegetation types could be incorporated into the same relationship for coefficient of drag as rigid, emergent cylinders.

An increase in vegetation density causes an increase in the streamwise and spanwise turbulence intensity magnitudes and hence more shedding of turbulent eddies, and a higher point velocity magnitude deficit between ADV measuring locations in the wake of the stems and between stems that increased with an increase in vegetation density. The point velocity magnitudes behind the stem were always less than the location in the free stream behind and between two stems, due to larger wake effects and eddy turbulence shedding that produced a lag effect on the velocity profiles in the stems. Similarly, streamwise and spanwise turbulence intensities were always larger in magnitude in the location behind a stem, for the same reason. Higher turbulence intensity magnitudes occur for submerged vegetation than emergent vegetation at the same vegetation density. It was shown that for all four types of vegetation, the normalized point velocity and turbulence intensity profiles were nearly uniform in the vertical direction within the stem layer, indicating that it can be assumed that submerged vegetation exhibits emergent vegetation properties within the stem layer as long as it is not deflected excessively. Relative location in the vegetative filter plays no role with respect to the vertical relative turbulence intensity magnitude, which was smaller than the streamwise and spanwise turbulence intensities in all four vegetation cases. The turbulence structure is dominated by a vegetation density-dependent wake flow and wake interference, and those effects decrease with a decrease in vegetation density. It was concluded that the turbulence structure satisfied the conditions for a plug-flow model relative to an exponential concentration decrease in the streamwise direction.

It is concluded that emergent vegetation produces higher drag and higher trap efficiencies than submerged vegetation at the same vegetation density. Presentation of the trap efficiencies of all four vegetation types as a function of the dimensionless settling efficiency along with the theoretical trap efficiency relationship for settling with no vegetation, was shown to be an effective method for generalizing the results to be used in design. It is concluded from the plot showing trap efficiency against settling efficiency

that, for the same vegetative filter length and grain size distribution of suspended sediment, the rate of increase of trap efficiency decreases as the flow rate increases. Moreover, the observation of trap efficiency curves leveling off for  $SEF > 6$  allows the determination of the maximum vegetative filter length for a design case.

It is concluded that the use of a combined seep berm – vegetative filter erosion control measure in series allows for more efficient suspended sediment trapping across a wider range of sediment grain sizes than the use of each control separately. The seep berm had a higher trap efficiency than the vegetative filter, however the grain size distribution of the suspended sediment in the seep berm outflow showed a higher percentage of fines than the original suspended sediment grain size distribution in the seep berm inflow. Thus, the presence of a vegetative filter immediately downstream of the seep berm was shown to address the issue of filtering out the finer suspended sediment particles in the stormwater runoff. Hence, the combination of both erosion control measures in series was shown to improve overall suspended sediment trapping from coarse to fine sediment particles.

### **7.3 Contributions of this Research**

The major contributions of this thesis are presented as follows:

- This research showed quantitatively for the first time that seep berms are superior to silt fences for erosion control from construction sites based on the collection of field data at two construction sites in the Atlanta metro area.
- The force balance approach on a control volume representing the vegetative filter was shown to be more useful and explanatory for presenting the variation of drag coefficient with Reynolds number when pore velocities that depended on the solid volume fraction of vegetation were used in the definition of both the drag coefficient and the stem Reynolds number.
- It was shown how porous media flow concepts for length scale could be extended to flat rectangular stems, and how the relative vegetation height should be

reflected in the drag coefficient expression for submerged flexible vegetation. These modifications resulted in the collapse of the coefficient of drag data for flexible, submerged vegetation strips into the same relationship as that for rigid, emergent cylinders.

- Measurement of the velocity and turbulence field was shown to justify a plug-flow assumption with an exponential decrease in sediment concentration with flow length in the vegetative filter which resulted in a dimensionless experimental relationship for trap efficiency as a function of settling efficiency, and type and density of vegetation.
- The overall sediment reduction performance for an innovative combined erosion control measure consisting of a seep berm and vegetative strip in series was demonstrated quantitatively using a suggested design procedure and the experimental results of this research.

#### **7.4 Future Research**

A challenge for the future would be to use natural vegetation, and study its effects on drag coefficient and sediment settling. The vegetation used in the lab experimental trials was employed to simulate natural vegetation as much as possible; however a more accurate understanding of the dynamics of natural vegetative filters would be possible through the use of several types of naturally-occurring vegetation. Moreover, since naturally-occurring vegetation grows in random patterns, the effect of the randomness on point velocity and turbulence intensity profiles must be studied further. This in turn affects sediment settling and the trap efficiency of the vegetation. In addition, very dense vegetation patterns (such as bush types) and very sparse vegetation patterns must be tested and observed. The effects of foliage on suspended sediment settling should be studied more in depth, as should the relationship between the increased drag due to the foliage and the trap efficiency of the vegetation. The drag coefficient, point velocity, turbulence intensity, and trap efficient data can be used as a building block for future research involving natural vegetation, by providing guidelines to vegetative

density experimental ranges, vegetative filter strip dimensions, and expected trap efficiency values. This future research can additionally be extended to rooftop gardens or green roofs, which are an upcoming trend in urban areas. Natural vegetative filters are placed on rooftops to encourage infiltration before the runoff gets to the gutter. By intercepting the rain runoff at the source, the green roof eliminates the potential multiplying effect further downstream of the runoff chain.

A very important observation in the experimental trials was the presence of a near-bed velocity spike, appearing more prominently with decreased density, and especially behind a stem. More research on momentum exchange in the near-bed region should be performed to understand this phenomenon, and to understand its effect on suspended sediment settling in the near-bed region.

For emergent vegetation, since all the flow is through the vegetation or resistance layer, the possibility of producing theoretical distributions for velocity and concentration profiles that take into account the nature of the turbulence structure as reflected by the turbulent eddy diffusivity should be studied. The result might produce a more general relationship for drag coefficient and trap efficiency to be used in vegetative filter design as a function of type of foliage and its flexibility and density. Moreover, more research should be performed on the free stream region above submerged vegetation to understand its dynamics and its role in suspended sediment transport and settling. The vegetation-free stream interface is a region of heavy momentum exchange, and the effect of that region on vegetative drag coefficient and trap efficiency should be explored further.

## APPENDIX A

### PHOTOS OF THE EXPERIMENTAL FLUME AND VEGETATIVE STEMS

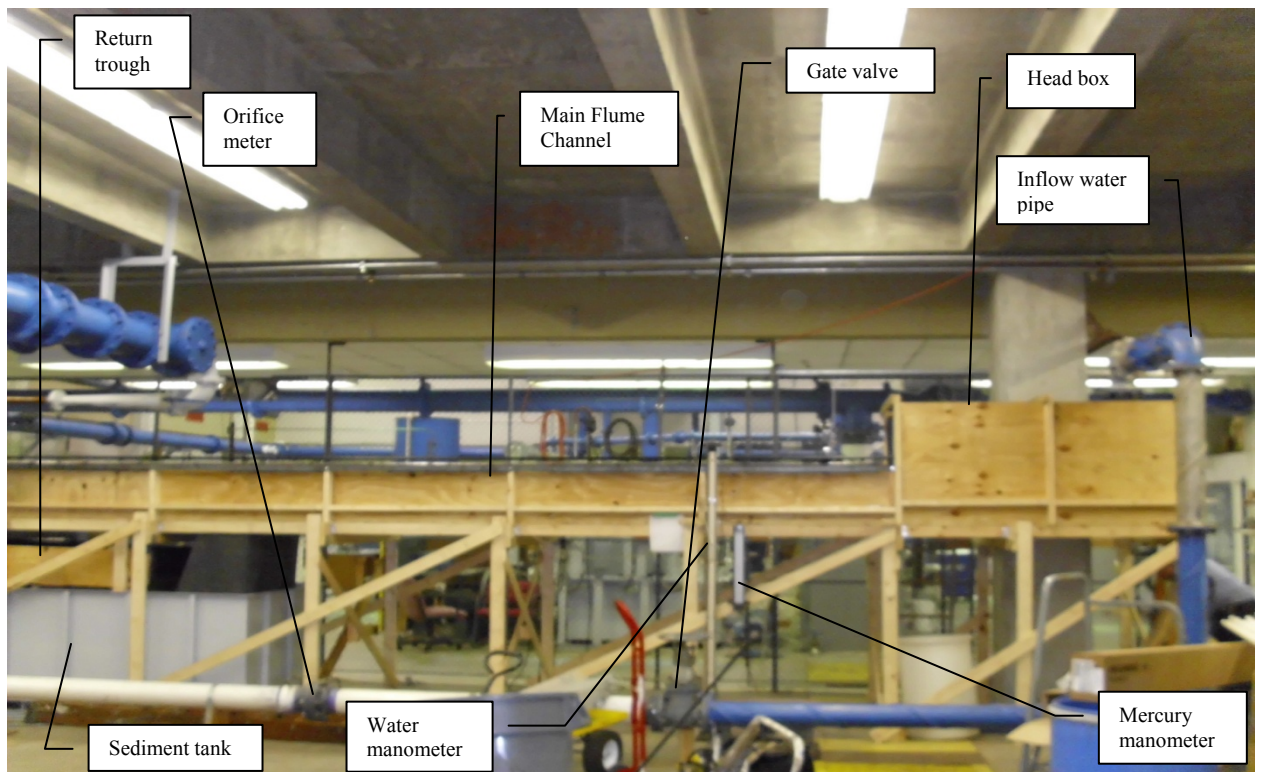


Figure A. 1 : Photo of flume. Flow travels from right to left.



Figure A. 2: Photo of the cylindrical wooden rods simulating emergent rigid vegetation,  $m = 101.9$  stems/ft<sup>2</sup>



Figure A. 3: Photo of the rectangular plastic strips simulating submerged flexible vegetation,  $m = 101.9$  stems/ft<sup>2</sup>

## APPENDIX B

### POROUS MEDIA ANALOGY FOR OPEN CHANNEL FLOW THROUGH VEGETATIVE FILTERS

One of the objectives of the experimental trials described in Chapter 5 was to develop a technique that would allow designers to determine the design depth  $H$  or  $y_n$  of water required when using vegetative filters as an extra erosion control measure downstream of seep berms. The applicability of porous media concepts to vegetative filters is analyzed, where a vegetative filter is treated as a porous media control volume. The analysis focuses on the relationship between the drag coefficient of the vegetation filter and the modified Reynolds number  $Re'$  used in porous media, to determine the design water depth  $H$  of a vegetative filter in the field. This relationship was approached by Cheng and Nguyen (2011), but will be explained thoroughly and validated in this subsection.

Flow through porous media is usually described by Darcy's Law, which is a one-dimensional flow formula:

$$\frac{K\Delta P}{\mu L} = \frac{Q}{A} \quad (\text{B - 1})$$

where  $K$  is the permeability,  $\mu$  is the fluid viscosity,  $Q$  is the flow through an area  $A$ , and  $\Delta P$  is the pressure drop over a length  $L$ . Hellstrom and Lundstrom (2006) stated that Darcy's law is applicable if the flow Reynolds number ( $Re$ ) is low. The Reynolds number is defined as a measure of the ratio of inertial forces to viscous forces for given flow conditions, when a fluid is in relative motion to a surface. However, once flow  $Re$  exceeds a certain threshold, Darcy's law becomes insufficient, and the pressure drop increases to values higher than what Darcy's law is able to predict. The Forchheimer's equation can then be used (Hellstrom & Lundstrom, 2006):

$$\frac{K\Delta P}{\mu L} = \frac{Q}{A} + b \left(\frac{Q}{A}\right)^m \quad (\text{B - 2})$$

where  $b$  is defined as a property of the porous media, and  $m$  is defined as a measure of the influence of fluid inertia. The Forchheimer's equation is considered the classical approach to characterize macroscopically the effect of inertia on flow through porous media (Andrade et al., 1999). Andrade et al. (1999) also presented the Forchheimer's equation as:

$$\frac{\Delta P}{L} = \alpha \mu U + \beta \rho U^2 \quad (\text{B - 3})$$

where  $U$  is the fluid velocity in the porous media, and  $\alpha$  describes the reciprocal permeability of the porous material, and  $\beta$  is the "inertial parameter". Both  $\alpha$  and  $\beta$  depend on  $\varepsilon$ , which is the porosity of the porous media. The Forchheimer's equation can further be rearranged to show a generalized friction factor-modified Reynolds number correlation, in the following form (Andrade et al., 1999):

$$f = \frac{1}{\text{Re}'} + 1 \quad (\text{B - 4})$$

In porous media, the modified Reynolds number is described as  $\text{Re}'$ . The length scale used is grain diameter  $d$ , similar to the use of stem diameter  $d$  for Stem  $\text{Re}$  in vegetative filters.  $\text{Re}'$  will be shown later to be equal to  $(\text{Stem Re})/\phi$ , where  $\phi$  is the solid fraction of the packed bed in porous media. For flow through vegetative filters, Cheng and Nguyen (2011) used the stem diameter  $d$  as the length scale, with  $\phi$  representing the solid volume fraction of the vegetative filter for calculating stem Reynolds number (Stem  $\text{Re}$ ) and modified stem Reynolds number ( $\text{Re}'$ ). In the upcoming derivations, the parameter  $d$  was used to represent grain size diameter in porous media, and stem diameter in open channel flow through vegetative filters.

The generalized friction factor-modified Reynolds number correlation in porous media is universal for all ranges of Reynolds numbers. It has been successfully used to correlate experimental data from a large spectrum of both porous materials and flow conditions (Dullien, 1979). Andrade et al. (1999) plotted the generalized friction factor  $f$  vs  $\text{Re}'$  for three different values of porosity  $\varepsilon$ . They computed the pressure drops for all

values of  $\varepsilon$  and Reynolds number  $Re$ , where the length scale used for  $Re$  was the grain diameter  $d$ . They then fit the results in Forchheimer's equation to calculate  $\alpha$  and  $\beta$ , and consequently obtained values for  $f$  and  $Re'$ . The logarithmic graph presented in Figure B.1 shows the dependence of  $f$  on  $Re'$ , taken from Andrade et al. (1999). The decreasing trend shows lower values of  $f$  for higher values of  $Re'$ , similar to the trend obtained for vegetative drag coefficient  $C_{Dv}$  (from Equation 26) when plotted against modified stem Reynolds number  $Re' = R_v$  (from Equations 22 and 21, respectively).

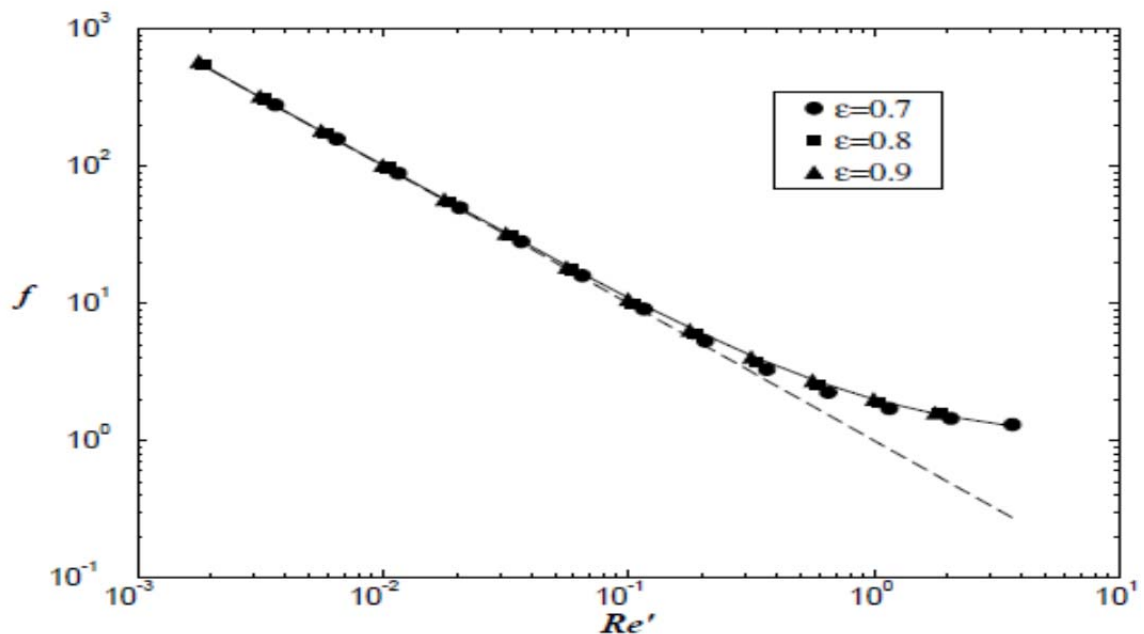


Figure B. 1: Friction factor  $f$  plotted against modified Reynolds number (Andrade et al., 1999)

The graphs from Figure B.1 and Figure 49 exhibit similar decreasing trends. The former is for porous media and the latter is for vegetative filters in open channel flow. The similarity of the graphs prompts a deeper look into the usage of the concept of modified Reynolds number  $Re'$  of porous media and its application to open channel flow through vegetative filters instead of the more common stem Reynolds number.

The Forchheimer's equation for porous media was modified by Ergun in 1952 (Hellstrom & Lundstrom, 2006). Ergun assumed that the sum of viscous and kinematic forces defined the total pressure drop across a fluidized bed. Through numerous experiments and by fittings to experimental data, Ergun devised the following equation applicable for a wide range of Reynolds numbers (Hellstrom & Lundstrom, 2006):

$$\frac{\Delta P}{L} g = 150 \frac{(1-\varepsilon)^2}{\varepsilon^3} \frac{\mu U}{d^2} + 1.75 \frac{(1-\varepsilon)}{\varepsilon^3} \frac{\rho U^2}{d} \quad (\text{B - 5})$$

where  $U = Q/A$  is the bulk flow velocity, and  $\varepsilon$  is the fractional void volume in the bed, and  $d$  is the effective diameter of the particles. The solid portion of the packed bed is defined as  $\phi = 1 - \varepsilon$ .

Niven (2002) provided a dimensional analysis of the Ergun equation in porous media. He stated that, for flow through packed beds, the traditional equation for hydraulic radius  $R=A/P$  (where  $A$  is the cross-sectional flow area and  $P$  is the wetted perimeter) is not favorable since packed beds are not straight conduits, but are variable diameter conduits. Thus, the hydraulic radius  $R$  will vary along the length of flow from point to point (Niven, 2002). A better description of length scale would be the ratio of the volume of voids to their surface area, or void length scale  $l_\varepsilon$ . For spherical particles (sphericity of particles = 1, similar to the identical stems in a vegetative filter), it is defined as (Niven, 2002):

$$l_\varepsilon = \frac{V_v}{A_v} = \frac{V_v/V_T}{A_v/V_T} = \frac{\varepsilon d}{6(1-\varepsilon)} \quad (\text{B - 6})$$

where  $V_v$  is the volume of voids,  $A_v$  is the surface area of voids,  $V_T$  is the total volume of the packing, and  $d$  is the spherical particle diameter. The porosity  $\varepsilon = V_v/V_T$ , and  $A_v/V_T$  is defined as the product of the surface area of a single particle ( $A=\pi d^2$ ) multiplied by the number of particles per unit volume  $N = [(1 - V_v)/V_p]/V_T = 6(1 - \varepsilon)/\pi d^3$ , and  $V_p$  is the volume of a single particle. This formulation of  $l_\varepsilon$  has also been mentioned in previous research (Bird et al., 1960; Churchill, 1988). For the purposes of the dimensional analysis, and since constants can be dropped from dimensionless groups,  $l_\varepsilon$  can be simplified to:

$$l_\varepsilon = \frac{\varepsilon d}{(1-\varepsilon)} \quad (\text{B - 7})$$

Bird et al. (1960) and Churchill (1988) stated that a more accurate representation of flow velocity through porous media would be the interstitial or pore velocity  $U_v$ , defined as  $U_v = U/\varepsilon$ , where  $U$  is the bulk flow velocity. Thus, the dimensional relationship for the Ergun equation in porous media can be written as:

$$\frac{\Delta P}{L} = f(\mu, \rho, U_v, l_\varepsilon, \rho g) \quad (\text{B - 8})$$

According to Glicksman et al. (1994) gravity does not act as a variable in its own right, hence the effect of gravity is taken as  $\rho g$  instead of  $g$ .

The results of the dimensional analysis were (Niven, 2002):

$$\frac{\Delta P/L}{\rho g} = f\left(\text{Re}' = \frac{\rho l_\varepsilon U_v}{\mu}, \text{Ga}^* = \frac{\rho^2 g l_\varepsilon^3}{\mu^2}\right) \quad (\text{B - 9})$$

where  $\text{Re}'$  is the modified Reynolds number based on the pore velocity, and  $\text{Ga}^*$  is a modified Galileo number based on the void length scale  $l_\varepsilon$ . The original fluid particle dimensionless Galileo number  $\text{Ga}$  is based on particle diameter  $d$ , and is defined as (Niven, 2002):

$$\text{Ga} = \frac{\rho^2 g d^3}{\mu^2} \quad (\text{B - 10})$$

Substituting for  $l_\varepsilon$  in  $\text{Re}'$  and  $\text{Ga}^*$ , the following expressions are obtained:

$$\text{Re}' = \frac{\rho d U}{\mu(1-\varepsilon)} \quad (\text{B - 11})$$

$$\text{Ga}^* = \frac{\rho^2 g d^3 \varepsilon^3}{\mu^2(1-\varepsilon)^3} \quad (\text{B - 12})$$

Hence, the Ergun equation for porous media can be rearranged as (Niven, 2002):

$$\frac{\Delta P d \varepsilon^3}{L \rho U^2 (1-\varepsilon)} = \frac{150}{\text{Re}'} + 1.75 \quad (\text{B - 13})$$

It is evident that the expression for  $Re'$  as presented by Niven (2002) in Equation B-13 is comparable to the modified Reynolds number  $Re'$  used in the Forchheimer's equation presented by Andrade et al. (1999) in Equation B-4, where both equations are of the same form.

Thus, dimensional analysis showed that a viable representation of velocity for porous media cases would be through the use of pore velocity instead of bulk velocity. It is seen that the effect of porosity is accounted for in the void length scale and pore velocity, and consequently reflected in the dimensional analysis results through the modified Reynolds number  $Re'$ . For those reasons, porosity was not included as a parameter in the dimensional analysis. The dimensional analysis, through the use of the void length scale and pore velocity instead of the grain diameter  $d$  and bulk velocity  $U$ , better reflects the fundamental physical processes of the Ergun equation (Niven, 2002).

Since the dimensional analysis for Ergun's equation for porous media showed the relevance of using pore velocity and modified Reynolds number as a better representation of data, it remains to be seen whether those dimensional analysis results could be exported to open channel flow through vegetative filters. Thus, in the analysis presented in the next paragraphs, the Ergun equation will be rearranged to reflect the relationship between vegetative drag coefficient and modified Reynolds number in vegetative filters.

The Ergun equation can be applied in flow through vegetated filters by assuming the vegetative filter to resemble a porous medium. In that case,  $\phi$  is defined as the volumetric solid fraction of the vegetative filter,  $d$  is the stem diameter, and  $U$  is the bulk flow velocity. The Ergun equation for vegetated filters can hence be rewritten as:

$$\frac{\Delta P}{L} g = 150 \frac{(\phi)^2}{(1-\phi)^3} \frac{\mu U}{d^2} + 1.75 \frac{(\phi)}{(1-\phi)^3} \frac{\rho U^2}{d} \quad (\text{B - 14})$$

Algebraic manipulation of Equation B-14 gives:

$$\frac{\Delta P}{L} \frac{g}{\mu} \frac{(1-\phi)^3}{\phi^2 U} d^2 = 150 + 1.75 \frac{\rho d U}{\mu \phi} \quad (\text{B - 15})$$

Substituting in Equation B-15 for stem Reynolds number and pore velocity (from Equations 11 and 18), and for the Cheng and Nguyen (2011) vegetated hydraulic radius (from Equation 20), the following expression is obtained:

$$\frac{\Delta P}{L} \frac{g}{\mu} \left(\frac{4}{\pi}\right)^2 \frac{r_v^2}{U_v} = 150 + 1.75 \frac{Re'}{\phi} \quad (\text{B - 16})$$

where  $Re' = (\text{Stem } Re)/\phi$ .

Substituting for  $\Delta P = h_L \rho g$  (where  $h_L$  is the friction loss, and the bed slope  $S = h_L/L$ ) in Equation B-16, then:

$$S \frac{\rho g^2}{\mu} \left(\frac{4}{\pi}\right)^2 \frac{r_v^2}{U_v} = 150 + 1.75 Re' \quad (\text{B - 17})$$

Through the introduction of the coefficient of drag expression as defined by Cheng and Nguyen (2011) (from Equation 26) and some algebraic manipulation, Equation (B - 17) is given as:

$$C_{Dv} \left(\frac{8g}{\pi^2}\right) = \frac{150}{Re'} + 1.75 \quad (\text{B - 18})$$

It is observed from applying the Ergun equation to open channel flow through vegetative filters that the drag coefficient  $C_{Dv}$  is a function of the modified Reynolds number  $Re'$ . The drag coefficient  $C_{Dv}$  is a function of the surface resistance factor  $f'$ , where  $C_{Dv} = f(f')$ . From Equation (B - 18), it is clear that the Ergun equation for vegetative filters has the same form of both the Forchheimer's equation described by Andrade et al. (1999) in Equation B-4 and the Ergun equation as presented by Niven (2002) in Equation B-13. It can be concluded that a viable representation of drag coefficient for vegetative filters would be through the use of pore velocity instead of bulk velocity, and through the use of the modified Reynolds number  $R_v$  from Equation 21 (or  $Re'$  from Equation 22), which has an identical expression to the porous media modified Reynolds number.

## APPENDIX C

### ADV PROFILES FOR ALL VEGETATION AND FLOW RATES

Appendix C presents the remaining normalized profiles of: point velocity, streamwise turbulence intensity, spanwise turbulence intensity, and vertical turbulence intensity; for all four cases of vegetation and their respective flow rates. All profiles were normalized by bulk velocity.

#### Emergent vegetation of density $m = 101.9$ stems/ft<sup>2</sup>

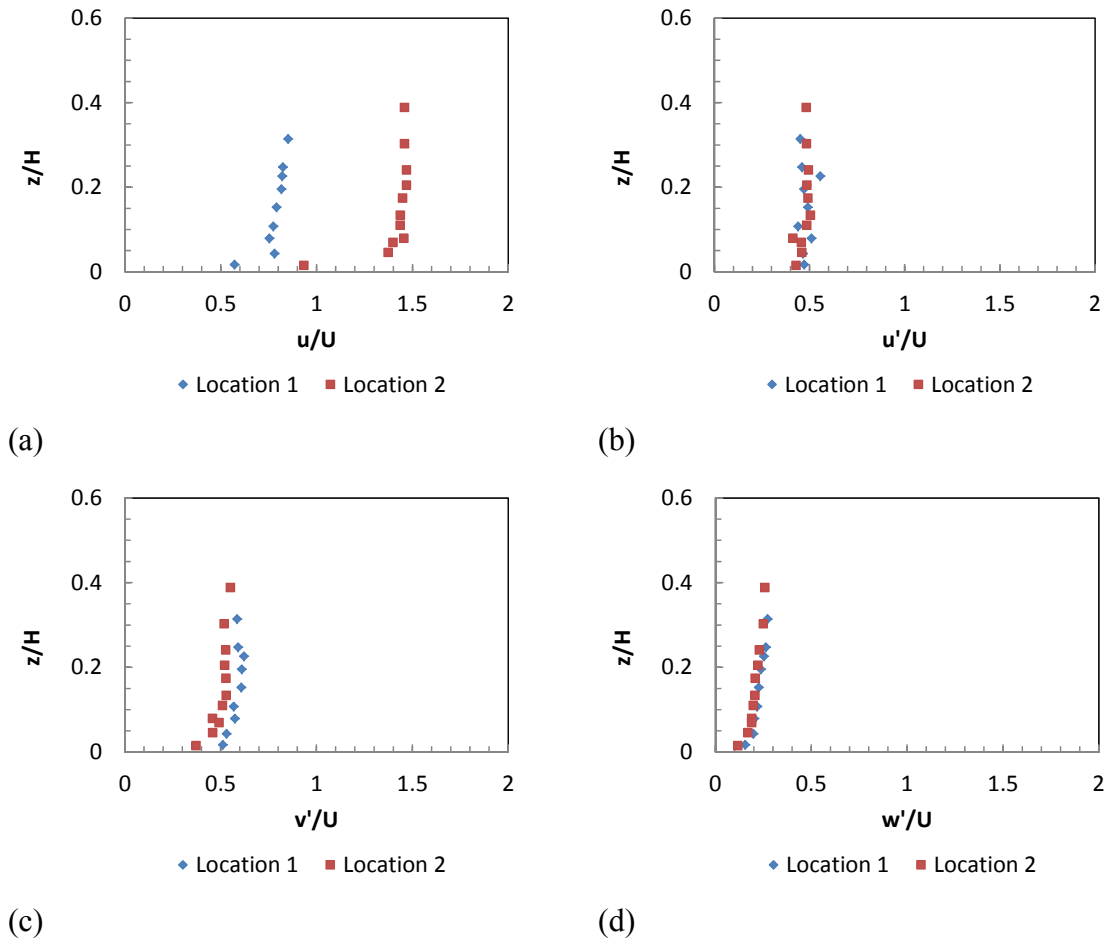


Figure C. 1: Normalized ADV results for: (a) point velocity; (b) streamwise turbulence intensity; (c) spanwise turbulence intensity; (d) vertical turbulence intensity; for emergent vegetation density  $m = 101.9$  stems/ft<sup>2</sup>,  $Q = 0.2$  cfs,  $H = 4.20$  in.,  $U = 0.174$  ft/sec

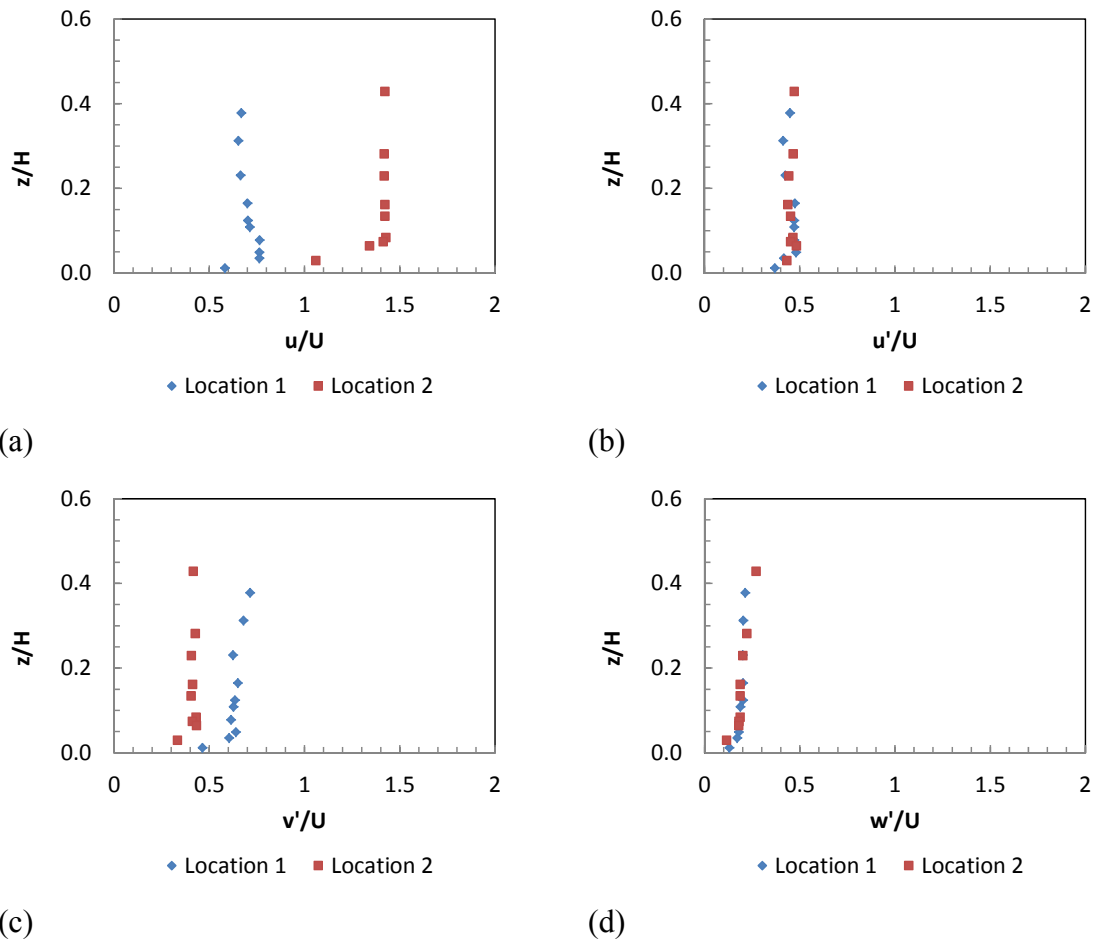


Figure C. 2: Normalized ADV results for: (a) point velocity; (b) streamwise turbulence intensity; (c) spanwise turbulence intensity; (d) vertical turbulence intensity; for emergent vegetation density  $m = 101.9$  stems/ft<sup>2</sup>,  $Q = 0.3$  cfs,  $H = 5.16$  in.,  $U = 0.213$  ft/sec

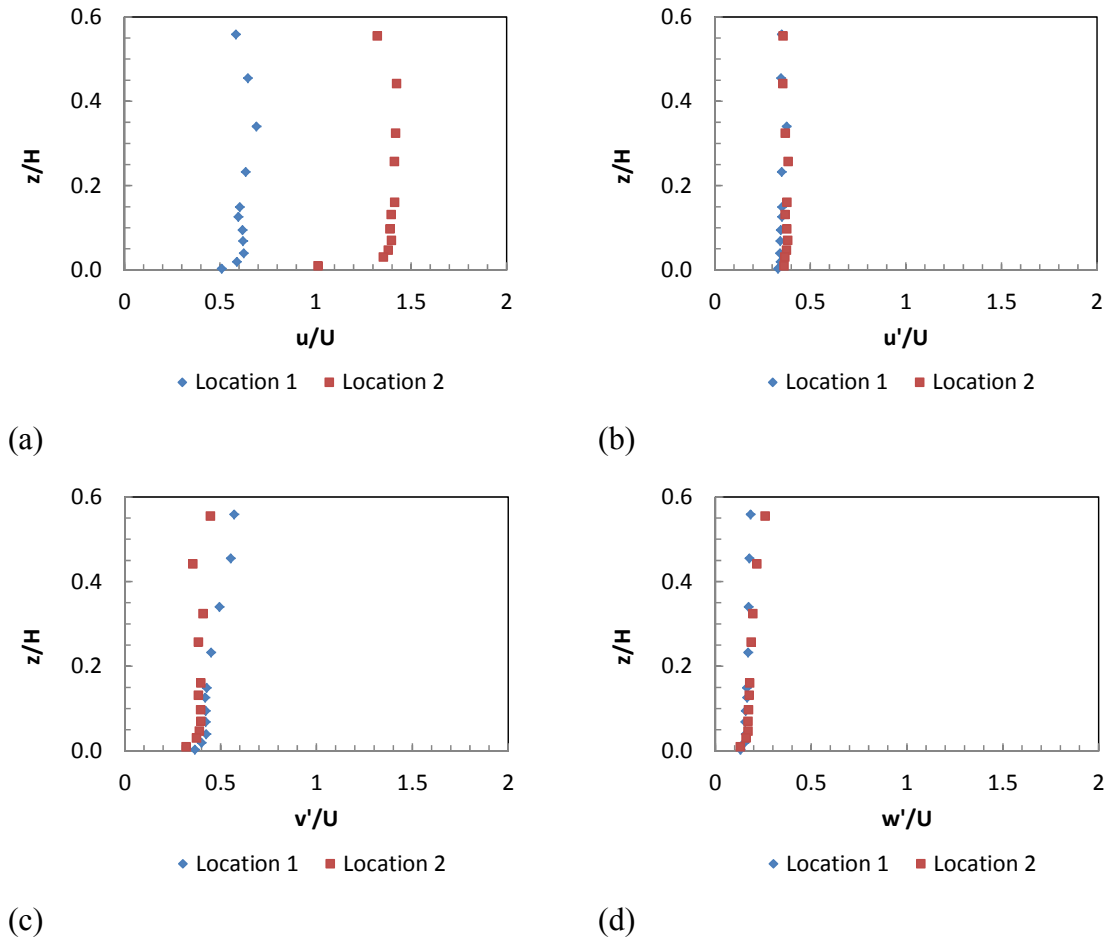


Figure C. 3: Normalized ADV results for: (a) point velocity; (b) streamwise turbulence intensity; (c) spanwise turbulence intensity; (d) vertical turbulence intensity; for emergent vegetation density  $m = 101.9$  stems/ft<sup>2</sup>,  $Q = 0.5$  cfs,  $H = 7.32$  in.,  $U = 0.250$  ft/sec

Emergent vegetation of density  $m = 25.5 \text{ stems/ft}^2$

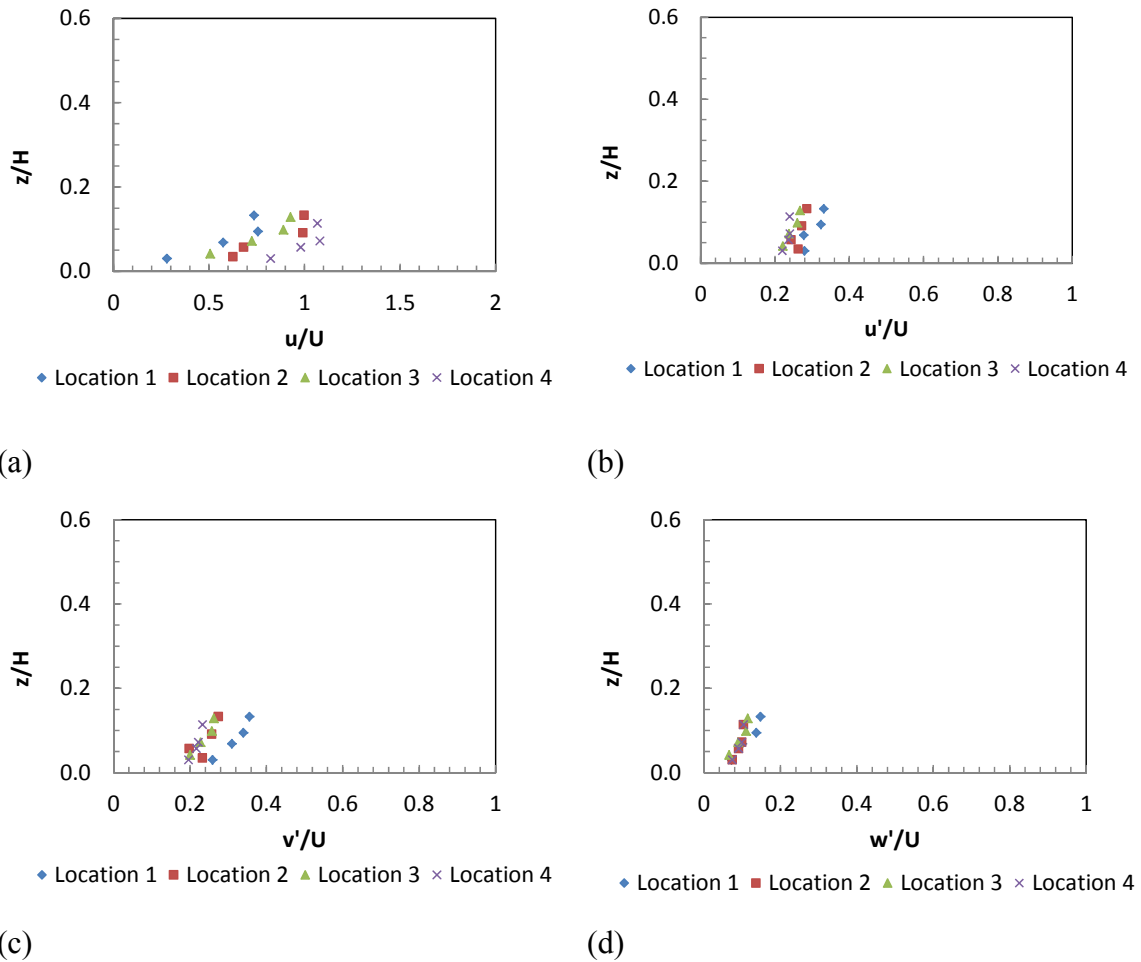


Figure C. 4: Normalized ADV results for: (a) point velocity; (b) streamwise turbulence intensity; (c) spanwise turbulence intensity; (d) vertical turbulence intensity; for emergent vegetation density  $m = 25.5 \text{ stems/ft}^2$ ,  $Q = 0.3 \text{ cfs}$ ,  $H = 2.64 \text{ in.}$ ,  $U = 0.416 \text{ ft/sec}$

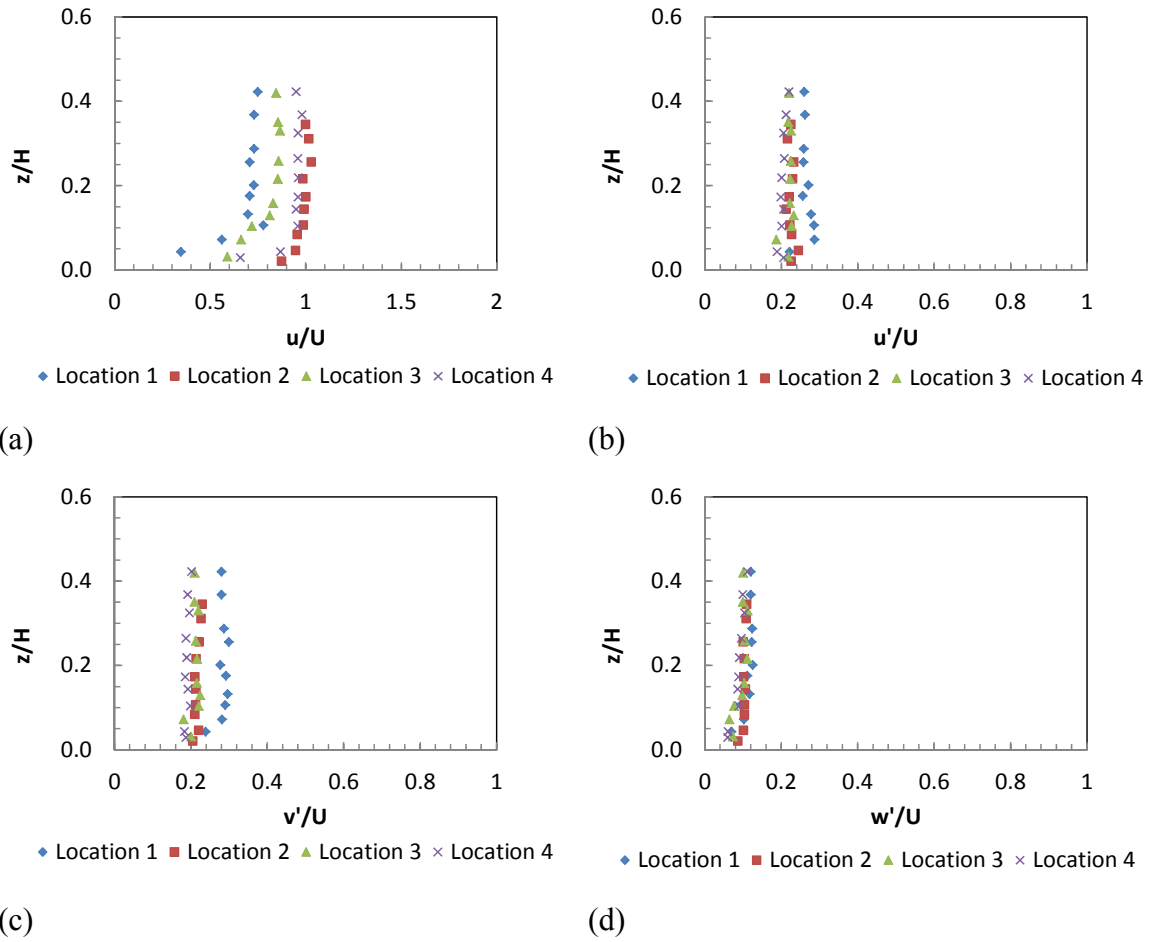


Figure C. 5: Normalized ADV results for: (a) point velocity; (b) streamwise turbulence intensity; (c) spanwise turbulence intensity; (d) vertical turbulence intensity; for emergent vegetation density  $m = 25.5$  stems/ft<sup>2</sup>,  $Q = 0.5$  cfs,  $H = 3.48$  in.,  $U = 0.526$  ft/sec

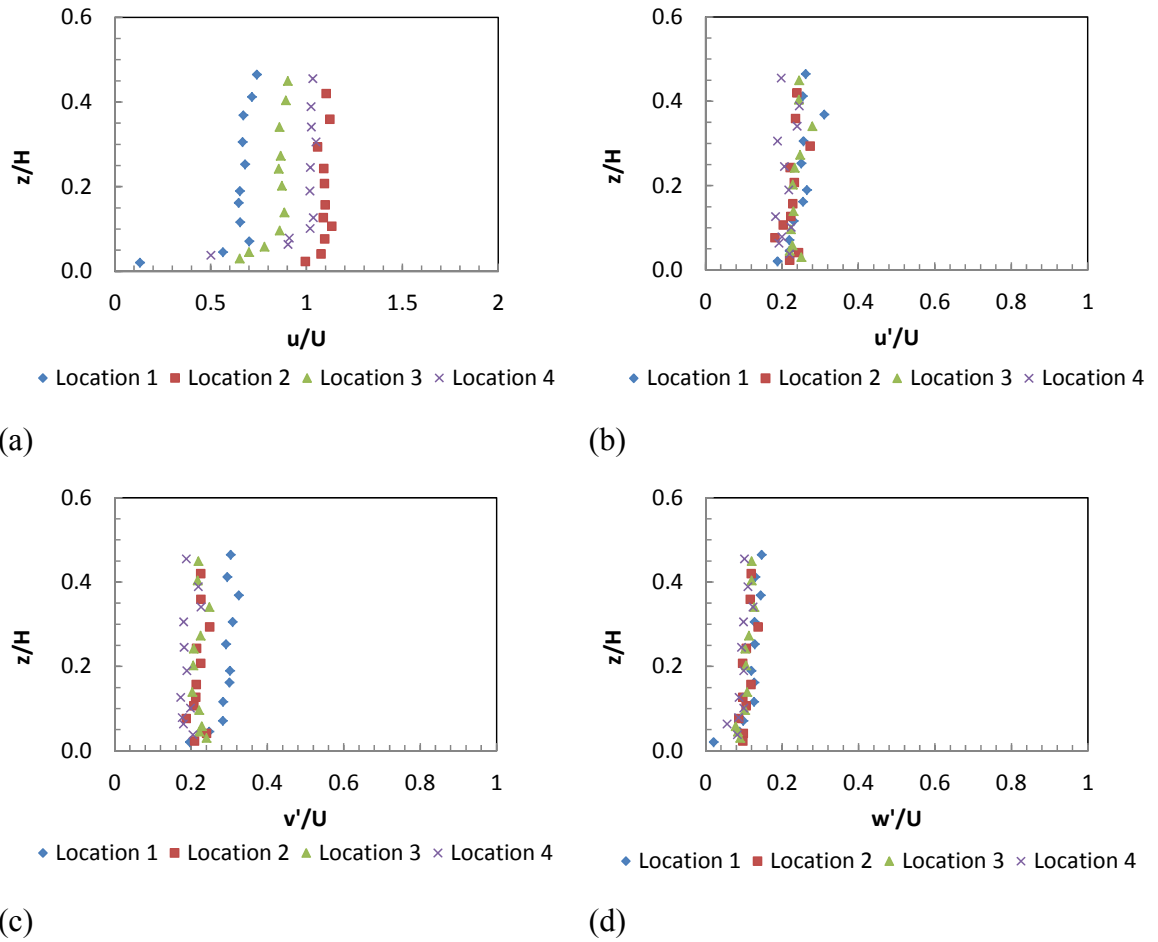


Figure C. 6: Normalized ADV results for: (a) point velocity; (b) streamwise turbulence intensity; (c) spanwise turbulence intensity; (d) vertical turbulence intensity; for emergent vegetation density  $m = 25.5$  stems/ft<sup>2</sup>,  $Q = 0.6$  cfs,  $H = 3.96$  in.,  $U = 0.554$  ft/sec

Submerged vegetation of density  $m = 101.9 \text{ stems/ft}^2$

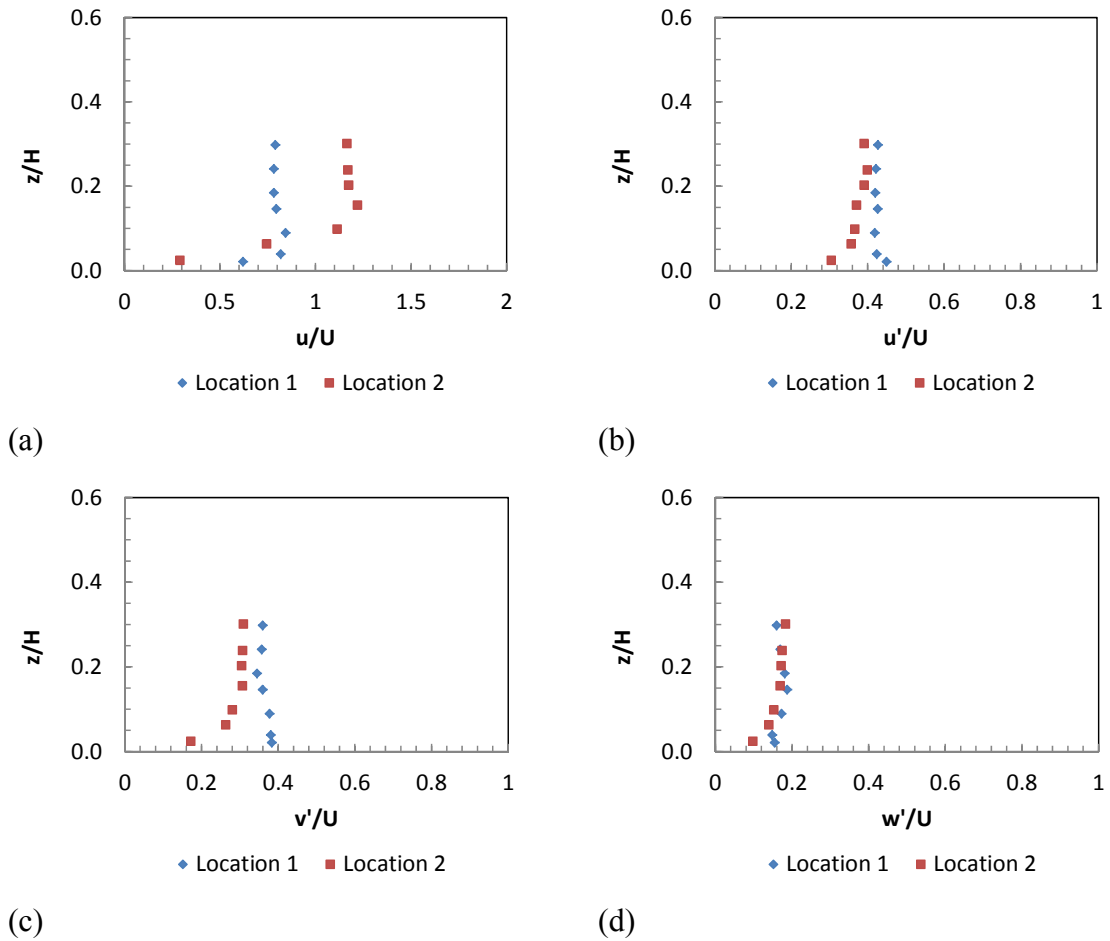


Figure C. 7: Normalized ADV results for: (a) point velocity; (b) streamwise turbulence intensity; (c) spanwise turbulence intensity; (d) vertical turbulence intensity; for submerged vegetation density  $m = 101.9 \text{ stems/ft}^2$ ,  $Q = 0.2 \text{ cfs}$ ,  $H = 3.36 \text{ in.}$ ,  $U = 0.218 \text{ ft/sec}$

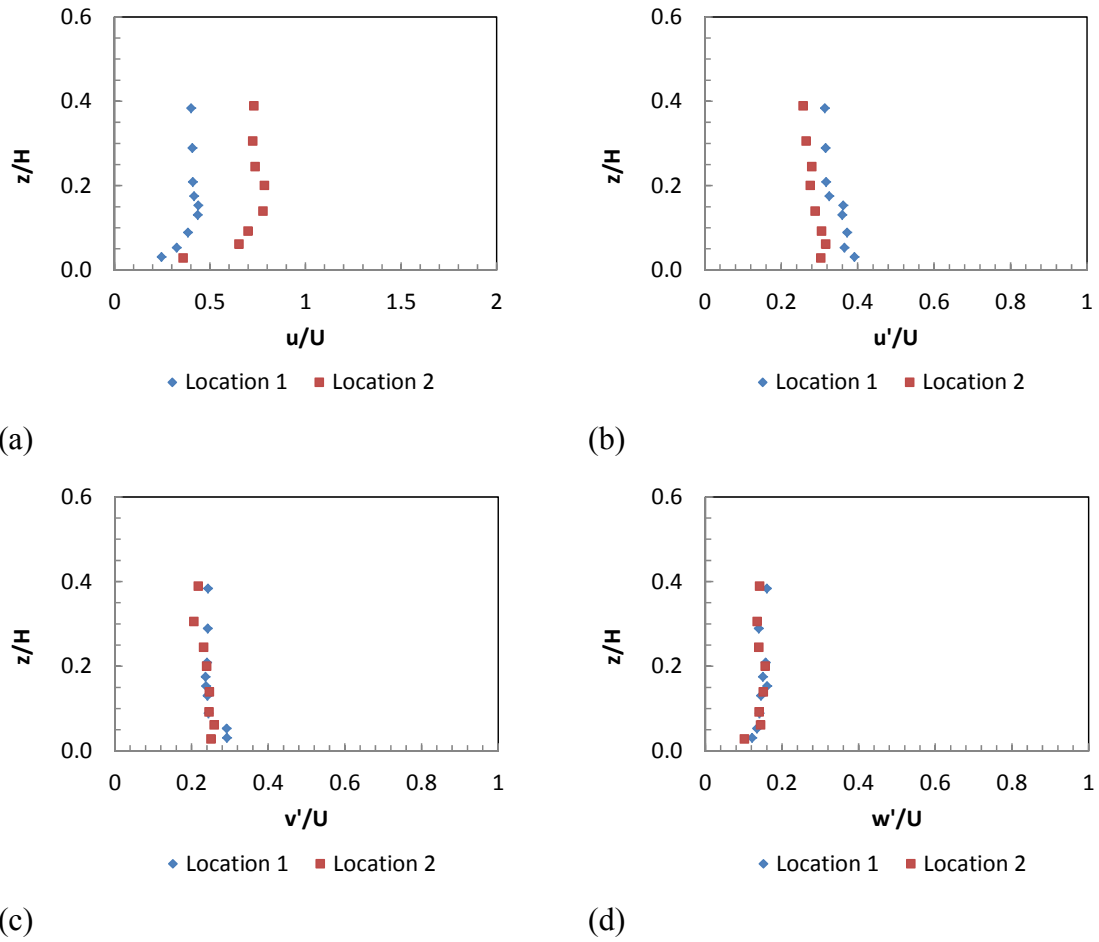


Figure C. 8: Normalized ADV results for: (a) point velocity; (b) streamwise turbulence intensity; (c) spanwise turbulence intensity; (d) vertical turbulence intensity; for submerged vegetation density  $m = 101.9$  stems/ft<sup>2</sup>,  $Q = 0.3$  cfs,  $H = 3.60$  in.,  $U = 0.310$  ft/sec

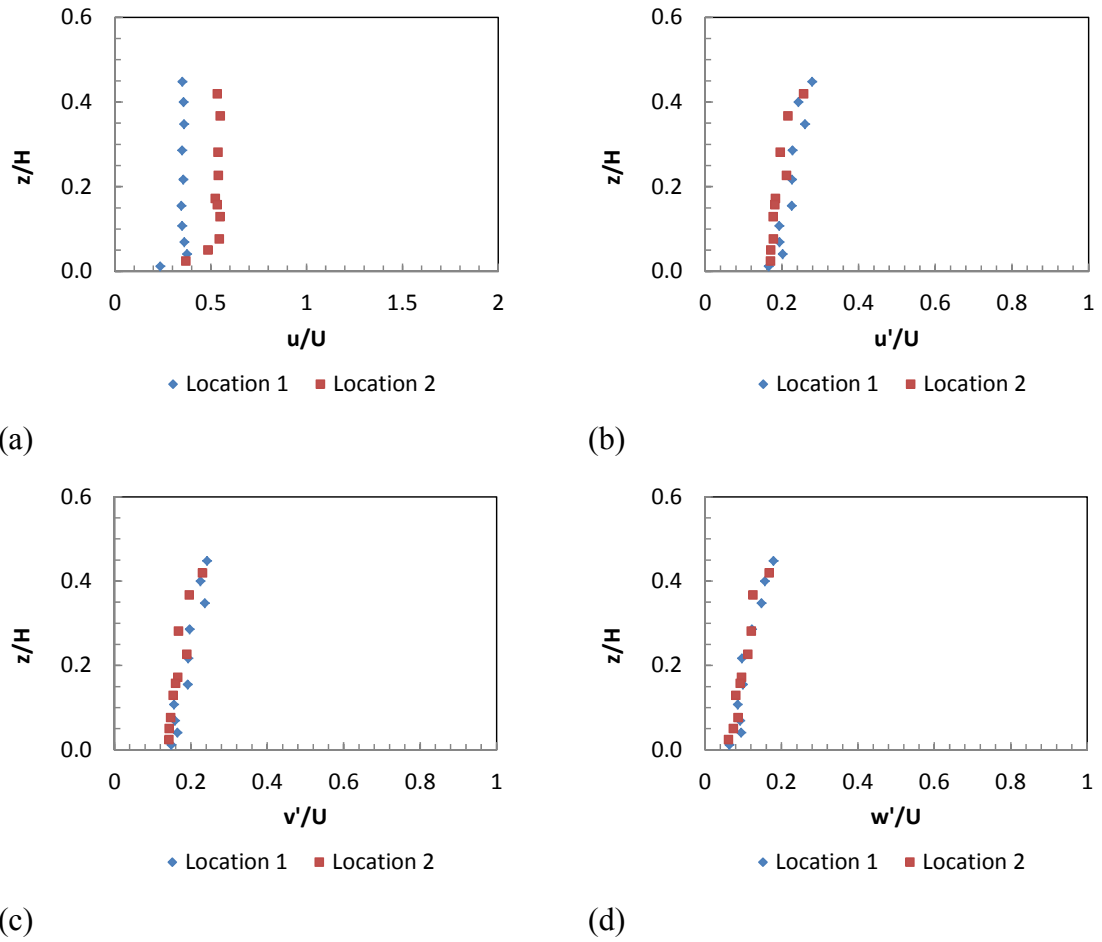


Figure C. 9: Normalized ADV results for: (a) point velocity; (b) streamwise turbulence intensity; (c) spanwise turbulence intensity; (d) vertical turbulence intensity; for submerged vegetation density  $m = 101.9$  stems/ft<sup>2</sup>,  $Q = 0.5$  cfs,  $H = 4.20$  in.,  $U = 0.436$  ft/sec

**Submerged vegetation of density  $m = 25.5$  stems/ft<sup>2</sup>**

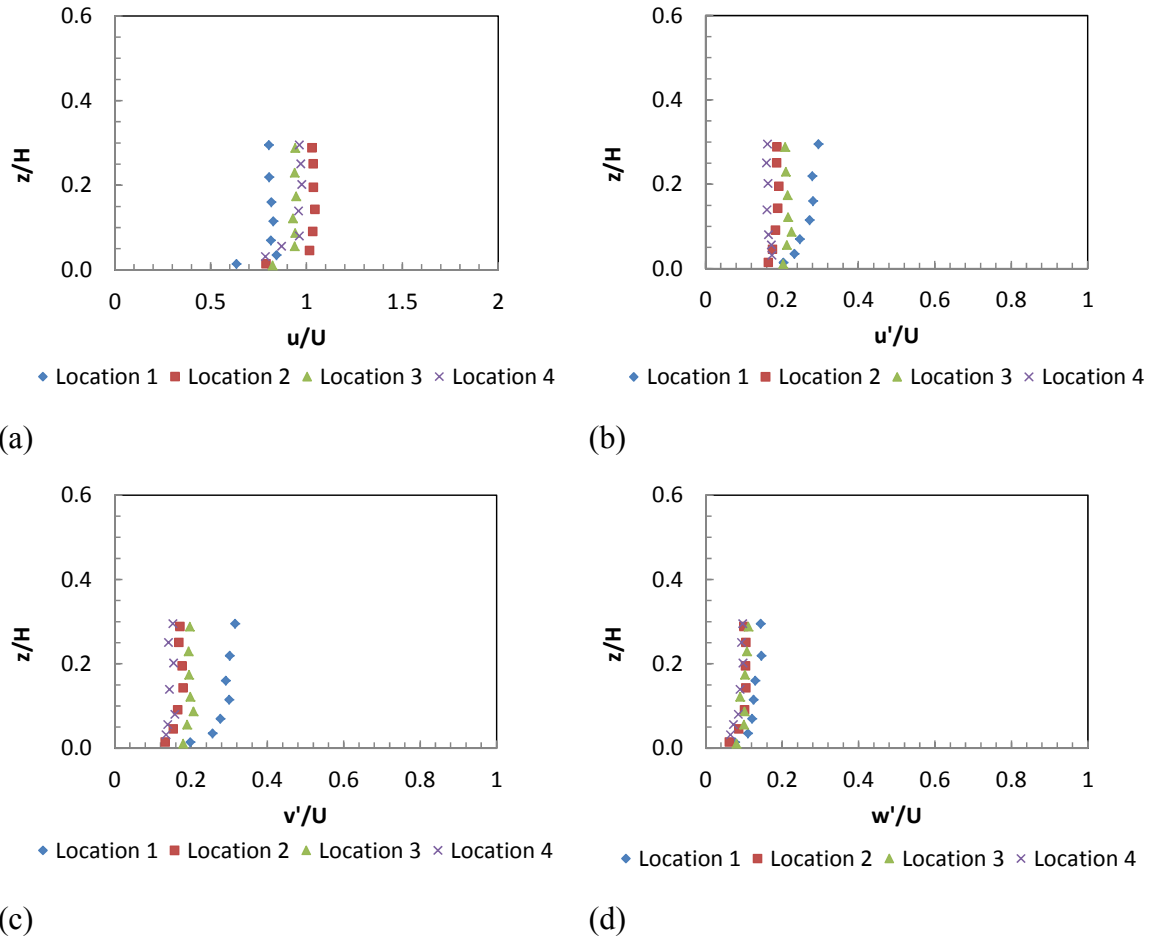


Figure C. 10: Normalized ADV results for: (a) point velocity; (b) streamwise turbulence intensity; (c) spanwise turbulence intensity; (d) vertical turbulence intensity; for submerged vegetation density  $m = 25.5$  stems/ft<sup>2</sup>,  $Q = 0.5$  cfs,  $H = 2.88$  in.,  $U = 0.635$  ft/sec

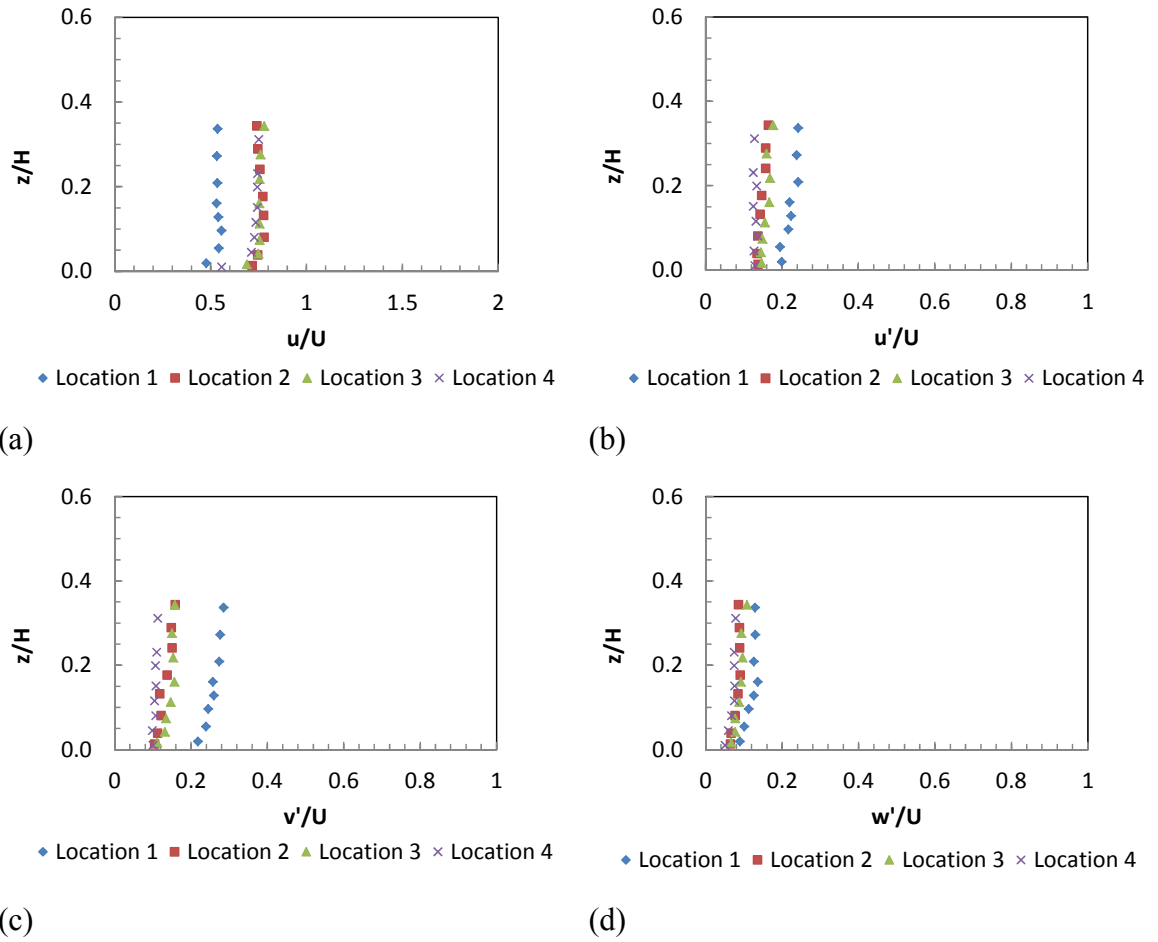


Figure C. 11: Normalized ADV results for: (a) point velocity; (b) streamwise turbulence intensity; (c) spanwise turbulence intensity; (d) vertical turbulence intensity; for submerged vegetation density  $m = 25.5$  stems/ft<sup>2</sup>,  $Q = 0.7$  cfs,  $H = 3.12$  in.,  $U = 0.821$  ft/sec

## REFERENCES

- Andrade, J. S., Costa, U. M. S., Almeida, M. P., Makse, H. A., & Stanley, H. E. (1999). *Inertial effects on fluid flow through disordered porous media*. *Physical Review Letters*, 82(26), 5249-5252.
- Barfield, B.J., Gasem, K.A.M., Arjunan, J., Yeri, S., & Stevens, E. (2005). *Application of Polyacrylamide to Enhance Silt Fence Performance*. Paper presented at the World Water Congress 2005: Impact of Global Climate Change, Anchorage, AK.
- Bird, R. B., Stewart, W. E., & Lightfoot, E. N. (1960). *Transport Phenomena*. New York: Wiley.
- Carollo, F. G., Ferro, V., & Termini, D. (2002). *Flow velocity measurements in vegetated channels*. *Journal of Hydraulic Engineering-Asce*, 128(7), 664-673.
- Cellino, M., & Graf, W. H. (2002). *Suspension flows in open channels; experimental study*. *Journal of Hydraulic Research*, 40(4), 435-447.
- Chen, Y.H., & Cotton, B.A. (1988). *Design of Roadside Channels with Flexible Linings*. Paper presented at the Hydraulic Engineering Circular No. 15 (HEC-15), FHWA, Publication No. FHWA-IP-87-7, USDOT/FHWA, McClean, VA.
- Cheng, N. S., & Nguyen, H. T. (2011). *Hydraulic Radius for Evaluating Resistance Induced by Simulated Emergent Vegetation in Open-Channel Flows*. *Journal of Hydraulic Engineering-Asce*, 137(9), 995-1004.
- Choi, S. U., & Kang, H. S. (2004). *Reynolds stress modeling of vegetated open-channel flows*. *Journal of Hydraulic Research*, 42(1), 3-11.
- Churchill, S.W. (1988). *Viscous Flows — the Practical Use of Theory*. Boston, MA: Butterworths.
- Dallaire, G. (1976). *Controlling Erosion and Sedimentation at Construction Sites*. *Civil Engineering*, 47(10), 73-77.
- Davies, K., Fullen, M. A., & Booth, C. A. (2006). *A pilot project on the potential contribution of palm-mat geotextiles to soil conservation*. *Earth Surface Processes and Landforms*, 31(5), 561-569.
- Dirt 2 Committee. (2001). *Repairing the Chattahoochee: The Dirt 2 Technical Panel Completion Report*. Franklin, GA.

- Dombroski, D.E., & Crimaldi, J.P. (2007). *The Accuracy of Acoustic Doppler Velocimetry Measurements in Turbulent Boundary Layer Flows Over a Smooth Bed*. *Limnol. Oceanogr., Methods* 5, 23–33.
- Dullien, F.A.L. (1979). *Porous Media-Fluid Transport and Pore Structure*. New York, NY: Academic Press, Inc., Harcourt Brace Jovanovich, Publishers.
- DVWK. (1991). *Hydraulische Berechnung von Fließgewässern (Hydraulic Calculation of Running Waters)*. Germany.
- Elliott, A. H. (2000). *Settling of fine sediment in a channel with emergent vegetation*. *Journal of Hydraulic Engineering-Asce*, 126(8), 570-577.
- Ferreira, R., Ricardo, A., & Franca, M. (2009). *Discussion of 'Laboratory Investigation of Mean Drag in a Random Array of Rigid, Emergent Cylinders' by Yukie Tanino and Heidi M. Nepf*. *J. Hydraul. Eng.*, 135 (8), 690–693.
- Fischer, H.B., List, E.J., Koh, R.C.Y, Imberger, J., & N.H.Brooks. (1979). *Mixing in Inland and Coastal Waters*. Orlando, FL: Academic Press, Inc.
- Fu Sheng Wu. (2008). *Characteristics of Flow Resistance in Open Channels with Non-Submerged Rigid Vegetation*. *Journal of Hydrodynamics*, 20(2), 239-245.
- GASWCC. (2000). *Manual for Erosion and Sediment Control in Georgia (Georgia Green Book), 5th Edition*. GA: Georgia Soil and Water Conservation Commission.
- Glicksman, L. R., Hyre, M. R., & Farrell, P. A. (1994). *Dynamic Similarity in Fluidization*. *International Journal of Multiphase Flow*, 20, 331-386.
- Graf, W.H. (1971). *Hydraulics of Sediment Transport*. New York, NY: MacGraw-Hill.
- Haan, C.T., Barfield, B.J., & Hayes, J.C. (1994). *Design Hydrology and Sedimentology for Small Catchments*. San Diego, CA: Academic Press, Inc.
- Hellstrom, J.G.I, & Lundstrom, T.S. (2006). *Flow through Porous Media at Moderate Reynolds Number*. Paper presented at the International Scientific Colloquium Modeling for Material Processing, Riga, Latvia.
- Hoffmann, M. R. (2004). *Application of a simple space-time averaged porous media model to flow in densely vegetated channels*. *Journal of Porous Media*, 7(3), 183-191.
- Holdich, R.G. (2002). *Fundamentals of Particle Technology*. Leicestershire, UK: Midland Information Technology and Publishing.
- Hsieh, T. (1964). *Resistance of cylinder Piers in Open-Channel Flow*. *Journal of the Hydraulics Division, ASCE*, Vol.90, No. HY1, Proc. Paper 3770 pp. 161-173.

- Hudson, N.W. (2001). *A Study of the Reasons for Success and Failures of Soil Conservation Projects*. Bedford, UK: FAO Soils Bulletin No. 64.
- James, C. S., Birkhead, A. L., Jordanova, A. A., & O'Sullivan, J. J. (2004). *Flow resistance of emergent vegetation*. Journal of Hydraulic Research, 42(4), 390-398.
- James, C. S., Goldbeck, U. K., Patini, A., & Jordanova, A. A. (2008). *Influence of foliage on flow resistance of emergent vegetation*. Journal of Hydraulic Research, 46(4), 536-542.
- James, C. S., & Sharpe, R. G. (2006). *Deposition of sediment from suspension in emergent vegetation*. Water Sa, 32(2), 211-218.
- Jarvela, J. (2002a). *Flow resistance of flexible and stiff vegetation: a flume study with natural plants*. Journal of Hydrology, 269(1-2), 44-54.
- Jarvela, J. (2002b). *Determination of Flow Resistance of Vegetated Channel Banks and Floodplains* Paper presented at the River Flow 2002 - Proceedings of the International Conference on Fluvial Hydraulics, Lisse, The Netherlands.
- Jarvela, J. (2004). *Determination of Flow Resistance Caused by Non-Submerged Woody Vegetation*. International Journal of River Basin Management Vol. 2(No.1), pp. 61-70.
- Jarvela, J. (2005). *Effect of submerged flexible vegetation on flow structure and resistance*. Journal of Hydrology, 307(1-4), 233-241.
- Kadlec, R.H., & Knight, R.L. (1996). *Treatment Wetlands*. Boca Raton, FL: Lewis Publishers.
- Kaufman, M. M. (2000). *Erosion control at construction sites: The science-policy gap*. Environmental Management, 26(1), 89-97.
- Kouwen, N. (1992). *Modern Approach to Design of Grassed Channels*. Journal of Irrigation and Drainage Engineering-Asce, 118(5), 733-743.
- Kouwen, N., & FathiMaghadam, M. (1997). *Nonrigid, nonsubmerged, vegetative roughness on floodplains*. Journal of Hydraulic Engineering-Asce, 123(1), 51-57.
- Kouwen, N., & Li, R. M. (1980). *Biomechanics of Vegetative Channel Linings*. Journal of the Hydraulics Division-Asce, 106(6), 1085-1106.
- Kouwen, N., Li, R.M., & Simons, D.B. (1980). *A Stability Criteria for Vegetated Waterways*. Paper presented at the Proc., Int. Symp. on Urban Storm Runoff, University of Kentucky, KY.
- Kouwen, N., Unny, T.E., & Hill, H.M. (1969). *Flow Retardance in Vegetated Channels*. Journal of the Irrigation and Drainage Division, ASCE, Vol. 95(No. 2), pp. 329-344.

- Kubrak, E., Kubrak, J., & Rowinski, P. M. (2008). *Vertical velocity distributions through and above submerged, flexible vegetation*. Hydrological Sciences Journal-Journal Des Sciences Hydrologiques, 53(4), 905-920.
- Kundu, P., & Cohen, I. (2004). *Fluid Mechanics*. Elsevier Academic Press, San Diego, CA, USA, 3rd Edition.
- Lee, J. K., Roig, L. C., Jenter, H. L., & Visser, H. M. (2004). *Drag coefficients for modeling flow through emergent vegetation in the Florida Everglades*. Ecological Engineering, 22(4-5), 237-248.
- Li, Y. X., Lau, S. L., Kayhanian, M., & Stenstrom, M. K. (2005). *Particle size distribution in highway runoff*. Journal of Environmental Engineering-Asce, 131(9), 1267-1276.
- Li, Y. X., Lau, S. L., Kayhanian, M., & Stenstrom, M. K. (2006). *Dynamic characteristics of particle size distribution in highway runoff: Implications for settling tank design*. Journal of Environmental Engineering-Asce, 132(8), 852-861.
- Licht, L., Aitchison, E., Schnabel, W., English, M., & Kaempf, M. (2001). *Landfill Capping with Woodland Ecosystems*. Practice Periodical of Hazardous, Toxic, and Radioactive Waste Management, 5(4), 175-184.
- Lindner, K. (1982). *The Flow Resistance of Cultivated Plants (Der Strömungswiderstand von Pflanzenbeständen)*. Leichtweiss Institute of Hydraulic Engineering, Technical University of Braunschweig, Germany.
- Liu, D., Diplas, P., Fairbanks, J. D., & Hodges, C. C. (2008). *An experimental study of flow through rigid vegetation*. Journal of Geophysical Research-Earth Surface, 113(F4).
- Lopez, F., & Garcia, M. (1997). *Open-Channel Flow Through Simulated Vegetation: Turbulence Modeling and Sediment Transport*. Wetlands Research Program Technical Report WRP-CP-10, August 1997 - Final Report
- McLaughlin, R. A., & Brown, T. T. (2006). *Evaluation of erosion control products with and without added polyacrylamide*. Journal of the American Water Resources Association, 42(3), 675-684.
- Meyer, L.D., & Wischmeier, W.H. (1969). *Mathematical Simulation of the Processes of Soil Erosion By Water* Transactions of the ASABE, 12(6), pp. 0754-0758.
- Morgan, R.P.C. (2005). *Soil Erosion and Conservation* (3rd Edition ed.). Oxford, UK: 3rd Edition, Blackwell Publishing.
- Morrow, S., Smolen, M., Stiegler, J., & Cole, J. (2003). *Using Vegetation for Erosion Control on Construction Sites*. Fact Sheet F-1514, Oklahoma Cooperative Extension Fact

Sheets, Division of Agricultural Sciences and Natural Resources, Oklahoma State University, Stillwater, OK.

Mostaghimi, S., Gidley, T. M., Dillaha, T. A., & Cooke, R. A. (1994). *Effectiveness of Different Approaches for Controlling Sediment and Nutrient Losses from Eroded Land*. Journal of Soil and Water Conservation, 49(6), 615-620.

Munson, B.R., Young, D.F., & Okiishi, T.H. (1999). *Fundamentals of Fluid Mechanics*. John Wiley & Sons, Inc., New York, 3rd Edition

Neary, V. S., Constantinescu, S. G., Bennett, S. J., & Diplas, P. (2012). *Effects of Vegetation on Turbulence, Sediment Transport, and Stream Morphology*. Journal of Hydraulic Engineering-Asce, 138(9), 765-776.

Nehal, L., Yan, Z. M., & Xia, J. H. (2005). *Study of the Flow Through Non-Submerged Vegetation*. Journal of Hydrodynamics, 17(4), 498-502.

Nezu, I., & Nakagawa, H. (1993). *Turbulence in Open Channel Flows*. Rotterdam, The Netherlands: International Association for Hydraulic Research: Monograph Series on Fluid Mechanics, A.A. Balkema Publishing.

Nezu, I., & Rodi, W. (1986). *Open-Channel Flow Measurements with a Laser Doppler Anemometer*. Journal of Hydraulic Engineering-Asce, 112(5), 335-355.

Niven, R. K. (2002). *Physical insight into the Ergun and Wen & Yu equations for fluid flow in packed and fluidised beds*. Chemical Engineering Science, 57(3), 527-534.

Ocktmann, M. (2000). *Vegetative Buffer Zones*. Farmnote 38/2000, Department of Agriculture and food Western Australia (DAFWA), Norham, Western Australia.

Pimentel, D., & Kounang, N. (1998). *Ecology of soil erosion in ecosystems*. Ecosystems, 1(5), 416-426.

Rickson, R. J. (2006). *Controlling sediment at source: an evaluation of erosion control geotextiles*. Earth Surface Processes and Landforms, 31(5), 550-560.

Rouse, H. (1937). *Modern Conceptions of the mechanics of Fluid Turbulence*. Transactions of the ASCE, Vol. 102(No. 1), pp. 523-543.

Stephan, U. (2002). *Zum Fließwiderstandsverhalten Flexible Vegetation (Resistance to the Flow Behavior of Flexible Vegetation)*. Technical University of Vienna, Austria.

Stoesser, T., Kim, S. J., & Diplas, P. (2010). *Turbulent Flow through Idealized Emergent Vegetation*. Journal of Hydraulic Engineering-Asce, 136(12), 1003-1017.

- Stoesser, T., Wilson, C. A. M. E., Bates, P. D., & Dittrich, A. (2003a). *Application of a 3D Numerical Model to a River with Vegetated Floodplains*. Journal of Hydroinformatics, Vol. 5(2), pp. 99-112.
- Stoesser, T., Wilson, Came, Bates, P. D., & Pinzen, A. B. (2003b). *Open channel flow through different forms of submerged flexible vegetation*. Journal of Hydraulic Engineering-Asce, 129(11), 847-853.
- Stone, B. M., & Shen, H. T. (2002). *Hydraulic resistance of flow in channels with cylindrical roughness*. Journal of Hydraulic Engineering-Asce, 128(5), 500-506.
- Sturm, T. (2001). *Open Channel Hydraulics*: McGraw-Hill Series in Water Resources and Environmental Engineering.
- Sturm, T., & Kirby, R. (1991). Sediment Reduction in Urban Stormwater Runoff from Construction Sites. Technical Completion Report for USDI/Geological Survey Project 14-08-0001-G1556 (06): Georgia Institute of Technology, School of Civil Engineering in cooperation with Environmental Resources Center, GA.
- Sturm, T., & Warner, R. (2007). *Seep Berm Design Manual*: Georgia EPD and U.S. Environmental Protection Agency, Atlanta, GA.
- Sturm, T., Warner, R., Hamade, F., & S.Torrealba. (2007). *Demonstration of a Performance-Based System of Storm Water and Erosion Controls on Small Residential/Commercial Sites in the Georgia Piedmont*. Georgia Institute of Technology, Georgia EPD Research Project.
- Tanino, Y., & Nepf, H. (2010). *Laboratory investigation of mean drag in a random array of rigid, emergent cylinders (Unpublished raw data)*.
- Tanino, Y., & Nepf, H. M. (2008). *Laboratory investigation of mean drag in a random array of rigid, emergent cylinders*. Journal of Hydraulic Engineering-Asce, 134(1), 34-41.
- Tanino, Y., & Nepf, H. M. (2009). *Laboratory investigation of lateral dispersion within dense arrays of randomly distributed cylinders at transitional Reynolds number*. Physics of Fluids, 21(4).
- Tsujimoto, T., Shimizu, Y., Kitamura, T., & Okada, T. (1992). *Turbulent Open Channel Flow over Bed Covered by Rigid Vegetation*. Journal of Hydrosience and Hydraulic Engineering, Vol 10(2), pp. 13-25.
- Turgeon, A.J. (2002). *Turfgrass Management* (6th Edition ed.). Upper Saddle River, NJ: Prentice Hall, 6th Edition.
- UM. (2004). *Occupational Safety and Environmental Health: Soil Erosion and Control Procedures*. University of Michigan, MI.

- USEPA. (2002). *National Water Quality Inventory*.: U.S. Environmental Protection Agency.
- Warner, R., Botts, S.D., Marticorena, M., & Mills, L. (2004). *Incorporating Indigenous Technologies Into Enhanced Stormwater, Erosion and Sediment Control Systems*. Paper presented at the Society for Mining, Metallurgy, and Exploration (SME) Annual Meeting, Feb 2004, Denver, CO.
- Warner, R., Schwab, P.J., & Marshall, D.J. (1998). *SEDCAD 4 Design Manual and User's Guide*. Civil Software Design
- Wilson, Came. (2007). *Flow resistance models for flexible submerged vegetation*. Journal of Hydrology, 342(3-4), 213-222.
- Wilson, Came, & Horritt, M. S. (2002). *Measuring the flow resistance of submerged grass*. Hydrological Processes, 16(13), 2589-2598.
- Wolman, M. G., & Schick, A. P. (1967). *Effects of Construction on Fluvial Sediment, Urban, and Suburban Areas of Maryland*. Water Resources Research, 3(2), 451-&.
- Wu, F. C., Shen, H. W., & Chou, Y. J. (1999). *Variation of roughness coefficients for unsubmerged and submerged vegetation*. Journal of Hydraulic Engineering-Asce, 125(9), 934-942.
- Yang, W., & Choi, S. U. (2010). *A two-layer approach for depth-limited open-channel flows with submerged vegetation*. Journal of Hydraulic Research, 48(4), 466-475.
- Yen, B. C. (2002). *Open channel flow resistance*. Journal of Hydraulic Engineering-Asce, 128(1), 20-39.